Studies on Helical Tubular Assemblies of Foldamers and Helix-in-Helix Inclusion Complex Formation of Syndiotactic Poly(methyl methacrylate) with Polylactides

フォルダマーのチューブ状らせん集合体および
シンジオタクチックポリメタクリル酸メチルと
ポリ乳酸からなるらせん状包接錯体形成に関する研究

Satoshi KAWABATA

川端　賢

2021

Studies on Helical Tubular Assemblies of Foldamers and Helix-in-Helix Inclusion Complex Formation of Syndiotactic Poly(methyl methacrylate) with Polylactides

フォルダマーのチューブ状らせん集合体および
シンジオタクチックポリメタクリル酸メチルと
ポリ乳酸からなるらせん状包接錯体形成に関する研究

Table of Contents

General Introduction

Proteins are an important class of biological polymers and fold into well-defined highly-ordered structures through noncovalent bonding interactions, such as hydrogen bonding and charged electrostatic interactions. Therefore, their functional groups are precisely arranged at the active sites, thus showing various sophisticated functions, such as enzymatic activity.[1] However, since these functions strongly depend on the stability of the highly-ordered architectures of proteins, these unique functions only take place under a limited range of conditions. Inspired by such sophisticated biological highly-ordered architectures and their functions, the development of helical polymers[2] and supramolecular helical aggregates from small molecules[3] has become one of the most emerging research areas in the world. Therefore, artificial helical systems with a controlled helical handedness have been applied as novel chiral materials in asymmetric catalysis, chiral recognition/separation, and circularly polarized luminescence.

Pioneering studies on artificial helical polymers were reported by Nolte et al. in 1974,[4] Okamoto et al. in 1979,[5] and Green et al. in 1988.[6] The artificial helical polymers synthesized to date can be classified into three types depending on their helical characteristics: 1) static helical polymers, 2) dynamic helical polymers, and 3) foldamers. Static helical polymers, such as polyisocyanide (**1**),[4] poly(triphenylmethyl methacrylate) (**2**),[5] polychloral (**3**),[7] poly(quinoxaline-2,3-diyl) (**4**),[8] and polycarbodiimide (**5**),[9] have high helix inversion barriers and their excess one-handed helical structures are maintained with high stability.

On the other hand, dynamic helical polymers, such as polyisocyanates (**6**),[2b,10] polysilanes (**7**),[11] and polyacetylenes (**8**–**10**),[12] have relatively low helix inversion barriers, therefore, the helix inversion between an equal amount of right (*P*)- and left (*M*)-handed helices easily occurs along a single polymer chain. Because these dynamic helical polymers have a relatively long helical persistence length, either a *P*- or *M*-handed helix can be biased in the entire polymer chain by copolymerizing an achiral monomer with a small amount of an enantiopure monomer. This chiral amplification phenomenon is known as the

"sergeants-and-soldiers" effect and is one of the intriguing characteristics of dynamic helical polymers.[2d,10] It has also been reported that an excess one-handed helical structure can be induced in a variety of dynamic helical polymers via noncovalent bonding interactions with nonracemic guest molecules.[2d,3f,13]

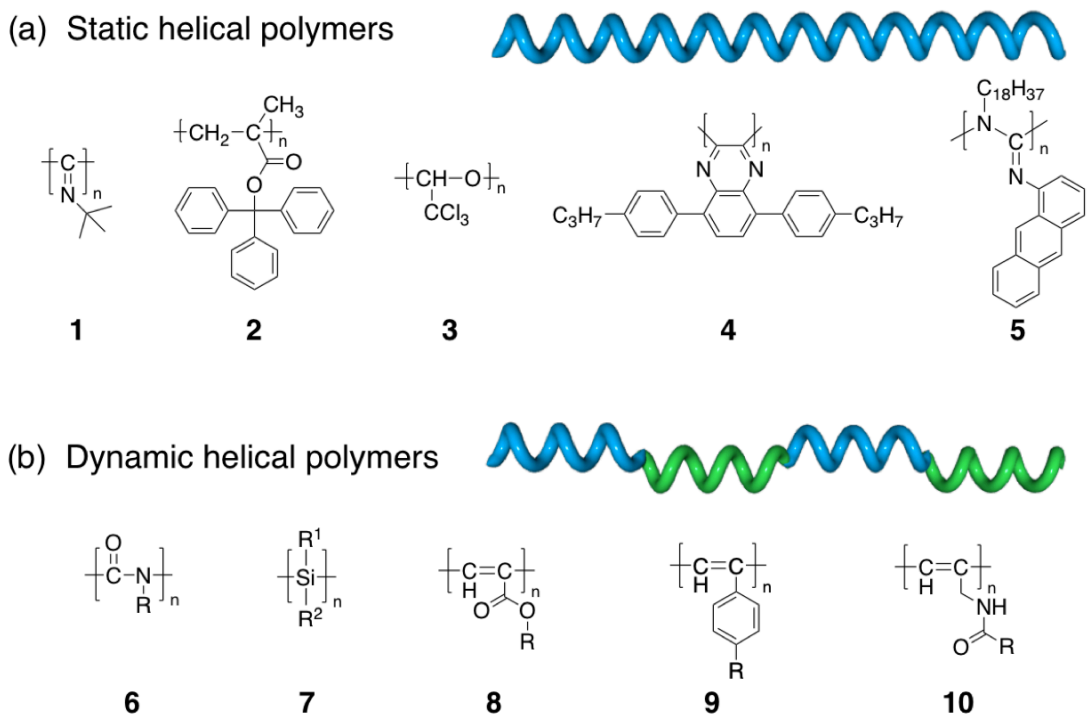

Figure 1. Structures of typical static (a) and dynamic (b) helical polymers.

Furthermore, research on foldamers, which are oligomers or polymers that fold into specific secondary structures under particular experimental conditions, such as solvent, temperature, and additives, has also attracted significant attention during the past two decades.[14] Helical foldamers with various skeletons have been designed and synthesized, and fold into a helical conformation driven by noncovalent bonding interactions, such as hydrogen bonding, solvophobic, and π–π interactions (Figure 2a). Aromatic oligoamides,[15–20] phenyleneethynylenes,[21–25] peptides,[26] indolocarbazoles,[27] aryltriazoles,[28–30] and pyridine-pyridazines[31] have been reported as the typical main chains of such helical foldamers (Figure 2b).

Hamilton and co-workers synthesized an aromatic oligoamide **11**, which folds into a helical structure driven by intramolecular hydrogen bonds as revealed by single-crystal X-ray and NMR analysis.[16] Moore and co-workers reported that a *m*-phenyleneethynylene (**12a**) forms a random coil structure in chloroform, but folds to form a helical structure with an inner cavity driven by solvophobic interactions in acetonitrile.[22] Furthermore, it has been discovered that a one-handed helix can be induced in **12b** by incorporating an optically active guest molecule (**13**) into its helical cavity.[23]

Foldamers can be structurally controlled and switched among random coils, racemic *P*- and *M*-handed helical conformations, and preferred-handed helical conformations using various external stimuli because of their unique dynamic nature. Structural control of the foldamers leads to the switching of their functions, such as the molecular recognition and asymmetric catalytic abilities. Huc, Lehn, and co-workers reported the conformational switching of an aromatic oligoamide **14** between its single and double helices in chloroform by controlling the concentration of the solution. The oligoamide **14** forms a single helix at a low concentration (1 mM) but a double helix at a high concentration (2.7 mM).[17] Furthermore, a one-handed helical conformation can be induced in **14** by intermolecular hydrogen bonding between a chiral guest molecule (**15**) and the terminal units of **14**.[18]

Li and co-workers prepared a series of aromatic oligohydrazides (**16–18**) with different chain lengths, which form a one-handed helical conformation by encapsulating sugars (**19a** and **20–21**).[32] It has been revealed that the association constants increase as the chain length gets longer because of the increase in the number of sites available to form intermolecular interactions with the sugars. Abe, Inoue, and co-workers have developed a series of oligo-*m*-ethynylpyridines (**22a**,**b**, and **23**) that selectively incorporate specific sugars (**19b**, **24**) among multiple sugars accompanied by a preferred-handed helicity induction.[33] Interestingly, the excess one-handed helical conformation was found to be retained utilizing copper coordination to the pyridine moiety after the replacement of the optically active sugar (**19b**) with achiral phenanthroline (**25**).[34]

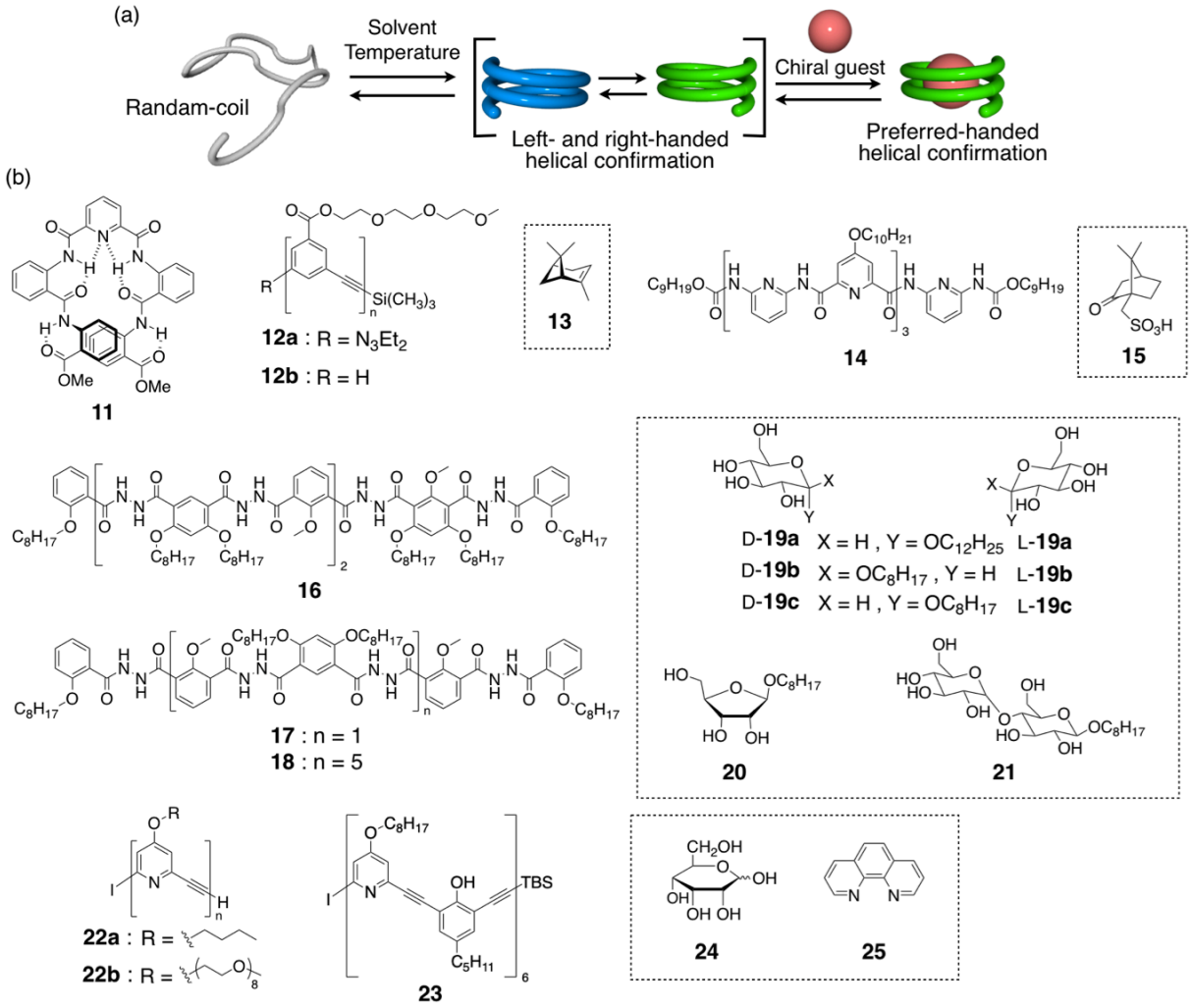

Figure 2. (a) Schematic representation of the preferred-handed helix formation induced by noncovalent bonding interactions with chiral guest compounds. (b) Structures of typical helical foldamers and guest molecules.

On the other hand, the external stimulus that controls the conformation of the foldamers is not limited to additives,[18,23,32–33,35] with an example of using light irradiation, has been reported in the literature (Figure 3a).[29,36–37] Hecht and co-workers synthesized a foldamer **26**, in which azobenzene units are introduced into the main chain of an oligo-*m*-phenyleneethynylene, and succeeded in conformational switching between a helical conformation and a random coil through isomerization of the photoresponsive azobenzene moieties upon irradiation of light (Figure 3b).[36] Flood and co-workers prepared an

aryl-triazole based foldamer (**27**) carrying photoresponsive azobenzene residues at the both ends of the foldamer backbone. Since the helical conformation of **27** is stabilized by internal π-π interactions at the terminal azobenzene moiety, it is possible to switch between the helix and random coil structures via photoisomerization. In addition, they succeeded in controlling the binding and release of guest anions utilizing the conformational switching of **27** (Figure 3b).[29]

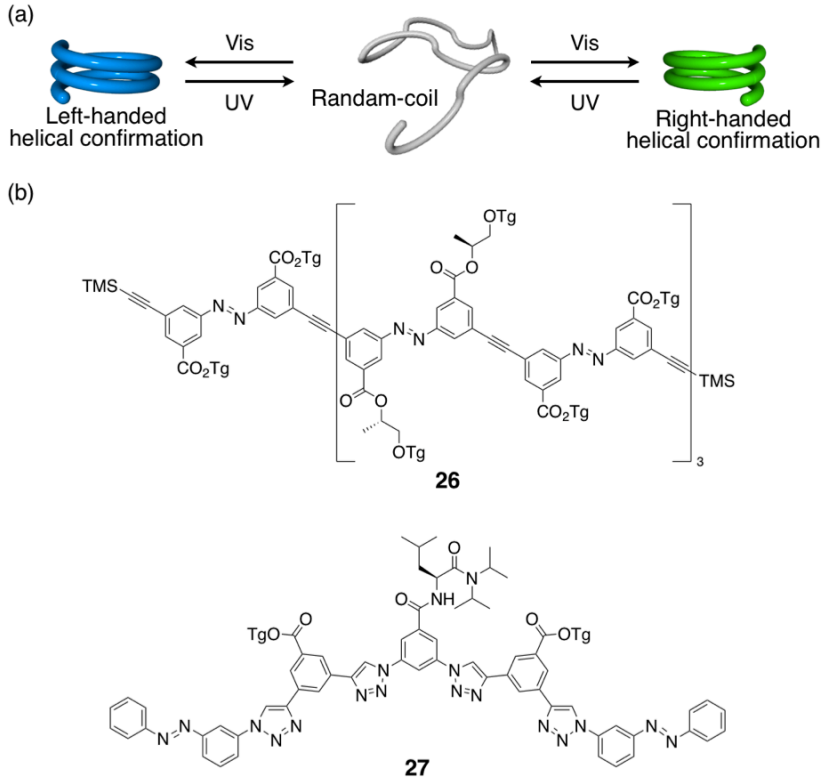

Figure 3. (a) Schematic representation of the structural switching of a foldamer induced upon irradiation of light. (b) Structures of photoresponsive foldamers.

As a method for controlling the excess one-handed helical conformation of covalent polymers and supramolecular polymers, not only the use of nonracemic guest molecules, but also the copolymerization of chiral and achiral monomers (the sergeants-and-soldiers effect) has been reported. The transfer of chiral information from a small amount of nonracemic "sergeant" molecules or monomer units to the achiral "soldier" molecules or monomer units

accompanied by significant amplification of the helix-sense excess plays an important role in inducing an excess one-handed helical structure.

Since the first example of such a chiral amplification (the sergeants-and-soldiers effect) was discovered in rigid-rod helical polyisocyanates, such as **28** by Green and co-workers,[10a] various helical polymers, such as polysilane (**29**),[38] polyisocyanide (**30**),[39] polyacetylenes (**31**–**33**),[40] and poly(quinoxaline-2,3-diyl) (**34**),[41] have been reported to show similar sergeants-and-soldiers effects (Figure 4).

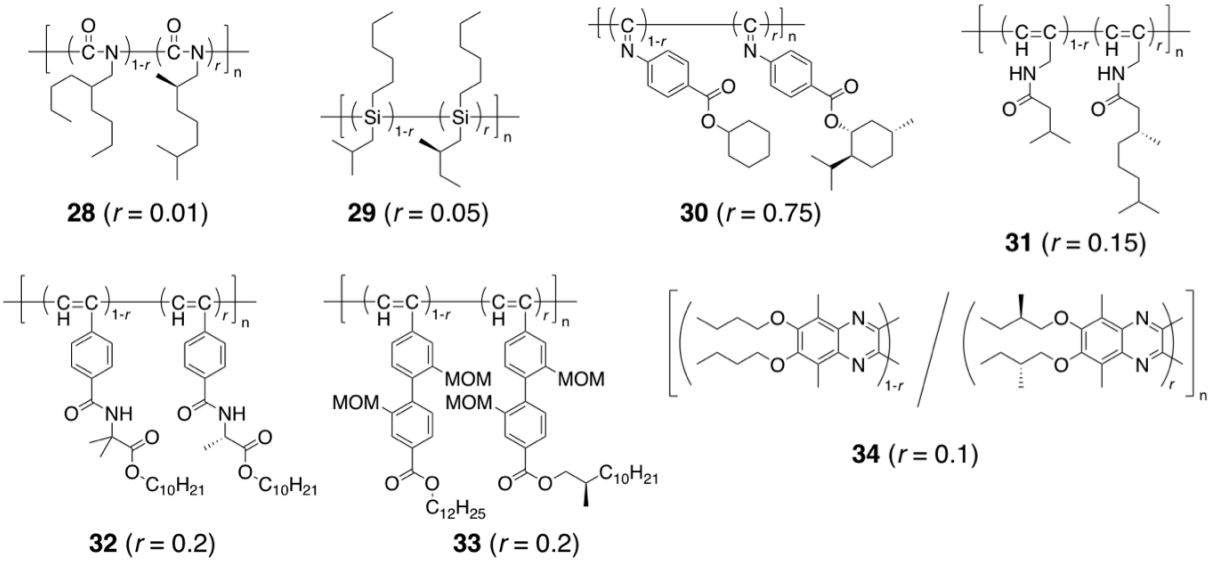

Figure 4. Structures of typical helical copolymers showing the sergeants-and-soldiers effect. The molar fraction (*r*) of chiral units shown in the parentheses denotes that the copolymers composed of chiral units (*r*) almost adopt a one-handed helical structure.

On the other hand, the sergeants-and-soldiers effect in supramolecular helical copolymers (**35a**/**b**) were, for the first time, reported by Meijer and co-workers in 1997.[42] Since then, various supramolecular helical copolymers consisting of chiral and achiral benzene-1,3,5-tricarboxamide (BTA) derivatives (**35c**/**d**, **35e**/**h**, **35f**/**h**, **35g**/**h**, and **35i**/**j**)[43] and oligo(phenyleneethynylene) (OPE)-based trisamide derivatives (**36a**/**c**, **36b**/**c**, **36d**/**f**, and **36e**/**f**),[44] have been reported to show the sergeants-and-soldiers-type chiral amplification (Figure 5).[3c,e,f]

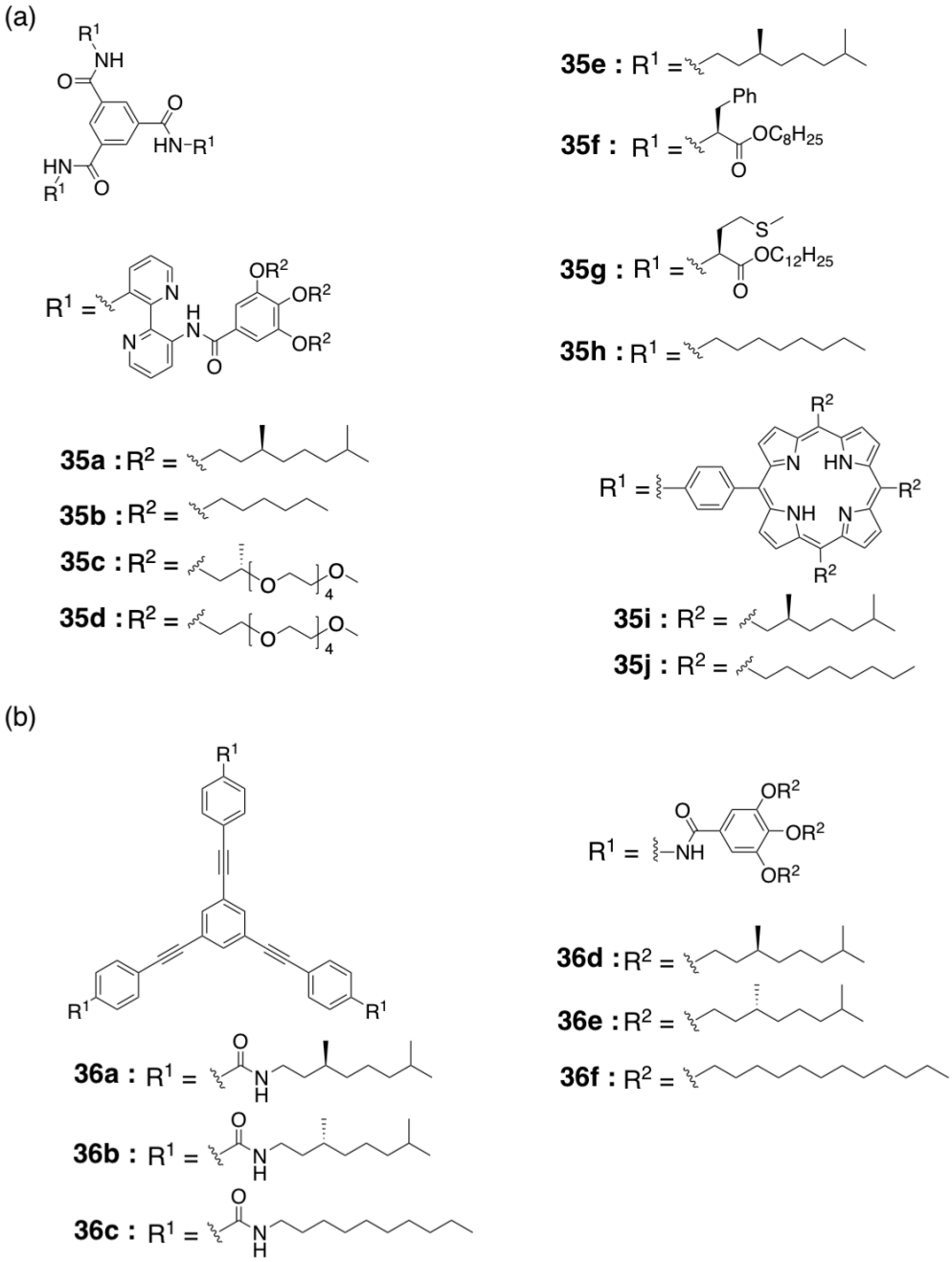

Figure 5. Structures of chiral and achiral benzene 1,3,5-tricarboxamide (BTA) derivatives (a) and oligo(phenyleneethynylene) (OPE)-based trisamides (b).

The sergeants-and-soldiers effect has also been reported to be operative in helical foldamers (Figure 6). Moore, Meijer, and co-workers prepared an excess one-handed helical oligo-*m*-phenyleneethynylene (**37**) bearing optically active pendants as the "sergeant" and found that the sergeants-and-soldiers-type amplification of chirality takes place during the

supramolecular co-assembly of **37** with a dynamically racemic foldamer (**12b**) used as a soldier.[24] The chiral/achiral foldamers **38** also showed a typical sergeants-and-soldiers effect.[25] Jiang and co-workers introduced an optically active side chain into the terminal unit of oligo(*m*-phenylene-1,2,3-triazole) (**39a**), which induced an excess one-handed helix in **39a**. Mixing chiral (**39a**) and achiral (**39b**) foldamers in a water/MeOH mixture, the co-assembled **39a** and **39b** exhibited a nonlinear effect of the circular dichroism (CD) intensity resulting from intermolecular chirality transfer from **39a** to **39b**.[30]

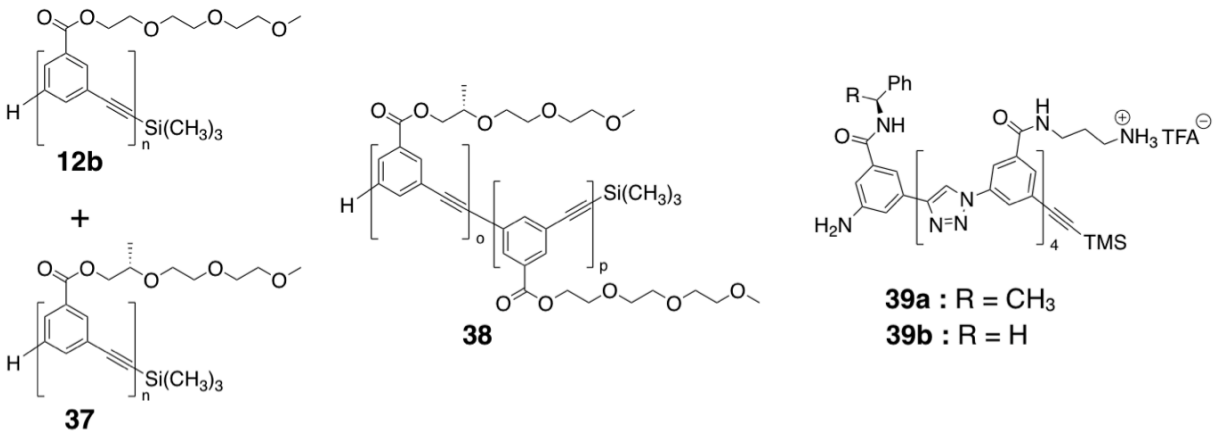

Figure 6. Structures of the helical foldamers showing the intermolecular (**12b**/**37** and **39a**/**39b**) and intramolecular (**38** and **39a**) sergeants-and-soldiers effect.

The chiral internal cavities formed by helical foldamers are expected to be applied as new chiral materials that can recognize the size, shape, and chirality of guest molecules in a selective manner (Figure 7).

Li, Wang, and co-workers prepared an aromatic oligohydrazide foldamer (**40a**) possessing optically active proline units at both ends and found that **40a** recognizes the chirality of L- and D-glucose derivatives (**19a**) in chloroform and forms an inclusion complex with a high affinity and diastereoselectivity (Figure 7a).[45] Huc and co-workers synthesized aromatic oligoamides **41a** and **41b**, whose sequences were optimized to encapsulate fructose (D-**42**) in a highly selective manner from various sugars.[19] The sequence-optimized aromatic oligoamide (**43**) forms a double helix, through which a pair of one xylose tautomer,

α-D-pyranose (D-**44**), was stereo-selectively encapsulated into the helical cavity of the double helix.[20]

Helical nanospace generated by helical foldamers has also been used for asymmetric catalysis (Figure 7b) and ion channels (Figure 7c). Ousaka, Yashima, and co-workers prepared optically active phenyleneethynylene-based foldamers (**45a** and **45b**) bearing a Mn(III)-salen linker at the center of the main chain, which catalyzed the asymmetric epoxidation of 2,2-dimethyl-2H-chromene-6-carbonitrile (**46**), producing epoxide **47** in up to 5.6% ee.[46] Hou, Li, and co-workers prepared a series of aromatic oligohydrazides (**48**) with various chain lengths and reported that these foldamers act as artificial ion channels in lipid membranes; **48a** with a shortest main chain efficiently permeates a thallium ion, while that of a longer **48c** selectively permeates an ammonium ion over a potassium ion. [47]

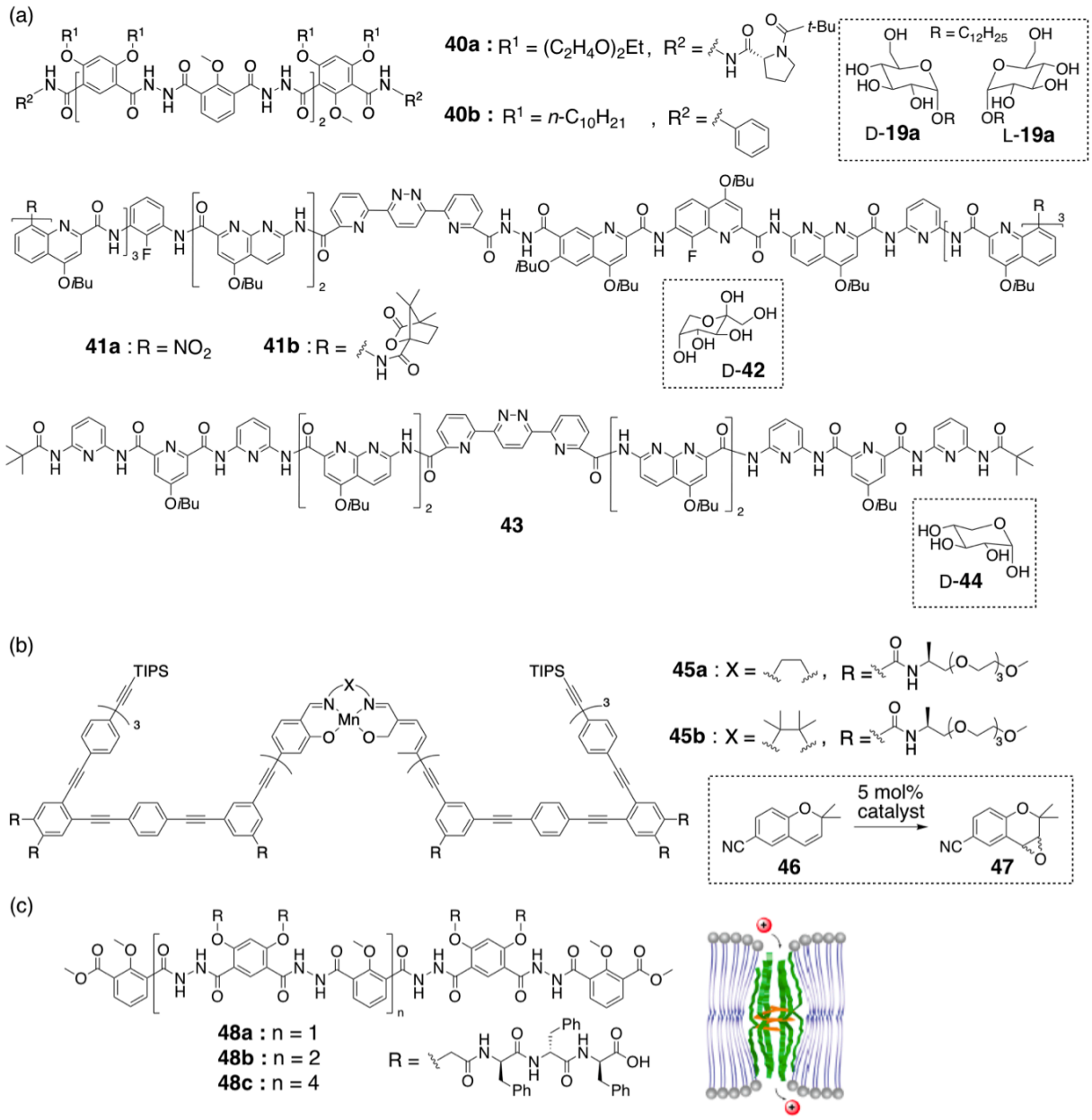

Figure 7. Structures of helical foldamers showing functions, such as chiral/molecular recognition (a), asymmetric catalysis (b), and artificial ion channel (c).

Most of the helical foldamers reported to date are oligomers and the size of the inner cavity is limited. Therefore, helical foldamers with a continuous long hollow interior are highly demanded. Li and co-workers demonstrated that the preferred-handed helical foldamer (**40b**) induced by encapsulation of an optically active glucose derivative (**19c**) (Figure 2b,7a), forms a columnar structure driven by intermolecular hydrogen bonding and π–π interactions.[48] Zeng

and co-workers found that foldamers (**49a,b** and **50**–**52**) can serve as artificial channels toward various ions, water, and solvents in a selective manner via stacking in the lipid membrane (Figure 8a).[49]

Liu and co-workers prepared a helical foldamer (**53**) consisting of phenanthroline and triazole units, thus forming an artificial channel via π-π stacking interactions. Interestingly, they also succeeded in controlling the ON/OFF switching of the channel performance utilizing the conformational change of **53** between a single helix with a large helical cavity and a double helix with an insufficient inner cavity in the absence and presence of copper ions, respectively (Figure 8b).[50]

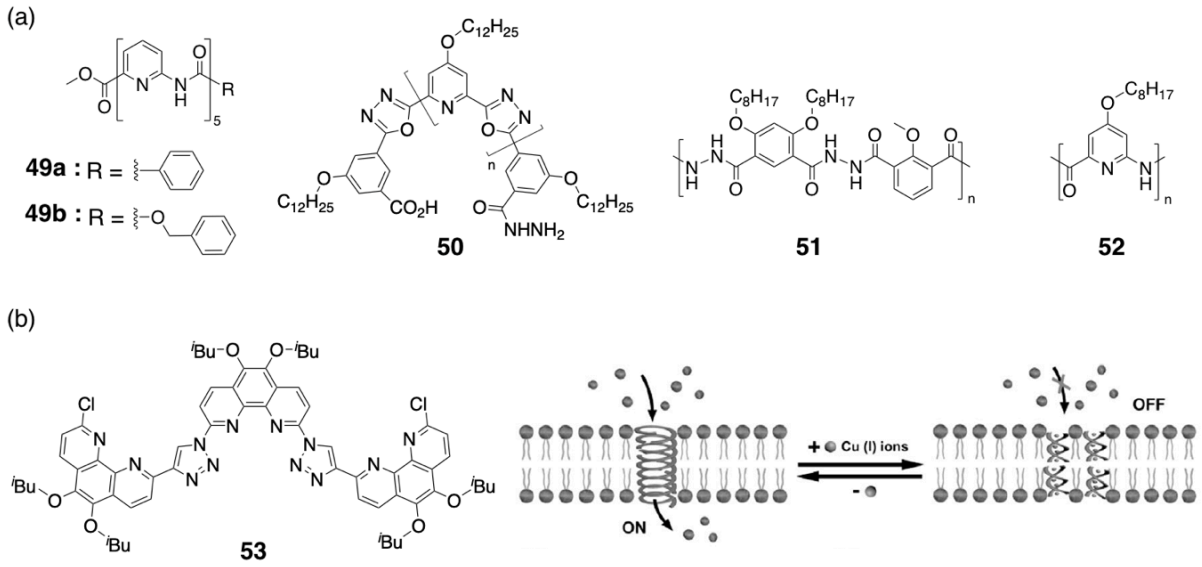

Figure 8. Structures of helical foldamers that serve as an artificial ion channel via π-π stacking interactions in the lipid membrane.

Polysaccharides, such as left-handed helical amylose,[51] and right-handed triple-stranded helical schizophyllan and curdlan,[52] are known to form inclusion complexes with a variety of molecules within a hydrophobic cavity of polysaccharides.[53] The typical small organic and inorganic molecules, oligomers, and polymers encapsulated in the polysaccharides are summarized in Figure 9.[54] Amylose, schizophyllan, and curdlan have been reported to induce a preferred-handed helical structure in oligosilanes when encapsulated in their hydrophobic helical inner cavities.[55] α-Sexithiophene also forms an excess-handed twisted conformation upon encapsulation with a partially carboxymethylated amylose and schizophyllan. The CD spectra induced in α-sexithiophene are mirror images to each other resulting from the opposite-handed helical structures of the amylose and schizophyllan.[56]

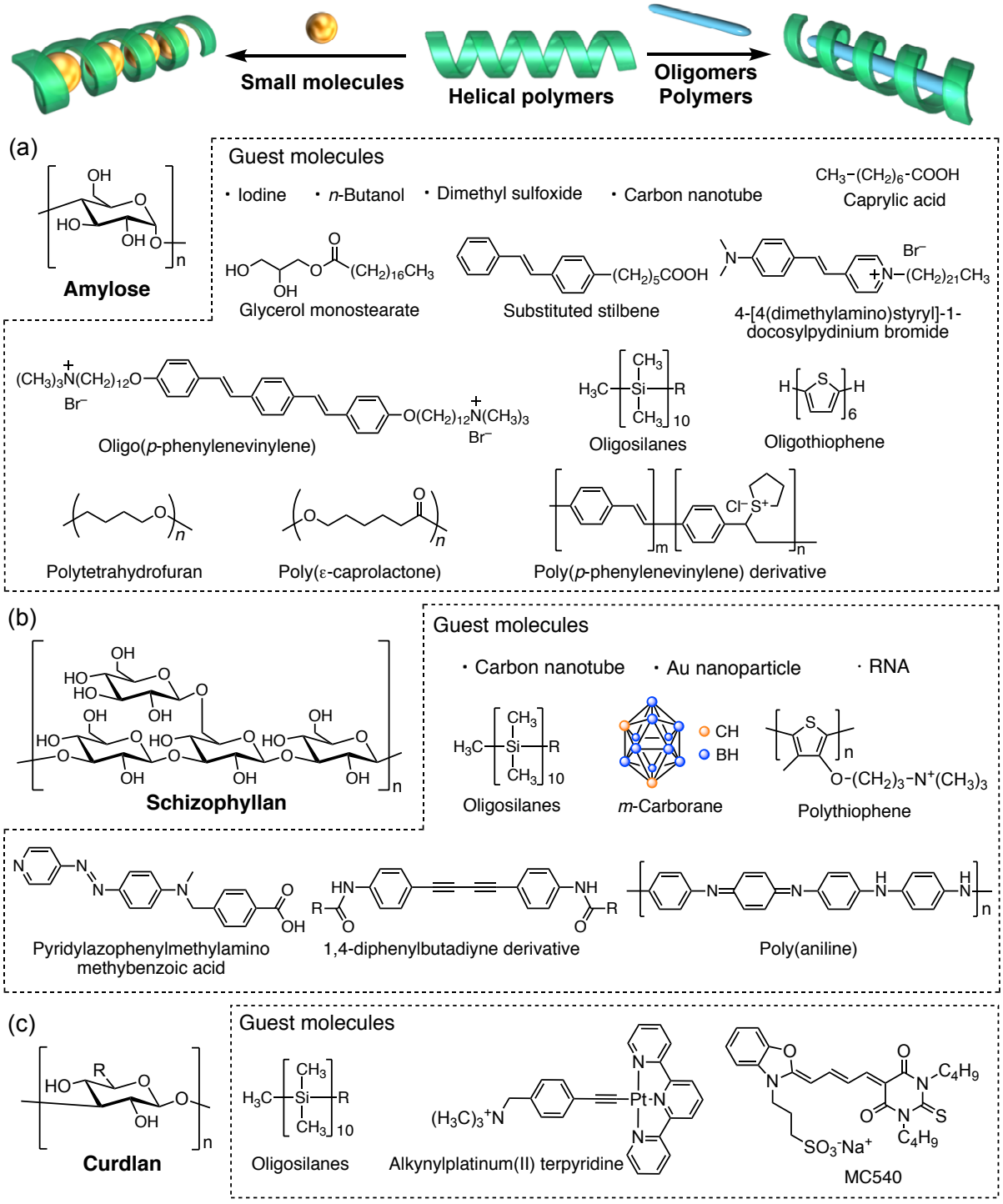

Figure 9. Schematic representation of helical polymers showing inclusion complex formation with small molecules and oligomers. Structures of small molecules and oligomers included in amylose (a), schizophyllan (b), and curdlan (c).

On the other hand, stereoregular syndiotactic poly(methyl methacrylate) (st-PMMA), a typical commodity plastic, has been reported to form a helical conformation with a large inner cavity of ca. 1 nm in aromatic solvents, such as toluene, upon heating followed by cooling, resulting in gelation accompanied by incorporation of solvent molecules into its helical cavity (Figure 10a).[57]

Kawauchi, Kumaki, Yashima, and co-workers reported that double-stranded helical isotactic (it)-PMMAs (Figure 10b)[58] and fullerenes of various sizes, such as C_{60}, C_{70}, and further higher fullerenes (Figure 10c),[59,60] can be included into the cavity of helical st-PMMA to produce crystalline stereocomplex and peapod-like inclusion complexes, respectively. Kawauchi et al. further found that polycyclic aromatic hydrocarbons, such as pyrene and phenanthrene (Figure 10d)[61] as well as C_{60}-end-capped poly(dimethylsiloxane) (**54**) (Figure 10e)[62] were also encapsulated within the helical cavity of st-PMMA to form crystalline inclusion complexes.

Taking advantage of the induced-fit mechanism observed during the inclusion complex formations between st-PMMA and higher fullerenes, Kawauchi, Yashima, and co-workers revealed that the gelation of st-PMMA in toluene containing a 1:1 mixture of C_{60} and C_{70} led to the encapsulation of fullerenes with significantly high size-selectivity toward C_{70} (99.8%) (Figure 10f).[59]

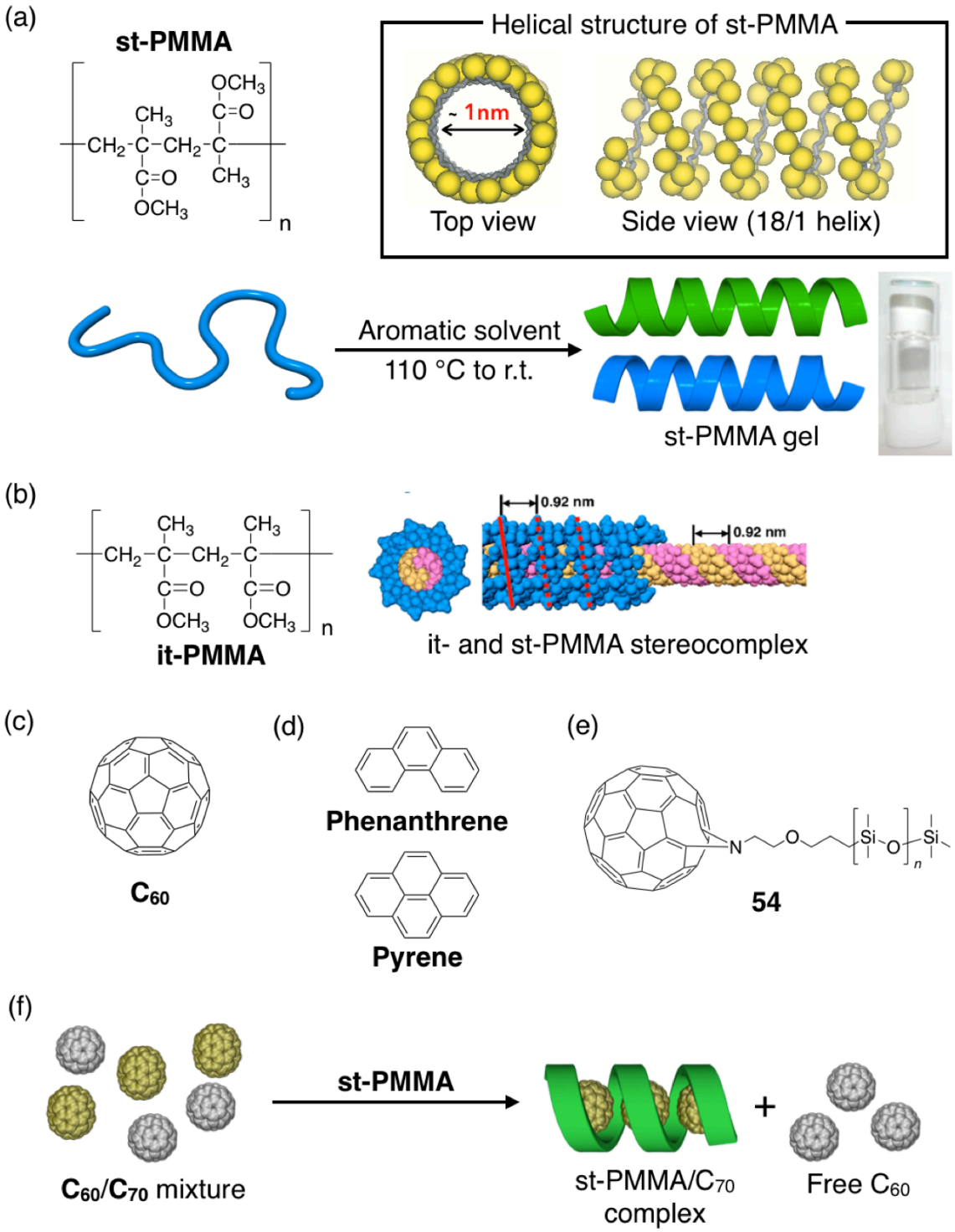

Figure 10. (a) Helical structure of st-PMMA and its helix formation in aromatic solvents accompanied by gelation. (b–e) Helical structure of it- and st-PMMA stereocomplex (b) and structures of C_{60} (c), phenanthrene and pyrene (d), and **54** (e). (f) Schematic representation of the size-selective extraction of C_{70} over C_{60} using helical st-PMMA.

An excess one-handed helical st-PMMA can be biased using enantiopure or nonracemic amines and alcohols (**55**–**60**) as solvents or additives during the gelation process. Interestingly, the induced st-PMMA helix with a preferred-handed helical conformation is retained (memorized) even after complete removal of the chiral molecules (Figure 11a).[59,63]

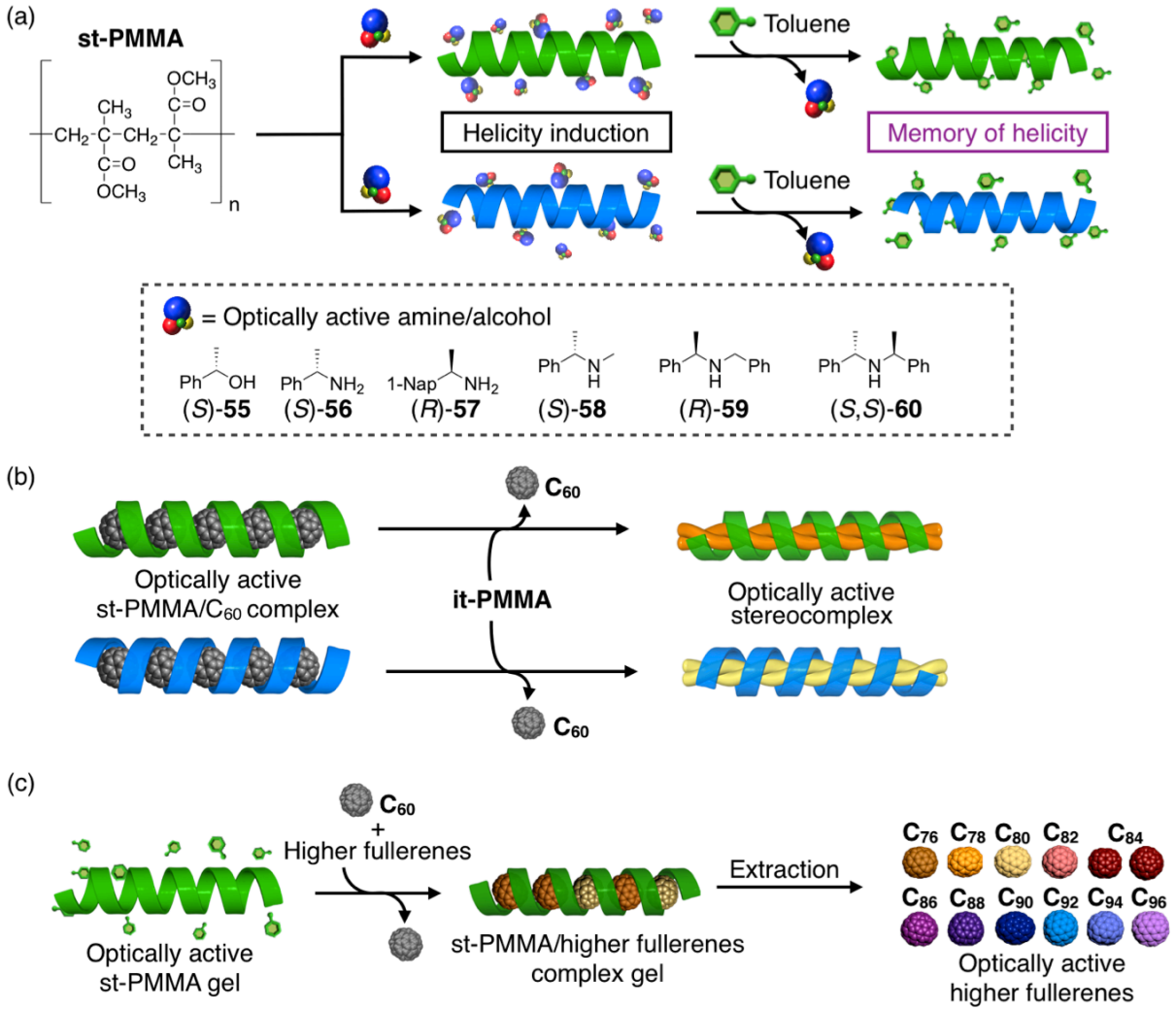

Figure 11. Schematic representations of the excess one-handed helicity induction in st-PMMA followed by memory of the induced helicity (a), optically active stereocomplex formation with it-PMMA (b), and size- and enantio-selective extraction of chiral higher fullerenes using optically active helical st-PMMA with a helicity memory (c).

The optically active st-PMMA with helicity memory complexed with C_{60} has been used as a template for producing the first optically active crystalline stereocomplex in a helix-sense-selective way by mixing with its complementary it-PMMA in a 2:1 molar ratio, through which the C_{60} molecules encapsulated in the helical cavity of st-PMMA helical cavity are released (Figure 11b).[64] It has also been reported that the optically active helicity-memorized st-PMMA can recognize the chirality of higher fullerenes and a series of higher fullerenes with optical activity are size- and enantio-selectively extracted from carbon soot (Figure 11c).[59]

Recently, Ousaka, Mamiya, Yashima, and co-workers have discovered that *P*- and *M*-handed 10_3-helical oligopeptides (L- and D- **62**, respectively) can also be efficiently entrapped in the st-PMMA helical cavity once a C_{60} unit is incorporated at one end of the peptides, thereby forming a unique crystalline "helix-in-helix" superstructure, through which the same-handed helical conformation as that of the encapsulated peptide is induced in the st-PMMA (Figure 12a,b).[65] Importantly, the st-PMMA cannot form such a "helix-in-helix" inclusion complex with the C_{60}-free L- and D- **61**. This result implies that various organic molecules and polymers would be encapsulated into the helical cavity of st-PMMA when a C_{60} derivative is attached at one end of their terminals because the C_{60} moiety may act as a molecular carrier or transporter even if the molecules and polymers themself hardly form such an inclusion complex with the st-PMMA. In fact, Mamiya further reported preliminary results of a similar "helix-in-helix" superstructure formation of C_{60}-bound *M*- and *P*-handed 10_3-helical polylactic acids (PLAs) (L- and D-**63**, respectively) with st-PMMA (Figure 12a,b) as well as an enantioselective inclusion complex formation of C_{60}-bound helical peptides (L- and D- **62**) and PLAs (L- and D-**63**) within a helical cavity of the st-PMMA with an excess handed helicity memory (Figure 12c).[66]

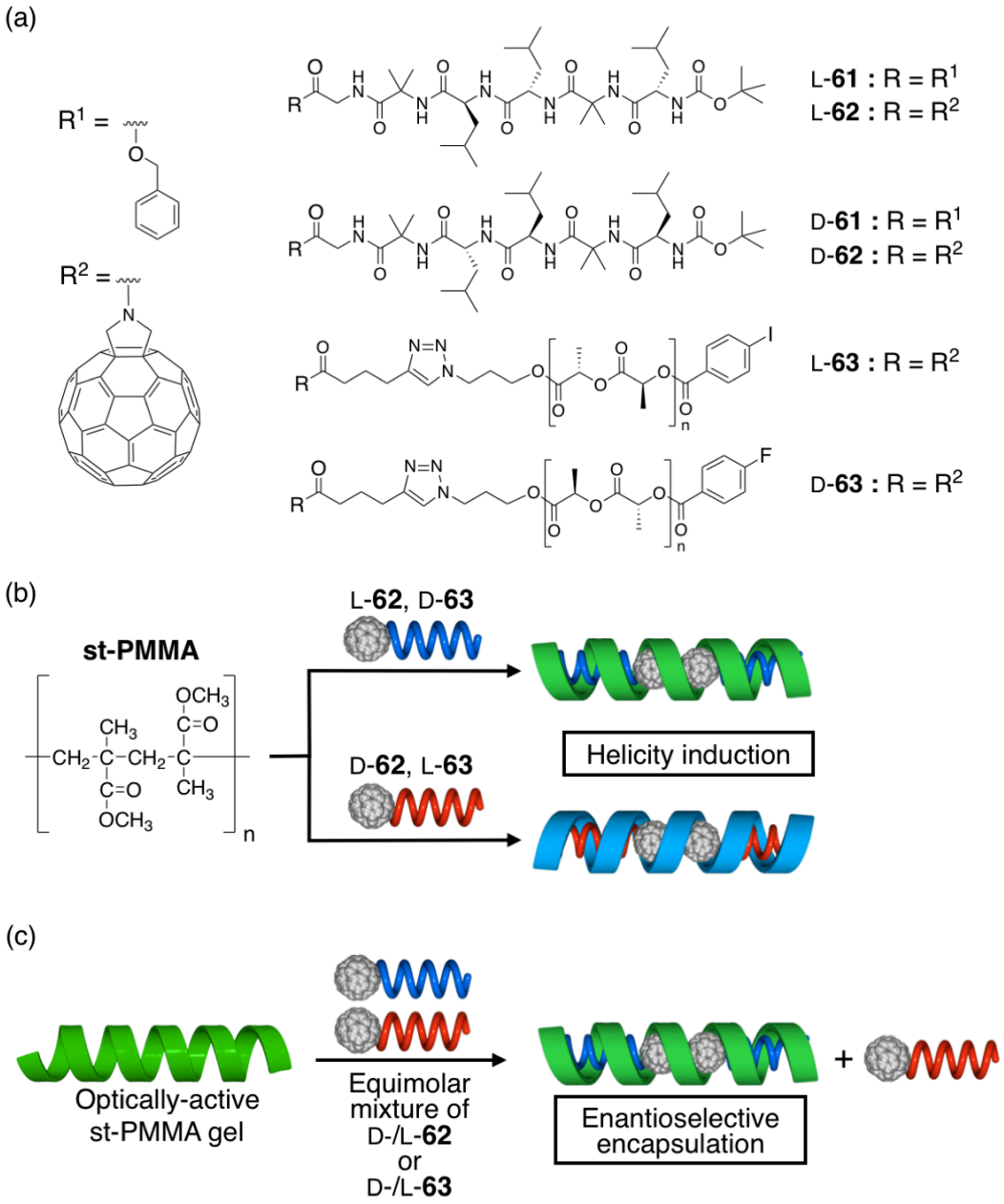

Figure 12. (a) Structures of the C_{60}-free (L-**61** and D-**61**) and C_{60}-bound (L-**62** and D-**62**) one-handed 10_3-helical peptides and C_{60}-bound one-handed 10_3-helical PLAs (L-**63** and D-**63**). (b) Schematic representations of the "helix-in-helix" superstructured inclusion complex formations of st-PMMA with C_{60}-bound *P*-handed L-**62** and D-**63** (top) and *M*-handed helical D-**62** and L-**63** (bottom) accompanied by induction of the same-handedness in st-PMMA. (c) Schematic representations of enantio- and helix-sense-selective inclusion complex formation of C_{60}-bound L-/D-**62** and L-/D-**63** in the helical cavity of st-PMMA with an excess handed helicity memory.

Based on this information, the author studied the following three areas concerning the helical tubular assemblies of foldamers and helix-in-helix inclusion complex formation of st-PMMA with C_{60}-bound and C_{60}-free *P*- and *M*-helical PLAs.

(1) Allosteric Regulation of Metal-Binding Sites Inside an Optically-Active Helical Foldamer and Its Tubular Assemblies

(2) Chiral Amplification of Supramolecular Co-Assemblies of Chiral and Achiral Acylhydrazine-Functionalized Biphenyls and Their Copolymers

(3) Helix-Sense-Selective Encapsulation of Helical Poly(lactic acid)s within a Helical Cavity of Syndiotactic Poly(methyl methacrylate) with Helicity Memory

These studies will be described in the following three chapters.

In chapter 1, the author describes the supramolecular helical assemblies of an enantiopure acylhydrazine-bound biphenyl derivative carrying L-alanine-derived oligoamide side chains (**64**) driven by intermolecular hydrogen bonding interactions. A helical folded polymer (foldamer) (poly-**64**) is also prepared by a polycondensation reaction of **64** with 2,6-pyridinedicarboxaldehyde (**65**), which further supramolecularly polymerizes through intermolecular hydrogen bonding, resulting in the formation of a helically twisted nanofiber. The nanofiber reversibly undergoes a unique helix-to-helix transition in a positive allosteric manner regulated by cooperative binding and release of Ag(I) ions to the metal-binding 2,6-pyridinebis(acylhydrazone) linker units located inside of the helical cavity of poly-**64**, through which the structure of the linkages changes from a W-shaped form to a U-shaped form (Chart 1).

Chart 1

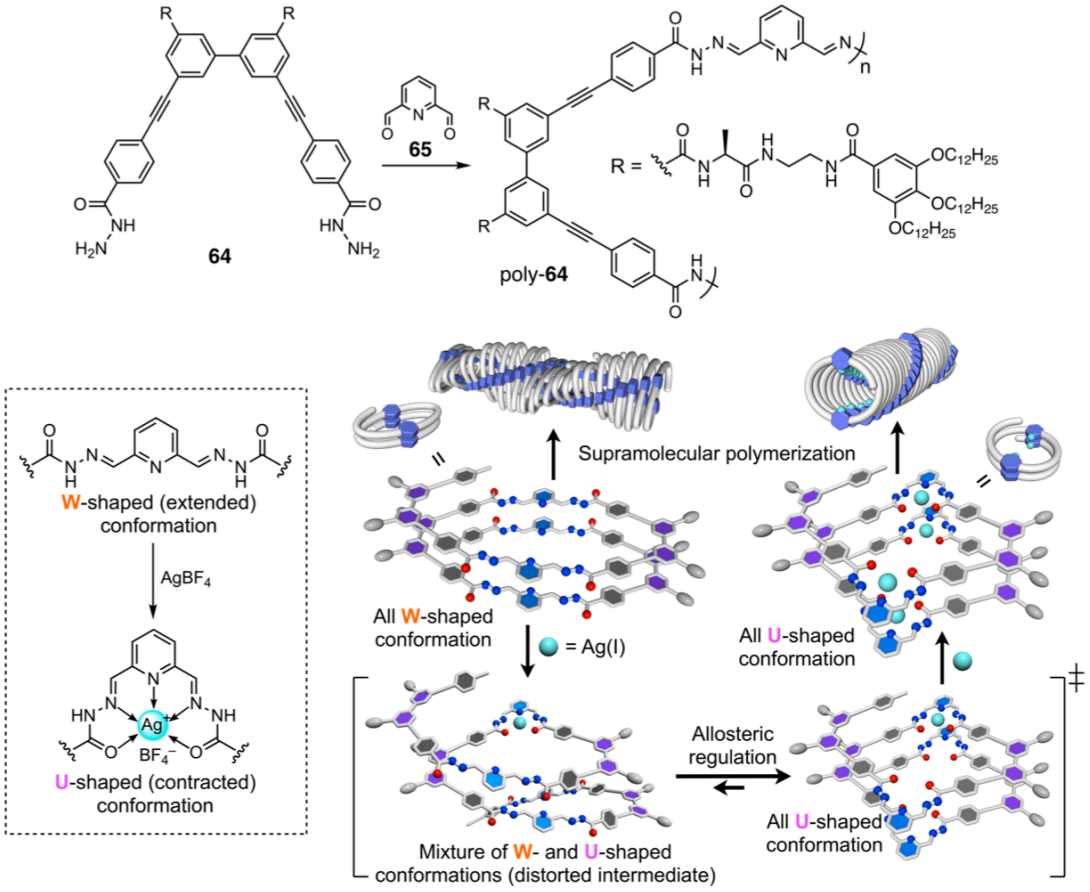

Chapter 2 deals with the sergeants-and-soldiers-type chiral amplification during the supramolecular co-assemblies of optically active (**64**) and achiral (**66**) acylhydrazine-functionalized biphenyl derivatives and their copolymers (poly(**64**$_r$-*co*-**66**$_{1-r}$)) with 2,6-pyridinedicarboxaldehyde (**65**) (Chart 2). A mixture of **64** and **66** at different molar ratios exhibits a modest chiral amplification as supported by their CD and absorption spectral changes driven by intermolecular hydrogen-bonding between the chiral and achiral pendant groups of **64** and **66**, respectively, resulting in the formation of a one-dimensional helical nanofiber. The copolymers of **64** and **66** at different molar ratios (poly(**64**$_r$-*co*-**66**$_{1-r}$)) also show amplification of the helical sense excess through the intramolecular hydrogen bonds followed by helical assembly of the copolymers via intermolecular hydrogen bonding network formation. In contrast, no chiral amplification of the helical sense excess takes place for the mixtures of the homopolymers of poly-**64** and poly-**66**.

Chart 2

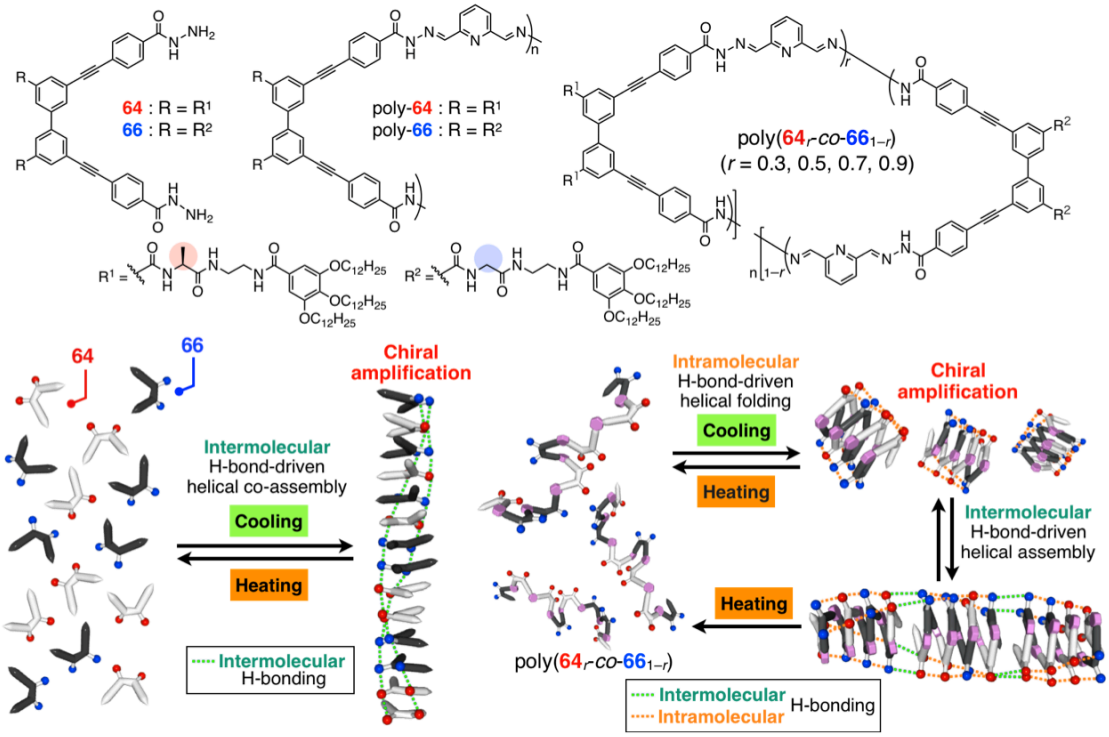

In chapter 3, the author describes his discovery that the C_{60}-free *M*- and *P*-helical PLAs (***M*-L$_{N3}$-67-I** and ***P*-D$_{N3}$-67-F**) (Chart 3) prepared as precursors for the C_{60}-bound *M*- and *P*-helical PLAs (***M*-L$_{C60}$-63-I** and ***P*-D$_{C60}$-63-F**) bearing the different terminal benzoate groups (4-iodo (**I**)- and 4-fluorobenzoyl (**F**) groups, respectively)[66] are also encapsulated in the helical nanotube of st-PMMA, thus forming a crystalline "helix-in-helix" superstructure as observed for the C_{60}-bound PLAs. Based on this serendipitous discovery, the author has thoroughly investigated the effect of the terminal C_{60} moiety of the PLAs along with the molar mass effect on the enantio- and helix-sense-selective inclusion complex formation within the helical cavity of st-PMMA with an excess one-handed helicity memory generated by optically active amines ((*S*)- and (*R*)-**56**). The excess one-handed helix induction capabilities of the C_{60}-free and C_{60}-bound *M*- and *P*-helical PLAs to the as-prepared optically inactive st-PMMA are also investigated. The results provide a versatile method to separate racemic helical PLAs into the *M*- and *P*-helices of PLAs through the helix-sense-selective

encapsulation with a helical st-PMMA with a helicity memory. It has been reported that cyclodextrins[67] and amylose[68,69] recognized the helicity of PLAs, but these chiral hosts cannot be used to separate the helical PLAs into the *M*- and *P*-helices and the mechanism for the helix-sense-selective complex formation at a molecular level remains unclear. The helical *M*- and *P*-st-PMMAs induced by *M*- and *P*-PLAs, respectively, during the "helix-in-helix" superstructure formation are found to be retained after complete replacement of the *M*- and *P*-PLAs with achiral C_{60}, thereby producing the helicity memorized st-PMMAs while retaining its optical activity; the results are also described in this chapter.

Chart 3

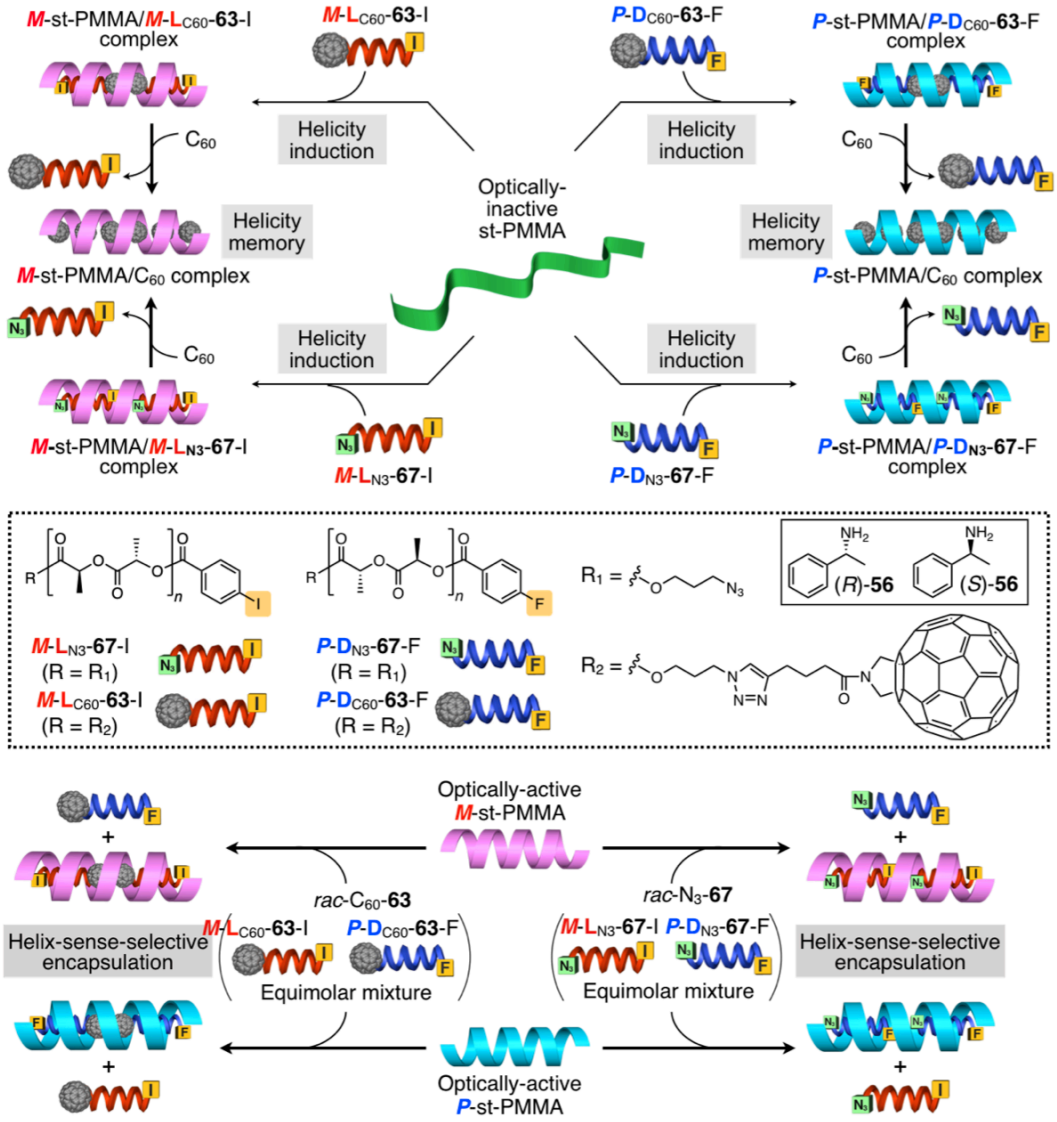
M-st-PMMA/M-LC60-63-I complex
M-LC60-63-I
P-DC60-63-F
P-st-PMMA/P-DC60-63-F complex
Helicity induction
Helicity induction
C60
C60
Optically-inactive st-PMMA
Helicity memory
Helicity memory
M-st-PMMA/C60 complex
P-st-PMMA/C60 complex
C60
C60
Helicity induction
Helicity induction
M-st-PMMA/M-LN3-67-I complex
M-LN3-67-I
P-DN3-67-F
P-st-PMMA/P-DN3-67-F complex
R1 =
(R)-56
(S)-56
M-LN3-67-I (R = R1)
M-LC60-63-I (R = R2)
P-DN3-67-F (R = R1)
P-DC60-63-F (R = R2)
R2 =
Optically-active M-st-PMMA
rac-C60-63
rac-N3-67
Helix-sense-selective encapsulation
M-LC60-63-I P-DC60-63-F
Equimolar mixture
M-LN3-67-I P-DN3-67-F
Equimolar mixture
Helix-sense-selective encapsulation
Optically-active P-st-PMMA

References

(1) (a) Pauling, L.; Corey, R. B.; Branson, H. R. *Proc. Natl. Acad. Sci. U. S. A.* **1951**, *37*, 205−211. (b) Monod, J.; Wyman, J.; Changeux, J.-P. *J. Mol. Biol.* **1965**, *12*, 88–118. (c) Klug, A. *Angew. Chem., Int. Ed. Engl.* **1983**, *22*, 565–582. (d) Egan, P.; Sinko, R.; LeDuc, P. R.; Keten, S. *Nat. Commun.* **2015**, *6*, 7418. (e) Luo, Q.; Hou, C.; Bai, Y.; Wang, R.; Liu, J. *Chem. Rev.* **2016**, *116*, 13571–13632. (f) Pieters, B. J. G. E.; van Eldijk, M. B.; Nolte, R. J. M.; Mecinović, J. *Chem. Soc. Rev.* **2016**, *45*, 24–39.

(2) (a) Okamoto, Y.; Nakano, T. *Chem. Rev.* **1994**, *94*, 349–372. (b) Nakano, T.; Okamoto, Y. *Chem. Rev.* **2001**, *101*, 4013–4038. (c) Cornelissen, J. J. L. M.; Rowan, A. E.; Nolte, R. J. M.; Sommerdijk, N. A. J. M. *Chem. Rev.* **2001**, *101*, 4039–4070. (d) Yashima, E.; Maeda, K.; Iida, H.; Furusho, Y.; Nagai, K. *Chem. Rev.* **2009**, *109*, 6102–6211.

(3) (a) Estroff, L. A.; Hamilton, A. D. *Chem. Rev.* **2004**, *104*, 1201–1218. (b) Shimizu, T.; Masuda, M.; Minamikawa, H. *Chem. Rev.* **2005**, *105*, 1401–1444. (c) De Greef, T. F. A.; Smulders, M. M. J.; Wolffs, M.; Schenning, A. P. H. J.; Sijbesma, R. P.; Meijer, E. W. *Chem. Rev.* **2009**, *109*, 5687–5754. (d) Babu, S. S.; Praveen, V. K.; Ajayaghosh, A. *Chem. Rev.* **2014**, *114*, 1973–2129. (e) Liu, M.; Zhang, L.; Wang, T. *Chem. Rev.* **2015**, *115*, 7304–7397. (f) Yashima, E.; Ousaka, N.; Taura, D.; Shimomura, K.; Ikai, T.; Maeda, K. *Chem. Rev.* **2016**, *116*, 13752–13990.

(4) Nolte, R. J. M.; Van Beijnen, A. J. M.; Drenth, W. *J. Am. Chem. Soc.* **1974**, *96*, 5932–5933.

(5) Okamoto, Y.; Suzuki, K.; Ohta, K.; Hatada, K.; Yuki, H. *J. Am. Chem. Soc.* **1979**, *101*, 4763–4765.

(6) Green, M. M.; Andreola, C.; Muñoz, B.; Reidy, M. P.; Zero, K. *J. Am. Chem. Soc.* **1988**, *110*, 4063–4065.

(7) (a) Corley, L. S.; Vogl, O. *Polym. Bull.* **1980**, *3*, 211–217. (b) Vogl, O.; Jaycox, G. D.; Kratky, C.; Simonsick, W. J. Jr.; Hatada, K. *Acc. Chem. Res.* **1992**, *25*, 408–413. (c) Ute, K.; Hirose, K.; Kashimoto, H.; Nakayama, H.; Hatada, K.; Vogl, O. *Polym. J.* **1993**, *25*, 1175–1186.

(8) Suginome, M.; Ito, Y. *Adv. Polym. Sci*. **2004**, *171*, 77–136.

(9) Tang, H.-Z.; Boyle, P. D.; Novak, B. M. *J. Am. Chem. Soc*. **2005**, *127*, 2136–2142.

(10) (a) Green, M. M.; Reidy, M. P.; Johnson, R. D.; Darling, G.; O'Leary, D. J.; Willson, G. *J. Am. Chem. Soc.* **1989**, *111*, 6452−6454. (b) Green, M. M.; Park, J.-W.; Sato, T.; Teramoto, A.; Lifson, S.; Selinger, R. L. B.; Selinger, V. S. *Angew. Chem., Int. Ed*. **1999**, *38*, 3138–3154.

(11) Fujiki, M. *J. Am. Chem. Soc.* **1994**, *116*, 6017−6018.

(12) (a) Ciardelli, F.; Benedetti, E.; Pieroni, O. *Makromol. Chem*. **1967**, *103*, 1–18. (b) Ciardelli, F.; Lanzillo, S.; Pieroni, O. *Macromolecules* **1974**, *7*, 174–179. (c) Aoki, T.; Kokai, M.; Shinohara, K.; Oikawa, E. *Chem. Lett.* **1993**, *22*, 2009–2012. (d) Yashima, E.; Huang, S.; Matsushima, T.; Okamoto, Y. *Macromolecules* **1995**, *28*, 4184–4193. (e) Nomura, R.; Nakako, H.; Masuda, T. *J. Mol. Catal. A: Chem.* **2002**, *190*, 197–205. (f) Nomura, R.; Tabei, J.; Nishiura, S.; Masuda, T. *Macromolecules* **2003**, *36*, 561–564. (g) Zhao, H.; Sanda, F.; Masuda, T. *J. Polym. Sci., Part A: Polym. Chem.* **2005**, *43*, 5168–5176.

(13) (a) Yashima, E.; Maeda, K. *Macromolecules* **2008**, *41*, 3–12. (b) Yashima, E.; Maeda, K.; Furusho, Y. *Acc. Chem. Res.* **2008**, *41*, 1166–1180. (c) Maeda, K.; Yashima, E. *Top. Curr. Chem*. **2017**, *375*, 72.

(14) (a) Hecht, S.; Huc, I. *Foldamers: Structure, Properties, and Applications*, Wiley-VCH, Weinheim, **2007**. (b) Juwaker, H.; Suk, J.-m.; Jeong, K.-S. *Chem. Soc. Rev.* **2009**, *38*, 3316–3325. (c) Zhang, D.-W.; Zhao, X.; Hou, J.-L.; Li, Z.-T. *Chem. Rev.* **2012**, *112*, 5271–5316.

(15) (a) Zhu, J.; Parra, R. D.; Zeng, H. Q.; Skrzypczak-Jankun, E.; Zeng, X. C.; Gong, B. *J. Am. Chem. Soc.* **2000**, *122*, 4219–4220. (b) Berl, V.; Krische, M. J.; Huc, I.; Lehn, J.-M.; Schmutz, M. *Chem. - Eur. J.* **2000**, *6*, 1938–1946. (c) Gong, B.; Zeng, H.; Zhu, J.; Yua, L.; Han, Y.; Cheng, S.; Furukawa, M.; Parra, R. D.; Kovalevsky, A. Y.; Mills, J. L.; Skrzypczak-Jankun, E.; Martinovic, S.; Smith, R. D.; Zheng, C.; Szyperski, T.; Zeng, X.

C. *Proc. Natl. Acad. Sci. U. S. A*. **2002**, *99*, 11583–11588. (d) Zhang, D.-W.; Zhao, X.; Hou, J.-L.; Li, Z.-T. *Chem. Rev*. **2012**, *112*, 5271–5316. (e) Zhang, D.-W.; Zhao, X.; Li, Z.-T. *ACC. Chem. Res*. **2014**, *47*, 1961–1970. (f) Zhang, D.-W.; Wang, W.-K.; Li, Z.-T. *Chem. Rec*. **2015**, *15*, 233–251.

(16) (a) Hamuro, Y.; Geib, S. J.; Hamilton, A. D. *Angew. Chem., Int. Ed.* **1994**, *33*, 446–448. (b) Hamuro, Y.; Geib, S. J.; Hamilton, A. D. *J. Am. Chem. Soc.* **1996**, *118*, 7529–7541.

(17) Berl, V.; Huc, I.; Khoury, R. G.; Krische, M. J.; Lehn, J.-M. *Nature* **2000**, *407*, 720–723.

(18) Maurizot, V.; Dolain, C.; Huc, I. *Eur. J. Org. Chem.* **2005**, *7*, 1293–1301.

(19) Chandramouli, N.; Ferrand, Y.; Lautrette, G.; Kauffmann, B.; Mackereth, C. D.; Laguerre, M.; Dubreuil, D.; Huc, I. *Nat. Chem*. **2015**, *7*, 334–341.

(20) Mateus, P.; Chandramouli, N.; Mackereth, C. D.; Kauffmann, B.; Ferrand, Y.; Huc, I. *Angew. Chem., Int. Ed.* **2020**, *59*, 5797–5805.

(21) (a) Hill, D. J.; Mio, M. J.; Prince, R. B.; Hughes, T. S.; Moore, J. S. *Chem. Rev.* **2001**, *101*, 3893–4012. (b) Toya, M.; Ito, H.; Itami, K. *Tetrahedron Lett*. **2018**, *59*, 1531–1547.

(22) Nelson, J. C.; Saven, J. G.; Moore, J. S.; Wolynes, P. G. *Science* **1997**, *277*, 1793–1796.

(23) Prince, R. B.; Barnes, S. A.; Moore, J. S. *J. Am. Chem. Soc.* **2000**, *122*, 2758–2762.

(24) Brunsveld, L.; Meijer, E. W.; Prince, R. B.; Moore, J. S. *J. Am. Chem. Soc.* **2001**, *123*, 7978–7984.

(25) Prince, R. B.; Moore, J. S.; Brunsveld, L.; Meijer, E. W. *Chem. - Eur. J.* **2001**, *7*, 4150–4154.

(26) (a) Gellman, S. H. *Acc. Chem. Res.* **1998**, *31*, 173–180. (b) Cheng, R. P.; Gellman, S. H.; DeGrado, W. F. *Chem. Rev.* **2001**, *101*, 3219–3232. (c) Ousaka, N.; Inai, Y.; Kuroda, R. *J. Am. Chem. Soc.* **2008**, *130*, 12266–12267.

(27) (a) Suk, J.-m.; Kim, D. A.; Jeong, K.-S. *Org. Lett.* **2012**, *14*, 5018–5021. (b) Jeon, H.-G.; Jung, J. Y.; Kang, P.; Choi, M.-G.; Jeong, K.-S. *J. Am. Chem. Soc.* **2016**, *138*, 92−95. (c) Kim, J. S.; Jeon, H.-G.; Jeong, K.-S. *Chem. Commun.* **2016**, *52*, 3406–3409. (d) Jeon, H.-G.; Lee, H. K.; Lee, S.; Jeong, K.-S. *Chem. Commun.* **2018**, *54*, 5740–5743. (e) Lee,

C.; Lee, H.; Lee, S.; Jeon, H.-G.; Jeong, K.-S. *Org. Chem. Front.* **2019**, *6*, 299–303. (f) Seo, S. B.; Lee, S.; Jeon, H.-G.; Jeong, K.-S. *Angew. Chem., Int. Ed.* **2020**, *59*, 10441–10445.

(28) (a) Pfukwa, R.; Kouwer, P. H. J.; Rowan, A. E.; Klumperman, B. *Angew. Chem., Int. Ed.* **2013**, *52*, 11040–11044. (b) Hua, Y. R.; Liu, Y.; Chen, C.-H.; Flood, A. H. *J. Am. Chem. Soc.* **2013**, *135*, 14401−14412.

(29) Parks, F. C.; Liu, Y.; Debnath, D.; Stutsman, S. R.; Raghavachari, K.; Flood, A. H. *J. Am. Chem. Soc.* **2018**, *140*, 17711−17723.

(30) Wang, Y.; Li, F.; Han, Y.; Wang, F.; Jiang, H. *Chem. - Eur. J.* **2009**, *15*, 9424–9433.

(31) (a) Hanan, G. S.; Lehn, J.-M.; Kyritsakas, N.; Fischer, J. *J. Chem. Soc., Chem. Commun.* **1995**, 765–766. (b) Ohkita, M.; Lehn, J.-M.; Baum, G.; Fenske, D. *Chem. - Eur. J.* **1999**, *5*, 3471–3481.

(32) Hou, J.-L.; Shao, X.-B.; Chen, G.-J.; Zhou, Y.-X.; Jiang, X.-K.; Li, Z.-T. *J. Am. Chem. Soc.* **2004**, *126*, 12386–12394.

(33) (a) Inouye, M.; Waki, M.; Abe, H. *J. Am. Chem. Soc.* **2004**, *126*, 2022–2027. (b) Waki, M.; Abe, H.; Inouye, M. *Chem. - Eur. J.* **2006**, *12*, 7839–7847. (c) Ohishi, Y.; Abe, H.; Inouye, M. *Chem. - Eur. J.* **2015**, *21*, 16504–16511.

(34) (a) Takashima, S.; Abe, H.; Inouye, M. *Chem. Commun.* **2012**, *48*, 3330–3332. (b) Takashima, S.; Abe, H.; Inouye, M. *Tetrahedron: Asymmetry* **2013**, *24*, 527–531.

(35) (a) Knipe, P. C.; Thompson, S.; Hamilton, A. D. *Chem. Commun.* **2016**, *52*, 6521–6524. (b) Wang, W.; Zhang, C.; Qi, S.; Deng, X.; Yang, B.; Liu, J.; Dong, Z. *J. Org. Chem.* **2018**, *83*, 1898−1902.

(36) Yu, M. S. Z.; Hecht, S. *Angew. Chem., Int. Ed.* **2011**, *50*, 1640–1643.

(37) Gole, B.; Kauffmann, B.; Maurizot, V.; Huc, I.; Ferrand, Y. *Angew. Chem., Int. Ed.* **2019**, *58*, 8063–8067.

(38) Fujiki, M. *Macromol. Rapid Commun.* **2001***, 22,* 539−563.

(39) (a) Takei, F.; Onitsuka, K.; Takahashi, S. *Polym. J.* **1999**, *31*, 1029−1032. (b) Takei, F.;

Onitsuka, K.; Takahashi, S. *Polym. J.* **2000**, *32*, 524−526.

(40) (a) Nomura, R.; Tabei, J.; Masuda, T. *Macromolecules* **2002**, *35*, 2955–2961. (b) Ohsawa, S.; Sakurai, S.; Nagai, K.; Banno, M.; Maeda, K.; Kumaki, J.; Yashima, E. *J. Am. Chem. Soc.* **2011**, *133*, 108–114. (c) Ishidate, R.; Markvoort, A. J.; Maeda, K.; Yashima, E. *J. Am. Chem. Soc.* **2019**, *141*, 7605−7614.

(41) Nagata, Y.; Yamada, T.; Adachi, T.; Akai, Y.; Yamamoto, T.; Suginome, M. *J. Am. Chem. Soc.* **2013**, *135*, 10104–10113.

(42) Palmans, A. R. A.; Vekemans, J.; Havinga, E. E.; Meijer, E. W. *Angew. Chem., Int. Ed. Engl.* **1997**, *36*, 2648–2651.

(43) (a) Brunsveld, L.; Lohmeijer, B. G. G.; Vekemans, J.; Meijer, E. W. *Chem. Commun.* **2000**, 2305–2306. (b) Brunsveld, L.; Schenning, A.; Broeren, M. A. C.; Janssen, H. M.; Vekemans, J.; Meijer, E. W. *Chem. Lett.* **2000**, *29*, 292–293. (c) Smulders, M. M. J.; Schenning, A. P. H. J.; Meijer, E. W. *J. Am. Chem. Soc.* **2008**, *130*, 606–611. (d) Desmarchelier, A.; Raynal, M.; Brocorens, P.; Vanthuyne, N.; Bouteiller, L. *Chem. Commun.* **2015**, *51*, 7397–7400. (e) Veling, N.; van Hameren, R.; van Buul, A. M.; Rowan, A. E.; Nolte, R. J. M.; Elemans, J. A. A. W. *Chem. Commun.* **2012**, *48*, 4371–4373.

(44) (a) García, F.; Viruela, P. M.; Matesanz, E.; Ortí, E.; Sánchez, L. *Chem. - Eur. J.* **2011**, *17*, 7755–7759. (b) Wang, F.; Gillissen, M. A. J.; Stals, P. J. M.; Palmans, A. R. A.; Meijer, E. W. *Chem. - Eur. J.* **2012**, *18*, 11761–11770.

(45) Li, C.; Wang, G.-T.; Yi, H.-P.; Jiang, X.-K.; Li, Z.-T.; Wang, R.-X. *Org. Lett.* **2007**, *9*, 1797–1800.

(46) Ousaka, N.; Yamaguchi, T.; Yashima, E. *Chem. Lett.* **2014**, *43*, 512–514.

(47) Xin, P.; Zhu, P.; Su, P.; Hou, J.-L.; Li, Z.-T. *J. Am. Chem. Soc.* **2014**, *136*, 13078−13081.

(48) Cai, W.; Wang, G.-T.; Du, P.; Wang, R.-X.; Jiang, X.-K.; Li, Z.-T. *J. Am. Chem. Soc.* **2008**, *130*, 13450–13459.

(49) (a) Zhao, H. Q.; Sheng, S.; Hong, Y. H.; Zeng, H. Q. *J. Am. Chem. Soc.* **2014**, *136*,

14270−14276. (b) Ma, W.; Wang, C.; Li, J. Zhang, K.; Lu, Y.-J.; Huo, Y.; Zeng, H. *Org. Biomol. Chem.* **2015**, *13*, 10613–10619. (c) Shen, J.; Ye, R.; Romanies, A.; Roy, A.; Chen, F.; Ren, C.; Liu, Z.; Zeng, H. *J. Am. Chem. Soc.* **2020**, *142*, 10050−10058. (d) Chen, F.; Shen, J.; Li, N.; Roy, A.; Ye, R.; Ren, C.; Zeng, H. *Angew. Chem., Int. Ed.* **2020**, *59*, 1440–1444. (e) Roy, A.; Joshi, H.; Ye, R.; Shen, J.; Chen, F.; Aksimentiev, A.; Zeng, H. *Angew. Chem., Int. Ed*. **2020**, *59*, 4806–4813. (f) Shen, J.; Fan, J.; Ye, R.; Li, N.; Mu, Y.; Zeng, H. *Angew. Chem., Int. Ed.* **2020**, *59*, 13328–13334.

(50) Bai, D.; Yan, T.; Wang, S.; Wang, Y.; Fu, J.; Fang, X.; Zhu, J.; Liu, J. *Angew. Chem., Int. Ed.* **2020**, *59*, 13602–13607.

(51) (a) Zugenmaier, P.; Sarko, A. *Biopolymers* **1976**, *15*, 2121–2136. (b) Wu, H. H.-C.; Sarko, A. *Carbohydr. Res*. **1978**, *61*, 7–25. (c) Wu, H. H.-C.; Sarko, A. *Carbohydr. Res.* **1978**, *61*, 27–40. (d) Tester, R. F.; Karkalas, J.; Qi, X. *J. Cereal Sci.* **2004**, *39*, 151–165. (e) Takahashi, Y.; Kumano, T.; Nishikawa, S. *Macromolecules* **2004**, *37*, 6827–6832.

(52) (a) Yanaki, T.; Norisue, T.; Fujita, H. *Macromolecules* **1980**, *13*, 1462–1466. (b) Deslandes, Y.; Marchessault, R. H.; Sarko, A. *Macromolecules* **1980**, *13*, 1466–1471. (c) Tabata, K.; Ito, W.; Kojima, T. *Carbohydr. Res.* **1981**, *89*, 121–135. (d) Kashiwagi, Y.; Norisue, T.; Fujita, H. *Macromolecules* **1981**, *14*, 1220–1225. (e) Bohn, J. A.; BeMiller, J. N. *Carbohydr. Res.* **1995**, *28*, 3–14.

(53) Koumoto, K.; Kimura, T.; Kobayashi, H.; Sakurai, K.; Shinkai, S. *Chem. Lett.* **2001**, 908–909.

(54) (a) French, A. D.; Zobel, H. F. *Biopolymers* **1967**, *5*, 457–464. (b) Hui, Y.; Russell, C. R.; Whitten, D. G. *J. Am. Chem. Soc.* **1983**, *105*, 1374–1376. (c) Helbert, W.; Chanzy, H. *Int. J. Biol. Macromol.* **1994**, *16*, 207–213. (d) Godet, M. C.; Tran, V.; Colonna, P.; Buleon, A.; Pezolet, M. *Int. J. Biol. Macromol.* **1995**, *17*, 405–408. (e) Kim, O.-K.; Choi, L.-S.; Zhang, H.-Y.; He, X.-H.; Shin, Y.-H. *J. Am. Chem. Soc.* **1996**, *118*, 12220–12221. (f) Sakurai, K.; Shinkai, S. *J. Am. Chem. Soc.* **2000**, *122*, 4520–4521. (g) Immel, S.; Lichtenthaler, F. H. *Starch/Stärke* **2000**, *52*, 1–8. (h) Star, A.; Steuerman, D. W.; Heath, J.

R.; Stoddart, J. F. *Angew. Chem., Int. Ed.* **2002**, *41*, 2508–2512. (i) Kim, O.-K.; Je, J.; Baldwin, J. W.; Kooi, S.; Pehrsson, P. E.; Buckley, L. J. *J. Am. Chem. Soc.* **2003**, *125*, 4426–4427. (j) Numata, M.; Hasegawa, T.; Fujisawa, T.; Sakurai, K.; Shinkai, S. *Org. Lett.* **2004**, *6*, 4447–4450. (k) Numata, M.; Asai, M.; Kaneko, K.; Hasegawa, T.; Fujita, N.; Kitada, Y.; Sakurai, K.; Shinkai, S. *Chem. Lett*. **2004**, *33*, 232–234. (l) Sakurai, K.; Uezu, K.; Numata, M.; Hasegawa, T.; Li, C.; Kaneko, K.; Shinkai, S. *Chem. Commun.* **2005**, 4383–4398. (m) Li, C.; Numata, M.; Bae, A.-H.; Sakurai, K.; Shinkai, S. *J. Am. Chem. Soc.* **2005**, *127*, 4548–4549. (n) Hasegawa, T.; Haraguchi, T.; Numata, M.; Li, C.; Bae, A. -H.; Fujisawa, T.; Kaneko, K.; Sakurai, K.; Shinkai, S. *Org. Biomol. Chem.* **2005**, *3*, 4321–4328. (o) Numata, M.; Tamesue, S.; Fujisawa, T.; Haraguchi, S.; Hasegawa, T.; Bae, A.-H.; Li, C.; Sakurai, T.; Shinkai, S. *Org. Lett.* **2006**, *8*, 5533–5536. (p) Numata, M.; Tamesue, S.; Nagasaki, T; Sakurai, K.; Shinkai, S. *Chem. Lett*. **2007**, *36*, 668–669. (q) Sletmoen, M.; Stokke, B. T. *Biopolymers* **2008**, *89*, 310–321. (r) Haraguchi, S.; Numata, M.; Kaneko, K.; Shinkai, S. *Bull. Chem. Soc. Jpn.* **2008**, *81*, 1002–1006. (s) Kato, N.; Sanji, T.; Tanaka, M. *Chem. Lett.* **2009**, *38*, 1192–1193. (t) Haraguchi, S.; Tsuchiya, Y.; Shiraki, T.; Sugikawa, K.; Sada, K.; Shinkai, S. *Chem. - Eur. J.* **2009**, *15*, 11221–11228. (u) Haraguchi, S.; Numata, M.; Li, M. C.; Nakano, Y.; Fujiki, M.; Shinkai, S. *Chem*. *Lett*. **2009**, *38*, 254–255. (v) Shiraki, T.; Haraguchi, S.; Tsuchiya, Y.; Shinkai, S. *Chem*. *Asian J*. **2009**, *4*, 1434–1441. (w) Shiraki, T.; Tsuchiya, Y.; Noguchi, T.; Tamaru, S.; Suzuki, N.; Taguchi, M.; Fujiki, M.; Shinkai, S. *Chem*. *Asian J*. **2014**, *9*, 218–222.

(55) (a) Haraguchi, S.; Hasegawa, T.; Numata, M.; Fujiki, M.; Uezu, K.; Sakurai, K.; Shinkai, S. *Org. Lett.* **2005**, *7*, 5605–5608. (b) Sanji, T.; Kato, N.; Kato, M.; Tanaka, M. *Angew. Chem., Int. Ed.* **2005**, *44*, 7301−7304. (c) Ikeda, M.; Hasegawa, T.; Numata, M.; Sugikawa, K.; Sakurai, K.; Fujiki, M.; Shinkai, S. *J. Am. Chem. Soc.* **2007**, *129*, 3979−3988.

(56) (a) Sanji, T.; Kato, N.; Tanaka, M. *Org. Lett.* **2006**, *8*, 235–238. (b) Sanji, T.; Kato, N.; Tanaka, M. *Chem. – Asian J.* **2008**, *3*, 46–50.

(57) (a) Kusuyama, H.; Takase, M.; Higashihata, Y.; Tseng, H.-T.; Chatani, Y.; Tadokoro, H. *Polymer* **1982**, *23*, 1256–1258. (b) Kusuyama, H.; Miyamoto, N.; Chatani, Y.; Tadokoro, H. *Polym. Commun.* **1983**, *24*, 119–122.

(58) Kumaki, J.; Kawauchi, T.; Okoshi, K.; Kusanagi, H.; Yashima, E. *Angew. Chem., Int. Ed.* **2007**, *46*, 5348–5351.

(59) Kawauchi, T.; Kitaura, A.; Kawauchi, M.; Takeichi, T.; Kumaki, J.; Iida, H.; Yashima, E. *J. Am. Chem. Soc.* **2010**, *132*, 12191–12193.

(60) Kawauchi, T.; Kumaki, J.; Kitaura, A.; Okoshi, K.; Kusanagi, H.; Kobayashi, K.; Sugai, T.; Shinohara, H.; Yashima, E. *Angew. Chem., Int. Ed.* **2008**, *47*, 515–519.

(61) Kawauchi, T.; Kawauchi, M.; Kodama, Y.; Takeichi, T. *Macromolecules* **2011**, *44*, 3452–3457.

(62) Kawauchi, T.; Ohnishi, K.; Kajihara, K.; Kawauchi, M.; Takeichi, T. *Macromolecules* **2019**, *52*, 5067–5073.

(63) Kitaura, A.; Iida, H.; Kawauchi, T.; Yashima, E. *Chem. Lett.* **2011**, *40*, 28–30.

(64) Kawauchi, T.; Kitaura, A.; Kumaki, J.; Kusanagi, H.; Yashima, E. *J. Am. Chem. Soc.* **2008**, *130*, 11889–11891.

(65) Ousaka, N.; Mamiya, F.; Iwata, Y.; Nishimura, N.; Yashima, E. *Angew. Chem., Int. Ed.* **2017**, *56*, 791–795.

(66) Mamiya, F. Studies on Synthesis of Chiral Cyclic Supramolecules and Supramolecular Helical Complex Formation of Syndiotactic Poly(methyl methacrylate) with Chiral Fullerene Derivatives. Ph.D. Thesis, Nagoya University, Japan, **2019**. http://hdl.handle.net/2237/00029969.

(67) Ohya, Y.; Takamido, S.; Nagahama, K.; Ouchi, T.; Ooya, T.; Katoono, R.; Yui, N. *Macromolecules* **2007**, *40*, 6441–6444.

(68) Kaneko, Y.; Ueno, K.; Yui, T.; Nakahara, K.; Kadokawa, J.-i. *Macromol. Biosci.* **2011**, *11*, 1407–1415.

(69) Tanaka, T.; Sasayama, S.; Yamamoto, K.; Kimura, Y.; Kadokawa, J.-i. *Macromol. Chem.*

Phys. **2015**, *216*, 794–800.

Chapter 1

Allosteric Regulation of Metal-Binding Sites Inside an Optically-Active Helical Foldamer and Its Tubular Assemblies

Abstract: A helical foldamer possessing conformationally switchable metal-binding linkers underwent supramolecular polymerization to form a helical nanofiber. A reversible helix-to-helix transition of the helical nanofiber took place upon cooperative binding and release of Ag(I) ions via metal-coordination-driven W-to-U-shape conformational change of the linkers in a positive allosteric manner.

Introduction

In living systems, the self-assembly of biopolymers is one of the most common processes to build complex chiral architectures that show various sophisticated functions. Among the artificial self-assembled systems, the supramolecular polymerization of small molecules to form helical assemblies with a controlled handedness has rapidly evolved into one of the most fascinating research topics in the field of supramolecular chemistry,[1] because of their unique applications and properties, such as asymmetric catalysis,[2] chiral recognition and separation,[3] helical templates for the synthesis of inorganic helices[4] and circular polarized luminescence.[5] However, most of these unique reaction and molecular recognition events take place on the outer surface of the assembled helices or at their side chains.[2,3] In contrast, the development of supramolecular helical polymers with an internal helical cavity is able to provide a well-defined continuous chiral nanospace inside a helical structure. Although tubular or helical assemblies of macrocyclic compounds with an inner space have been extensively studied,[6] there are limited examples of supramolecular polymers assembled from helical oligomers (foldamers) and polymers[1e,7] possessing an internal helical cavity capable of guest inclusion.[8]

The author now reports hydrogen-bond-driven supramolecular helical assemblies of an optically-active acylhydrazine-functionalized biphenyl derivative (**1C**) bearing tris(alkoxy)benzene-appended chiral oligoamide side chains and its corresponding helical polymer (foldamer) (poly-**1C**) whose monomer units are linked by multidentate 2,6-pyridinebis(acylhydrazone) ligands formed by a condensation reaction between the acylhydrazine groups of **1C** and aldehyde groups of 2,6-pyridinedicarboxaldehyde (**2**) (Figure 1-1a,c(i)).[9] Interestingly, the binding of Ag(I) ions to the metal binding W-shaped linker units located inside the helical cavity of poly-**1C** proceeds in a positive allosteric fashion,[10] resulting in a cooperative helix-to-helix transition of poly-**1C** triggered by an Ag(I) coordination-driven conformational change of the linker units from a W-shaped form to a U-shaped one (Figure 1-1b)[11] that further induces conformational changes in the neighboring linker units thereby facilitating the following metal-binding at the linker units and producing

another helical foldamer composed of all the U-shaped linker units (Figure 1-1b,c(ii)). To the best of the author's knowledge, there are only a few examples of the allosteric regulation of metal binding sites located inside or outside the helices.[12]

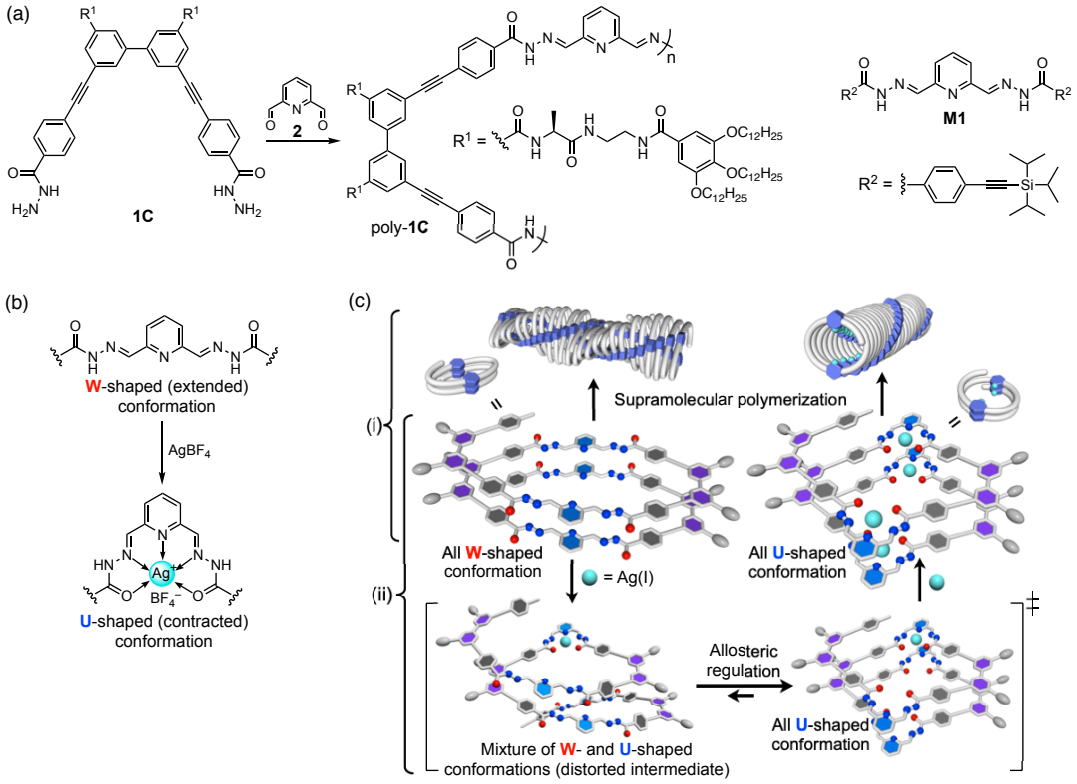

Figure 1-1. (a) Synthesis of foldamer poly-**1C** and chemical structure of its model **M1**. (b) Schematic representation of an Ag(I) ion-triggered W-to-U-shaped conformational change of the 2,6-pyridinebis(acylhydrazone) linker units of poly-**1C**. (c) Schematic representations of tubular assemblies of helical foldamer poly-**1C** and its complex with Ag(I) ions through supramolecular polymerization (i) and of allosteric regulation of a helix-to-helix transition of poly-**1C** triggered by binding of Ag(I) ions to W-shaped linker units of poly-**1C** (ii). The blue color represents the W- or U-shaped linker units (top). The first binding of an Ag(I) ion to one of the W-shaped linker units of poly-**1C** induces the W-to-U-shape conformational change, resulting in further conformational changes in the neighboring linker units via an unstable intermediated helical structure composed of a mixture of the W- and U-shaped linker units thereby facilitating the following metal-binding at the linker units inside the helical cavity of poly-**1C** (ii).

Results and Discussion

The optically-active monomer (**1C**) and achiral model compound (**M1**)[13] were prepared according to Schemes 1-S1 and 1-S2, respectively. The optically-active foldamer (poly-**1C**) was synthesized by the polycondensation reaction of the corresponding monomer **1C** with 1 equiv. of **2** in a DMSO/THF mixture (3/7, v/v) containing a catalytic amount of trifluoroacetic acid, followed by size-exclusion chromatography (SEC) purification, producing an acylhydrazone-linked foldamer poly-**1C** in a moderate yield (34%) (Figure 1-1a and Scheme 1-S1).[14] The number-average molar mass (M_n) and its distribution (M_w/M_n) of poly-**1C** were estimated to be 1.7×10^4 and 1.2, respectively, by SEC with polystyrene (PSt) standards using a DMSO/$CHCl_3$ mixture (1/9, v/v) containing tetra-*n*-butylammonium bromide (TBAB) (0.5 wt%) as the eluent.[15] In the absence of TBAB, however, poly-**1C** self-assembled to form a higher molar mass supramolecular polymer ($M_n = 1.1 \times 10^5$, $M_w/M_n = 5.6$) (Figure 1-S1) as supported by its broad ^{1}H NMR signals except for the pendant alkyl signals in DMSO-d_6/$CDCl_3$ (1/9, v/v) at 50 °C (Figure 1-S2a).

The author thus anticipated that the monomer **1C** would also self-assemble to form an optically-active supramolecular polymer due to the chiral oligoamide side chains that facilitate intermolecular hydrogen-bonding between the monomers **1C**. In fact, the ^{1}H NMR spectrum of **1C** in $CDCl_3$ at 25 °C exhibited significantly broad signals except for the pendant alkyl signals (Figure 1-S3a), which became sharper ones upon heating to 50 °C and/or by the addition of hydrogen-bond disrupting solvents, such as DMSO-d_6 (Figure 1-S3b–d), indicating the formation of a hydrogen-bond-driven supramolecular polymer. In addition, the circular dichroism (CD) spectrum of a freshly prepared 0.1 mM solution of **1C** in $CHCl_3$ showed an intense bisignate Cotton effect assigned to a predominantly left-handed (*M*)-twist conformation of the biphenyl moiety based on the exciton chirality theory (Figures 1-2a(i) and 1-S4a),[16] although **1C** possesses the chiral L-Ala residues at the side chains that are far away from the biphenyl core and cannot contribute to induce a preferred-handed twist-sense in the monomeric state.[17]

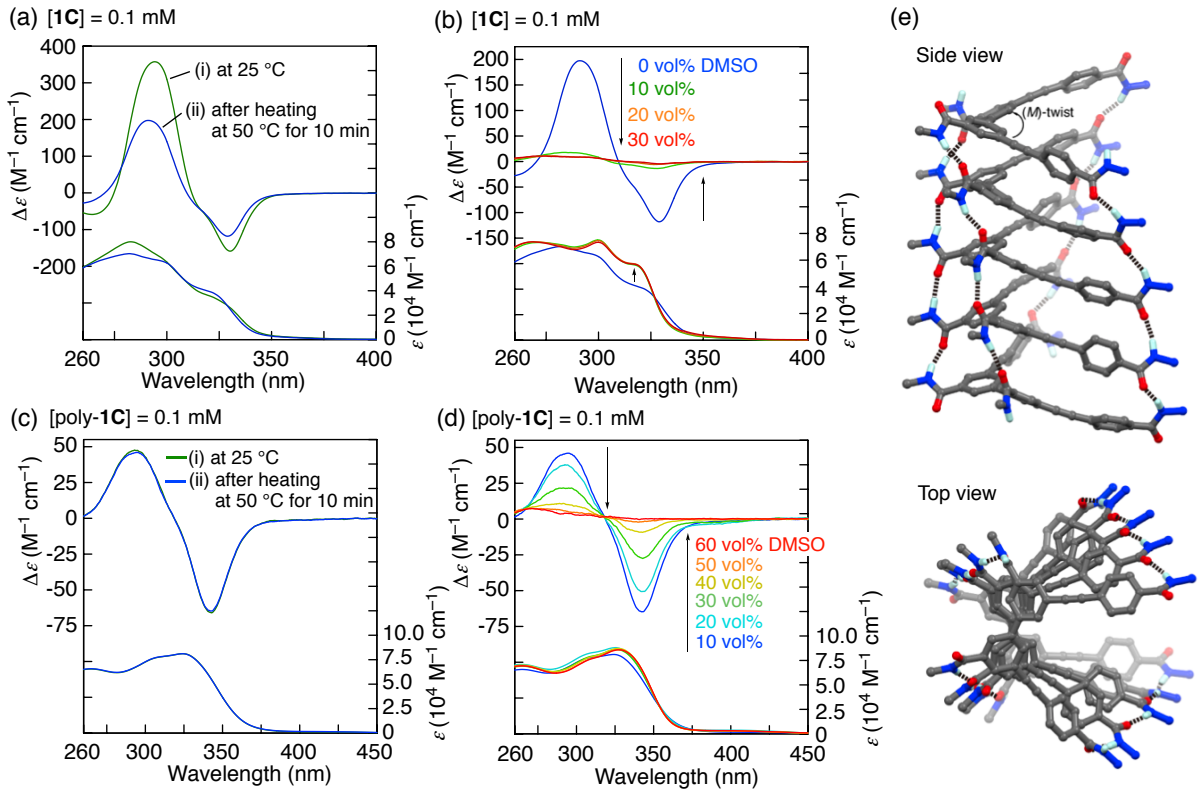

Figure 1-2. (a,b) CD and absorption spectra (0.1 mM, 25 °C) of **1C** in $CHCl_3$ before (i) and after heating at 50 °C for 10 min (ii) (a) and those in various DMSO/$CHCl_3$ mixtures (b). The CD and absorption spectra of **1C** in $CHCl_3$ (b) are identical to those shown in Figure 1-1a(ii). (c,d) CD and absorption spectra (0.1 mM per monomer unit, 25 °C) of poly-**1C** in DMSO/$CHCl_3$ (1/9, v/v) before (i) and after heating at 50 °C for 10 min (ii) (c) and those in various DMSO/$CHCl_3$ mixtures (d). (e) Side (upper) and top (bottom) views of the energy-minimized stacked structure of (**1C**)$_5$ with an (*M*)-twist conformation of the biphenyl moieties. Hydrogen atoms except for the amide protons are omitted for clarity. Black dotted lines represent the intermolecular hydrogen bonds. The oligoamide side-chains were replaced with –$CONHCH_3$ groups to simplify the calculations.

Interestingly, the optical activity of **1C** in $CHCl_3$ remained upon heating the as-prepared solution of **1C** at 50 °C for 10 min accompanied by a change in its absorption spectrum that was irreversible (Figures 1-2a(ii) and 1-S4a), as a result of transformation of the kinetically-formed helically assembled supramolecular polymer of **1C** into a thermodynamically stable one with a decrease in its molecular length.[18]

The observed unusual stability of the self-assembled **1C** in $CHCl_3$ relies solely on the intermolecular hydrogen bonds between the chiral oligoamide side chains including the terminal acylhydrazine moieties, as supported by a DMSO-mediated dissociation of the self-assembled **1C** into the monomeric **1C**, resulting in a disappearance of the induced CD accompanied by a significant change in its absorption spectrum (Figure 1-2b). In addition, the molecular modeling study of the linear pentameric assembly of **1C** ((**1C**)$_5$) suggested that all the pendant amide groups as well as the terminal acylhydrazine moieties participate in the intermolecular hydrogen-bonding network (Figure 1-2e). The atomic force microscopy (AFM) images observed for the self-assembled **1C** on a mica substrate provided further convincing evidence for the supramolecular polymer formation, in which **1C** self-assembled into micrometer-scale helical coiled-coil fibrils with a right-handed helical structure (Figures 1-3a and 1-S5).

In contrast to **1C**, foldamer poly-**1C** exhibited an obvious CD even in a DMSO/$CHCl_3$ mixture (1/9, v/v), whose CD intensity was approximately 2.6 times higher than that of **1C** measured under the same condition (Figure 1-2c) and was highly tolerant toward thermal annealing (Figure 1-S6b), dilution and the addition of DMSO (Figure 1-2d), as compared to **1C** (Figures 1-S6 and 1-S7). These results indicated that the helically-folded structure of poly-**1C** was stabilized by intramolecular hydrogen-bonding interactions as well as intermolecular ones in a DMSO/$CHCl_3$ mixture (1/9, v/v), in which poly-**1C** assembled to form a higher molar mass supramolecular polymer, which dissociated into single polymer chains in the presence of TBAB as already described (Figure 1-S1). This TBAB-triggered dissociation resulted in slight changes in its CD and absorption spectra of poly-**1C** (Figure

1-S8). Therefore, such a supramolecular polymerization of foldamer poly-**1C** hardly affects the helically-folded structure of poly-**1C**.

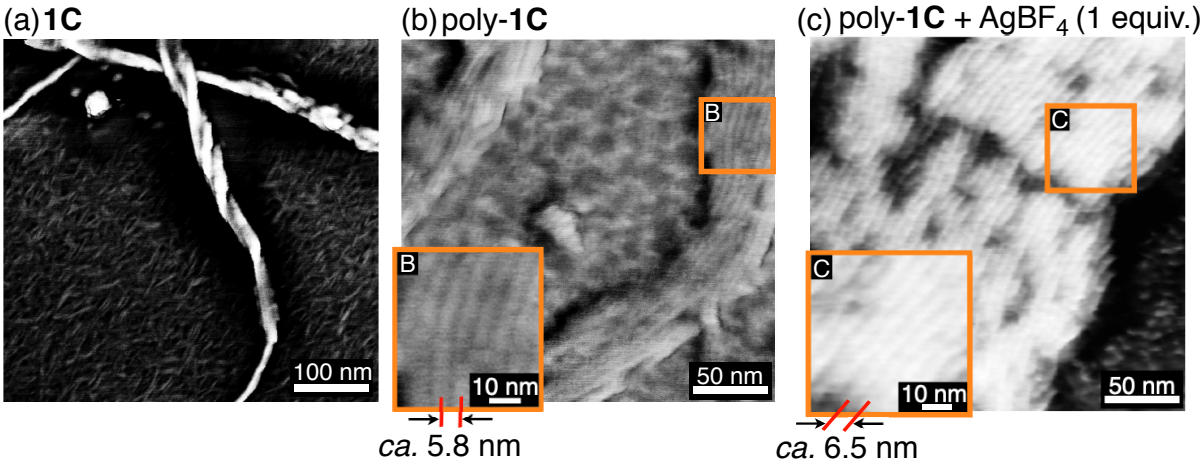

Figure 1-3. AFM phase (a,b) and height (c) images of self-assembled helical coiled-coil of **1C** (a) and helically assembled foldamer poly-**1C** -based supramolecular polymer in the absence (b) and presence of 1 equiv. of $AgBF_4$ (c). AFM images were observed on mica cast from dilute $CHCl_3$ (a) and dilute DMSO/$CHCl_3$ (*ca.* 2/98 (b) and *ca.* 1/99 (c), v/v) solutions (0.02 (a,c) and 0.04 mg mL^{-1} (b)). The insets (B,C) indicate magnified AFM phase (B) and height (C) images of poly-**1C** in the absence (B) and presence of 1 equiv. of $AgBF_4$ (C), respectively, which correspond to the area indicated by the squares in (b) and (c), respectively.

Supramolecular polymer formation of poly-**1C** in a DMSO/$CHCl_3$ mixture (1/9, v/v) was unambiguously revealed by AFM. Figure 1-3b shows a typical AFM image of poly-**1C** drop cast on mica from a dilute DMSO/$CHCl_3$ solution (*ca.* 2/98, v/v). The foldamer poly-**1C** underwent hydrogen-bond-mediated supramolecular polymerization to produce several ten to hundred nm long, rod- or tubular-like one-dimensional (1D) supramolecular nanofibers, which further assembled to form two-dimensional (2D) bundles packed parallel to each other with a height of *ca*. 4.4 nm and fiber-fiber spacing of *ca*. 5.8 nm (Figure 1-S9), which were close to the molecular diameter of the helically-assembled, left-handed model polymer of

poly-**1C** (*ca*. 5.6 nm) (Figure 1-S9f).[19,20]

The 2,6-pyridinebis(acylhydrazone) linker units of poly-**1C** are known to coordinate to various metal ions, such as Zn(II) and lanthanide(III) ions, in a pentadentate fashion with a nearly pentagonal-planar coordination geometry, accompanied by a change in its shape from W to U (Figure 1-1b).[11,21,22] The author then investigated the metal-coordination-driven shape transition of the linker units of poly-**1C** using an Ag(I) ion toward its model **M1** by UV-vis and ^{1}H NMR titrations. The absorption spectrum of **M1** in a DMSO/$CHCl_3$ mixture (1/9, v/v) gradually changed upon the addition of $AgBF_4$ with clear isosbestic points at 286, 316 and 346 nm, accompanied by an increase in the absorbance in the longer wavelength regions, suggesting the binding of an Ag(I) ion to **M1** with a 1:1 stoichiometry (Figure 1-S10), as further supported by the ^{1}H NMR spectral changes of **M1** with $AgBF_4$ (Figure 1-S11). The W-to-U-shape conformational change of **M1** upon complexation with $AgBF_4$ was confirmed by the ROESY spectrum (Figure 1-S12).

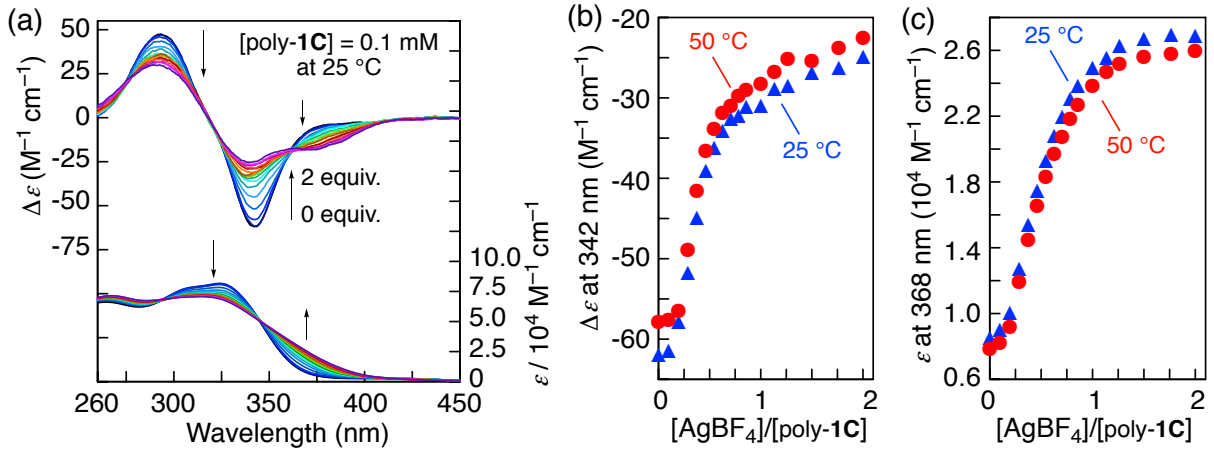

Figure 1-4. (a) CD and UV–vis titrations of poly-**1C** (DMSO/$CHCl_3$ (1/9, v/v), 0.1 mM per monomer unit, 25 °C) with $AgBF_4$. (b,c) Plots of $\Delta\varepsilon$ at 342 nm (b) and ε at 368 nm (c) for poly-**1C** as a function of [$AgBF_4$]/[poly-**1C**] at 25 (▲) and 50 °C (●).

The CD and UV-vis titrations of $AgBF_4$ with poly-**1C** in the same solvent mixture were then performed, showing clear isodichroic and isosbestic points, respectively (Figure 1-4a). Most interestingly, the plots of the CD and absorption intensities at 342 and 368 nm of poly-**1C** *versus* the $AgBF_4$ molar ratio, respectively, exhibited sigmoidal curvatures (Figure 1-4b,c) different from the UV-vis titration curve for the complexation of **M1** with $AgBF_4$ (Figure 1-S10). These results indicate the cooperative binding of Ag(I) ions to the linker units of poly-**1C**. Namely, the first Ag(I) binding to one of the W-shaped linker units induces a substantial W-to-U-shape conformational change, which further facilitates the conformational changes of the neighboring linker units suitable for the subsequent Ag(I) binding events in a highly allosteric manner. Aa a result, the overall helical structure of the Ag-bound poly-**1C** composed of all the U-shaped linker units significantly changed to a cylindrical helix (Figure 1-1b,c) while keeping its thermal stability (Figure 1-4b,c) and supramolecular polymerizability. The resulting Ag-bound poly-**1C** also assembled to produce similar 2D-bundled supramolecular nanofibers with a height of *ca*. 4.9 nm (Figure 1-S13) and fiber-fiber spacing of *ca*. 6.5 nm (Figure 1-3c) as revealed by its AFM images, which were slightly larger than those of the supramolecular nanofibers produced from poly-**1C** in the absence of $AgBF_4$ (Figures 1-3b and 1-S9) probably due to the rigid cylindrical helical structure of the Ag-bound poly-**1C** (Figure 1-1c).[24]

In order to demonstrate a reversible helix-to-helix transition of poly-**1C** upon the binding and release of Ag(I) ions to the metal-binding linker units of poly-**1C**, the CD and absorption spectral changes of poly-**1C** were followed by the sequential addition of $AgBF_4$ (2 equiv.) and [2.2.1]cryptand, a strong receptor for Ag(I) ions, in DMSO/$CHCl_3$ (1/9, v/v) at 25 °C. As shown in Figure 1-5, the absorption spectrum of poly-**1C** complexed with $AgBF_4$ (2 equiv.) (ii) was almost restored to that of poly-**1C** after the addition of [2.2.1]cryptand (2.0 equiv.), which trapped the Ag(I) ions from poly-**1C**, although the CD intensity of poly-**1C** did not recover completely (Figure 1-5(i–iii)). This is due to a large excess amount of BF_4^- anions that most likely bind to the acylhydrazone NH groups of the linker moieties and/or the

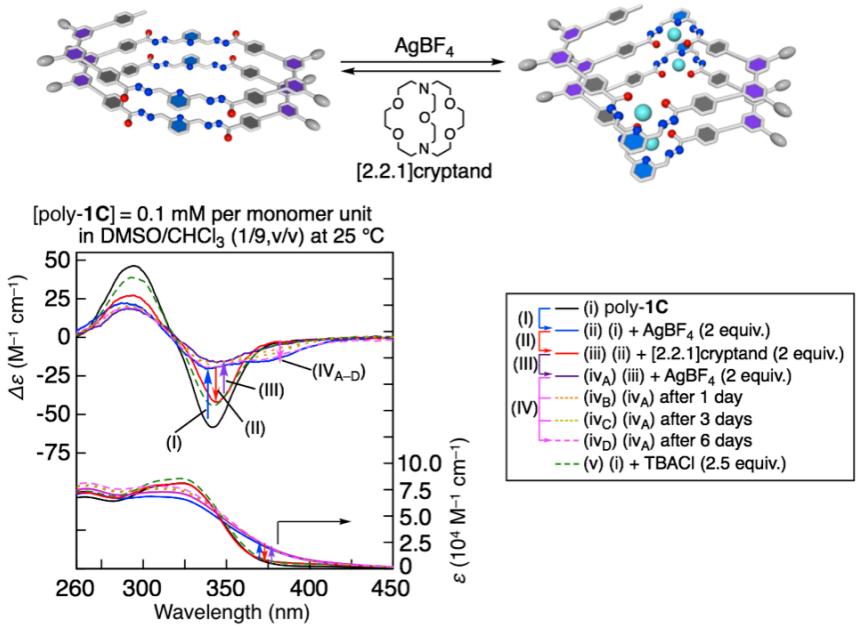

Figure 1-5. CD and absorption spectra of poly-**1C** ($DMSO/CHCl_3$ (1/9, v/v), 0.1 mM per monomer unit, 25 °C) after heating the solutions at 50 °C for 10 min (i), (i) + $AgBF_4$ (2 equiv.) (ii), (ii) + [2.2.1]cryptand (2 equiv.) (iii), and those just after the further addition of $AgBF_4$ (2 equiv.) (iv_A) followed by standing at 25 °C for 1 (iv_B), 3 (iv_C), and 6 days (iv_D). The CD and absorption spectra of poly-**1C** in the presence of TBA chloride (TBACl, 2.5 equiv.) in $DMSO/CHCl_3$ (1/9, v/v) are also shown (v).

oligoamide NH groups of poly-**1C**.[25] In fact, the CD spectrum of poly-**1C** complexed with $AgBF_4$ (2 equiv.) after the addition of [2.2.1]cryptand (2.0 equiv.) was similar to that of poly-**1C** in the presence of TBACl (2.5 equiv.) (Figure 1-5(iii,v)). Upon the further addition of $AgBF_4$ (2 equiv.), the CD and absorption spectra gradually changed with time (Figure 1-5(iv_A–iv_D)) and were almost switched back to the original ones after six days (Figure 1-5(ii,iv_D)). The observed time-dependent CD intensity changes can be ascribed to an excess amount of BF_4^- anions binding to the pendant NH groups of poly-**1C** as mentioned above, resulting in dissociation of the self-assembled polymeric poly-**1C** into a monomeric or an oligomeric poly-**1C** as supported by the SEC experiments of poly-**1C** in the presence and

absence of TBAB (Figure 1-S1). Therefore, the resulting monomeric or oligomeric poly-**1C** slowly re-assembled into its tubular poly-**1C**-based supramolecular polymer upon complexation with Ag(I) ions. Although the remaining anions slightly affect the CD spectral pattern of poly-**1C**, such a unique helix-to-helix transition of poly-**1C** was found to be reversibly controlled and switched by the sequential addition of $AgBF_4$ (2 equiv.) and [2.2.1]cryptand in an alternate manner.

Conclusions

In summary, the author has demonstrated a unique hydrogen-bond-driven supramolecular polymerization of an optically-active helical foldamer bearing conformationally switchable metal-binding linker units located inside the helical cavity to produce several ten to hundred nm long, supramolecular helical nanofibers. Upon cooperative and allosteric binding of Ag(I) ions to the linker units, an intriguing helix-to-helix transition takes place as a result of a metal coordination-driven W-to-U-shaped conformational change of the linkers. The present supramolecular helical polymers, of which the metal-binding sites are regularly located inside the helical cavity, may be applicable to developing novel foldamer-based asymmetric catalysts.[26]

Experimental Section

Instruments. The melting points were measured on a Yanaco MP-500D micromelting point apparatus (Yanako, Kyoto, Japan) and were uncorrected. The IR spectra were recorded on a JASCO FT/IR-680 spectrophotometer (JASCO, Tokyo, Japan). The NMR spectra were measured using a Bruker Ascend 500 (Bruker Biospin, Billerica, MA) or a Varian 500AS (Varian, Palo Alto, CA) spectrometer operating at 500 MHz for ^{1}H and 125 MHz for ^{13}C using tetramethylsilane (TMS) or a solvent residual peak as the internal standard. The absorption and CD spectra were measured in a 0.1-, 0.2-, or 1.0-cm quartz cell on a JASCO V-570 spectrophotometer and a JASCO J-1500 spectropolarimeter, respectively. The temperature was controlled with a JASCO ETC-505 apparatus. The electrospray ionization (ESI) mass spectra were recorded using a JEOL JMS-T100CS mass spectrometer (JEOL, Akishima, Japan). The size exclusion chromatography (SEC) measurements were performed with a JASCO PU-980 liquid chromatograph equipped with an UV-visible detector (324 nm, JASCO UV-2075) and a column oven (JASCO CO-2060). The wide-angle X-ray diffraction (WAXD) measurements were carried out by a Rigaku FR-E/R-AXIS IV system with a rotating-anode generator with graphite monochromated Cu *K*α radiation (l = 0.15418 nm) focused through a 0.3 mm pinhole collimator, which was supplied at 45 kV and 45 mA current, equipped with a flat imaging plate camera having a specimen-to-plate distance of 300 mm. The small-angle X-ray diffraction (SAXD) measurements were carried out by a Rigaku NANO-Viewer X-ray diffractometer using Cu *K*α radiation (l = 0.15418 nm) as an X-ray source and an imaging plate (Fujifilm) for detection. An image was obtained by exposure for 8–22 h. The diameter of the pinhole slit-collimated X-ray beam was in the range of 0.3–0.6 mm. The camera length was set at 955 mm. The number-average molar mass (M_n) and its distribution (M_w/M_n) were determined at 50 °C using a TSKgel G4000H$_{HR}$ (0.78 (i.d.) × 30 cm) SEC column (Tosoh, Tokyo, Japan), and DMSO/$CHCl_3$ (1/9, v/v) with 0.5 wt% tetra-*n*-butylammonium bromide (TBAB) was used as the eluent at a flow rate of 0.4 mL/min. The molar mass calibration curve was obtained with polystyrene standards (Tosoh). The atomic force microscopy (AFM) measurements were performed using a NanoScope V microscope (Bruker AXS, Santa

Barbara, CA) in air at room temperature with standard cantilevers (TESP–V2, Bruker AXS) in the tapping mode.

Materials. All starting materials were purchased from commercial suppliers and were used without further purification unless otherwise noted. *N*-(2-Aminoethyl)-3,4,5-tris(dodecyloxy)benzamide (**3**) was prepared according to the literature.[27]

Synthetic Procedures.

Abbreviations of chemicals:

Boc: *tert*-butoxycarbonyl,

dppf: 1,1'-bis(diphenylphosphino)ferrocene,

EDC·HCl: 1-ethyl-3-(3-dimethylaminopropyl)-carbodiimide hydrochloride,

HOBt·H_2O: 1-hydroxybenzotriazole monohydrate,

$^{i}Pr_2NH$: diisopropylamine,

NMM: *N*-methylmorpholine,

TFA: trifluoroacetic acid.

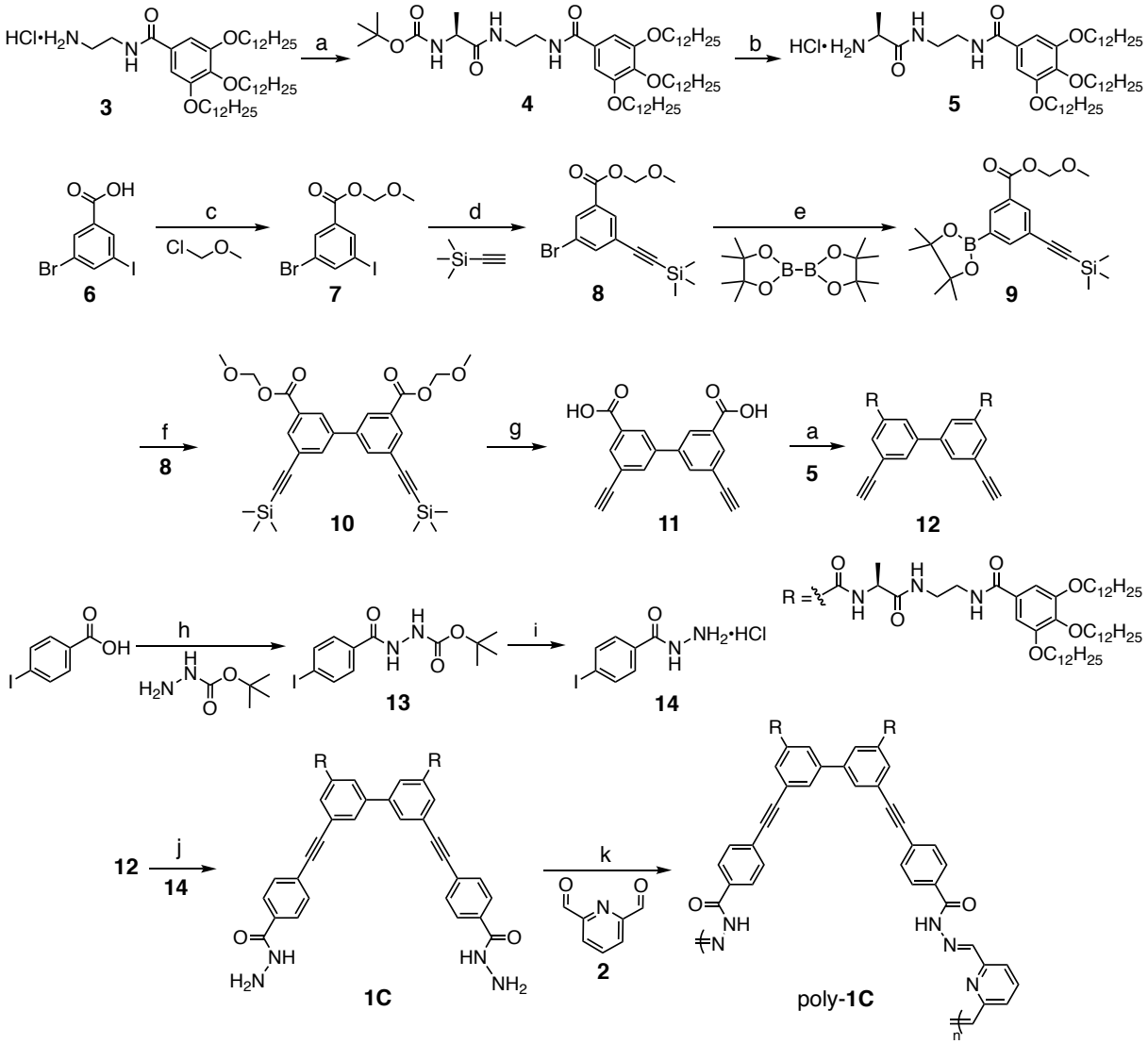

Scheme 1-S1. Synthesis of poly-**1C**. Reagents and conditions: a) HOBt·H_2O, EDC·HCl, NMM, DMF, 0 °C to r.t. b) 4N HCl in 1,4-dioxane, 0 ºC. c) Et_3N, THF, 0 °C to r.t. d) $Pd(PPh_3)_2Cl_2$, PPh_3, CuI, Et_3N, THF, 0 °C to r.t. e) $Pd(dppf)Cl_2·CH_2Cl_2$, KOAc, 1,4-dioxane, 80 °C. f) K_3PO_4, $Pd(PPh_3)_4$, 1,4-dioxane, 110 ºC. g) aqueous NaOH, MeOH, THF, r.t. h) EDC·HCl, CH_2Cl_2, 0°C to r.t. i) 4N HCl in 1,4-dioxane, 0 ºC to r.t. j) $Pd(PPh_3)_4$, CuI, $^iPr_2NH$, THF, 40 °C. k) TFA, THF, DMSO, 50 °C.

Synthesis of 4. To a solution of **3** (1.00 g, 1.33 mmol), Boc-L-alanine (278 mg, 1.47 mmol), and HOBt·H_2O (265 mg, 1.73 mmol) in DMF (20 mL) was added EDC·HCl (258 mg, 1.34 mmol) at 0 ºC under N_2, and the reaction mixture was stirred at 0 °C for 1 h. After NMM (0.151 mL, 1.37 mmol) was added to this at 0 ºC, the reaction mixture was stirred at 0 ºC for 30 min and further at room temperature for 11.5 h. After evaporating the solvent under reduced pressure, the residue was dissolved in $CHCl_3$, and the solution was washed with 1N aqueous HCl, 5% aqueous $NaHCO_3$, and brine, dried over $MgSO_4$, filtered, and evaporated to dryness under reduced pressure, affording **4** (1.05 g, 89.3%) as a white solid. Mp: 85–87 °C. ^{1}H NMR (500 MHz, $CDCl_3$, 25 °C): δ 7.18 (br, 1H, NH), 7.04 (s, 2H, Ar-H), 6.88 (br, 1H, NH), 5.00 (br, 1H, NH), 4.13 (br, 1H, NCHCO), 4.02-3.97 (m, 6H, OCH_2), 3.58-3.49 (m, 4H, NCH_2), 1.82-1.72 (m, 6H, CH_2), 1.46-1.26 (m, 66H, CH_2, CH_3), 0.89-0.87 (m, 9H, CH_3). ^{13}C NMR (125 MHz, $CDCl_3$, 25 °C): δ 174.36, 167.89, 155.60, 153.04, 141.01, 128.82, 105.61, 80.38, 73.47, 69.20, 50.46, 41.13, 39.68, 31.94, 30.34, 29.77, 29.75, 29.73, 29.676, 29.61, 29.44, 29.40, 29.38, 28.28, 26.13, 26.10, 22.71, 18.19, 14.13. IR (KBr, cm^{-1}): 3289 (ν_{N-H}), 1688 ($\nu_{C=O}$), 1659 ($\nu_{C=O}$), 1582 (ν_{N-H}), 1539 (ν_{N-H}). HRMS (ESI-MS): *m*/*z* calcd for $[M(C_{53}H_{97}N_3O) + H]^+$, 888.7405; found 888.7398.

Synthesis of 5. Into a two-neck round bottom flask containing **4** (993 mg, 1.12 mmol) was added 4N HCl in 1,4-dioxane (20 mL) at 0 ºC under N_2, and the reaction mixture was stirred at 0 ºC for 5 h. After evaporating the solvent under reduced pressure, the residue was washed with Et_2O to afford **5** (902 mg, 98%) as a white solid. Mp: 210–212 °C. ^{1}H NMR (500 MHz, DMSO-d_6/$CDCl_3$ (1/9, v/v), 25 °C): δ 8.82 (br, 1H, NH), 8.61 (br, 1H, NH), 8.44 (s, 3H, NH_3^+), 7.34 (s, 2H, Ar-H), 4.10-3.95 (m, 7H, OCH_2, N-CH-CO), 3.63-3.33 (m, 4H, N-CH_2), 1.82-1.70 (m, 6H, CH_2), 1.51-1.47 (m, 9H, CH_2, CH_3), 1.30-1.26 (m, 48H, CH_2), 0.88 (m, 9H, CH_2). ^{13}C NMR (125 MHz, DMSO-d_6/$CDCl_3$ (1/9, v/v), 25 °C): δ 169.64, 167.14, 152.72, 140.33, 129.04, 106.08, 73.26, 69.16, 49.68, 40.60, 40.44, 40.27, 40.10, 39.93, 39.77, 39.60, 38.98, 31.85, 31.84, 30.28, 29.67, 29.65, 29.63, 29.59, 29.58, 29.53, 29.41, 29.37, 29.30, 29.28, 26.113, 26.04, 22.60, 17.00, 14.10. IR (KBr, cm^{-1}): 3266 (ν_{N-H}), 1681 ($\nu_{C=O}$), 1634

($\nu_{C=O}$), 1582 (ν_{N-H}), 1549 (ν_{N-H}). HRMS (ESI-MS): *m*/*z* calcd for $[M(C_{48}H_{89}N_3O_5) + H]^+$, 788.6880; found 788.6889.

Synthesis of 7. To a solution of 3-bromo-5-iodobenzoic acid (**6**) (9.96 g, 30.5 mmol) in THF (80 mL) were added Et_3N (5.0 mL) and chloromethyl methyl ether (2.80 mL, 37.0 mmol) at 0 °C under Ar, and the reaction mixture was stirred at 0 °C for 1 h and further at room temperature for 12 h. After evaporating the solvent under reduced pressure, the residue was dissolved in EtOAc, and the solution was washed with 5% aqueous $NaHCO_3$ and brine, dried over $MgSO_4$, filtered, and concentrated under reduced pressure. The crude product was purified by column chromatography (SiO_2, *n*-hexane/EtOAc (1/1, v/v)) to afford **7** (11.0 g, 98%) as a white solid. Mp: 72-73 °C. ^{1}H NMR (500 MHz, $CDCl_3$, 25 °C): δ 8.32 (dd, *J* =1.5, 1.5 Hz, 1H, Ar-H), 8.16 (dd, *J* =1.5, 1.7 Hz, 1H, Ar-H), 8.06 (dd, *J* =1.8, 1.7 Hz, 1H, Ar-H), 5.48 (s, 2H, CH_2), 3.56 (s, 3H, OCH_3). ^{13}C NMR (125 MHz, $CDCl_3$, 25 °C): δ 163.51, 144.24, 137.42, 133.16, 132.23, 123.23, 94.22, 91.83, 58.20. IR (KBr, cm^{-1}): 1727 ($\nu_{C=O}$). Anal. Calcd for $C_9H_8BrIO_3$: C, 29.14; H, 2.17; Found: C, 29.14; H, 2.10.

Synthesis of 8. Into a two-neck round bottom flask containing **7** (7.00g, 18.9 mmol), $Pd(PPh_3)_2Cl_2$ (265 mg, 0.377 mmol), PPh_3 (98.9 mg, 0.377 mmol), and CuI (71.8 mg, 0.377 mmol) were added THF (100 mL) and Et_3N (70 mL) under Ar. After dissolving, the flask was cooled to −78 °C (dry ice-methanol), and subjected to three evacuation/Ar fill cycles. The flask was then warmed to 0 °C, trimethylsilyl acetylene (2.80 mL, 19.8 mmol) was added to this under Ar with stirring. The reaction mixture was stirred at 0 °C for 1 h and further at room temperature for 12 h. After evaporating the solvent under reduced pressure, the residue was dissolved in EtOAc, and the solution was washed with 1N aqueous HCl and brine, dried over $MgSO_4$, filtered, and concentrated under reduced pressure. The crude product was purified by column chromatography (SiO_2, *n*-hexane/EtOAc (9/1, v/v)) to afford **8** (5.94 g, 92%) as a white solid. Mp: 79-80 °C. ^{1}H NMR (500 MHz, $CDCl_3$, 25 °C): δ 8.13 (dd, *J* = 2.0, 1.5 Hz, 1H, Ar-H), 8.07 (dd, *J* =1.5, 1.5 Hz, 1H, Ar-H), 7.80 (dd, *J* =1.5, 1.5 Hz, 1H, Ar-H),

5.48 (s, 2H, CH_2), 3.56 (s, 3H, OCH_3), 0.26 (s, 9H, $Si(CH_3)_3$). ^{13}C NMR (125 MHz, $CDCl_3$, 25 °C): δ 164.25, 139.03, 132.67, 131.88, 131.81, 125.67, 122.32, 102.24, 97.50, 91.68, 58.13, -0.11. IR (KBr, cm^{-1}): 2158 ($\nu_{C\equiv C}$), 1729 ($\nu_{C=O}$). Anal. Calcd for $C_{14}H_{17}BrO_3Si$: C, 49.27; H, 5.02. Found: C, 49.28; H, 5.01.

Synthesis of 9. Into a two-neck round bottom flask containing **8** (5.92 g, 17.3 mmol), bis(pinacolato)diboron (4.68 g, 18.4 mmol), $Pd(dppf)Cl_2 \cdot CH_2Cl_2$ (1.25 g, 1.53 mmol), and KOAc (5.11 g, 52.0 mmol) was added 1,4-dioxane (110 mL) under Ar. After dissolving, the flask was subjected to five evacuation/Ar fill cycles, and the reaction mixture was stirred at 80 °C for 16 h. After evaporating the solvent under reduced pressure, the residue was dissolved in EtOAc, and the solution was washed with H_2O and brine, dried over $MgSO_4$, filtered, and concentrated under reduced pressure. The crude product was purified by column chromatography (SiO_2, *n*-hexane/EtOAc (9/1, v/v)) to afford **9** (5.93 g, 88%) as a colorless oil. ^1H NMR (500 MHz, $CDCl_3$, 25 °C): δ 8.42 (dd, J = 1.7, 1.2 Hz, 1H, Ar-H), 8.24 (dd, J = 1.8, 1.8 Hz, 1H, Ar-H), 8.11 (dd, J = 1.6, 1.2 Hz, 1H, Ar-H), 5.49 (s, 2H, OCH_2), 3.55 (s, 3H, OCH_3), 1.35 (s, 12H, $C(CH_3)_2$), 0.25 (s, 9H, $Si(CH_3)_3$). ^{13}C NMR (125 MHz, $CDCl_3$, 25 °C): δ 165.59, 142.88, 135.75, 135.67, 129.61, 123.43, 103.90, 95.59, 91.23, 84.48, 58.03, 58.01, 25.00, 0.02. IR (KBr, cm^{-1}): 2159 ($\nu_{C\equiv C}$), 1733 ($\nu_{C=O}$). HRMS (ESI-MS): *m*/*z* calcd for $[M(C_{20}H_{29}BO_5Si) + Na]^+$, 411.1779; found 411.1792.

Synthesis of 10. Into a two-neck round bottom flask containing **8** (1.94 g, 5.69 mmol), **9** (2.00 g, 5.14 mmol), K_3PO_4 (2.22 g, 10.4 mmol), and $Pd(PPh_3)_4$ (597 mg, 516 mmol) was added 1,4-dioxane (60 mL) under Ar. The flask was then subjected to three evacuation/Ar fill cycles, and the reaction mixture was stirred at 110 °C for 16 h. After cooling to room temperature, the solvent was evaporated to dryness under reduced pressure. The residue was dissolved in EtOAc, and the solution was washed with H_2O and brine, dried over $MgSO_4$, filtered, and concentrated under reduced pressure. The crude product was purified by column chromatography (SiO_2, *n*-hexane/EtOAc (4/1, v/v)) to afford **10** (1.58 g, 59%) as a colorless

oil. ^{1}H NMR (500 MHz, $CDCl_3$, 25 °C): δ 8.25 (dd, J = 1.5, 1.5 Hz, 2H, Ar-H), 8.19 (dd, J = 1.5, 1.5 Hz, 2H, Ar-H), 7.92 (dd, J = 1.5, 1.5 Hz, 2H, Ar-H), 5.53 (s, 4H, OCH_2), 3.59 (s, 6H, OCH_3), 0.29 (s, 18H, $Si(CH_3)_3$). ^{13}C NMR (125 MHz, $CDCl_3$, 25 °C): δ 165.26, 139.97, 135.03, 132.71, 131.01, 128.33, 124.69, 103.46, 96.47, 91.52, 58.12, -0.0184. IR (KBr, cm^{-1}): 2158 ($\nu_{C\equiv C}$), 1730 ($\nu_{C=O}$). HRMS (ESI-MS): m/z calcd for $[M(C_{28}H_{34}O_6Si_2) + Na]^+$, 545.1792; found 545.1790.

Synthesis of 11. To a solution of **10** (1.28 g, 2.46 mmol) in MeOH (8.0 mL) and THF (16.0 mL) was added 1N aqueous NaOH (16.0 mL, 16.0 mmol) at 0 °C under N_2, and the reaction mixture was stirred at 0 °C for 5 min and further at room temperature for 3 h. After most of the organic solvents was removed under reduced pressure, the solution was washed with Et_2O and then acidified to pH 1–2 by 1N aqueous HCl. The precipitate was collected by filtration, washed with water and *n*-hexane, and dried in vacuo, affording **11** (717 mg, quant.) as a white sold. Mp: 219 °C (dec.). ^{1}H NMR (500 MHz, DMSO-d_6, 25 °C): δ 13.41 (s, 2H, COOH), 8.19 (dd, J = 1.6, 1.6 Hz, 2H, Ar-H), 8.10 (dd, J = 1.6, 1.6 Hz, 2H, Ar-H), 8.00 (dd, J = 1.6, 1.6 Hz, 2H, Ar-H), 4.39 (s, 2H, C≡CH). ^{13}C NMR (125 MHz, DMSO-d_6, 25 °C): δ 166.21, 139.28, 134.10, 132.25, 131.80, 127.95, 123.11, 82.22. IR (KBr, cm^{-1}): 3290 ($\nu_{\equiv C-H}$), 2975 (ν_{O-H}). HRMS (ESI-MS): m/z calcd for $[M(C_{18}H_{10}O_4) - H]^-$, 289.0501; found 289.0492.

Synthesis of 12. To a solution of **11** (148 mg, 0.509 mmol), **5** (879 mg, 1.07 mmol), and HOBt·H_2O (195 mg, 1.28 mmol) in DMF (15 mL) was added EDC·HCl (198 mg, 1.03 mmol) at 0 ºC under N_2, and the reaction mixture was stirred at 0 °C for 1 h. After NMM (0.125mL, 1.14 mmol) was added to this at 0 ºC, the reaction mixture was stirred at 0 ºC for 30 min and further at room temperature for 25 h. After evaporating the solvent under reduced pressure, the residue was dissolved in $CHCl_3$, and the solution was washed with 1N aqueous HCl, 5% aqueous $NaHCO_3$, and brine, dried over $MgSO_4$, filtered, and concentrated under reduced pressure. The crude product was purified by column chromatography (SiO_2, MeOH/$CHCl_3$ (1/9, v/v)) to afford **12** (616 mg, 66%) as a slightly yellowish solid. Mp: 201–203 °C. ^{1}H

NMR (500 MHz, DMSO-d_6/$CDCl_3$ (1/9, v/v), 50 °C): δ 8.47 (s, 2H, NH), 8.17 (s, 2H, Ar-H), 7.98 (s, 2H, Ar-H), 7.82 (s, 2H, NH), 7.76 (s, 2H, Ar-H), 7.71 (s, 2H, NH), 7.05 (s, 4H, Ar-H), 4.73 (m, 2H, NCHCO), 3.96-3.89 (s, 6H, OCH_2), 3.51 (m, 4H, NCH_2), 3.40 (m, 4H, NCH_2), 3.19 (s, 2H, C≡CH), 1.77-1.68 (m, 12H, CH_2), 1.49-1.40 (m, 18H, CH_2, CH_3), 1.26 (m, 96H, CH_2), 0.88 (m, 18H, CH_3). ^{13}C NMR (125 MHz, DMSO-d_6/$CDCl_3$ (1/9, v/v), 50 °C): δ 173.68, 167.63, 165.60, 152.61, 140.87, 139.66, 134.66132.95, 130.69, 128.96, 126.03, 122.93, 106.04, 82.33, 78.45, 73.11, 69.03, 49.77, 31.59, 31.58, 30.08, 29.40, 29.38, 29.36, 29.33, 29.31, 29.27, 29.18, 29.12, 29.01, 29.00, 25.85, 25.81, 22.32, 17.76, 13.74. IR (KBr, cm^{-1}): 3265 ($\nu_{\equiv C-H}$), 1634 ($\nu_{C=O}$), 1538 (ν_{N-H}). HRMS (ESI-MS): *m*/*z* calcd for $[M(C_{114}H_{184}N_6O_{12}) + Na]^+$, 1852.3870; found 1852.3797.

Synthesis of 13. To a solution of 4-iodobenzoic acid (5.37 g, 21.6 mmol) in CH_2Cl_2 (200 mL) was added EDC·HCl (5.06 g, 26.4 mmol) at 0 ºC under N_2 and the reaction mixture was stirred at 0 °C for 30 min. After *tert*-butyl carbazate (3.00 g, 22.7 mmol) was added to this at 0 ºC, the reaction mixture was stirred at 0 ºC for 30 min and further at room temperature for 84 h. The solution was diluted with CH_2Cl_2, and the solution was washed with 5% aqueous $NaHCO_3$ and brine, dried over Na_2SO_4, filtered, and evaporated to dryness under reduced pressure. The crude product was purified by column chromatography (SiO_2, $CHCl_3$/*n*-hexane/EtOAc (1/1/2, v/v/v)) to afford **13** (5.87 g, 75%) as a white solid. Mp: 166–167 °C. ^{1}H NMR (500 MHz, $CDCl_3$, 25 °C): δ 8.79 (br, 1H, NH), 7.72 (d, J = 8.3 Hz, 2H, Ar-H), 7.49 (d, J = 8.3 Hz, 2H, Ar-H), 6.83 (br, 1H, NH), 1.48 (s, 9H, CH_3). ^{13}C NMR (125 MHz, $CDCl_3$, 25 °C): δ 166.21, 156.21, 137.93, 131.05, 128.90, 99.70, 82.43, 28.28. IR (KBr, cm^{-1}): 3339 (ν_{N-H}), 3230 (ν_{N-H}), 1720 ($\nu_{C=O}$), 1664 ($\nu_{C=O}$). HRMS (ESI-MS): *m*/*z* calcd for $[M(C_{12}H_{15}N_2O_3I) - H]^-$, 361.0049; found 361.0060.

Synthesis of 1C. 13 was dissolved in 4N HCl in 1,4-dioxane at 0 °C. The reaction mixture was stirred at room temperature for 4 h and the solvent was evaporated to dryness under reduced pressure, affording **14** as a white solid, which was used without further purification in

the next step. Into a two-neck round bottom flask containing **12** (251 mg, 0.137 mmol) and **14** (205 mg, 0.687 mmol) was added dry THF (10 mL) under Ar. After dissolving, the solution was frozen by liq. N_2 and degassed by three freeze-pump-thaw cycles. After the flask was warmed to 0 °C, to this were added $Pd(PPh_3)_4$ (5.11 mg, 7.28 μmol), CuI (1.39 mg, 7.30 μmol), and degassed $^{i}Pr_2NH$ (2.5 mL) under Ar, and the solution was gradually warmed to room temperature. The reaction mixture was stirred at room temperature for 20 min and further at 40 °C for 17 h. After cooling to room temperature, to this was added excess MeOH (100 mL) and the precipitate was collected by filtration and washed with MeOH, affording **1C** (253 mg, 88%) as a brown solid. Mp: 270 °C (dec.). ^{1}H NMR (500 MHz, DMSO-d_6/$CDCl_3$ (3/7, v/v), 25 °C): δ 9.81 (br, 2H, NH), 8.66 (br, 2H, NH), 8.34 (s, 2H, Ar-H), 8.22 (br, 2H, NH), 8.13 (s, 2H, Ar-H), 8.03 (br, 2H, NH), 8.00 (s, 2H, Ar-H), 7.90 (d, J = 7.5 Hz, 4H, Ar-H), 7.58 (d, J = 7.5 Hz, 4H, Ar-H), 7.10 (s, 4H, Ar-H), 4.66 (m, 2H, NCHCO), 4.38 (br, 4H, NH_2), 3.94-3.89 (m, 12H, OCH_2), 3.52-3.46 (m, 4H, NCH_2), 3.42-3.41 (m, 4H, NCH_2), 1.77-1.65 (m, 12H, CH_2), 1.47 (d, J = 7.0 Hz, 6H, CH_3), 1.44-1.41 (m, 12H, CH_2), 1.28-1.24 (m, 96H, CH_2), 0.88-0.85 (m, 18H, CH_3). ^{13}C NMR (125 MHz, DMSO-d_6/$CDCl_3$ (3/7, v/v), 25 °C): δ 172.85, 166.76, 165.25, 152.04, 139.70, 139.11, 134.86, 131.89, 130.85, 129.97, 128.77, 126.96, 125.99, 124.86, 122.96, 105.27, 89.99, 89.27, 77.96, 72.54, 68.29, 49.25, 38.84, 31.22, 31.21, 29.68, 29.05, 29.04, 29.02, 29.00, 28.97, 28.96, 28.95, 28.930, 28.89, 28.74, 28.66, 28.64, 25.50, 25.43, 21.99, 21.98, 17.51, 13.59. IR (KBr, cm^{-1}): 3310 (ν_{N-H}), 1637 ($\nu_{C=O}$), 1541 (ν_{N-H}). HRMS (ESI-MS): m/z calcd for $[M(C_{128}H_{196}N_{10}O_{14}) + Na]^+$, 2120.4830; found 2120.4793.

Polymerization of 1C with 2. Into a two-neck round bottom flask containing **1C** (72.7 mg, 34.6 μmol) was added **2** (4.70 mg, 34.8 μmol) in DMSO (0.6 mL) and THF (1.5 mL), and the reaction mixture was stirred at 50 °C for 30 min. After a catalytic amount of TFA (3.5 μmol) in DMSO (60 μL) and THF (140 μL) was added to this, the reaction mixture was stirred at 50 °C for 3 days. To this was then added excess MeOH (20 mL) and the precipitate was collected and washed with MeOH. The crude product was purified by SEC (TOYOPEARL

HW-50S (1.5 (i.d.) × 88 cm), DMF/THF (3/7, v/v)), affording poly-**1C** (25.9 mg, 34%) as a yellow solid. The M_n and M_w/M_n of poly-**1C** were estimated to be 1.7×10^4 and 1.2, respectively, by SEC with polystyrene standard using DMSO/$CHCl_3$ (1/9, v/v) with 0.5 wt% TBAB as the eluent at a flow rate of 0.4 mL/min.

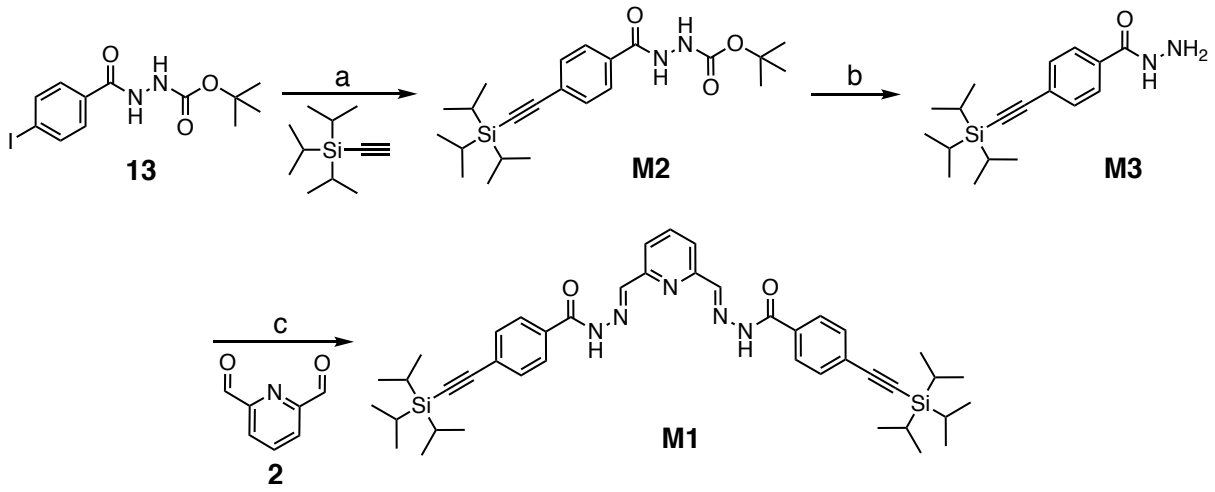

Scheme 1-S2. Synthesis of **M1**. Reagents and conditions: a) $Pd(PPh_3)_2Cl_2$, PPh_3, CuI, Et_3N, THF, 40 ºC. b) 4N HCl in 1,4-dioxane, 0°C to r.t. c) THF, 40 °C.

Synthesis of M2. Into a two-neck round bottom flask containing **13** (700 mg, 1.93 mmol), $Pd(PPh_3)_2Cl_2$ (68.2 mg, 97.1 μmol), PPh_3 (28.1 mg, 0.107 mmol), and CuI (19.2 mg, 0.101 mmol) were added THF (2.0 mL) and Et_3N (5.4 mL) under N_2. After dissolving, the flask was cooled to −78 °C (dry ice-methanol), and subjected to three evacuation/N_2 fill cycles. After the flask was warmed to 0 °C, to this was added triisopropylsilylacetylene (0.57 mL, 2.5 mmol). The reaction mixture was stirred at 0 °C for 10 min and further at 40 °C for 15 h. After evaporating the solvent under reduced pressure, the residue was dissolved in EtOAc, and the solution was washed with H_2O and brine, dried over Na_2SO_4, filtered, and concentrated under reduced pressure. The crude product was purified by column chromatography (SiO_2, $CHCl_3$/EtOAc (9/1, v/v)) to afford **M2** (655 mg, 81%) as a white solid. Mp: 193–194 °C. ^{1}H NMR (500 MHz, $CDCl_3$, 25 °C): δ 8.75 (br, 1H, NH), 7.72 (d, J = 8.3

Hz, 2H, Ar-H), 7.46 (d, J = 8.3 Hz, 2H, Ar-H), 6.88 (br, 1H, NH), 1.45 (s, 9H, CH_3), 1.16-1.10 (m, 21H, CH, CH_3). ^{13}C NMR (125 MHz, $CDCl_3$, 25 °C): δ 166.25, 156.14, 132.25, 131.05, 127.64, 127.28, 106.09, 94.15, 82.297, 28.27, 18.78, 11.40. IR (KBr, cm^{-1}): 3335 (ν_{N-H}), 3220 (ν_{N-H}), 2156 ($\nu_{C\equiv C}$), 1721 ($\nu_{C=O}$), 1659 ($\nu_{C=O}$). HRMS (ESI-MS): m/z calcd for $[M(C_{23}H_{36}N_2O_3Si) + Na]^+$, 439.2393; found 439.2399.

Synthesis of M3. M2 (512 mg, 1.23 mmol) was dissolved in 4N HCl in 1,4-dioxane at 0 ºC under N_2, and the reaction mixture was stirred at 0 ºC for 1 h and further at room temperature for 2 h. After evaporating the solvent under reduced pressure, the residue was dissolved in EtOAc, and the solution was washed with 5% aqueous $NaHCO_3$ and brine, dried over Na_2SO_4, filtered, and evaporated to dryness under reduced pressure. The residue was washed with *n*-hexane to afford **M3** (349 mg, 89%) as a white solid. Mp: 118–119 °C. ^1H NMR (500 MHz, $CDCl_3$, 25 °C): δ 7.87 (br, 1H, NH), 7.71 (d, J = 8.3 Hz, 2H, Ar-H), 7.53 (d, J = 8.3 Hz, 2H, Ar-H), 4.16 (br, 2H, NH_2), 1.16-1.10 (m, 21H, CH, CH_3). ^{13}C NMR (125 MHz, $CDCl_3$, 25 °C): δ 168.10, 132.37, 132.03, 127.36, 126.89, 106.02, 94.09, 18.76, 11.38. IR (KBr, cm^{-1}): 3314 (ν_{N-H}), 2155 ($\nu_{C\equiv C}$), 1667 ($\nu_{C=O}$). HRMS (ESI-MS): m/z calcd for $[M(C_{23}H_{36}N_2O_3Si) + Na]^+$, 339.1869; found 339.1875.

Synthesis of M1. M3 (253 mg, 799 mmol) and **2** (51.2 mg, 379 mmol) were dissolved in THF (2.5 mL) under N_2, and the reaction mixture was stirred at room temperature for 1 h and further at 40 °C for 7 h. After evaporating the solvent under reduced pressure, the residue was washed with Et_2O to afford **M1** (244 mg, 88%) as a white solid. Mp: 271–272 °C. ^1H NMR (500 MHz, DMSO-d_6, 25 °C): δ 12.16 (br, 2H, NH), 8.53 (s, 2H, N=CH), 8.01 (br, 3H, Py-H), 7.97 (d, J = 8.0 Hz, 4H, Ar-H), 7.64 (d, J = 8.0 Hz, 4H, Ar-H), 1.16-1.10 (m, 42H, CH, CH_3). ^{13}C NMR (125 MHz, DMSO-d_6, 25 °C): δ 162.42, 153.23, 147.81, 137.76, 132.93, 131.86, 128.10, 125.73, 120.57, 106.31, 92.97, 18.50, 10.69. IR (KBr, cm^{-1}): 3447 (ν_{N-H}), 2156 ($\nu_{C\equiv C}$), 1655 ($\nu_{C=O}$). HRMS (ESI-MS): m/z calcd for $[M(C_{43}H_{57}N_5O_2Si_2) + Na]^+$, 754.3948; found 754.3923.

Atomic Force Microscopy (AFM) Measurements

AFM Measurements of Assemblies of 1C on Mica

A solution of **1C** in $CHCl_3$ (10 μM) was prepared. Samples for the AFM measurements of **1C** were prepared by casting 30 μL aliquots of the stock solution on a freshly cleaved mica at room temperature (ca. 25 °C), and the solvents were then slowly evaporated under a $CHCl_3$ vapor atmosphere. After **1C** had been deposited on the mica, the mica substrates were exposed to $CHCl_3$ vapors at room temperature for 12 h, and the substrates were then dried under vacuum for 1 h. The organic solvent vapors were prepared by putting 1 mL of $CHCl_3$ into a 2 mL flask that was inside a 50 mL flask, and the mica substrates were then placed in the 50 mL flask. The AFM measurements were performed using a NanoScope V microscope in air at room temperature with standard silicon cantilevers (TESP–V2) in the tapping mode. The typical settings of the AFM for the high-magnification observations were as follows: a free amplitude of the oscillation frequency of 280 mV, a set-point amplitude of 180–250 mV, and a scan rate of 1.0 Hz. The NanoScope image processing software was used for the image analysis.

AFM Measurements of 2D Assemblies of poly-1C on Mica

A solution of poly-**1C** in a DMSO/$CHCl_3$ mixture (1/9, v/v, 0.1 mM) was prepared and 5-fold diluted with $CHCl_3$ ([poly-**1C**] = 20 μM, DMSO/$CHCl_3$ (*ca.* 2/98, v/v)). Samples for the AFM measurements of poly-**1C** were prepared by casting 30 μL aliquots of the stock solution on a freshly cleaved mica at room temperature (ca. 25 °C), and the solvents were then slowly evaporated under a $CHCl_3$ vapor atmosphere. After poly-**1C** had been deposited on the mica, the mica substrates were exposed to $CHCl_3$ vapors at room temperature for 13 h, and the substrates were then dried under vacuum for 1 h. The organic solvent vapors were prepared by putting 1 mL of $CHCl_3$ into a 2 mL flask that was inside a 50 mL flask, and the mica substrates were then placed in the 50 mL flask. The AFM measurements were performed using a NanoScope V microscope in air at room temperature with standard silicon cantilevers

(TEPS–V2) in the tapping mode. The typical settings of the AFM for the high-magnification observations were as follows: a free amplitude of the oscillation frequency of 280 mV, a set-point amplitude of 200–250 mV, and a scan rate of 1.0 Hz. The NanoScope image processing software was used for the image analysis.

AFM Measurements of 2D Assemblies of poly-1C with $AgBF_4$ on Mica

A solution of poly-**1C** in the presence of $AgBF_4$ (1 equiv.) in a DMSO/$CHCl_3$ mixture (1/9, v/v, 0.1 mM) was prepared and 10-fold diluted with $CHCl_3$ ([poly-**1C**] = 10 μM, DMSO/$CHCl_3$ (*ca.* 1/99, v/v)). Samples for the AFM measurements of poly-**1C** were prepared by casting 30 μL aliquots of the stock solution on a freshly cleaved mica at room temperature (ca. 25 °C), and the solvents were then slowly evaporated under a $CHCl_3$ vapor atmosphere. After poly-**1C** had been deposited on the mica, the mica substrates were exposed to $CHCl_3$ vapors at room temperature for 12 h, and the substrates were then dried under vacuum for 1 h. The organic solvent vapors were prepared by putting 1 mL of $CHCl_3$ into a 2 mL flask that was inside a 50 mL flask, and the mica substrates were then placed in the 50 mL flask. The AFM measurements were performed using a NanoScope V microscope in air at room temperature with standard silicon cantilevers (TEPS–V2) in the tapping mode. The typical settings of the AFM for the high-magnification observations were as follows: a free amplitude of the oscillation frequency of 280 mV, a set-point amplitude of 200–250 mV, and a scan rate of 1.0 Hz. The NanoScope image processing software was used for the image analysis.

Molecular Modeling of the Stacked Assemblies of 1C, poly-$1C_{(n=8)}$ and poly-$1C_{(n=8)}$ Complexed with Ag(I) Ions (poly-$1C_{(n=8)}$·Ag(I)) to Form $(1C)_5$, $(\text{poly-}1C_{(n=8)})_4$ and $(\text{poly-}1C_{(n=8)}\cdot\text{Ag(I)})_4$.

The molecular modeling was performed on a Windows 7 or 10 PC with the ArgusLab software[28] or the MS modeling software (version 8.0, BIOVIA, San Diego, CA).

(1C)$_5$. The initial structure of **1C** was constructed according to the following procedures: the chiral oligoamide side chains of **1C** were replaced with –$CONHCH_3$ groups to simplify the calculations. Based on the CD spectral pattern of the assembled **1C** (Figures 1-2a and 1-S4), the twist angle between the two phenyl rings of the biphenylene moiety was set to be –45°.[29] The monomer **1C** was then allowed to manually construct a pentamer (**1C**)$_5$ so as to stack each other via intermolecular hydrogen-bonding interactions. The initial model of the stacked (**1C**)$_5$ was fully optimized by the semi-empirical molecular orbital (MO) calculations (PM6 method[30] in MOPAC2012[31]) (Figure 1-2e).

(poly-1C$_{(n=8)}$)$_4$. The initial structure of poly-**1C**$_{(n=8)}$ (8 repeating monomer units) was constructed according to the following procedures: tris(dodecyloxy)benzene groups of the chiral oligoamide side chains of poly-**1C**$_{(n=8)}$ were replaced with tris(methoxy)benzene groups to simplify the calculations. The twist angle between the two phenyl rings of the biphenylene moiety was set to be –45°.[29] The 2,6-pyridinebis(acylhydrazone) linker units were constructed in such a way to form a planar, extended W-shaped conformation based on the related crystal structure.[11,21a] The initial model of poly-**1C**$_{(n=8)}$ was fully optimized by the molecular mechanics (MM) calculations (Compass II force field[32] as implemented in the MS modeling software) (Figure 1-S9f, left). In order to estimate the molecular diameter of the self-assembled nanofiber of poly-**1C**$_{(n=8)}$, helically-stacked tetrameric poly-**1C**$_{(n=8)}$ ((poly-**1C**$_{(n=8)}$)$_4$) was constructed according to the following procedures: the energy-minimized poly-**1C**$_{(n=8)}$ was allowed to manually construct a tetramer (poly-**1C**$_{(n=8)}$)$_4$ with a twisting angle of –30º between the adjacent poly-**1C**$_{(n=8)}$ foldamers so as to helically stack each other. The initial model of (poly-**1C**$_{(n=8)}$)$_4$ was fully optimized by the MM calculations (Compass II force field) (Figure 1-S9f, right).

(poly-1C$_{(n=8)}$·Ag(I))$_4$. The initial structure of Ag(I)-bound poly-**1C**$_{(n=8)}$ (poly-**1C** $_{(n=8)}$·Ag(I)) was constructed according to the following procedures: tris(dodecyloxy)benzene groups of the chiral oligoamide side chains of poly-**1C**$_{(n=8)}$·Ag(I) were replaced with tris(methoxy)benzene groups to simplify the calculations. The twist angle between the two

phenyl rings of the biphenylene moiety was set to be –45°.[29] The U-shaped 2,6-pyridinebis(acylhydrazone) linker unit coordinating with the Ag(I) ion was constructed on the basis of the related crystal structure[11,21a] and then fully optimized by the DFT calculations using the dispersion corrected B3LYP (B3LYP-D3)[33] functional with the LANL2DZ (for the Ag(I) ion) and the 6-31G* (for H, C, N, and O atoms) basis sets in *Gaussian 16* software (Gaussian, Inc., Pittsburgh, PA).[34] Computer resources for the DFT calculations were provided by the Information Technology Center of Nagoya University. The initial model of poly-**1C**$_{(n=8)}$·Ag(I) was optimized by the MM calculations (Compass II force field) with the geometrical constraints of the Ag(I)-bound linker moieties obtained by the DFT calculations (Figure 1-S13d, left). In order to estimate the molecular diameter of the self-assembled nanofiber of poly-**1C**$_{(n=8)}$·Ag(I), helically-stacked tetrameric poly-**1C**$_{(n=8)}$·Ag(I) ((poly-**1C**$_{(n=8)}$·Ag(I))$_4$) was then constructed according to the following procedures: the energy-minimized poly-**1C**$_{(n=8)}$·Ag(I) was allowed to manually construct a tetramer (poly-**1C**$_{(n=8)}$·Ag(I))$_4$ with a twisting angle of –30º between the adjacent poly-**1C**$_{(n=8)}$·Ag(I) foldamers so as to helically stack each other. The initial model of (poly-**1C**$_{(n=8)}$·Ag(I))$_4$ was optimized by the MM calculations (Compass II force field) with the geometrical constraints of the Ag(I)-bound linker moieties (Figure 1-S13d, right).

Notes and References

(1) For recent reviews: (a) Estroff, L. A.; Hamilton, A. D. *Chem. Rev.* **2004**, *104*, 1201–1218. (b) Shimizu, T.; Masuda, M.; Minamikawa, H. *Chem. Rev.* **2005**, *105*, 1401–1444. (c) De Greef, T. F. A.; Smulders, M. M. J.; Wolffs, M.; Schenning, A. P. H. J.; Sijbesma, R. P.; Meijer, E. W. *Chem. Rev.* **2009**, *109*, 5687–5754. (d) Babu, S. S.; Praveen, V. K.; Ajayaghosh, A. *Chem. Rev.* **2014**, *114*, 1973–2129. (e) Liu, M.; Zhang, L.; Wang, T. *Chem. Rev.* **2015**, *115*, 7304–7397. (f) Yashima, E.; Ousaka, N.; Taura, D.; Shimomura, K.; Ikai, T.; Maeda, K. *Chem. Rev.* **2016**, *116*, 13752–13990.

(2) For examples, see: (a) Jin, Q.; Zhang, L.; Cao, H.; Wang, T.; Zhu, X.; Jiang, J.; Liu, M. *Langmuir* **2011**, *27*, 13847–13653. (b) Raynal, M.; Portier, F.; van Leeuwen, P. W. N. M.; Bouteiller, L. *J. Am. Chem. Soc.* 2013, **135**, 17687–17690. (c) Raynal, M.; Ballester, P.; Vidal-Ferran, A.; van Leeuwen, P. W. N. M. *Chem. Soc. Rev.* **2014**, *43*, 1660–1733. (d) Raynal, M.; Ballester, P.; Vidal-Ferran, A.; van Leeuwen, P. W. N. M. *Chem. Soc. Rev.* **2014**, *43*, 1734–1787. (e) Huerta, E.; van Genabeek, B.; Lamers, B. A. G.; Koenigs, M. M. E.; Meijer, E. W.; Palmans, A. R. A. *Chem. – Eur. J.* **2015**, *21*, 3682–3690. (f) Jiang, J.; Meng, Y.; Zhang, L.; Liu, M. *J. Am. Chem. Soc.* **2016**, *138*, 15629.

(3) (a) Qiu, H.; Inoue, Y.; Che, S. *Angew. Chem., Int. Ed.* **2009**, *48*, 3069–3072. (b) Chen, X.; Huang, Z.; Chen, S.-Y.; Li, K.; Yu, X.-Q.; Pu, L. *J. Am. Chem. Soc.* **2010**, *132*, 7297–7299. (c) Jung, J. H.; Moon, S.-J.; Ahn, J.; Jaworski, J.; Shinkai, S. *ACS Nano* 2013, **7**, 2595–2601.

(4) For recent reviews, see: (a) Jung, J. H.; Park, M.; Shinkai, S. *Chem. Soc. Rev.* **2010**, *39*, 4286–4302. (b) Qiu, H.; Che, S. *Chem. Soc. Rev.* **2011**, *40*, 1259–1268.

(5) For examples, see: (a) Phillips, K. E. S.; Katz, T. J.; Jockusch, S.; Lovinger, A. J.; Turro, N. J. *J. Am. Chem. Soc.* **2001**, *123*, 11899–11907. (b) Tsumatori, H.; Nakashima, T.; Kawai, T. *Org. Lett.* **2010**, *12*, 2362–2365. (c) Kaseyama, T.;

Furumi, S.; Zhang, X.; Tanaka, K.; Takeuchi, M. *Angew. Chem., Int. Ed.* **2011**, *50*, 3684–3687.

(6) For reviews on tubular or helical assemblies of macrocyclic compounds, see: (a) Bong, D. T.; Clark, T. D.; Granja, J. R.; Ghadiri, M. R. *Angew. Chem., Int. Ed.* **2001**, *40*, 988–1011. (b) Gong, B.; Shao, Z. F. *Acc. Chem. Res.* **2013**, *46*, 2856–2866. (c) Kim, Y.; Kim, T.; Lee, M. *Polym. Chem.* **2013**, *4*, 1300–1308. (d) Shimizu, L. S.; Salpage, S. R.; Korous, A. A. *Acc. Chem. Res.* **2014**, *47*, 2116–2127.

(7) (a) Cuccia, L. A.; Lehn, J.-M.; Homo J. C.; Schmutz, M. *Angew. Chem., Int. Ed.* **2000**, *39*, 233–237. (b) Brunsveld, L.; Meijer, E. W.; Prince, R. B.; Moore, J. S. *J. Am. Chem. Soc.* **2001**, *123*, 7978–7984. For reviews on helical oligomers (foldamers) and polymers, see: 1e and (c) Green, M. M.; Park, J.-W.; Sato, T.; Teramoto, A.; Lifson, S.; Selinger, R. L. B.; Selinger, J. V. *Angew. Chem., Int. Ed.* **1999**, *38*, 3138–3154. (d) Cheng, R. P.; Gellman, S. H.; DeGrado, W. F. *Chem. Rev.* **2001**, *101*, 3219–3231. (e) Hill, D. J.; Mio, M. J.; Prince, R. B.; Hughes, T. S.; Moore, J. S. *Chem. Rev.* **2001**, *101*, 3893–4012. (f) Nakano, T.; Okamoto, Y. *Chem. Rev.* **2001**, *101*, 4013–4038. (g) Cornelissen, J. J. L. M.; Rowan, A. E.; Nolte, R. J. M.; Sommerdijk, N. A. J. M. *Chem. Rev.* **2001**, *101*, 4039–4070. (h) Hecht, S.; Huc, I. *Foldamers: Structure, Properties, and Applications*. Wiley-VCH, Weinheim, **2007**. (i) Yashima, E.; Maeda, K.; Iida, H.; Furusho, Y.; Nagai, K. *Chem. Rev.* **2009**, *109*, 6102–6211. (j) Zhang, D.-W.; Zhao, X.; Hou, J.-L.; Li, Z.-T. *Chem. Rev.*, **2012**, *112*, 5271–5316.

(8) (a) Berl, V.; Krische, M. J.; Huc, I.; Lehn, J.-M.; Schmutz, M. *Chem. – Eur. J.* **2000**, *6*, 1938–1946. (b) Petitjean, A.; Cuccia, L. A.; Lehn, J.-M.; Nierengarten, H.; Schmutz, M. *Angew. Chem., Int. Ed.* **2002**, *41*, 1195–1198. (c) Cai, W.; Wang, G.-T.; Du, P.; Wang, R.-X.; Jiang, X.-K.; Li, Z.-T. *J. Am. Chem. Soc.* **2008**, *130*, 13450–13459. (d) Pfukwa, R.; Kouwer, P. H. J.; Rowan, A. E.; Klumperman, B.

Angew. Chem., Int. Ed. **2013**, *52*, 11040–11044. (e) Zhao, H. Q.; Sheng, S.; Hong, Y. H.; Zeng, H. Q. *J. Am. Chem. Soc.* **2014**, *136*, 14270–14276.

(9) For examples of acylhydrazone-linked polymers, see: (a) Skene, W. G.; Lehn, J.-M. P. *Proc. Natl. Acad. Sci. U. S. A.* **2004**, *101*, 8270–8275. (b) Folmer-Andersen, J. F.; Lehn, J.-M. *J. Am. Chem. Soc.* **2011**, *133*, 10966–10973.

(10) For reviews on synthetic allosteric receptors, see: (a) Rebek, Jr. J. *Acc. Chem. Res.* **1984**, *17*, 258–264. (b) Nabeshima, T. *Coord. Chem. Rev.* **1996**, *148*, 151–169. (c) Shinkai, S.; Ikeda, M.; Sugasaki, A.; Takeuchi, M. *Acc. Chem. Res.* **2001**, *34*, 494–503. (d) Kovbasyuk, L.; Krämer, R. *Chem. Rev.* **2004**, *104*, 3161–3188. (e) von Krbek, L. K. S.; Schalley, C. A.; Thordarson, P. *Chem. Soc. Rev.* **2017**, *46*, 2622–2637.

(11) For an example of a metal coordination-driven W-to-U-shaped conformational change of the related 2,6-pyridinebis(acylhydrazone) ligands, see: Ratjen, L.; Lehn, J.-M. *RSC Adv.* **2014**, *4*, 50554–50557.

(12) (a) Prince, R. B.; Okada, T.; Moore, J. S. *Angew. Chem., Int. Ed.* **1999**, *38*, 233–236. (b) Makida, H.; Abe, H.; Inouye, M. *Org. Biomol. Chem.* **2015**, *13*, 1700–1707. (c) Suzuki, Y.; Nakamura, T.; Iida, H.; Ousaka, N.; Yashima, E. *J. Am. Chem. Soc.*, **2016**, *138*, 4852–4859. (d) Horeau, M.; Lautrette, G.; Wicher, B.; Blot, V.; Lebreton, J.; Pipelier, M.; Dubreuil, D.; Ferrand, Y.; Huc, I. *Angew. Chem., Int. Ed.*, **2017**, *56*, 6823–6827.

(13) **M1** was synthesized as a model of poly-**1C** to investigate an Ag(I) coordination-driven W-to-U shape transition as well as to stress the importance of hydrogen-bond forming side chains of poly-**1C** for supramolecular polymerization to form a tubular-like nanofiber.

(14) poly-**1C** is hardly soluble in $CHCl_3$ and DMSO, but readily soluble in DMSO/$CHCl_3$ mixtures (1/9–6/4, v/v).

(15) The degree of polymerization (DP) of poly-**1C** was roughly estimated to be *ca*. 8 based on PSt standards.

(16) Berova, N.; Nakanishi, K.; Woody, R. W. *Circular dichroism: principles and applications*. (2nd Ed.), **2000**, Wiley-VCH.

(17) Storch, G.; Trapp, O. *Nat. Chem.* **2017**, *9*, 179–187.

(18) The CD and absorption spectra of **1C** in $CHCl_3$ (0.1 and 0.01 mM) after annealing at 50 °C for 10 min were less sensitive to temperature changes ranging from 25 to 50 °C, although the latter diluted solution of **1C** showed a weaker CD due to dissociation into shorter chains (Figure 1-S4b–d).

(19) The helical sense (right- or left-handed helix) of the self-assembled poly-**1C** could not be identified by AFM. For the determination of the helical handedness of helical polymers by AFM, see: (a) Sakurai, S.-i.; Okoshi, K.; Kumaki, J.; Yashima, E. *Angew. Chem., Int. Ed*. **2006**, *45*, 1245–1248. (b) Kajitani, T.; Okoshi, K.; Sakurai, S.-i.; Kumaki, J.; Yashima, E. *J. Am. Chem. Soc*. **2006**, *128*, 708–709. (c) Kumaki, J.; Sakurai, S.-i.; Yashima, E. *Chem. Soc. Rev.* **2009**, *38*, 737–746.

(20) Based on the DP of poly-**1C** (*ca*. 8) estimated by SEC and its molecular model (Figure 1-S9f), the number of poly-**1C** stacked in a 100 nm-long, supramolecular nanofiber is estimated to be *ca*. 45.

(21) (a) Dumitru, F.; Legrand, Y.-M.; Barboiu, M.; Petit, E.; van der Lee, A. *Cryst. Growth Des.* **2009**, *9*, 2917–2921. (b) Albrecht, M.; Yulia, Y.; Exarchos, A.; Nachev, P.; Fröhlich, R. *Dalton Trans.* **2009**, *36*, 7421–7427.

(22) In contrast to Zn(II) and lanthanide(III) ions, an Ag(I) ion is known to coordinate with penta-dentate ligands without an additional coordination of an apical ligand.[23] The author then chose an Ag(I) ion for further experiments.

(23) (a) Constable, E. C.; Drew, M. G. B.; Forsyth, G.; Ward, M. D. *J. Chem. Soc., Chem. Commun*. **1988**, 1450–1451. (b) Matthews, R. W.; McPartlin, M.; Scowen, I. J. *J. Chem. Soc., Dalton Trans.* **1997**, 2861–2864.

(24) The observed changes in the fiber-fiber distances by AFM are also supported by the small-angle X-ray diffraction profiles of poly-**1C**-based supramolecular polymer and its complex with Ag(I) ions (Figure 1-S14).

(25) Choi, Y.; Kang, J. *J. Incl. Phenom. Macrocycl. Chem.* **2014**, *79*, 95–102.

(26) (a) Ousaka, N.; Yamaguchi, T.; Yashima, E. *Chem. Lett.* **2014**, *43*, 512–514. (b) Zurro, M.; Asmus, S.; Beckendorf, S.; Mück-Lichtenfeld, C.; Mancheño, O. G. *J. Am. Chem. Soc.* **2014**, *136*, 13999–14002.

(27) Stone, D. A.; Tayi, A. S.; Goldberger, J. E.; Palmer, L. C.; Stupp, S. I. *Chem. Commun.* **2011**, *47*, 5702–5704.

(27) Thompson, M. ArgusLab, Planaria Software LLC, Seattle, WA (**1996**).

(28) Grein, F. *J. Phys. Chem. A* **2002**, *106*, 3823–3827.

(29) (a) Stewart, J. J. P. *J. Mol. Model.* **2007**, *13*, 1173–1213; (b) Stewart, J. J. P. *Int. J. Quantum Chem.* **1996**, *58*, 133–146.

(30) Stewart, J. J. P. MOPAC2012, Stewart Computational Chemistry, Colorado Springs, CO, USA, http://openmopac.net/ **2012**.

(31) Sun, H.; Jin, Z.; Yang, C.; Akkermans, R. L. C.; Robertson, S. H.; Spenley, N. A.; Miller, S.; Todd, S. M. *J. Mol. Model.* **2016**, *22*, 47.

(32) Grimme, S.; Antony, J.; Ehrlich, S.; Krieg, H. *J. Chem. Phys*. **2010**, *132*, 154104.

(33) Gaussian 16, Revision A.03, Frisch, M. J.; Trucks, G. W.; Schlegel, H. B.; Scuseria, G. E.; Robb, M. A.; Cheeseman, J. R.; Scalmani, G.; Barone, V.; Petersson, G. A.; Nakatsuji, H.; Li, X.; Caricato, M.; Marenich, A. V.; Bloino, J.; Janesko, B. G.; Gomperts, R.; Mennucci, B.; Hratchian, H. P.; Ortiz, J. V.; Izmaylov, A. F.; Sonnenberg, J. L.; Williams-Young, D.; Ding, F.; Lipparini, F.; Egidi, F.; Goings, J.; Peng, B.; Petrone, A.; Henderson, T.; Ranasinghe, D.; Zakrzewski, V. G.; Gao, J.; Rega, N.; Zheng, G.; Liang, W.; Hada, M.; Ehara, M.; Toyota, K.; Fukuda, R.; Hasegawa, J.; Ishida, M.; Nakajima, T.; Honda, Y.; Kitao, O.; Nakai, H.; Vreven, T.; Throssell, K.; Montgomery, Jr. J. A.; Peralta, J. E.; Ogliaro, F.; Bearpark, M. J.; Heyd, J. J.; Brothers,

E. N.; Kudin, K. N.; Staroverov, V. N.; Keith, T. A.; Kobayashi, R.; Normand, K.; Raghavachari, A. P.; Rendell, J. C.; Burant, S. S.; Iyengar, J.; Tomasi, M.; Cossi, J.; Millam, J. M.; Klene, M.; Adamo, C.; Cammi, R.; Ochterski, J. W.; Martin, R. L.; Morokuma, K.; Farkas, O.; Foresman, J. B.; Fox, D. J. Gaussian, Inc., Wallingford CT, 2016.

Supporting Data

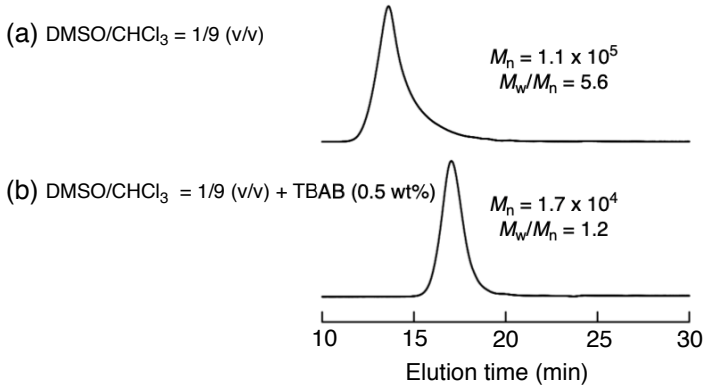

Figure 1-S1. UV (324 nm) detected SEC chromatograms of poly-**1C.** SEC conditions: column, TSKgel G4000H_{HR} (0.78 (i.d.) × 30 cm); eluent, DMSO/$CHCl_3$ (1/9, v/v) (a) and DMSO/$CHCl_3$ (1/9, v/v) containing TBAB (0.5 wt%) (b); flow rate, 0.4 mL/min; column temperature, 50 °C.

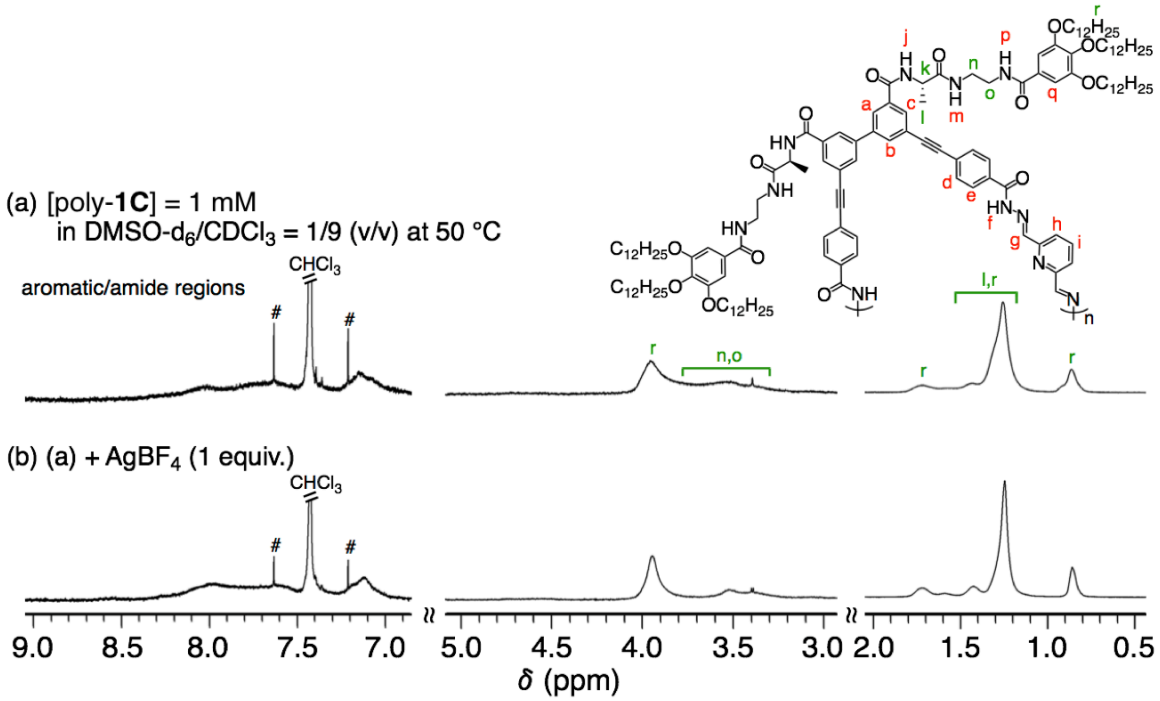

Figure 1-S2. Partial ^{1}H NMR spectra (500 MHz, DMSO-d_6/$CDCl_3$ (1/9, v/v), 1.0 mM, 50 °C) of poly-**1C** (a) and (a) + $AgBF_4$ (1 equiv.) (b). # denotes the ^{13}C satellite peaks of the solvent.

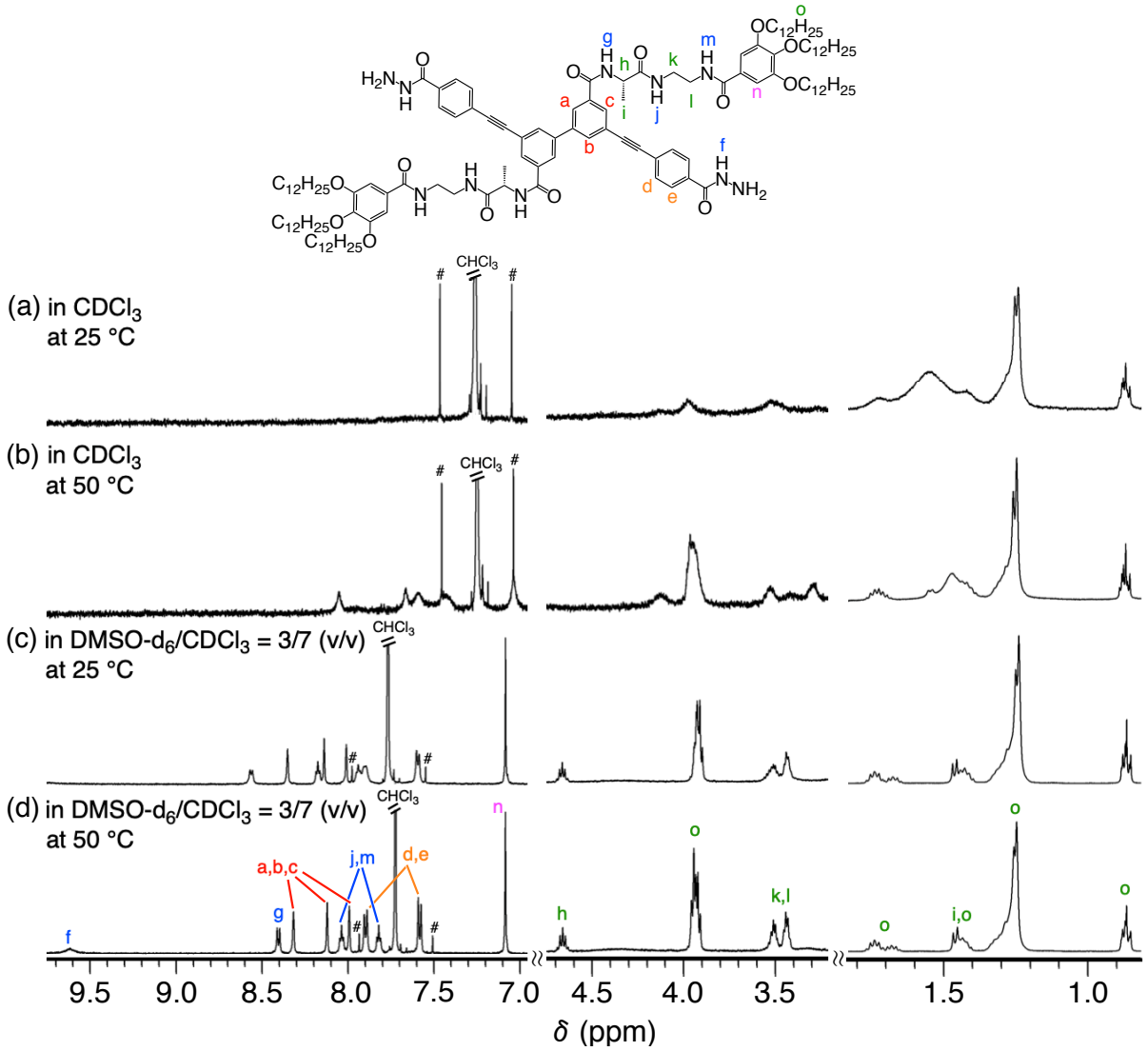

Figure 1-S3. Partial ^{1}H NMR spectra (500 MHz, 0.4 mM) of **1C** in $CDCl_3$ (a,b) at 25 (a) and 50 °C (b) and in DMSO-d_6/$CDCl_3$ (3/7, v/v) (c,d) at 25 (c) and 50 °C (d). # denotes the ^{13}C satellite peaks of the solvent.

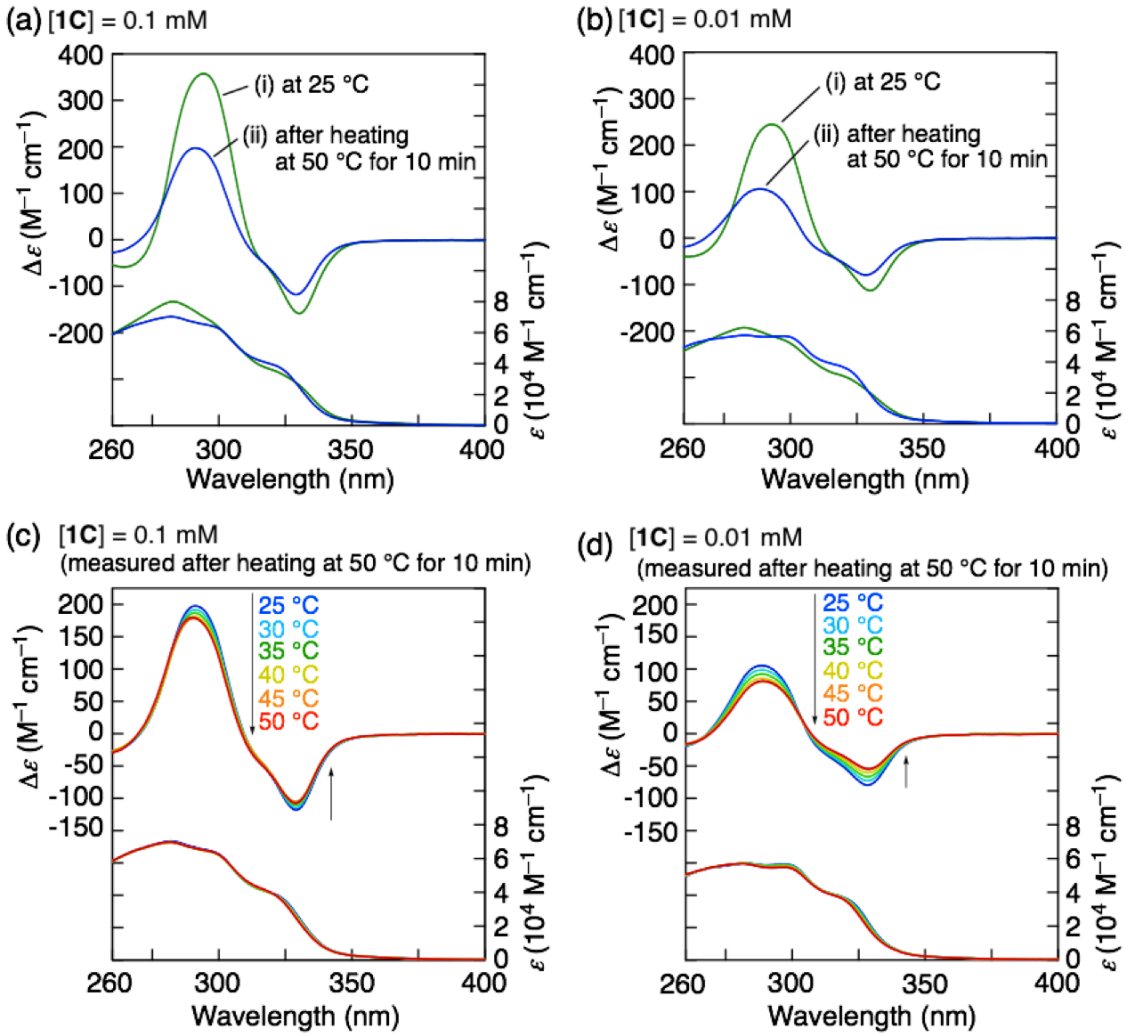

Figure 1-S4. (a) CD and absorption spectra ($CHCl_3$, 25 °C) of **1C** (0.1 mM (a), 0.01 mM (b)) before (i) and after heating at 50 °C for 10 min (ii). These measurements were performed by the following procedures; solutions of **1C** (0.1 and 0.01 mM) in $CHCl_3$ were prepared at room temperature and their CD and absorption spectra were measured at 25 °C within 30 min (i). The solutions were then heated at 50 °C for 10 min until reaching an equilibrium state. After cooling to 25 °C, the CD and absorption spectra were measured (ii). Figure 1-S4a is identical to Figure 1-2a. (c,d) Temperature-dependent CD and absorption spectral changes of **1C** (0.1 mM (c), 0.01 mM (d)) in $CHCl_3$. These measurements were carried out after heating the $CHCl_3$ solutions of **1C** at 50 °C for 10 min.

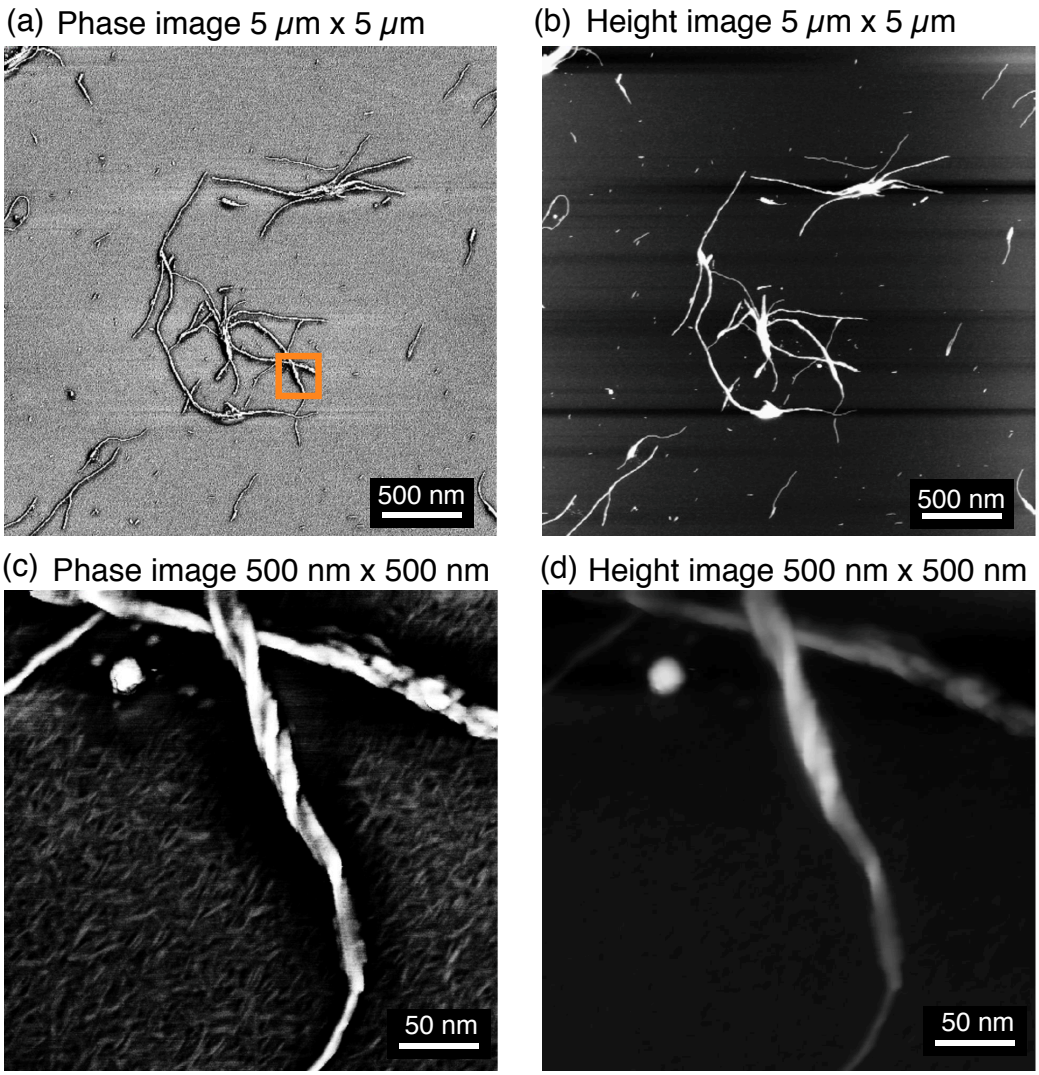

Figure 1-S5. AFM observation of **1C** on mica cast from a dilute $CHCl_3$ solution (0.02 mg mL^{-1}). AFM phase (a,c) and height (b,d) images of **1C**. The magnified AFM phase image (c) corresponds to the area indicated by the square in (a).

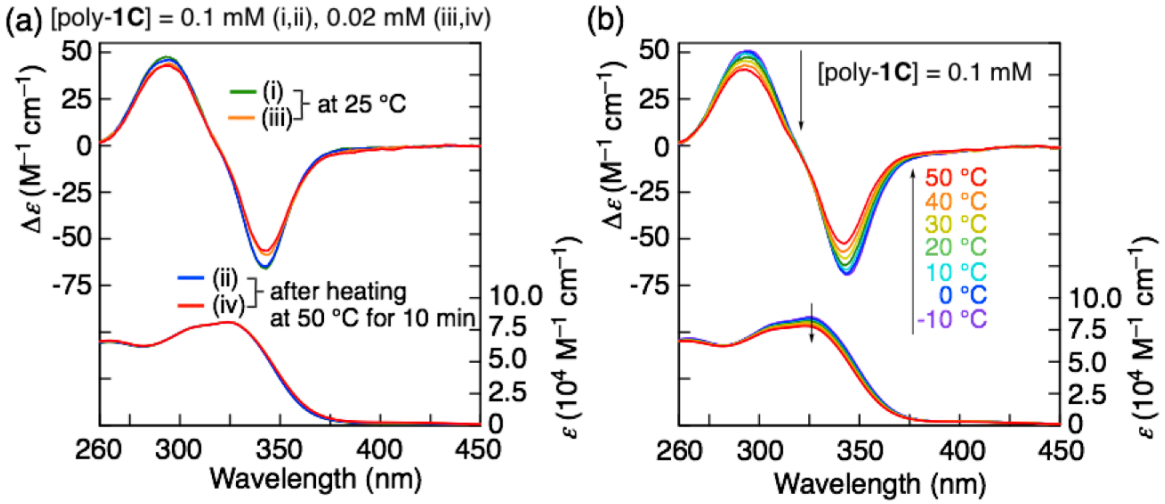

Figure 1-S6. (a) CD and absorption spectra (DMSO/$CHCl_3$ (1/9, v/v), 0.1 mM per monomer unit (i,ii), 0.02 mM per monomer unit (iii,iv), 25 °C) of poly-**1C** before (i,iii) and after heating at 50 °C for 10 min (ii,iv). Solutions of poly-**1C** (0.1 and 0.02 mM) were prepared in a DMSO/$CHCl_3$ mixture (1/9, v/v) at room temperature and their CD and absorption spectra were measured at 25 °C within 30 min (i,iii), which were then heated at 50 °C for 10 min. After cooling to 25 °C, the CD and absorption spectra were measured (ii,iv). (b) Temperature-dependent CD and absorption spectral changes (DMSO/$CHCl_3$ (1/9, v/v), 0.1 mM per monomer unit) of poly-**1C**.

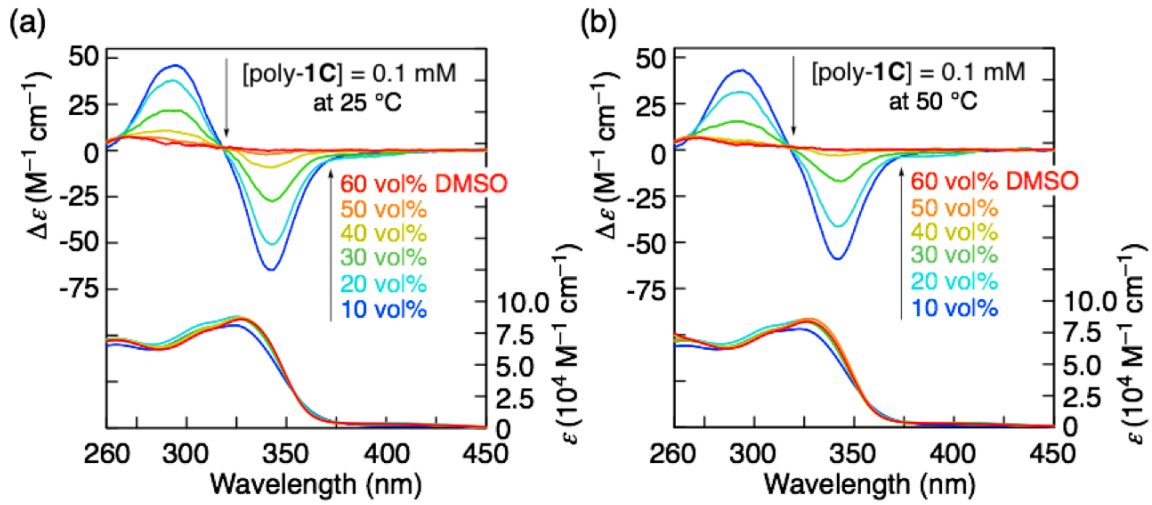

Figure 1-S7. CD and absorption spectra of poly-**1C** (0.1 mM) in various DMSO/$CHCl_3$ mixtures (v/v) at 25 (a) and 50 °C (b).

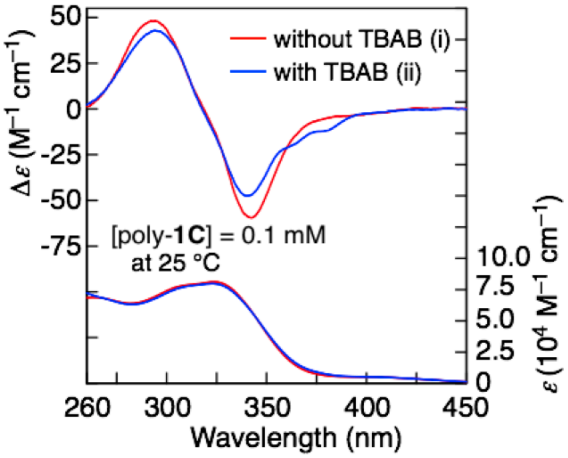

Figure 1-S8. CD and absorption spectra (0.1 mM per monomer unit, 25 °C) of poly-**1C** in DMSO/$CHCl_3$ (1/9, v/v) (i) and DMSO/$CHCl_3$ (1/9, v/v) containing TBAB (0.5 wt% (22 mM)) (ii). The CD and absorption spectra of poly-**1C** were measured at 25 °C after heating the solutions at 50 °C for 10 min.

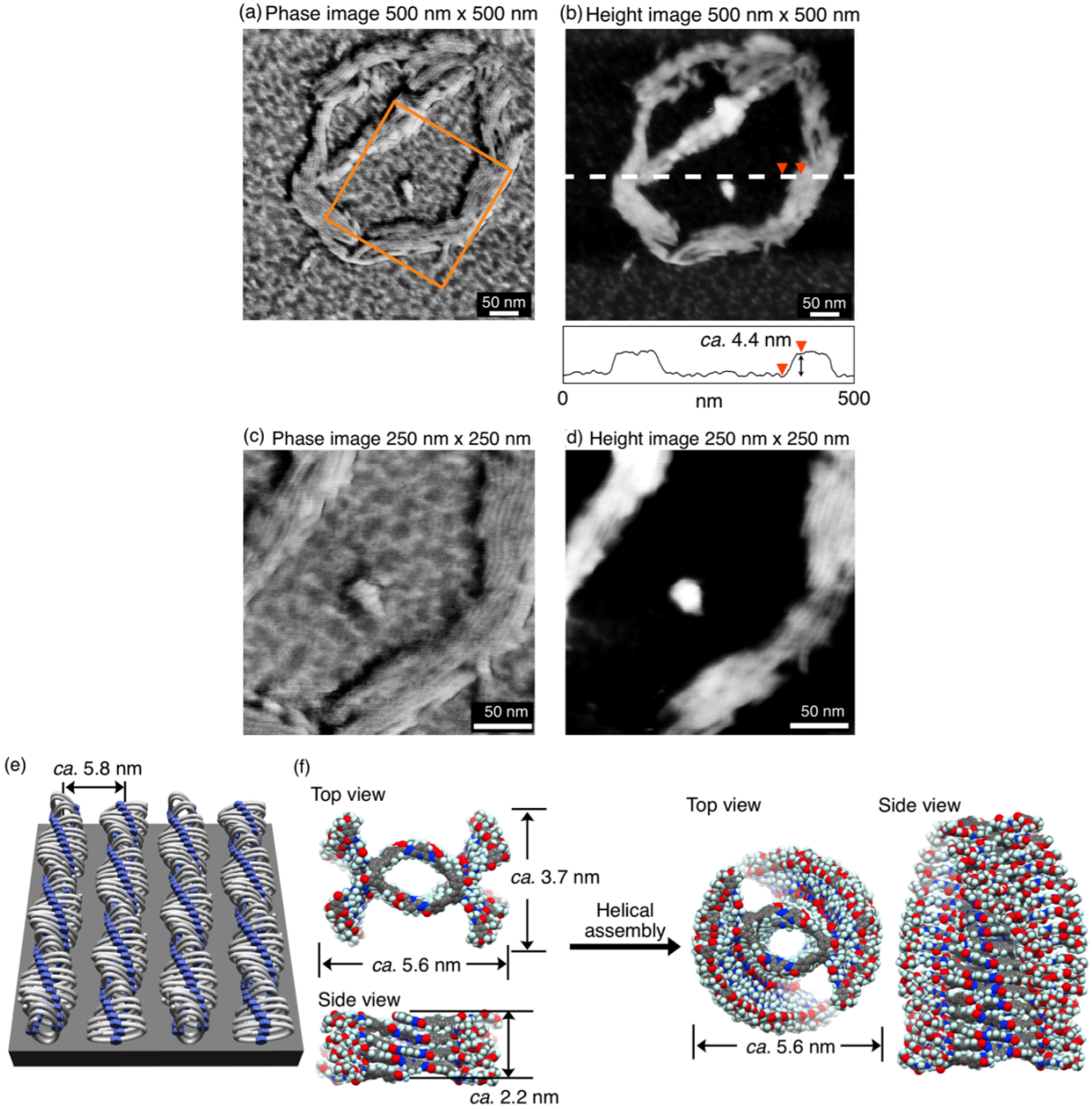

Figure 1-S9. (a-d) AFM observation of poly-**1C** on mica cast from a dilute DMSO/$CHCl_3$ (*ca.* 2/98, v/v) solution (0.04 mg mL^{-1}). AFM phase (a,c) and height (b,d) images of poly-**1C**. The cross-sectional profile denoted by the white dashed line is also shown in (b). The magnified AFM phase (c) and height (d) images correspond to the area indicated by the square in (a). (e) Schematic representation of a possible bundle structure of supramolecular helical assemblies of poly-**1C** on mica. The blue color represents the W-shaped linker units. (f) Top and side views of the molecular models of foldamer poly-$\mathbf{1C}_{(n=8)}$ (octamer of poly-**1C**) (left) and its tetrameric helical assembly ((poly-$\mathbf{1C}_{(n=8)}$)$_4$) (right). For simplicity, the dodecyloxy chains were replaced with methoxy groups.

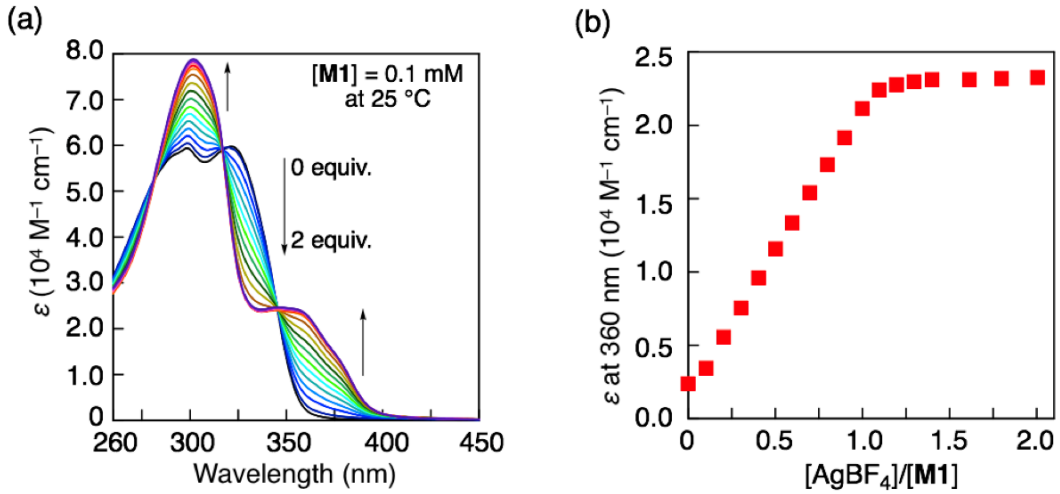

Figure 1-S10. (a) UV–vis titrations of **M1** (DMSO/$CHCl_3$ (1/9, v/v), 0.1 mM, 25 °C) with $AgBF_4$. (b) Plots of ε at 360 nm for **M1** as a function of [$AgBF_4$]/[**M1**] at 25 °C.

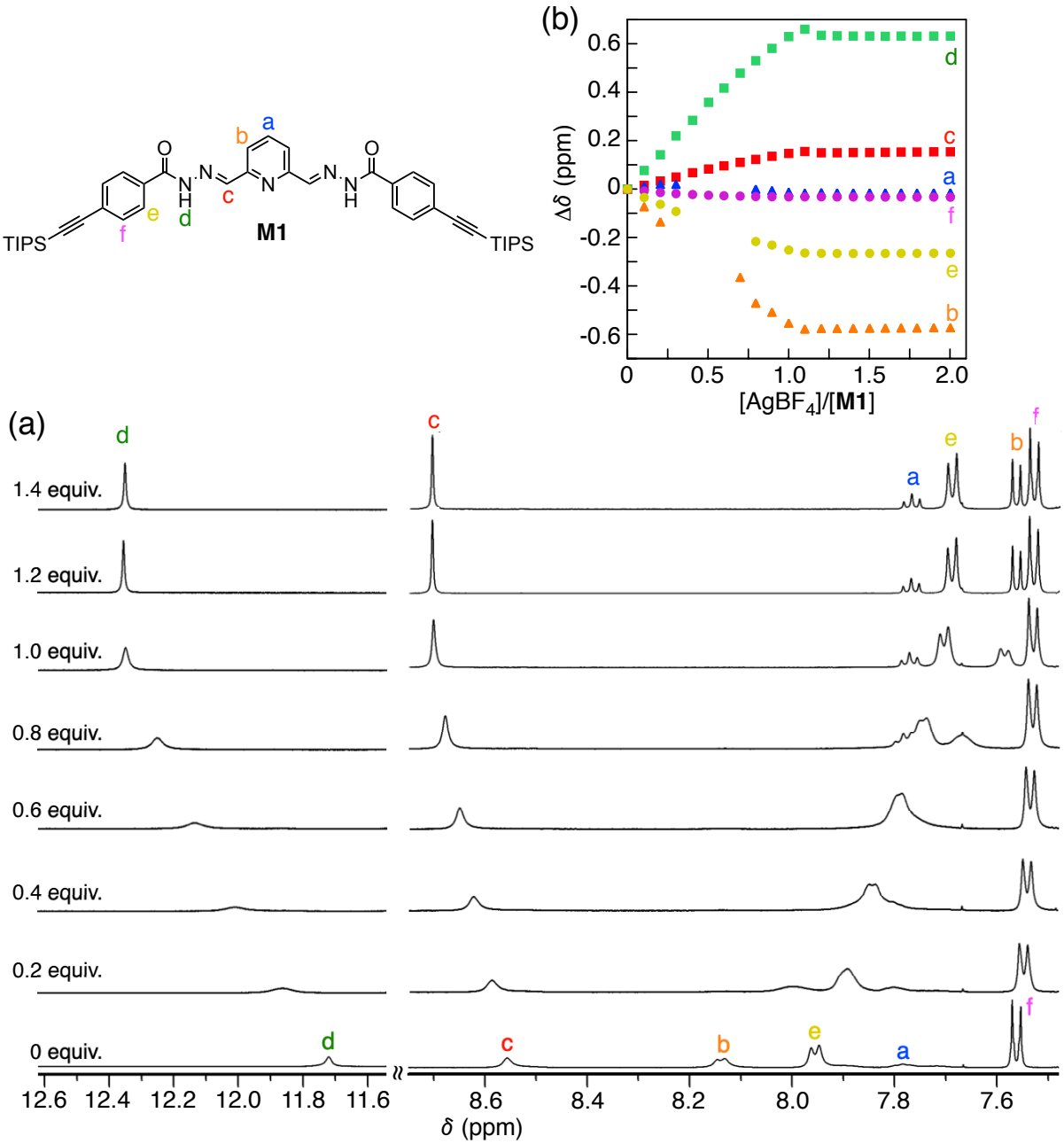

Figure 1-S11. (a) ^{1}H NMR (500 MHz, DMSO-d_6/$CDCl_3$ (1/9, v/v), 25 °C) spectral changes of **M1** (3.0 mM) in the presence of $AgBF_4$ (0–1.4 equiv.). (b) Plots of chemical shift changes ($\Delta\delta$) for **M1** as a function of [$AgBF_4$]/[**M1**].

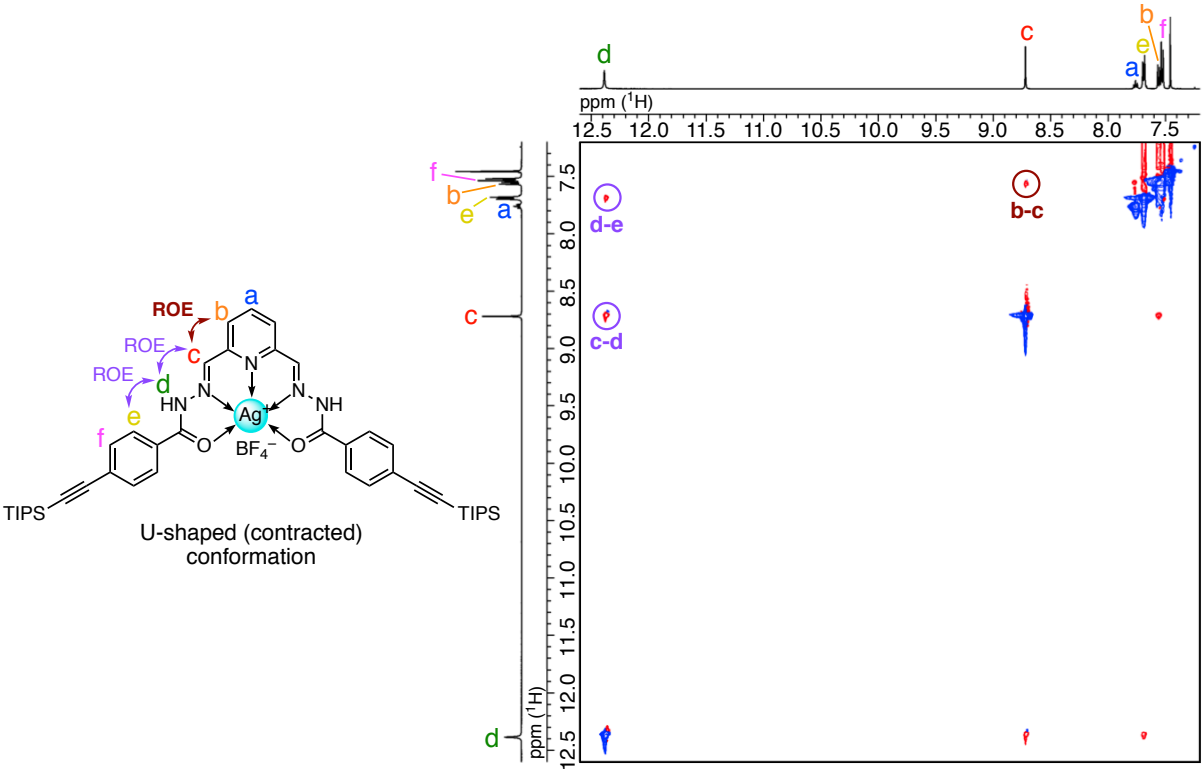

Figure 1-S12. Partial ROESY (500 MHz, 3.0 mM, DMSO-d_6/$CDCl_3$ (1/9, v/v), 25 °C, mixing time = 0.2 sec) spectrum of **M1** in the presence of 1.4 equiv. of $AgBF_4$.

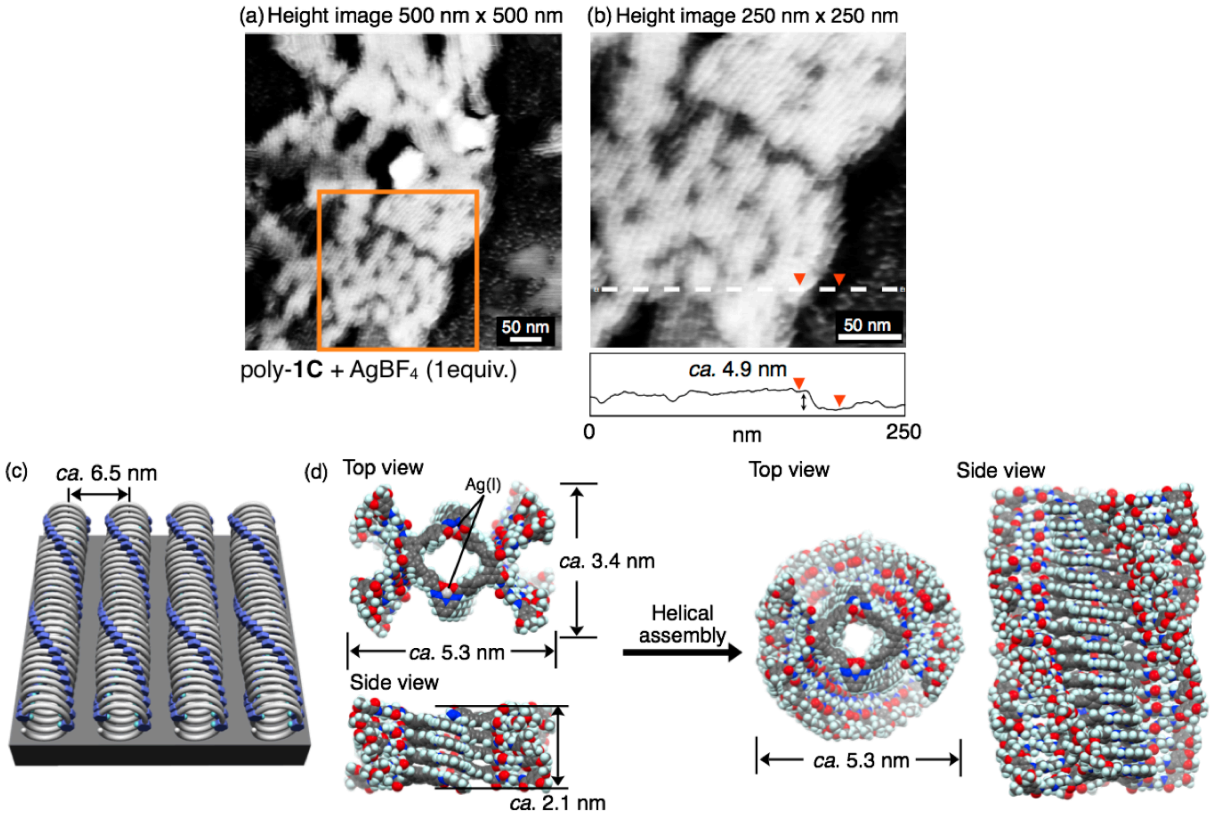

Figure 1-S13. (a,b) AFM observation of poly-**1C** in the presence of $AgBF_4$ (1 equiv.) on mica cast from a dilute DMSO/$CHCl_3$ (*ca.* 1/99, v/v) solution (0.02 mg mL^{-1}). AFM height (a,b) images of poly-**1C** in the presence of $AgBF_4$ (1 equiv.). The cross-sectional profile denoted by the white dashed line is also shown in (b). The magnified AFM height image (b) correspond to the area indicated by the square in (a). (c) Schematic representation of a possible bundle structure of supramolecular helical assemblies of poly-**1C** in the presence of $AgBF_4$ (1 equiv.) on mica. The blue color represents the U-shaped linker units. (d) Top and side views of the molecular models of Ag(I)-bound poly-$\mathbf{1C}_{(n=8)}$ (poly-$\mathbf{1C}_{(n=8)}$·Ag(I)) (left) and its tetrameric helical assembly (poly-$\mathbf{1C}_{(n=8)}$·Ag(I))$_4$ (right). For simplicity, the dodecyloxy chains were replaced with methoxy groups.

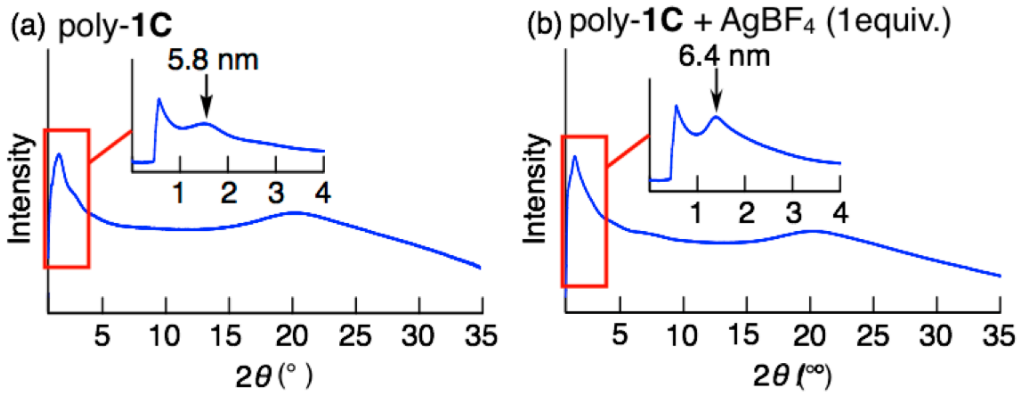

Figure 1-S14. WAXD and SAXD (inset) profiles of powder samples of poly-**1C** (a) and its complex with Ag(I) ions (b). The samples were prepared from each solution (0.1 mM per monomer unit) in DMSO/$CHCl_3$ (1/9, v/v) after evaporation of the solvents.

As anticipated, the WAXD profiles of powder samples of poly-**1C**-based supramolecular polymer and its complex with Ag(I) ions exhibited a diffuse halo in the wide-angle region (15~20°, 4–6 Å) probably due to reflections arising from the disordered side-chains and/or hydrogen-bonded stacked repeating units. On the other hand, the poly-**1C**-based supramolecular polymer and its complex with Ag(I) ions showed characteristic reflections at 5.8 and 6.4 nm, respectively, in their SAXD profiles, which are in good agreement with the fiber-fiber spacing values observed in the AFM images (5.8 and 6.5 nm, respectively; see Figures 1-3b,c, 1-S9 and 1-S13). Although these XRD profiles did not provide exact packing arrangements and helical structural information of poly-**1C**-based supramolecular polymer and its complex with Ag(I) ions, the observed XRD measurement results also support tubular-like assembled helical structures of poly-**1C**-based supramolecular polymer and its complex with Ag(I) ions as shown in Figure 1-1c.

Chapter 2

Chiral Amplification of Supramolecular Co-Assemblies of Chiral and Achiral Acylhydrazine-Functionalized Biphenyls and Their Copolymers

Abstract: An optically-active acylhydrazine-functionalized biphenyl (AHB) bearing L-alanine-derived oligoamide side chains with tris(alkoxy)phenyl residues at the periphery supramolecularly co-assembles with its achiral AHB to form a one-dimensional helical nanofiber accompanied by a modest chiral amplification (the sergeants-and-soldiers effect) through intermolecular hydrogen-bonding between the chiral/achiral oligoamide pendant units. The chiral and achiral AHBs copolymerize with 2,6-pyridinedicarboxaldehyde to form preferred-handed helical copolymers with amplification of the helical sense excess driven by intramolecular hydrogen bonds.

Introduction

Chiral amplification is a unique phenomenon and has been believed to be significantly associated with the origin of biological homochirality,[1] because a small chiral bias is significantly amplified through covalent and/or noncovalent bonding interactions, thereby generating dynamic covalent and noncovalent helical polymers with an excess one-handedness. In 1989, Green and co-workers, for the first time, reported that helical polyisocyanates with a large excess of a one-handed helical conformation can be produced by the copolymerization of achiral isocyanates with a very small amount of optically-active ones;[2] this unique phenomenon is known as the "sergeants-and-soldiers" effect. Since this discovery, a wide variety of covalent helical polymers[3–11] and noncovalent supramolecular helical polymers[12–23] with a controlled handedness has been prepared based on this universal concept.

The author previously reported that an optically-active acylhydrazine-functionalized biphenyl (AHB) (**1C**) bearing L-alanine-derived oligoamide side chains with tris(alkoxy)phenyl residues at the periphery (Figure 2-1a) formed intermolecular hydrogen-bond-driven supramolecular helical assemblies in less polar solvents, such as chloroform.[24] In addition, an optically-active homopolymer of **1C** (poly-**1C**), prepared by the polycondensation of **1C** with 2,6-pyridinedicarboxaldehyde (**3**),[25] folded into a preferred-handed helical structure, which further polymerized to afford a higher molar mass supramolecular helical polymer stabilized by end-to-end intermolecular hydrogen-bonding.[26,27]

In this study, the author synthesized an achiral AHB (**2A**) carrying glycine-derived oligoamide pendants, and investigated the sergeants-and-soldiers effect during the intermolecular hydrogen-bond-driven supramolecular co-assemblies of **1C** and **2A** in 1,1,2,2-tetrachloroethane (TCE) (Figure 2-1a,c). Furthermore, a series of copolymers of **1C** and **2A** with **3** were also prepared (poly(**1C**$_r$-*co*-**2A**$_{1-r}$), r = 0.3, 0.5, 0.7, 0.9), and amplification of the helical sense excess of the copolymers assisted by the intramolecular hydrogen bonding formation was also investigated (Figure 2-1b,d).

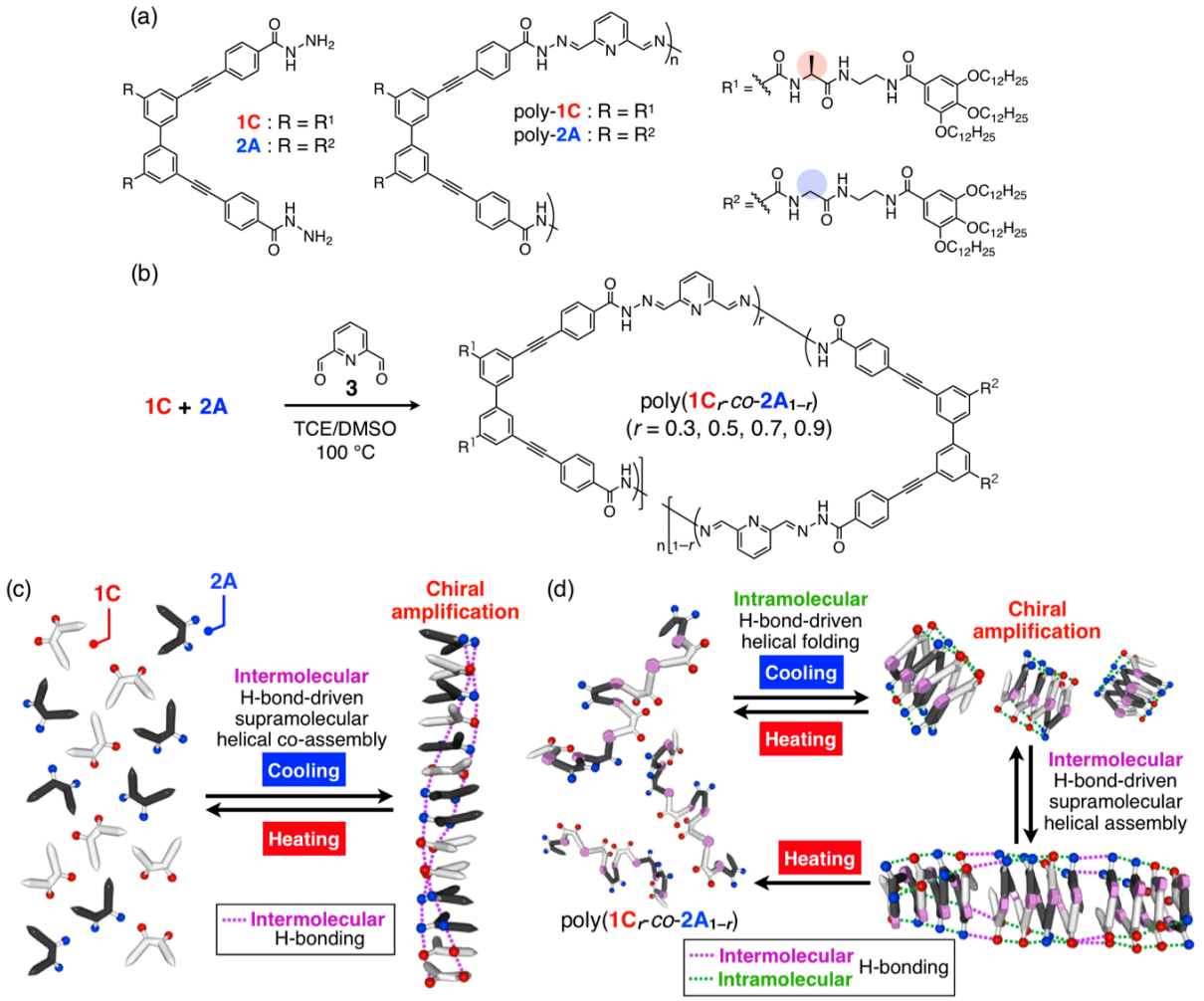

Figure 2-1. (a) Structures of **1C**, **2A**, poly-**1C**, and poly-**2A**. (b) Synthesis of poly(**1C**$_r$-*co*-**2A**$_{1-r}$) through ternary polycondensation of **1C**, **2A**, and **3**. (c) Schematic illustration of the intermolecular hydrogen-bond-driven supramolecular helical co-assemblies of **1C** and **2A** accompanied by the sergeants-and-soldiers-type chiral amplification. (d) Schematic illustration of the intramolecular hydrogen-bond-driven helical folding of poly(**1C**$_r$-*co*-**2A**$_{1-r}$) with amplification of the helical sense excess and further intermolecular hydrogen-bond-driven supramolecular helical assembly.

Results and Discussion

Prior to investigating the sergeants-and-soldiers effect in the co-assembly of **1C** and **2A**, the author examined the chiroptical property and self-assembly behavior of enantiopure **1C** in TCE. TCE was used as a solvent instead of chloroform,[24] which allowed higher-temperature spectroscopic measurements. **1C** showed a negligibly weak circular dichroism (CD) band in TCE at 110 °C, but displayed an apparent split-type Cotton effect in the π-conjugated chromophore absorption region at 50 °C. The CD intensity further increased with the decreasing temperature to –20 °C (Figure 2-2a). The observed bisignated CD signals were most likely derived from a predominantly left-handed (*M*)-twist conformation of the biphenyl unit with a dynamic axial chirality based on the exciton chirality theory, probably through the supramolecular helical assembly with a helical sense bias induced by an intermolecular hydrogen-bonding network between the L-alanine-derived oligoamide side chains as previously reported using chloroform as the solvent.[24] Such a supramolecular helical assembly of **1C** occurring at low temperatures was supported by the variable-temperature ^{1}H NMR spectral changes in TCE-d_2 from 25 to 110 °C, in which sharp proton signals were observed above 70 °C, but became considerably broadened below 50 °C (Figure 2-S1).

Figure 2-2b shows a typical atomic force microscopy (AFM) image of the self-assembled **1C** prepared by spin-casting a dilute TCE solution (0.10 mM) at ca. 25 °C on a highly oriented pyrolytic graphite (HOPG) substrate. The AFM image revealed that the self-assembled **1C** formed sub-micrometer length supramolecular nanofibers with a height of approximately 4.0 – 4.1 nm (Figure 2-2b), which was in good agreement with that of the computer-generated supramolecular polymer structure of **1C** (ca. 3.8 nm) (Figure 2-S2c).

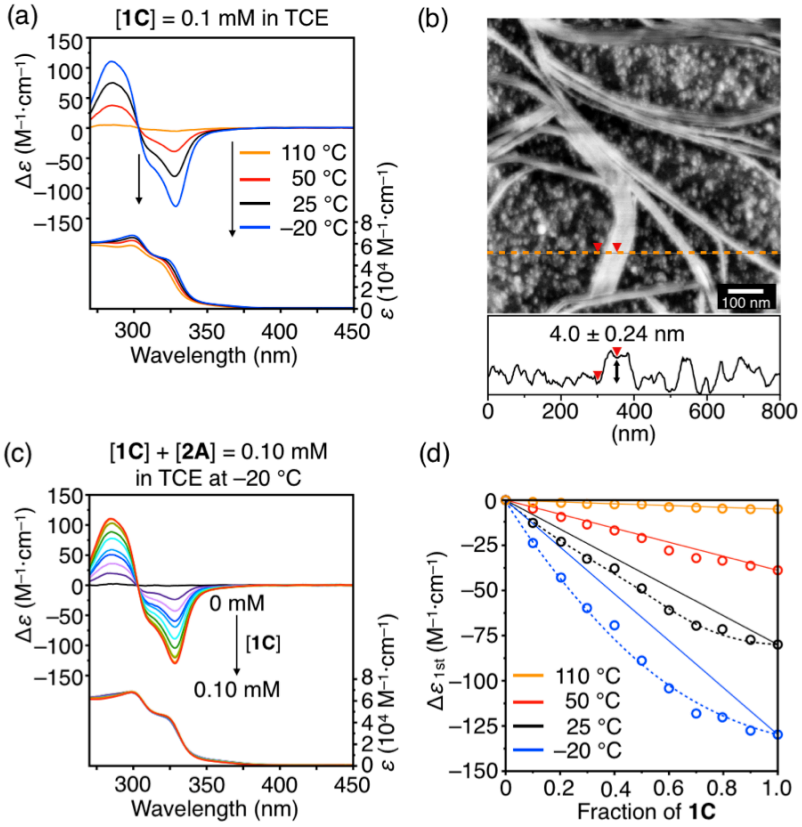

Figure 2-2. (a) Temperature-dependent CD and absorption spectral changes of **1C** (0.10 mM) in TCE. (b) AFM height image of self-assembled nanofibers formed from **1C**. AFM image was observed on HOPG cast from TCE solution (0.10 mM). The cross-sectional profile denoted by an orange dashed line is also shown in (b). (c) CD and absorption spectra of a mixture of **1C** and **2A** with various molar ratios ([**1C**] + [**2A**] = 0.10 mM) in TCE at –20 °C. (d) Plots of the first Cotton intensity ($\Delta\varepsilon_{1st}$) at 328 nm of the **1C**/**2A** mixture in TCE at –20 (blue circles), 25 (black circles), 50 (red circles), and 110 (orange circles) °C versus the mole fraction of **1C** versus the mole fraction of **1C**.

The author then investigated the sergeants-and-soldiers effect during the co-assembly process of **1C** and **2A** driven by intermolecular hydrogen bonding interactions by measuring the variable-temperature CD spectral changes of a mixture of **1C** and **2A** at different molar ratios (Figures 2-2c,d and 2-S3). The first Cotton effect ($\Delta\varepsilon_{1st}$) intensity of the **1C**/**2A** mixtures in TCE at –20 and 25 °C nonlinearly increased with an increase in the molar fraction of **1C** (Figures 2-2c,d and 2-S3a), indicating that the sergeants-and-soldiers effect is operative during the dynamic helical co-assembly of chiral **1C** and achiral **2A** at –20 and 25 °C. The CD spectral patterns of the chiral/achiral co-assembled polymers were virtually the same as that of the supramolecular helical homopolymer of the enantiopure **1C** (Figure 2-2a,c), indicating that the achiral **2A** co-assembled with **1C**, thereby forming supramolecular helical copolymers, in which axially chiral biphenyl units of achiral **2A** are also twisted with an excess twist-sense as those of **1C** (for the AFM observations of supramolecular nanofibers prepared from an equimolar mixture of **1C** and **2A**, see Figure 2-S2b).

As anticipated, the degree of chiral amplification significantly decreased at the higher temperatures (50 and 110 °C) (Figures 2-2d and 2-S3b,c) or by adding polar dimethyl sulfoxide (DMSO) as a co-solvent (Figure 2-S4) due to dissociation of the helically co-assembled **1C** and **2A** into the monomers at high temperatures or in the presence of the hydrogen-bond disrupting DMSO. These results indicated the primary importance of intermolecular hydrogen bonding network formations between the chiral/achiral AHBs for promoting the supramolecular helical co-assembly.

Table 2-1 Polymerization results of **1C** and/or **2A** with **3** in TCE/DMSO (1/1, v/v) at 100 °C for 12 h[a]

Entry	Monomer in feed		Polymer					
	1C (mol%)	**2A** (mol%)	Sample code	Yield[b] (%)	M_n[c] (10^4)	M_w/M_n[c]	$DP_{n,NMR}$[d]	**1C**[d] (mol%)
1	0	100	poly-**2A**	33	1.3	1.2	7.8	0
2	30	70	poly(**1C**$_{0.3}$-*co*-**2A**$_{0.7}$)	43	1.2	1.2	7.8	28
3	50	50	poly(**1C**$_{0.5}$-*co*-**2A**$_{0.5}$)	55	1.2	1.2	7.8	47
4	70	30	poly(**1C**$_{0.7}$-*co*-**2A**$_{0.3}$)	62	1.1	1.2	7.8	71
5	87	13	poly(**1C**$_{0.9}$-*co*-**2A**$_{0.1}$)	56	1.3	1.3	7.7	87
6	100	0	poly-**1C**	24	1.1	1.2	7.8	100

[a] [**1C**] + [**2A**] = [**3**] = 30 mM. [b] Isolated yield after the purification by SEC. [c] Determined by SEC (polystyrene standards) with TCE/DMSO (90/10, v/v) containing TBAB (0.5 wt%) as the eluent. [d] Estimated by ^{1}H NMR analysis in $CDCl_3$/DMSO-d_6 (1/1, v/v) at 50 °C.

The sergeants-and-soldiers-type chiral amplification during the copolymerization of **1C** and **2A** with **3** was then investigated. A series of copolymers was synthesized by the ternary polycondensation of **1C**,

2A, and **3** at different feed monomer ratios in TCE/DMSO at 100 °C for 12 h according to our previously reported procedure (Figure 2-1b),[24] affording optically-active copolymers (poly(**1C**$_r$-*co*-**2A**$_{1-r}$); r = 0.3, 0.5, 0.7, 0.9) (Table 2-1). The chiral/achiral molar ratios in the copolymers were confirmed to be nearly equal to those in the feed by ^{1}H NMR analysis. For comparison, optically-active (poly-**1C**) and optically-inactive (poly-**2A**) homopolymers were also prepared in the same way. The number-average molar masses, M_n, of the resulting homo- and copolymers were estimated to be more than 1.1×10^4 by size-exclusion chromatography (SEC) using a TCE/DMSO mixture (90/10, v/v) containing tetra-*n*-butylammonium bromide (TBAB) (0.5 wt%) as the eluent (Table 2-1 and Figure 2-S5b).

In contrast to the noncovalent supramolecular helical system with **1C** and **2A** described above, no chiral amplification was observed for the copolymers of **1C** and **2A** in TCE at –20

– 110 °C, giving an almost linear relationship between the CD intensity ($\Delta\varepsilon_{1st}$) and the molar fractions of the **1C** unit (Figures 2-3a,d and 2-S6). Unexpectedly, when a small amount of polar DMSO was used as a co-solvent in TCE (TCE/DMSO = 90/10, v/v), poly(**1C**$_r$-*co*-**2A**$_{1-r}$) showed a moderate, but apparent chiral amplification below 50 °C (Figures 2-3b,e and 2-S7). In the presence of an increasing amount of DMSO (20 – 40 vol% in TCE), however, the CD intensity significantly decreased, showing an almost linear relationship mostly due to a large amount of polar DMSO, which hampers intramolecular hydrogen bonding along the copolymer backbones (Figure 2-S8).

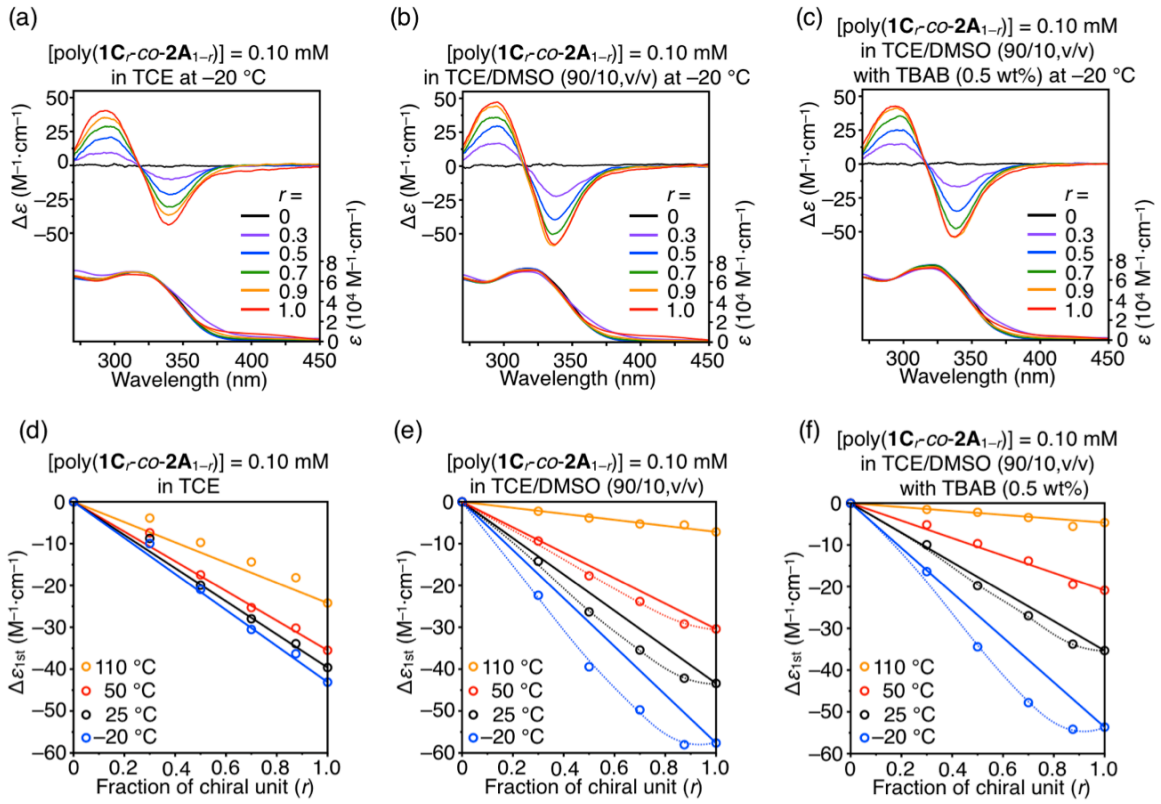

Figure 2-3. (a–c) CD and absorption spectra of poly(**1C**$_r$-*co*-**2A**$_{1-r}$) in TCE (a) and TCE/DMSO (90/10, v/v) in the absence (b) and presence (c) of TBAB (0.5 wt% (22 mM)) at –20 °C. (d–f) Plots of the first Cotton intensity ($\Delta\varepsilon_{1st}$) at 338 nm of poly(**1C**$_r$-*co*-**2A**$_{1-r}$) in TCE (d) and TCE/DMSO (90/10, v/v) in the absence (e) and presence (f) of TBAB (0.5 wt% (22 mM)) at –20 (blue circles), 25 (black circles), 50 (red circles), and 110 (orange circles) °C versus the content of the **1C**-based chiral monomer unit. [polymer] = 0.10 mM (calculated based on the monomer units).

As previously reported,[24] poly-**1C** self-assembled to form a higher molar mass supramolecular helical polymer in a chloroform/DMSO mixture (90/10, v/v) at 25 °C, which dissociated into single poly-**1C** chains in the presence of TBAB as supported by SEC analysis, while the CD signals remained almost unchanged. As shown in Figure 2-S5, similar supramolecular polymer formations and further TBAB-triggered dissociations were also observed for the copolymers of poly(**1C**$_r$-*co*-**2A**$_{1-r}$) in a TCE/DMSO mixture (90/10, v/v) at 25 °C as evidenced by the SEC chromatograms in the absence and presence of TBAB. The variable-temperature CD spectra of the copolymers were then measured in TCE/DMSO (90/10, v/v) in the presence of TBAB (Figures 2-3c,f and 2-S9). The CD intensities of the copolymers tended to slightly decrease in the presence of TBAB (Figure 2-3e,f), but exhibiting an almost similar amplification of the helical sense excess within the temperature range. These results suggest that the copolymers maintained their preferred-handed helical structures in the assembled and molecularly dispersed states in a specific solvent mixture, such as a TCE/DMSO mixture (90/10, v/v). As a result, the chiral amplification of the copolymers was achieved assisted by the intramolecular hydrogen bonding rather than the interchain interaction through supramolecular polymer formations. The author speculates that an appropriate amount of DMSO would prevent or destabilize the undesired intramolecular hydrogen bonding irregularly or randomly formed along the poly(**1C**$_r$-*co*-**2A**$_{1-r}$) chains, thereby forming an energetically-favorable helical conformation with a higher helix-sense excess being responsible for the observed modest sergeants-and-soldiers effect in the covalent polymer system.

On the other hand, no chiral amplification of the macromolecular helicity took place for the mixtures of the homopolymers, poly-**1C** and poly-**2A**, in TCE (Figures 2-4a,c and 2-S10) and TCE/DMSO (90/10, v/v) (Figures 2-4b,d and 2-S11) even at –20 °C, indicating that the interchain interactions through intermolecular hydrogen bonding hardly contribute to the helical sense bias toward the achiral or dynamically racemic helical poly-**2A** chains. The possibility that poly-**1C** and poly-**2A** self-assemble to form supramolecular homo-aggregates

in a self-sorting manner could not be completely excluded.[28]

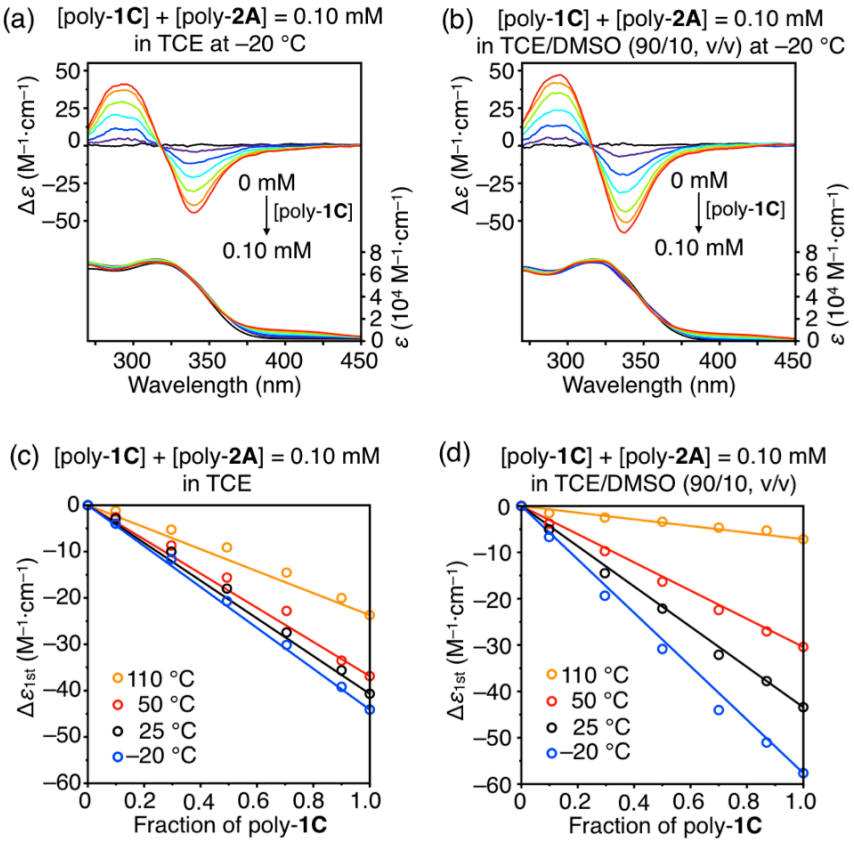

Figure 2-4. (a,b) CD and absorption spectra of a mixture of poly-**1C** and poly-**2A** with various molar ratios ([poly-**1C**] + [poly-**2A**] = 0.10 mM per monomer unit) in TCE (a) and TCE/DMSO (90/10, v/v) (b) at –20 °C. (c,d) Plots of the first Cotton intensity ($\Delta\varepsilon_{1st}$) at 328 nm of the poly-**1C**/poly-**2A** mixture in TCE (c) and TCE/DMSO (90/10, v/v) (d) at –20 (blue circles), 25 (black circles), 50 (red circles), and 110 (orange circles) °C versus the mole fraction of poly-**1C**.

Conclusions

In summary, the author has reported the sergeants-and-soldiers-type chiral amplification during the intermolecular hydrogen-bond-driven supramolecular co-assemblies of optically-active and -inactive AHBs carrying L-alanine- and glycine-derived oligoamide pendants, respectively, affording a one-dimensional helical nanofiber. The helical sense excess of the chiral/achiral AHB-based covalent copolymers was also amplified through the intramolecular hydrogen bonds followed by helical assembly of the copolymers via intermolecular hydrogen bonding network formations. The author believes that the present supramolecular helical systems will contribute to the development of novel chiral materials for sensing of chiral molecules by taking advantage of the chiroptical changes accompanied by structural alterations of the covalent and noncovalent helical polymers through noncovalent interactions with chiral guests.[29,30]

Experimental Section

Instruments. The melting points were measured on a Yanako melting point apparatus (Yanako, Kyoto, Japan) and were uncorrected. The IR spectra were recorded on a JASCO FT/IR-680 spectrophotometer (JASCO, Tokyo, Japan). The NMR spectra were measured using a Bruker Ascend 500 (Bruker Biospin, Billerica, MA) or a Varian 500AS (Varian, Palo Alto, CA) spectrometer operating at 500 MHz for ^{1}H and 126 MHz for ^{13}C using tetramethylsilane (TMS) or a solvent residual peak as the internal standard. The absorption and CD spectra were measured in 0.020-, 0.20-, or 1.0-cm quartz cell on a JASCO V-750 spectrophotometer and a JASCO J-1500 spectropolarimeter, respectively. The electrospray ionization (ESI) mass spectra were recorded using a JEOL JMS-T100CS mass spectrometer (JEOL, Akishima, Japan). The size exclusion chromatography (SEC) measurements were performed with a JASCO PU-4185 liquid chromatograph equipped with an UV-visible detector (338 nm, JASCO MD-4010) and a column oven (JASCO CO-2060). The number-average molar mass (M_n) and its distribution (M_w/M_n) were determined at 25 °C using a TSKgel G4000H$_{HR}$ (0.78 (i.d.) × 30 cm) SEC column (Tosoh, Tokyo, Japan), and 1,1,2,2-tetrachloroethane (TCE)/dimethyl sulfoxide (DMSO) (90/10, v/v) with 0.5 wt% tetra-*n*-butylammonium bromide (TBAB) was used as the eluent at a flow rate of 0.3 mL/min. The molar mass calibration curve was obtained with polystyrene standards (Tosoh). The atomic force microscopy (AFM) measurements were performed using a Nanoscope V microscope (Bruker AXS, Santa Barbara, CA) in air at room temperature with standard cantilevers (TESP–V2, Bruker AXS) in the tapping mode.

Materials. All starting materials were purchased from commercial suppliers and were used without further purification unless otherwise noted. *N*-(2-Aminoethyl)-3,4,5-tris(dodecyloxy)benzamide (**4**), **7**, **9**, **1C**, and poly-**1C** were prepared according to the literature.[24,31]

Synthetic Procedures

Abbreviations of chemicals:

Boc: *tert*-butoxycarbonyl,

EDC·HCl: 1-ethyl-3-(3-dimethylaminopropyl)-carbodiimide hydrochloride,

HOBt·H_2O: 1-hydroxybenzotriazole monohydrate,

$^{i}Pr_2NH$: diisopropylamine,

NMM: *N*-methylmorpholine.

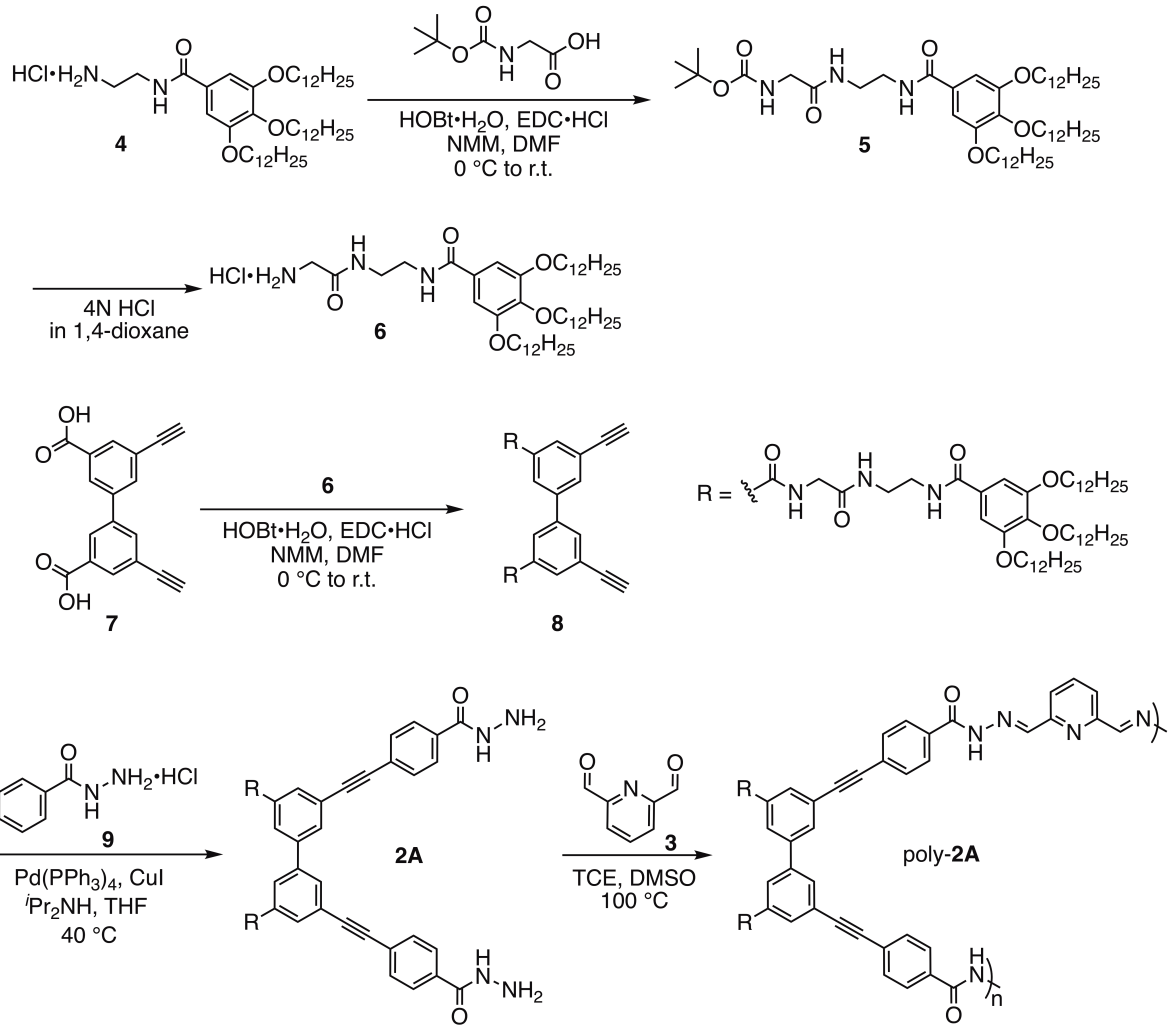

Scheme 2-S1. Synthesis of **2A** and poly-**2A**.

Synthesis of 5. To a mixture of **4** (501 mg, 666 μmol), Boc-glycine (139 mg, 734 μmol), and HOBt·H_2O (228 mg, 863 μmol) in DMF (10 mL) was added EDC·HCl (129 mg, 674 μmol) at 0 ºC under nitrogen, and the reaction mixture was stirred at 0 °C for 1 h. After NMM (75.1 μL, 683 mmol) was added to this at 0 ºC, the reaction mixture was stirred at 0 ºC for 30 min and further at room temperature for 22 h. After evaporating the solvent under reduced pressure, the residue was dissolved in $CHCl_3$ and the solution was washed with 1N aqueous HCl, 5% aqueous $NaHCO_3$, and brine, dried over $MgSO_4$, filtered, and evaporated to dryness under reduced pressure, affording **5** (487 mg, 84%) as a white solid. Mp: 86.1–87.0 °C. ^{1}H NMR (500 MHz, $CDCl_3$/DMSO-d_6 (9/1, v/v), 25 °C): δ 8.19 (br, 1H, NH) , 7.75 (br, 1H, NH), 7.12 (s, 2H, Ar–H), 6.39 (br, 1H, NH), 4.01 (t, J = 6.3 Hz, 4H, OCH_2), 3.94 (t, J = 6.5 Hz, 2H, OCH_2), 3.69 (d, J = 5.0 Hz 2H, NCH_2CO), 3.44-3.39 (m, 4H, NCH_2), 1.82-1.67 (m, 6H, CH_2), 1.51-1.26 (m, 63H, CH_2, CH_3), 0.88 (t, J = 6.8 Hz, 9H, CH_3). ^{13}C NMR (126 MHz, $CDCl_3$/DMSO-d_6 (9/1, v/v), 25 °C): δ 170.23, 166.95, 155.88, 152.46, 140.08, 129.26, 105.71, 78.79, 72.96, 68.74, 43.87, 39.00, 31.62, 30.07, 29.46, 29.42, 29.40, 29.36, 29.33, 29.29, 29.15, 29.13, 29.08, 29.05, 28.26, 25.91, 25.84, 22.40, 14.01. IR (KBr, cm^{-1}): 3290 (ν_{N-H}), 1687 ($\nu_{C=O}$), 1656 ($\nu_{C=O}$), 1580 (ν_{N-H}), 1542 (ν_{N-H}). HRMS (ESI-MS): m/z calcd for $[M(C_{52}H_{95}N_3O_7) + Na]^+$, 896.7068; found 896.7065.

Synthesis of 6. Into a two-neck round bottom flask containing **5** (400 mg, 458 mmol) was added 4N HCl in 1,4-dioxane (10 mL) at 0 ºC under nitrogen, and the reaction mixture was stirred at 0 ºC for 7 h. After evaporating the solvent under reduced pressure, the residue was washed with Et_2O to afford **6** (317 mg, 91%) as a white solid. Mp: 208.2–210.0 °C. ^{1}H NMR (500 MHz, $CDCl_3$/DMSO-d_6 (9/1, v/v), 25 °C): δ 8.79 (t, J = 4.9 Hz, 1H, NH), 8.42 (t, J = 5.8 Hz, 1H, NH), 8.37 (s, 3H, NH_3^+), 7.29 (s, 2H, Ar–H), 4.07 (t, J = 6.3 Hz, 6H, OCH_2), 3.96 (t, J = 6.5 Hz, 6H, OCH_2), 3.69 (br, 2H, NCH_2CO), 3.60 (br, 2H, NCH_2), 3.46 (br, 2H, NCH_2), 1.82-1.69 (m, 6H, CH_2), 1.50-1.47 (m, 6H, CH_2), 1.46-1.26 (m, 48H, CH_2), 0.88 (t, J = 6.9 Hz, 9H, CH_3). ^{13}C NMR (126 MHz, $CDCl_3$/DMSO-d_6 (9/1, v/v), 25 °C): δ 170.62, 167.62, 152.77, 140.60, 129.25, 105.85, 73.30, 69.07, 44.11, 39.48, 31.84, 31.82, 30.24, 29.65, 29.62, 29.60,

29.58, 29.55, 29.54, 29.49, 29.32, 29.31, 29.28, 29.26, 28.31, 26.06, 26.01, 22.59, 22.57, 22.55, 14.08, 14.04. IR (KBr, cm^{-1}): 3294 (ν_{N-H}), 1687 ($\nu_{C=O}$), 1635 ($\nu_{C=O}$), 1581 (ν_{N-H}), 1540 (ν_{N-H}). HRMS (ESI-MS): *m*/*z* calcd for $[M(C_{47}H_{87}N_3O_5) + Na]^+$, 796.6543; found 796.6546.

Synthesis of 8. To a mixture of **6** (283 mg, 349 μmol), **7** (48.1 mg, 166 μmol), and HOBt·H_2O (54.6 mg, 357 μmol) in DMF (10 mL) was added EDC·HCl (56.3 mg, 341 μmol) at 0 ºC under nitrogen, and the reaction mixture was stirred at 0 °C for 1 h. After NMM (40.2 μL, 366 μmol) was added to this at 0 ºC, the reaction mixture was stirred at 0 ºC for 30 min and further at room temperature for 21 h. After evaporating the solvent under reduced pressure, the residue was dissolved in $CHCl_3$ and the solution was washed with 1N aqueous HCl, 5% aqueous $NaHCO_3$, and brine, dried over $MgSO_4$, filtered, and concentrated under reduced pressure. The crude product was purified by column chromatography (SiO_2, MeOH/$CHCl_3$ (1/9, v/v)) to afford **8** (214 mg, 71%) as a slightly yellowish solid. Mp: 200.2–201.4 °C. ^{1}H NMR (500 MHz, $CDCl_3$/DMSO-d_6 (7/3, v/v), 25 °C): δ 8.88 (t, J = 5.8 Hz, 2H, NH), 8.31 (s, 2H, Ar–H), 8.22 (t, J = 5.3 Hz, 2H, NH), 8.08 (s, 2H, Ar–H), 8.02 (t, J = 5.4Hz, 2H, NH), 7.95 (s, 2H, Ar–H), 7.10 (s, 4H, Ar–H), 4.03 (d, J = 5.8 Hz, 4H, NCH_2CO), 3.96 (t, J = 6.3 Hz, 8H, OCH_2), 3.92 (t, J = 6.5 Hz, 4H, OCH_2), 3.52 (s, 2H, C≡CH), 3.49-3.40 (m, 8H, NCH_2), 1.78-1.66 (m, 12H, CH_2), 1.47-1.41 (m, 12H, CH_2), 1.25 (br, 96H, CH_2), 0.89-0.86 (m, 18H, CH_3). ^{13}C NMR (126 MHz, $CDCl_3$/DMSO-d_6 (7/3, v/v), 25 °C): δ 170.01, 167.21, 166.21, 152.57, 140.23, 140.23, 139.33, 135.27, 132.71, 130.80, 129.27, 126.54, 122.99, 105.92, 82.64, 79.61, 73.07, 68.82, 43.51, 39.36, 31.75, 31.73, 30.20, 29.57, 29.56, 29.54, 29.52, 29.49, 29.47, 29.46, 29.41, 29.26, 29.19, 29.17, 26.02, 25.95, 22.50, 14.10. IR (KBr, cm^{-1}): 3310 (ν_{N-H}), 1638 ($\nu_{C=O}$), 1544 (ν_{N-H}). HRMS (ESI-MS): *m*/*z* calcd for $[M(C_{112}H_{180}N_6O_{12}) + Na]^+$, 1824.3557; found 1824.3559.

Synthesis of 2A. Into a two-neck round bottom flask containing **8** (211 mg, 117 μmol) and **9** (181 mg, 606 μmol) was added dry THF (10 mL) under argon. After dissolving, the solution was frozen by liq. nitrogen and degassed by three freeze-pump-thaw cycles. After the flask was warmed to 0 °C, to this were added $Pd(PPh_3)_4$ (4.15 mg, 3.59 μmol), CuI (1.12 mg, 5.88

μmol), and degassed $^{i}Pr_2NH$ (2.0 mL) under argon, and the solution was gradually warmed to room temperature. The reaction mixture was stirred at room temperature for 30 min and further at 40 °C for 18 h. After cooling to room temperature, to this was added excess MeOH (100 mL) and the precipitate was collected by filtration and washed with MeOH, affording **2A** (182 mg, 75%) as a brown solid. Mp: 267 °C (dec.). ^{1}H NMR (500 MHz, $CDCl_3$/DMSO-d_6 (7/3, v/v), 50 °C): δ 9.62 (br, 2H, NH), 8.70 (t, J = 5.5 Hz, 2H, NH), 8.34 (s, 2H, Ar–H), 8.14 (s, 2H, Ar–H), 8.10 (t, J = 5.0 Hz, 2H, NH), 8.04 (s, 2H, Ar–H), 7.91-7.875 (m, 6H, Ar–H, NH), 7.59 (d, J = 8.0 Hz, 4H, Ar–H), 7.10 (s, 4H, Ar–H), 4.29 (br, 4H, NH_2), 4.04 (d, J = 5.5 Hz, 4H, NCH_2CO), 3.96 (t, J = 6.5 Hz, 8H, OCH_2), 3.92 (t, J = 6.5 Hz, 4H, OCH_2), 3.49-3.42 (m, 8H, NCH_2), 1.77-1.65 (m, 12H, CH_2), 1.44 (br, 12H, CH_2), 1.26 (br, 96H, CH_2), 0.88-0.83 (m, 18H, CH_3). ^{13}C NMR (126 MHz, $CDCl_3$/DMSO-d_6 (7/3, v/v), 50 °C): δ 169.91, 167.33, 166.31, 152.64, 140.71, 139.60, 135.51, 133.17, 132.33, 131.35, 130.36, 129.30, 127.41, 125.40, 123.69, 106.23, 90.45, 89.85, 73.11, 69.07, 43.58, 31.66, 30.17, 29.47, 29.46, 29.43, 29.40, 29.39, 29.33, 29.29, 29.20, 29.09, 29.07, 25.98, 25.91, 22.41, 13.95. IR (KBr, cm^{-1}): 3310 (ν_{N-H}), 1639 ($\nu_{C=O}$), 1543 (ν_{N-H}). HRMS (ESI-MS): m/z calcd for $[M(C_{126}H_{192}N_{10}O_{14}) + Na]^+$, 2092.4517; found 2092.4467.

Polymerization. A typical procedure for the polymerization of **2A** and **3** is described as follows. Into a two-neck round bottom flask containing **2A** (102 mg, 49.2 μmol) was added **3** (6.67 mg, 49.2 μmol) in TCE/DMSO (1/1, v/v; 1.6 mL), and the reaction mixture was stirred at 100 °C for 12 h. To this was then added excess MeOH and the precipitate was collected and washed with MeOH. The crude product was purified by SEC (TSKgel G4000H$_{HR}$ (0.78 (i.d.) × 30 cm), $CHCl_3$/DMSO (9/1, v/v) with 0.5 wt% TBAB), followed by washing with MeOH, affording poly-**2A** (35.3 mg, 33%) as a yellow solid. In the same way, poly-**1C** and poly(**1C**$_r$-*co*-**2A**$_{1-r}$) (r = 0.3, 0.5, 0.7, and 0.9) were prepared. The M_n and M_w/M_n were estimated by SEC with polystyrene standard using TCE/DMSO (9/1, v/v) with 0.5 wt% TBAB as the eluent at a flow rate of 0.3 mL/min. The degree of polymerization ($DP_{n,NMR}$)

was also estimated by ^{1}H NMR end-group analysis in $CDCl_3$/DMSO-d_6 (1/1, v/v). The polymerization results are summarized in Table 2-1.

Spectroscopic data of poly-**2A**: ^{1}H NMR (500 MHz, $CDCl_3$/DMSO (1/1, v/v), 50 °C): δ 11.98 (br, 2H, NH), 10.04 (br, 0.13H, CHO), 8.89 (br, 2H, NH), 8.38 (br, 1H, Ar–H), 8.22-8.02 (m, 14H, Ar–H, NH, N=CH, partially overlapping with $CHCl_3$ signal), 7.69 (d, J = 8.0 Hz, 4H, Ar–H), 7.11 (s, 4H, Ar–H), 4.01 (s, 4H, NCH_2CO), 3.96-3.88 (m, 12H, OCH_2), 3.43-3.39 (m, 8H, NCH_2), 1.74-1.64 (m, 12H, CH_2), 1.43 (br, 12H, CH_2), 1.23 (br, 96H, CH_2), 0.85 (br, 18H, CH_3). IR (KBr, cm^{-1}): 3310 (ν_{N-H}), 1655 ($\nu_{C=O}$), 1541 (ν_{N-H}).

Spectroscopic data of poly(**1C**$_{0.3}$-*co*-**2A**$_{0.7}$): ^{1}H NMR (500 MHz, $CDCl_3$/DMSO (1/1, v/v), 50 °C): δ 11.98 (br, 2H, NH), 10.04 (br, 0.13H, CHO), 8.89 (br, 1.4H, NH), 8.64 (br, 1.6H, NH, Ar–H), 8.22-7.85 (m, 14H, Ar–H, NH, HC=N, partially overlapping with $CHCl_3$ signal), 7.69 (d, J = 8.0 Hz, 4H, Ar–H), 7.11 (s, 4H, Ar–H), 4.61 (br, 0.6H, NCH), 4.01 (s, 2.8H, NCH_2CO), 3.95-3.88 (m, 12H, OCH_2), 3.44-3.39 (m, 8H, NCH_2), 1.72-1.64 (m, 12H, CH_2), 1.43 (br, 12H, CH_2), 1.24 (br, 97.8H, CH_3, CH_2), 0.85 (br, 18H, CH_3). IR (KBr, cm^{-1}): 3315 (ν_{N-H}), 1655 ($\nu_{C=O}$), 1542 (ν_{N-H}).

Spectroscopic data of poly(**1C**$_{0.5}$-*co*-**2A**$_{0.5}$): ^{1}H NMR (500 MHz, $CDCl_3$/DMSO (1/1, v/v), 50 °C): δ 11.98 (br, 2H, NH), 10.04 (br, 0.13H, CHO), 8.88 (br, 1H, NH), 8.65 (br, 2H, NH, Ar–H), 8.38-7.85 (m, 14H, Ar–H, NH, HC=N, partially overlapping with $CHCl_3$ signal), 7.69 (d, J = 8.0 Hz, 4H, Ar–H), 7.10 (s, 4H, Ar–H), 4.61 (br, 1H, NCH), 4.02 (s, 2H, NCH_2CO), 3.95-3.88 (m, 12H, OCH_2), 3.45-3.38 (m, 8H, NCH_2), 1.74-1.64 (m, 12H, CH_2), 1.43 (br, 12H, CH_2), 1.24 (br, 99H, CH_3, CH_2), 0.85 (br, 18H, CH_3). IR (KBr, cm^{-1}): 3322 (ν_{N-H}), 1655 ($\nu_{C=O}$), 1543 (ν_{N-H}).

Spectroscopic data of poly(**1C**$_{0.7}$-*co*-**2A**$_{0.3}$): ^{1}H NMR (500 MHz, $CDCl_3$/DMSO (1/1, v/v),

50 °C): δ 11.98 (br, 2H, NH), 10.04 (br, 0.13H, CHO), 8.88 (br, 0.6H, NH), 8.63 (br, 2.4H, NH, Ar–H), 8.38-7.85 (m, 14H, Ar–H, NH, HC=N, partially overlapping with $CHCl_3$ signal), 7.69 (d, J = 8.0 Hz, 4H, Ar–H), 7.10 (s, 4H, Ar–H), 4.61 (br, 1.4H, NCH), 4.02 (s, 1.2H, NCH_2CO), 3.94-3.88 (m, 12H, OCH_2), 3.45-3.39 (m, 8H, NCH_2), 1.74-1.64 (m, 12H, CH_2), 1.43 (br, 12H, CH_2), 1.24 (br, 100.2H, CH_3, CH_2), 0.85 (br, 18H, CH_3). IR (KBr, cm^{-1}): 3316 (ν_{N-H}), 1655 ($\nu_{C=O}$), 1543 (ν_{N-H}).

Spectroscopic data of poly(**1C**$_{0.9}$-*co*-**2A**$_{0.1}$): ^{1}H NMR (500 MHz, $CDCl_3$/DMSO (1/1, v/v), 50 °C): δ 11.98 (br, 2H, NH), 10.04 (br, 0.13H, CHO), 8.88 (br, 0.26H, NH), 8.63 (br, 2.74H, NH, Ar–H), 8.36-7.85 (m, 14H, Ar–H, NH, HC=N, partially overlapping with $CHCl_3$ signal), 7.69 (d, J = 8.0 Hz, 4H, Ar–H), 7.10 (s, 4H, Ar–H), 4.61 (br, 1.74H, NCHCO), 4.01 (s, 0.52H, NCH_2CO), 3.94-3.88 (m, 12H, OCH_2), 3.45-3.39 (m, 8H, NCH_2), 1.72-1.64 (m, 12H, CH_2), 1.44 (br, 12H, CH_2), 1.23 (br, 101.4H, CH_3, CH_2), 0.85 (br, 18H, CH_3). IR (KBr, cm^{-1}): 3304 (ν_{N-H}), 1655 ($\nu_{C=O}$), 1542 (ν_{N-H}).

AFM Measurements of Assemblies of 1C, 2A, and Their Equimolar Mixture on HOPG

A typical procedure for the AFM measurements of assemblies of **1C** is described as follows. A solution of **1C** in TCE (0.10 mM) was prepared. Samples for the AFM measurements of **1C** were prepared by spin casting 20 μL aliquots of the stock solution on a freshly cleaved highly oriented pyrolytic graphite (HOPG) at room temperature (ca. 25 °C), and the solvents were then slowly evaporated under a TCE vapor atmosphere. After **1C** had been deposited on the HOPG, the HOPG substrates were exposed to TCE vapors at 30 °C for 24 h, and the substrates were then dried under vacuum for 2 h. The organic solvent vapors were prepared by putting 1 mL of TCE into a 2 mL flask that was inside a 50 mL flask, and the HOPG substrates were then placed in the 50 mL flask. The AFM measurements were performed using a Nanoscope V microscope in air at room temperature with standard silicon cantilevers

(TESP–V2) in the tapping mode. The typical settings of the AFM for the high-magnification observations were as follows: a free amplitude of the oscillation frequency of 280 mV, a set-point amplitude of 180–250 mV, and a scan rate of 1.0 Hz. The Nanoscope image processing software was used for the image analysis. The AFM measurements of assemblies of **2A** and an equimolar mixture of **1C** and **2A** were also performed in a similar manner.

Molecular Modeling of 1C

The molecular modeling was performed on a Windows 10 PC with the Materials Studio Package (version 8.0; Dassault Systèmes BIOVIA, San Diego, CA, USA). The initial structure of **1C** was constructed according to the following procedures: tris(dodecyloxy)benzene groups of the chiral oligoamide side chains of **1C** were replaced with tris(methoxy)benzene groups to simplify the calculations. Based on the CD spectral pattern of the assembled **1C** (Figure 2-2a), the twist angle between the two phenyl rings of the biphenylene moiety was set to be –45°.[32] The **1C** was then allowed to manually construct a $(\mathbf{1C})_{64}$ so as to stack each other via intermolecular hydrogen-bonding interactions. The initial model of **1C** was fully optimized by the molecular mechanics (MM) calculations (Compass II force field[33] as implemented in the Material Studio package) (Figure 2-S2c).

References

(1) Feringa, B. L.; van Delden, R. A. *Angew. Chem., Int. Ed*. **1999**, *38*, 3418–3438.

(2) Green, M. M.; Reidy M. P. *J. Am. Chem. Soc*. **1989**, *111*, 6452–6454.

(3) Green, M. M.; Peterson, N. C.; Sato, T.; Teramoto, A.; Cook, R.; Lifson, S. *Science* **1995**, *268*, 1860–1866.

(4) Nakano, T.; Okamoto, Y. *Chem. Rev*. **2001**, *101*, 4013–4038.

(5) Cornelissen, J. J. L. M.; Rowan, A. E.; Nolte, R. J. M.; Sommerdijk, N. A. J. M. *Chem. Rev.* **2001**, *101*, 4039–4070.

(6) Suginome, M.; Yamamoto, T.; Nagata, Y.; Yamada, T.; Akai, Y. *Pure Appl. Chem*. **2012**, *84*, 1759–1769.

(7) Fujiki, M. *Symmetry* **2014**, *6*, 677–703.

(8) Freire, F.; Quiñoá, E.; Riguera, R. *Chem. Rev.* **2016**, *116*, 1242–1271.

(9) Yashima, E.; Ousaka, N.; Taura, D.; Shimomura, K.; Ikai, T.; Maeda, K. *Chem. Rev*. **2016**, *116*, 13752–13990.

(10) Worch, J. C.; Prydderch, H.; Jimaja, S.; Bexis, P.; Becker, M. L.; Dove, A. P. *Nat. Rev. Chem*. **2019**, *3*, 514–535.

(11) Zhang, C.; Liu, L.; Okamoto, Y. *TrAC Trends Anal. Chem*. **2020**, *123*, 115762.

(12) Mateos-Timoneda, M. A.; Crego-Calama, M.; Reinhoudt, D. N. *Chem. Soc. Rev.* **2004**, *33*, 363–372.

(13) Palmans, A. R. A.; Meijer, E. W. *Angew. Chem., Int. Ed.* **2007**, *46*, 8948–8968.

(14) Pijper, D.; Feringa, B. L. *Soft. Matter*. **2008**, *4*, 1349–1372.

(15) Zhang, D.-W.; Zhao, X.; Li, Z.-T. *Acc. Chem. Res*. **2014**, *47*, 1961–1970.

(16) Xing, P.; Zhao, Y. *Acc. Chem. Res*. **2018**, *51*, 2324–2334.

(17) Adelizzi, B.; Van Zee, N. J.; de Windt, L. N. J.; Palmans, A. R. A.; Meijer, E. W. *J. Am. Chem. Soc*. **2019**, *141*, 6110–6121.

(18) Dorca, Y.; Greciano, E. E.; Valera, J. S.; Gómez, R.; Sánchez, L. *Chem. - Eur. J*. **2019**, *25*, 5848–5864.

(19) Haino, T. *Polym. J*. **2019**, *51*, 303–318.

(20) Ariga, K.; Mori, T.; Kitao, T.; Uemura, T. *Adv. Mater*. **2020**, *32*, 1905657.

(21) Haino, T.; Hirano, T. *Chem. Lett*. **2020**, *49*, 574–584.

(22) Hashim, P. K.; Bergueiro, J.; Meijer, E. W.; Aida, T. *Prog. Polym. Sci*. **2020**, *105*, 101250.

(23) Yan, X.; Wang, Q.; Chen, X.; Jiang, Y.-B. *Adv. Mater*. **2020**, *32*, 1905667.

(24) Kawabata, S.; Ousaka, N.; Yashima, E. *Chem. Commun*. **2018**, *54*, 2417–2420.

(25) For an example of acylhydrazone-linked polymers, see: Skene, W. G.; Lehn, J.-M. P. *Proc. Natl. Acad. Sci. U. S. A*. **2004**, *101*, 8270–8275.

(26) For an example of supramolecular polymers assembled from helical oligomers (foldamers), see: Brunsveld, L.; Meijer, E. W.; Prince, R. B.; Moore, J. S. *J. Am. Chem. Soc*. **2001**, *123*, 7978–7984.

(27) For one-dimensional supramolecular polymerization of one-handed helical polyisocyanides through end-to-end multiple hydrogen bonding interactions accompanied by a remarkable amplification of the helical handedness excess, see: Wada, Y.; Shinohara, K.; Asakawa, H.; Matsui, S.; Taima, T.; Ikai, T. *J. Am. Chem. Soc*. **2019**, *141*, 13995–14002.

(28) Helmich, F.; Smulders, M. M. J.; Lee, C. C.; Schenning, A. P. H. J.; Meijer, E. W. *J. Am. Chem. Soc*. **2011**, *133*, 12238–12246.

(29) Ikeda, M. *Polym. J*. **2019**, *51*, 371–380.

(30) Zhang, L.; Wang, H.-X.; Li, S.; Liu, M. *Chem. Soc. Rev*. **2020**, *49*, 9095–9120.

(31) Stone, D. A.; Tayi, A. S.; Goldberger, J. E.; Palmer, L. C.; Stupp, S. I. *Chem. Commun.* **2011**, *47*, 5702–5704.

(32) Grein, F. *J. Phys. Chem. A* **2002**, *106*, 3823–3827.

(33) Sun, H.; Jin, Z.; Yang, C.; Akkermans, R. L. C.; Robertson, S. H.; Spenley, N. A.; Miller, S.; Todd, S. M. *J. Mol. Model.* **2016**, *22*, 47.

Supporting Data

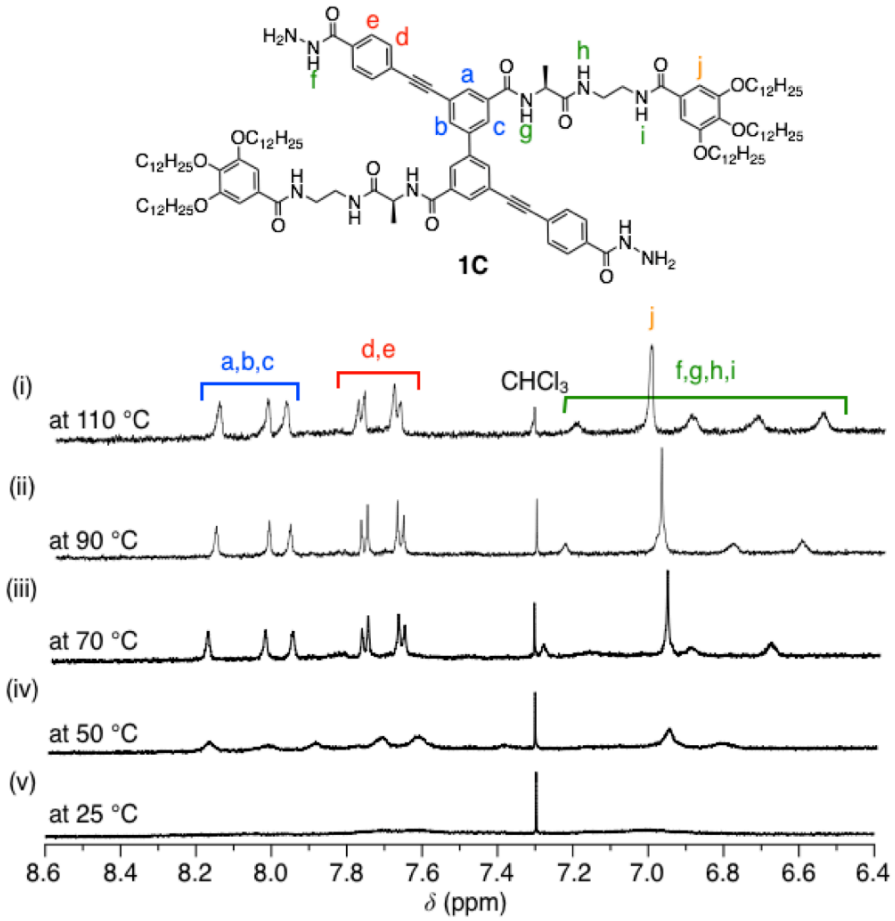

Figure 2-S1. Partial ^{1}H NMR spectra (500 MHz, TCE-d_2) of **1C** at 110 (i), 90 (ii), 70 (iii), 50 (iv), and 25 (v) °C. [**1C**] = 0.10 mM.

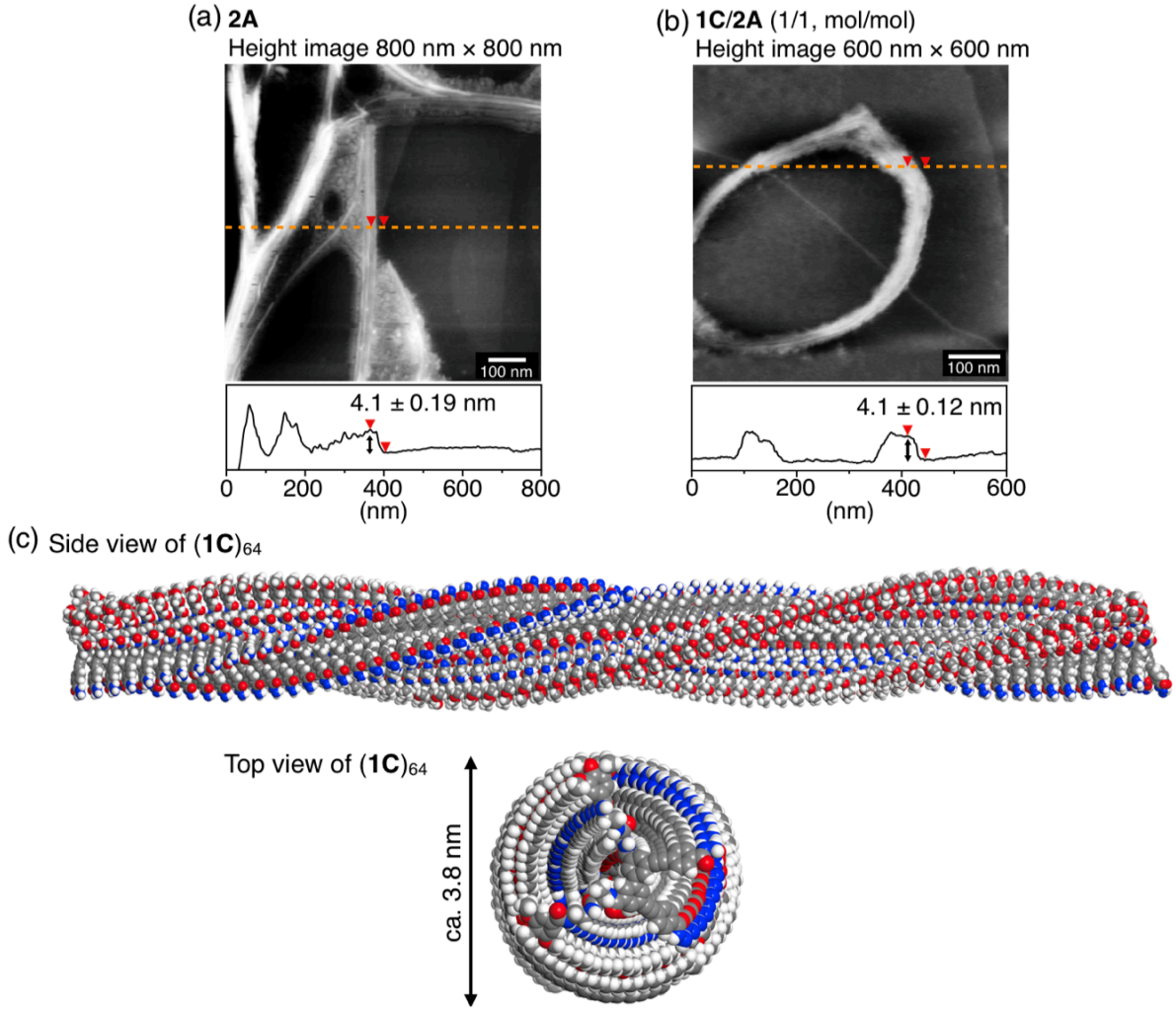

Figure 2-S2. (a,b) AFM height images of self-assembled nanofibers formed from **2A** (a) and an equimolar mixture of **1C** and **2A** (b) on HOPG cast from TCE solutions (0.10 mM). The cross-sectional profiles denoted by orange dashed lines are also shown in (a) and (b). (c) Side (upper) and top (bottom) views of the geometry-optimized stacked structure of $(\mathbf{1C})_{64}$ with an (*M*)-twist conformation of the biphenyl moieties. For simplicity, the dodecyloxy chains were replaced with methoxy groups.

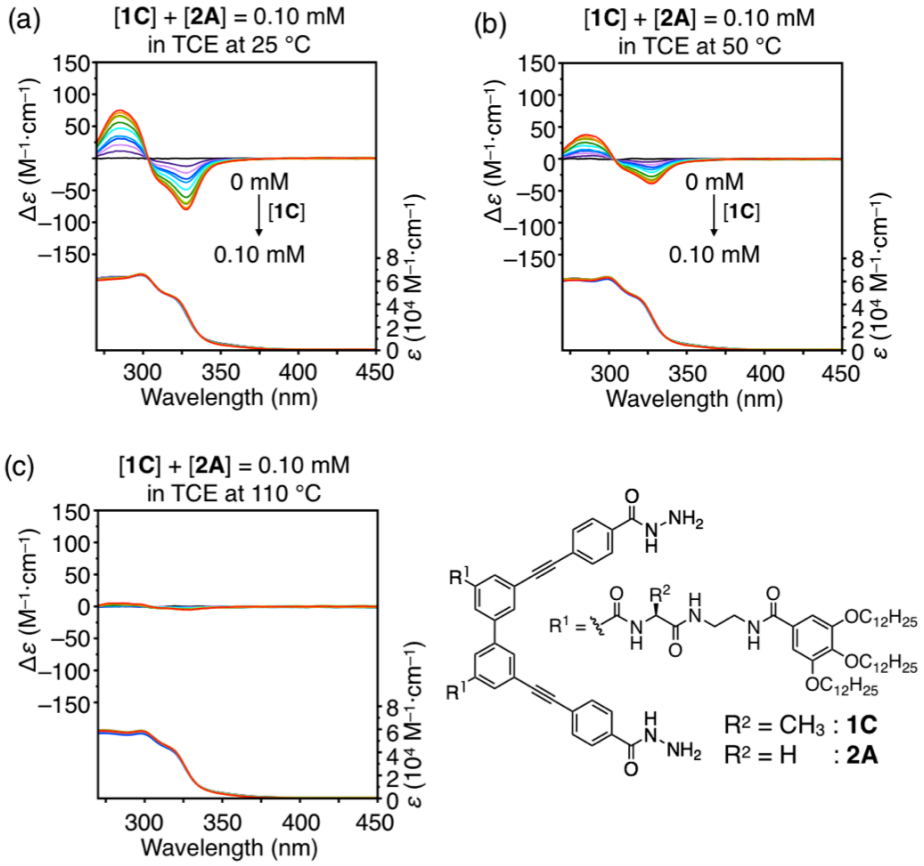

Figure 2-S3. CD and absorption spectra of a mixture of **1C** and **2A** with various molar ratios ([**1C**] + [**2A**] = 0.10 mM) in TCE at 25 (a), 50 (b), and 110 (c) °C.

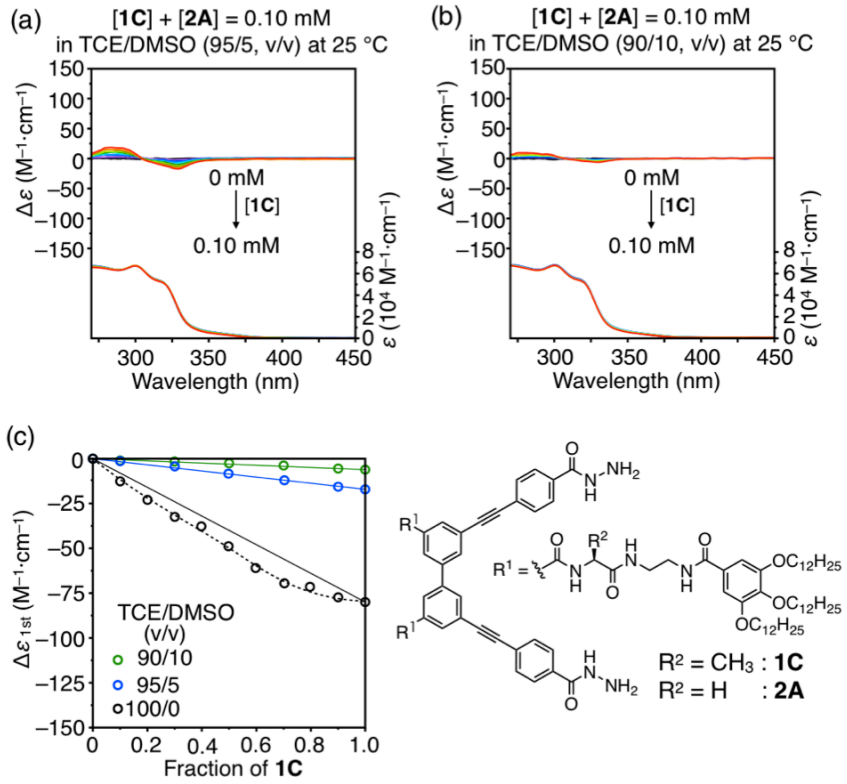

Figure 2-S4. (a,b) CD and absorption spectra of a mixture of **1C** and **2A** with various molar ratios ([**1C**] + [**2A**] = 0.10 mM) in TCE/DMSO (95/5 (a) and 90/10 (b), v/v) at 25 °C. (c) Plots of the first Cotton intensity ($\Delta\varepsilon_{1st}$) at 328 nm of the **1C**/**2A** mixture in TCE/DMSO (95/5 (blue circles) and 90/10 (green circles), v/v) at 25 °C versus the mole fraction of **1C**. The corresponding plots obtained in TCE at 25 °C (black circles) that are identical to those in Figure 2-2d (black circles) are also shown.

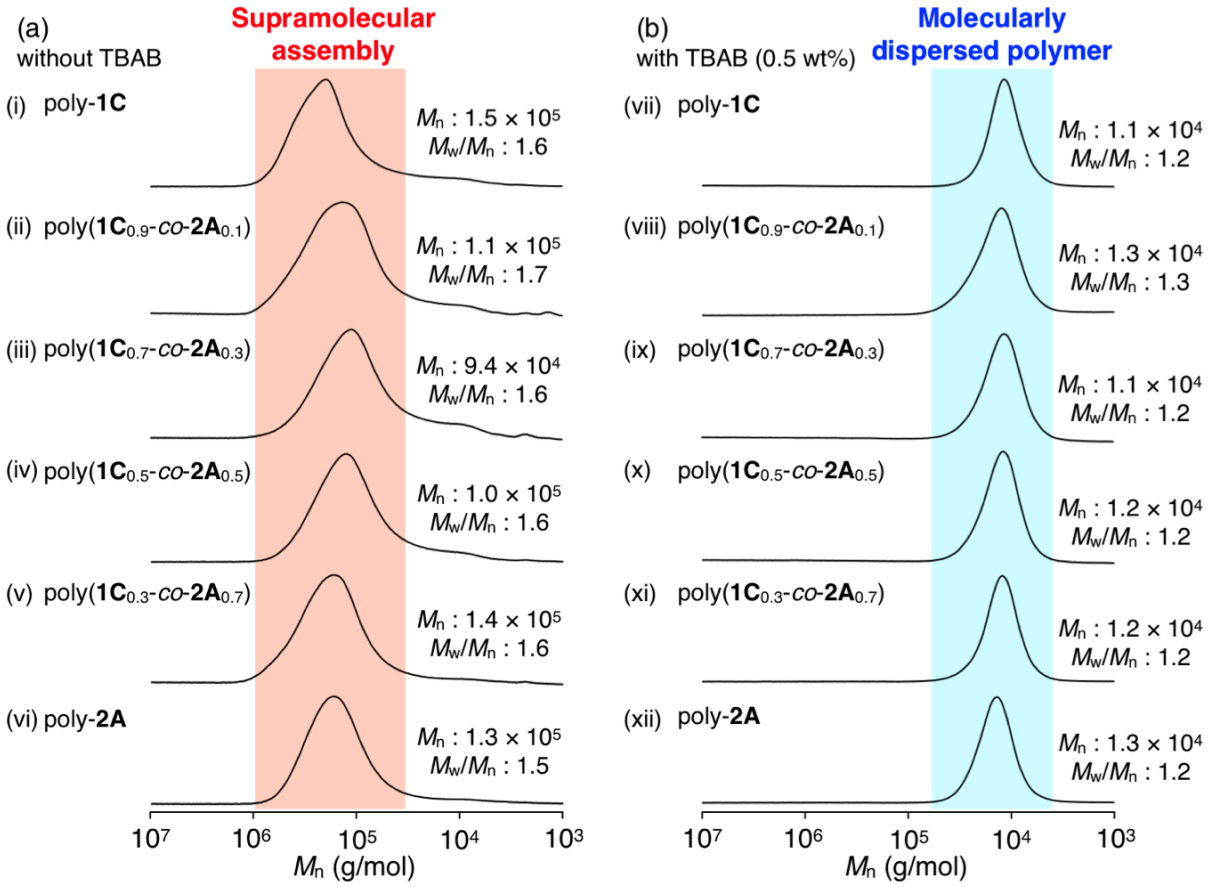

Figure 2-S5. UV (328 nm) detected SEC chromatograms of poly-**1C** (i, vii), poly(**1C**$_{0.9}$-*co*-**2A**$_{0.1}$) (ii, viii), poly(**1C**$_{0.7}$-*co*-**2A**$_{0.3}$) (iii, ix), poly(**1C**$_{0.5}$-*co*-**2A**$_{0.5}$) (iv, x), poly(**1C**$_{0.3}$-*co*-**2A**$_{0.7}$) (v, xi), and poly-**2A** (vi, xii). SEC conditions: column, TSKgel G4000H$_{HR}$ (0.78 (i.d.) × 30 cm); eluent, TCE/DMSO (90/10, v/v) in the absence (a) and presence (b) of TBAB (0.5 wt%); flow rate 0.3 mL/min; column temperature, 25 °C.

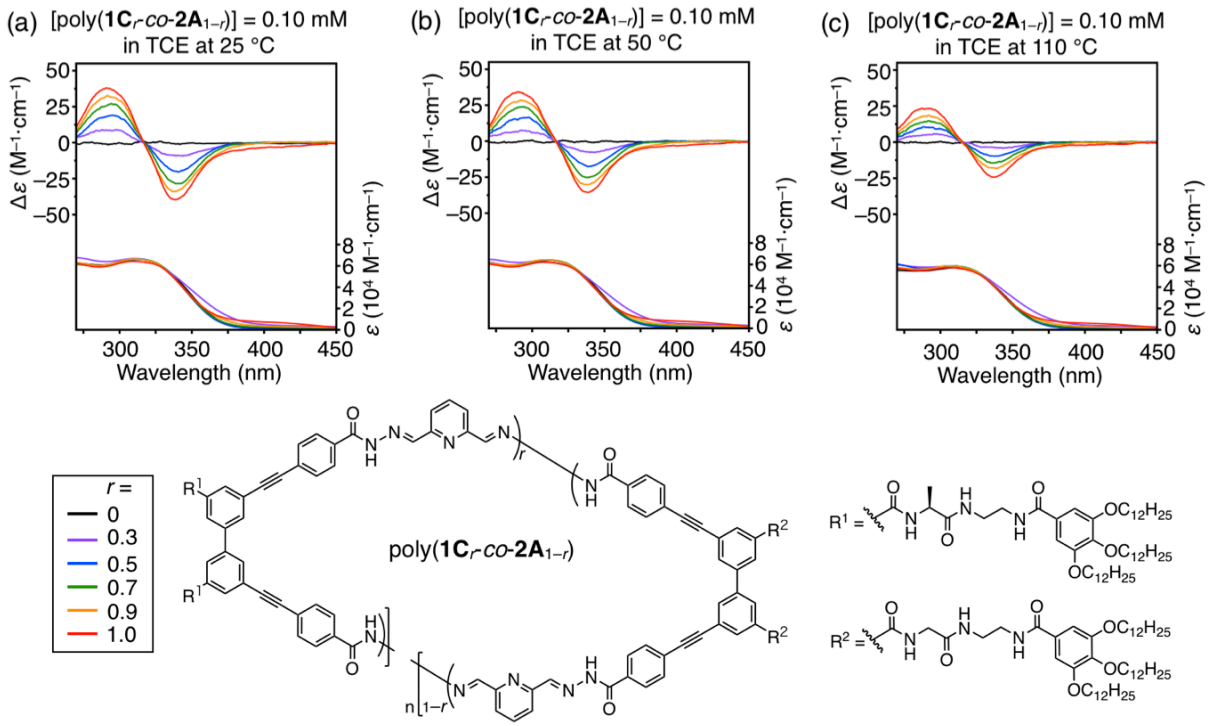

Figure 2-S6. CD and absorption spectra of poly(**1C**$_r$-*co*-**2A**$_{1-r}$) (0.10 mM per monomer unit) in TCE at 25 (a), 50 (b), and 110 (c) °C.

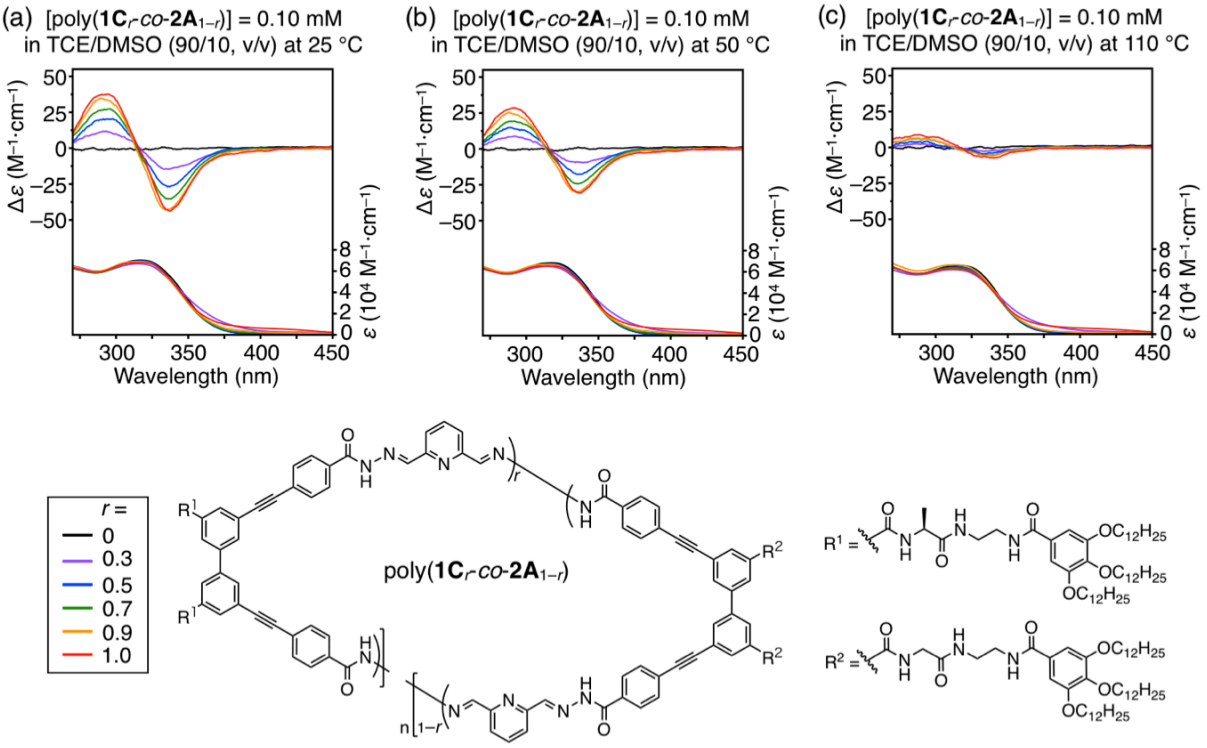

Figure 2-S7. CD and absorption spectra of poly(**1C**$_r$-*co*-**2A**$_{1-r}$) (0.10 mM per monomer unit) in TCE/DMSO (90/10, v/v) at 25 (a), 50 (b), and 110 (c) °C.

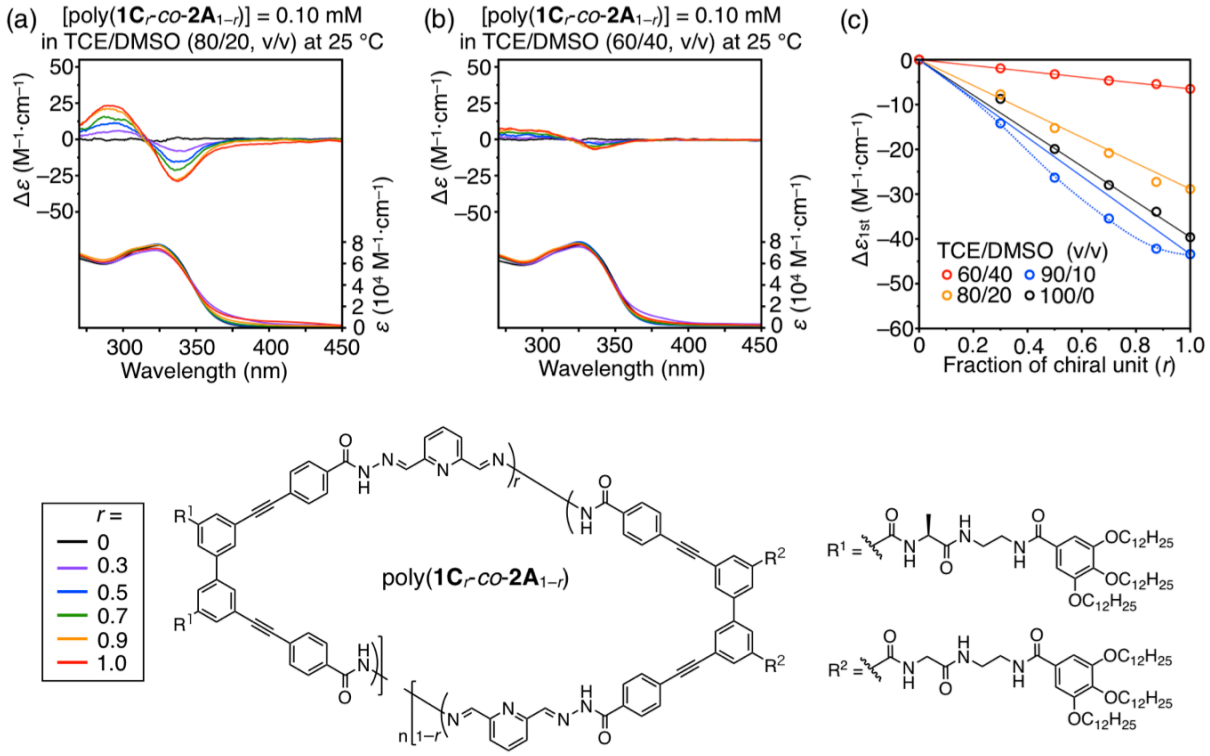

Figure 2-S8. (a,b) CD and absorption spectra of poly(**1C**$_r$-*co*-**2A**$_{1-r}$) (0.10 mM per monomer unit) in TCE/DMSO (80/20 (a) and 60/40 (b), v/v) at 25 °C. (c) Plots of the first Cotton intensity ($\Delta\varepsilon_{1st}$) at 338 nm of poly(**1C**$_r$-*co*-**2A**$_{1-r}$) in TCE/DMSO (100/0 (black circles), 90/10 (blue circles), 80/20 (orange circles), and 60/40 (red circles), v/v) at 25 °C versus the content of the **1C**-based chiral monomer unit. Because of poor solubility of the copolymers in TCE/DMSO mixtures at low temperatures, the CD and absorption spectra were measured at 25 °C.

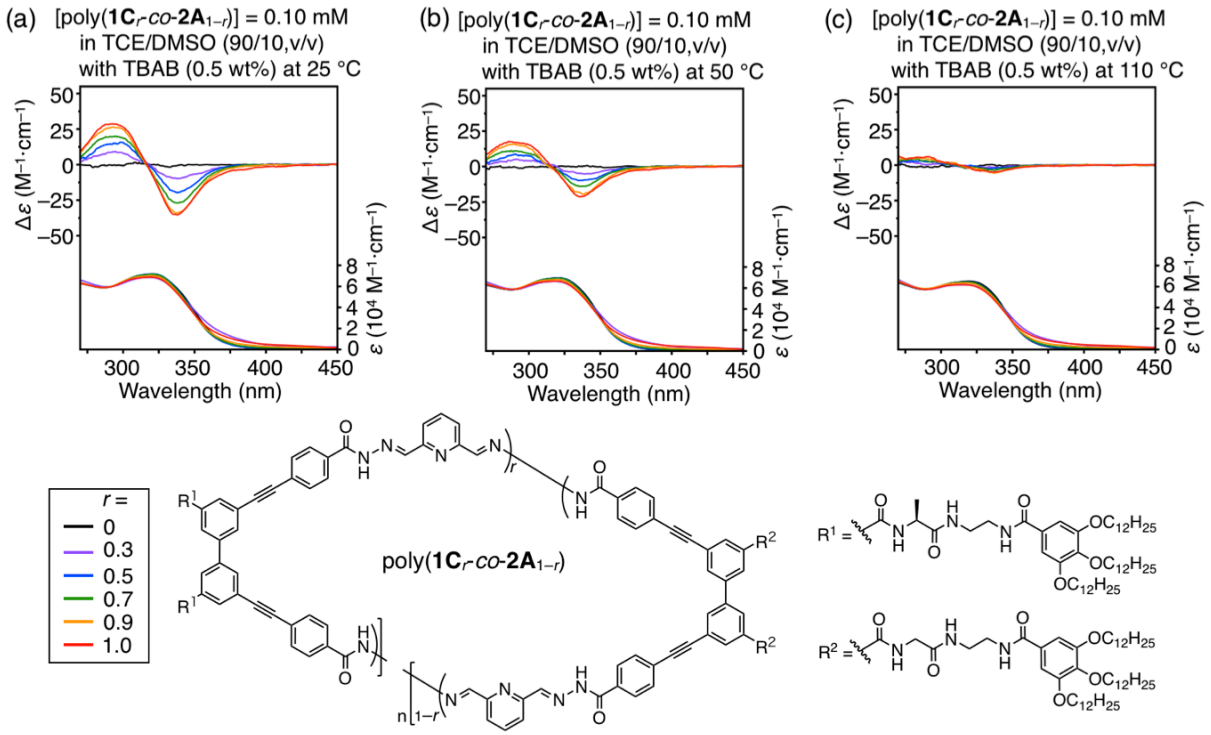

Figure 2-S9. CD and absorption spectra of poly(**1C**$_r$-*co*-**2A**$_{1-r}$) (0.10 mM per monomer unit) in TCE/DMSO (90/10, v/v) containing TBAB (0.5 wt% (22 mM)) at 25 (a), 50 (b), and 110 (c) °C.

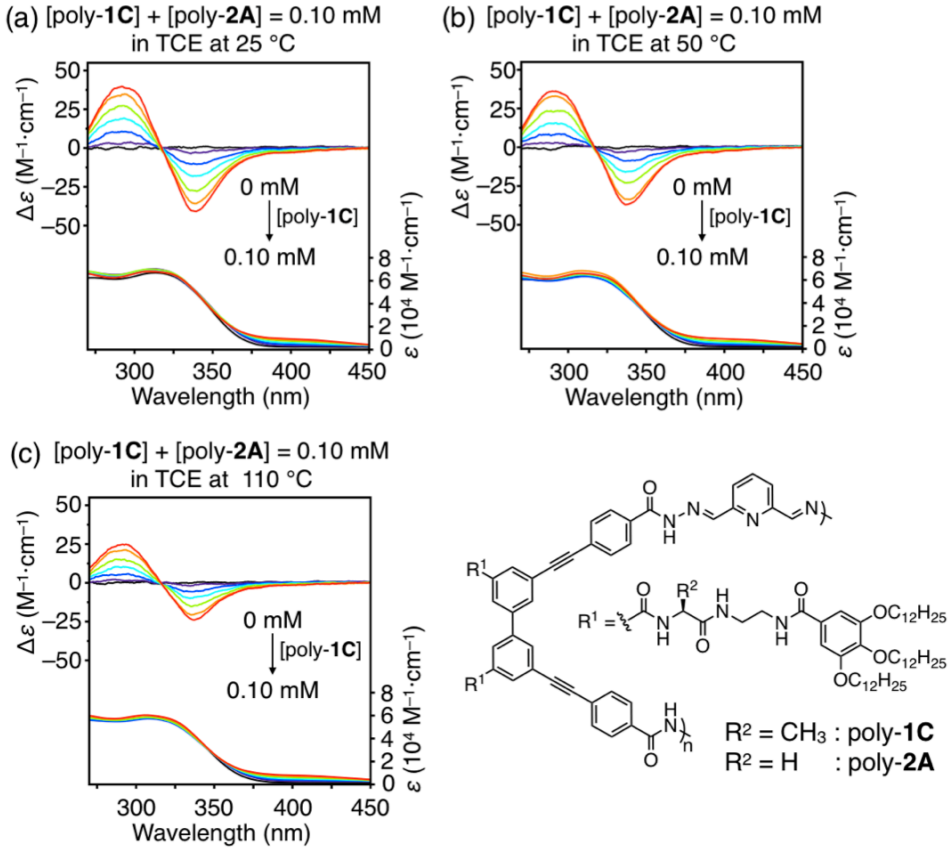

Figure 2-S10. CD and absorption spectra of a mixture of poly-**1C** and poly-**2A** with various molar ratios ([poly-**1C**] + [poly-**2A**] = 0.10 mM per monomer unit) in TCE at 25 (a), 50 (b), and 110 (c) °C.

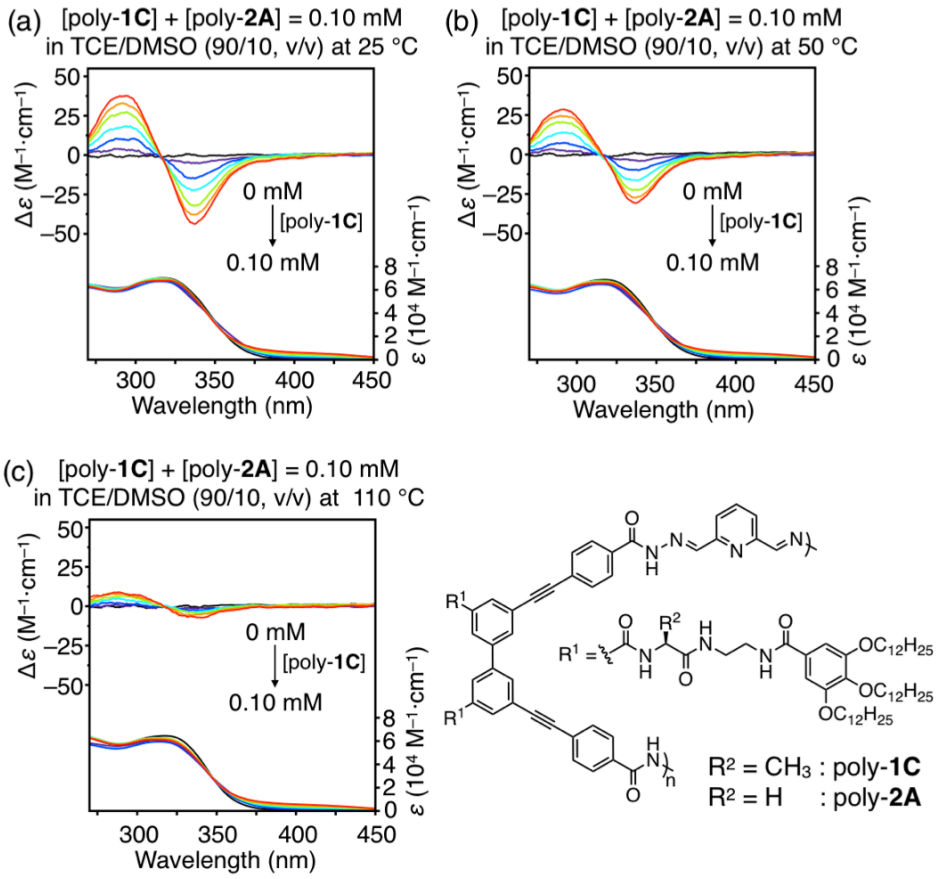

Figure 2-S11. CD and absorption spectra of a mixture of poly-**1C** and poly-**2A** with various molar ratios ([poly-**1C**] + [poly-**2A**] = 0.10 mM per monomer unit) in TCE/DMSO (90/10, v/v) at 25 (a), 50 (b), and 110 (c) °C.

Chapter 3

Helix-Sense-Selective Encapsulation of Helical Poly(lactic acid)s within a Helical Cavity of Syndiotactic Poly(methyl methacrylate) with Helicity Memory

Abstract: The author reports a highly enantio- and helix-sense-selective encapsulation of helical poly(lactic acid)s (PLAs) through a unique "helix-in-helix" superstructure formation within the helical cavity of syndiotactic poly(methyl methacrylate) (st-PMMA) with a one-handed helicity memory, which enables the separation of the enantiomeric helices of the left (*M*)- and right (*P*)-handed-PLAs. The *M*- and *P*-helical PLAs with different molar masses and a narrow molar mass distribution were prepared by the ring-opening living polymerization of the optically pure L- and D-lactides, respectively, followed by end-capping of the terminal residues of the PLAs with a 4-halobenzoate and then a C_{60} unit, giving the C_{60}-free and C_{60}-bound *M*- and *P*-PLAs. The C_{60}-free and C_{60}-bound *M*- and *P*-PLAs formed crystalline inclusion complexes with achiral st-PMMA accompanied by a preferred-handed helix induction in the st-PMMA backbone, thereby producing helix-in-helix superstructures with the same-handedness to each other. The induced helical st-PMMAs were retained after replacement with the achiral C_{60}, indicating the memory of the induced helicity of the st-PMMAs. Both the C_{60}-free and C_{60}-bound helical PLAs were enantio- and helix-sense selectively encapsulated into the helical hollow space of the optically active *M*- and *P*-st-PMMAs with the helicity memory prepared using chiral amines. The *M*- and *P*-PLAs are preferentially encapsulated within the *M*- and *P*-st-PMMA helical cavity with the same-handedness to each other, respectively, independent of the terminal units. The C_{60}-bound PLAs were more efficiently and enantioselectively trapped in the st-PMMA compared to the C_{60}-free PLAs. The enantioselectivities were highly dependent on the molar mass of the C_{60}-bound and C_{60}-free PLAs and significantly increased as the molar mass of the PLAs increased.

Introduction

Biological polymers, such as polysaccharides (e.g., amylose and schizophyllan)[1–10] and assembled proteins,[11–16] are known to possess a unique helical cavity or pore, within which a variety of small molecules and polymers are encapsulated in a size- and shape-selective manner, thereby producing discrete supramolecular inclusion complexes with specific functionalities that involve molecular/chiral recognition, catalysis, and ion/water transport.[9,17–21] Inspired by such biopolymer-based helical host systems, a large number of macrocyclic host molecules,[22–30] self-assembled organic/inorganic cages and capsules,[31–38] and helical foldamers[39–46] possessing a confined nanospace or cylindrical helical cavity suitable for encapsulating specific small molecules or oligomers has been extensively developed. However, because of their molecular-scale space, the encapsulating of polymers, in particular, helical polymers within their space or helical cavities is virtually impossible. Hence, the development of synthetic helical polymers with an optical activity showing an enantioselective or helix-sense-selective inclusion capability for helical polymers is an attractive challenge because of potential applications for separating enantiomers as chiral stationary phases (CSPs),[47] supramolecular liquid crystals,[6] and electronic and optoelectronic materials[2–9,18,48–55] as well as circularly polarized luminescence (CPL) when complexed with photoluminescent achiral polymers in a one-handed helical cavity.[56,57]

Previously, Yashima and co-workers found that syndiotactic poly(methyl methacrylate) (st-PMMA), a commodity plastic widely used as plastic optical fibers,[58] folds into either an excess left (*M*)- or right (*P*)-handed 18_1-helical conformation (18 monomer units per one turn) assisted by an optically active alcohol or amine in toluene upon gelation, thus creating a helical cavity of about 1 nm in diameter,[59–62] in which achiral and chiral fullerenes can be encapsulated in a size- or enantioselective manner through an induced-fit mechanism,[59,61,63–65] thereby producing unique peapod-like inclusion complexes with an optical activity that are retained (memorized) after complete removal of the chiral additives.[59–62] Such a one-handed helical cavity of the st-PMMA with a helicity memory is self-adjustable while maintaining its helical handedness, thus allowing the helix-sense-selective encapsulation of the

complementary isotactic PMMA (it-PMMA) to produce the first optically active PMMA stereocomplex[60] composed of an inner it-PMMA double-helix surrounded by the st-PMMA single-helix with the same handedness to each other.[66–74]

Taking advantage of the specific interactions between fullerenes and the hydrophobic helical cavity of st-PMMA, Mamiya, Yashima, and co-workers recently succeeded in the construction of a unique "helix-in-helix" superstructure through encapsulation of the *M*- and *P*-10_3-helical peptides (Figure 3-1a) within the st-PMMA helical cavity when a C_{60} moiety was introduced at one end of the peptides, through which a preferred-handed helix with the same-handedness as that of the encapsulated peptide was, at the same time, induced in the st-PMMA backbone.[75] Of particular importance is the terminal C_{60} unit of the peptides that is essential for the inclusion complex formation with the st-PMMA or no inclusion complexation took place. The results imply that a C_{60} unit can serve as a molecular carrier or transporter of particular organic molecules and polymers into the helical cavity of the st-PMMA once introduced at their terminals, resulting in unique supramolecular inclusion complexes.[76]

Poly(lactic acid) (PLA) is one of the popular bio-based, biocompatible, and biodegradable polyesters,[77] and would also be encapsulated in the st-PMMA helical cavity once the PLA is end-capped with a C_{60} unit because the homochiral PLAs, namely, poly(L-lactic acid) (PLLA) and poly(D-lactic acid) (PDLA) take *M*- and *P*-10_3-helical structures, respectively,[78–80] which resemble the helical polypeptides, specifically, poly(D- or L-alanine).[81,82] In fact, Mamiya reported preliminary results of a similar "helix-in-helix" superstructure formation of C_{60}-bound *M*- and *P*-handed 10_3-helical PLAs with st-PMMA and found an enantioselective inclusion complex formation of C_{60}-bound helical PLAs within a helical cavity of the st-PMMA with a one-handed helicity memory.[83] The author, however, discovered that the C_{60}-free *M*- and *P*-helical PLAs (***M***-N_3-**L**-**1**-I and ***P***-N_3-**D**-**1**-F) (Scheme 3-1 and Figure 3-1b) prepared as precursors for the C_{60}-bound *M*- and *P*-helical PLAs (***M***-C_{60}-**L**-**2**-I and ***P***-C_{60}-**D**-**2**-F) (Scheme 3-1 and Figure 3-1b) are also helix-sense selectively included in the

st-PMMA helical nanotube, resulting in a similar "helix-in-helix" superstructure.

Based on this serendipitous discovery, the author has thoroughly investigated the effects of the end-capped C_{60} unit and molar mass of the PLAs on the enantio- and helix-sense-selective inclusion complexations within the helical cavity of the preferred-handed helical st-PMMA prepared by the helicity induction and memory strategy[42,59–62] using chiral amines, such as (*R*)- and (*S*)-1-phenylethylamine ((*R*)- and (*S*)-**3**),[61,62] based on a unique "helix-in-helix" superstructure formation, which would enable us to separate the enantiomeric helices of PLAs (Figure 3-1c). The separation of enantiomers of optically active polymers, in particular, helical polymers, is quite rare.[84–86] Although chiral recognition of the enantiomeric helical PLAs has been reported using cyclodextrins[87] and amylose,[88,89] the *M*- and *P*-helical PLAs were neither separated nor isolated, providing little information about the enantioselective inclusion complex formation at a molecular level as well as its enantioselectivity (helix-sense selectivity). The helical *M*- and *P*-st-PMMAs induced by C_{60}-bound and C_{60}-free *M*- and *P*-PLAs, respectively, are found to be retained after complete replacement of the encapsulated *M*- and *P*-PLAs with achiral C_{60}, indicating the memory of the induced helicity of the st-PMMAs (Figure 3-1b); the results are also described in this chapter.

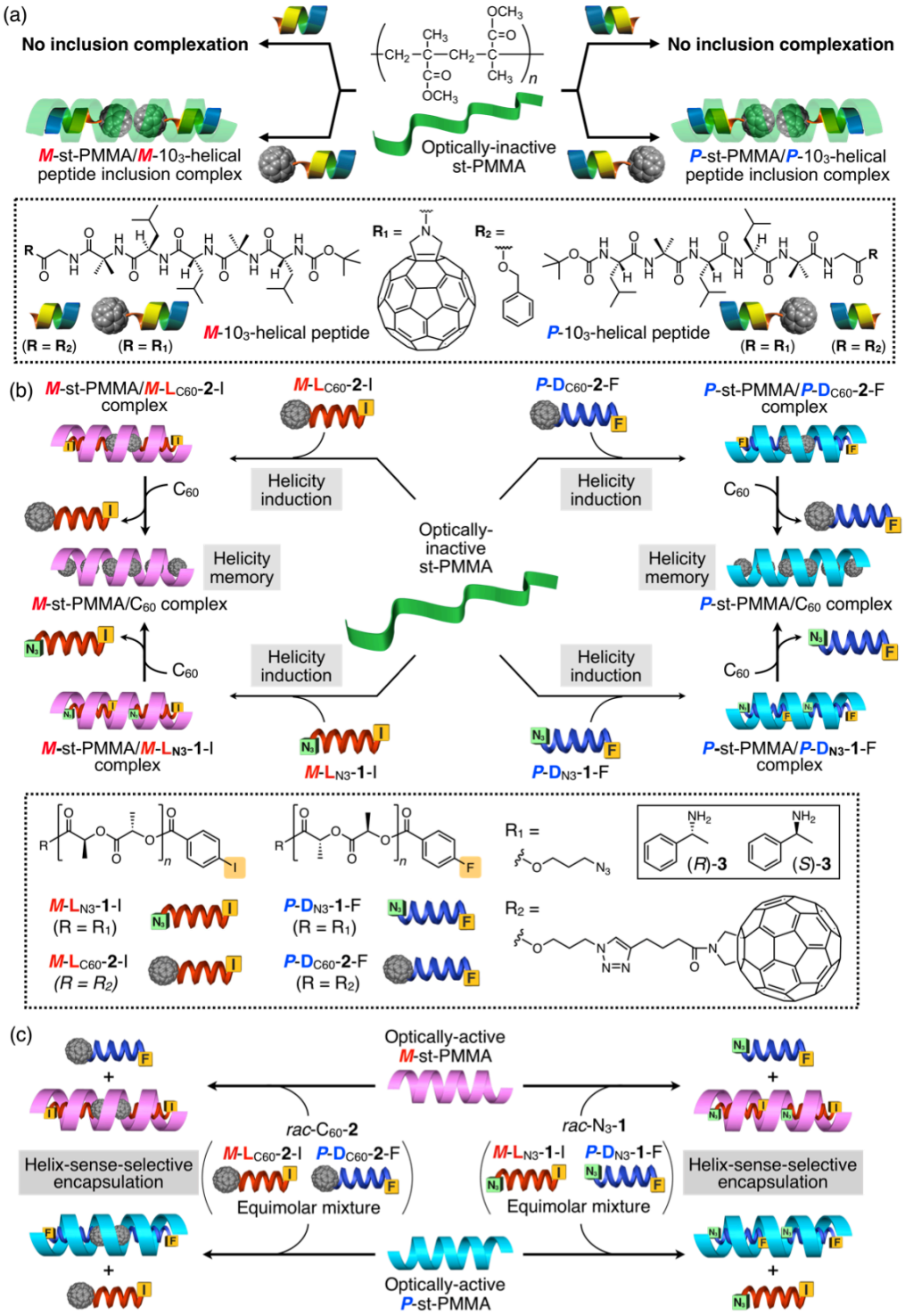

Figure 3-1. (a) Schematic illustration of the "helix-in-helix" superstructure formation through encapsulation of C_{60}-bound *M*- and *P*-10_3-helical peptides within the st-PMMA helical cavity.[75] (b) Structures of C_{60}-bound (***M*-L**$_{C60}$**-2**-I and ***P*- D**$_{C60}$**-2**-F) and C_{60}-free (***M*-L**$_{N3}$**-1**-I and ***P*-D**$_{N3}$**-1**-F) *M*- and *P*-helical PLAs and optically active amines ((*R*)- and (*S*)-**3**) and a

schematic illustration of the macromolecular helicity induction in st-PMMA upon inclusion complex formations with the C_{60}-bound and C_{60}-free *M*- and *P*-helical PLAs and subsequent memory of the induced macromolecular helicities of st-PMMA by replacing the encapsulated *M*- and *P*-helical PLAs with the achiral C_{60}. (c) Helix-sense-selective encapsulation of C_{60}-bound and C_{60}-free *M*- and *P*-helical PLAs within a helical cavity of st-PMMA with a one-handed helicity memory based on the "helix-in-helix" superstructure formation.

Scheme 3-1. Synthesis of the C_{60}-Free (*M*-L_{N3}-1-I and *P*-D_{N3}-1-F) and C_{60}-Bound (*M*-L_{C60}-2-I and *P*-D_{C60}-2-F) Optically-Active Polylactides

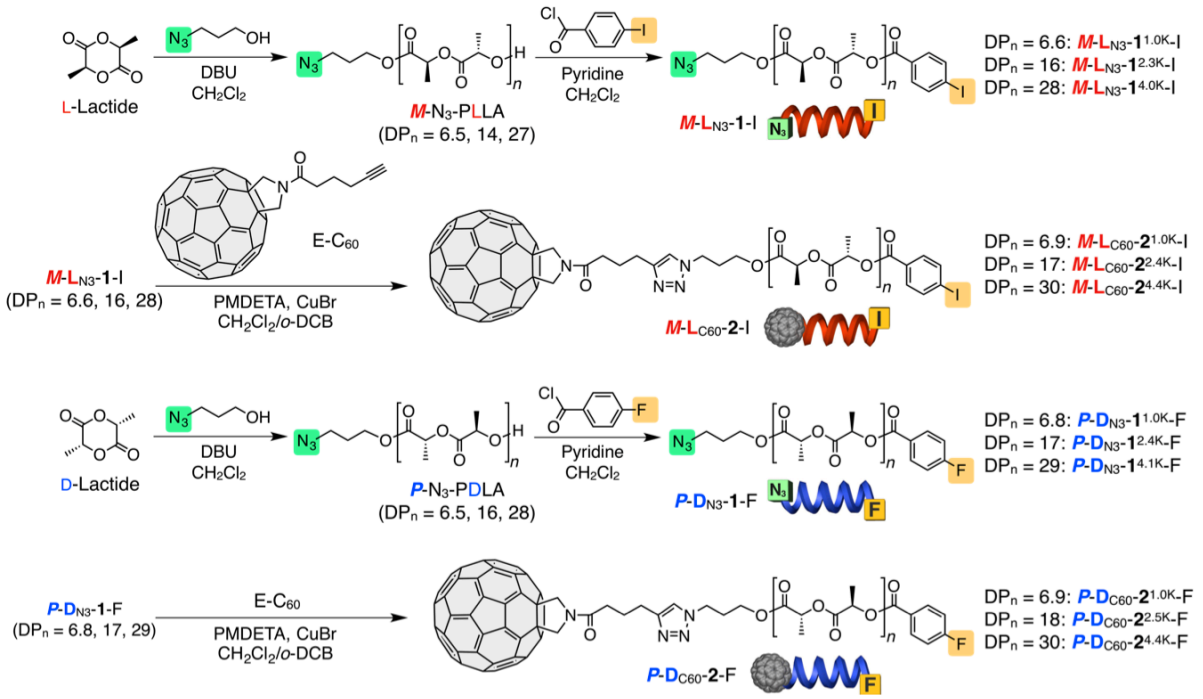

Results and Discussion

Synthesis and Characterization of C_{60}-Free and C_{60}-Bound *M*- and *P*-Helical PLAs. The C_{60}-free (N_3-**1**) and C_{60}-bound *M*-L- and *P*-D-helical PLAs (C_{60}-**2**) with different molar masses and a narrow molar mass distribution were synthesized according to Scheme 3-1. The ring-opening living polymerization of the optically pure L- and D-lactides (enantiomeric excess (ee) > 99% (Figure 3-S1)) initiated with 3-azido-1-propanol in the presence of 1,8-diazabicyclo[5.4.0]-7-undecene (DBU) as a catalyst (Table 3-S1),[90] followed by esterification of the terminal hydroxy groups using 4-iodo- and 4-fluorobenzoyl chlorides, respectively, afforded the C_{60}-free *M*- and *P*-helical PLAs (***M***-$\mathbf{L}_{N3}$-**1**-I and ***P***-$\mathbf{D}_{N3}$-**1**-F) (Table 3-S2). The copper(I)-catalyzed click reaction of the resulting PLAs bearing an azido residue (***M***-$\mathbf{L}_{N3}$-**1**-I and ***P***-$\mathbf{D}_{N3}$-**1**-F) with an alkyne-terminated C_{60} derivative (E-C_{60}) produced the C_{60}-bound *M*- and *P*-helical PLAs (***M***-$\mathbf{L}_{C60}$-**2**-I and ***P***-$\mathbf{D}_{C60}$-**2**-F) in good yields (Table 3-S3). The different terminal benzoate groups were introduced to the C_{60}-free and C_{60}-bound *M*-L- and *P*-D-helical PLAs to determine the ee of the nonracemic **1** and **2** by ^{1}H NMR spectroscopy after enantioselective extractions, respectively (see below (Figure 3-6a)), since the L- and D-PLA enantiomers could not be separated by chiral HPLC.

The polymerization results of the L- and D-lactides and characteristics of the PLA prepolymers and the C_{60}-free and C_{60}-bound *M*- and *P*-helical PLAs are summarized in Table 3-1. The structures were fully characterized and identified using size exclusion chromatography (SEC), NMR and IR spectroscopies, and matrix-assisted laser desorption-ionization time-of-flight mass (MALDI-TOF-MS) measurements (see the Experimental Section and Figures 3-2 and 3-S2 – 3-S6). The number-average molar masses ($M_{n,NMR}$) of the PLA chains and the functionalities ($f_{end\ group}$) of the 4-iodo- or 4-fluorobenzoate ($f_{benzoate}$) and C_{60} (f_{C60}) of the isolated C_{60}-free and C_{60}-bound PLAs were estimated based on the ^{1}H NMR end group analyses, showing the almost complete functionalizations of the PLA terminal ends, which were further supported by the MALDI-TOF-MS measurements. The MALDI-TOF-MS spectra of a series of ***M***-N_3–PLLA and ***P***-N_3–PDLA with different $M_{n,NMR}$ values before and after end-capping with 4-iodo- or

4-fluorobenzoyl chloride followed by C_{60} showed one main series of peaks, whose intervals were regular and separated by approximately 144.0 (*m*/*z*) mass corresponding to the molar mass of the lactic acid monomer; each molecular peak equals the molecular mass expected for the as-prepared PLAs (***M***-N_3–PLLA and ***P***-N_3–PDLA) end-capped with 4-iodo- or 4-fluorobenzoate (***M***-$\mathbf{L}_{N3}$-**1**-I and ***P***-$\mathbf{D}_{N3}$-**1**-F) and further with C_{60} (***M***-$\mathbf{L}_{C60}$-**2**-I and ***P***-$\mathbf{D}_{C60}$-**2**-F) (Figures 3-2b and 3-S2 – 3-S6). Sample codes are abbreviated using the helicity of PLA (*M* or *P*), the absolute configuration of the lactide (L or D), $M_{n,NMR}$, and the end groups such that ***M***-$\mathbf{L}_{C60}$-$\mathbf{2}^{1.0K}$-I, for example, stands for the *M*-PLLA end-capped with 4-iodobenzoate and C_{60} with the $M_{n,NMR}$ of the PLA chain (ca. 1.0 K) (Scheme 3-1 and Table 3-1).

The st-PMMA was sy*n*thesized using the stereospecific polymerization technique.[91] The M_n, its distribution (M_w/M_n), and stereoregularities (*mm* : *mr* : *rr*) were as follows: M_n = 616 kDa, M_w/M_n = 1.36, and *mm* : *mr* : *rr* = 0 : 4 : 96, in which *m* and *r* represent the isotactic (it) and st dyads of the meso and racemo sequences, respectively, and *mm*, *mr*, and *rr* are the corresponding triad sequences.

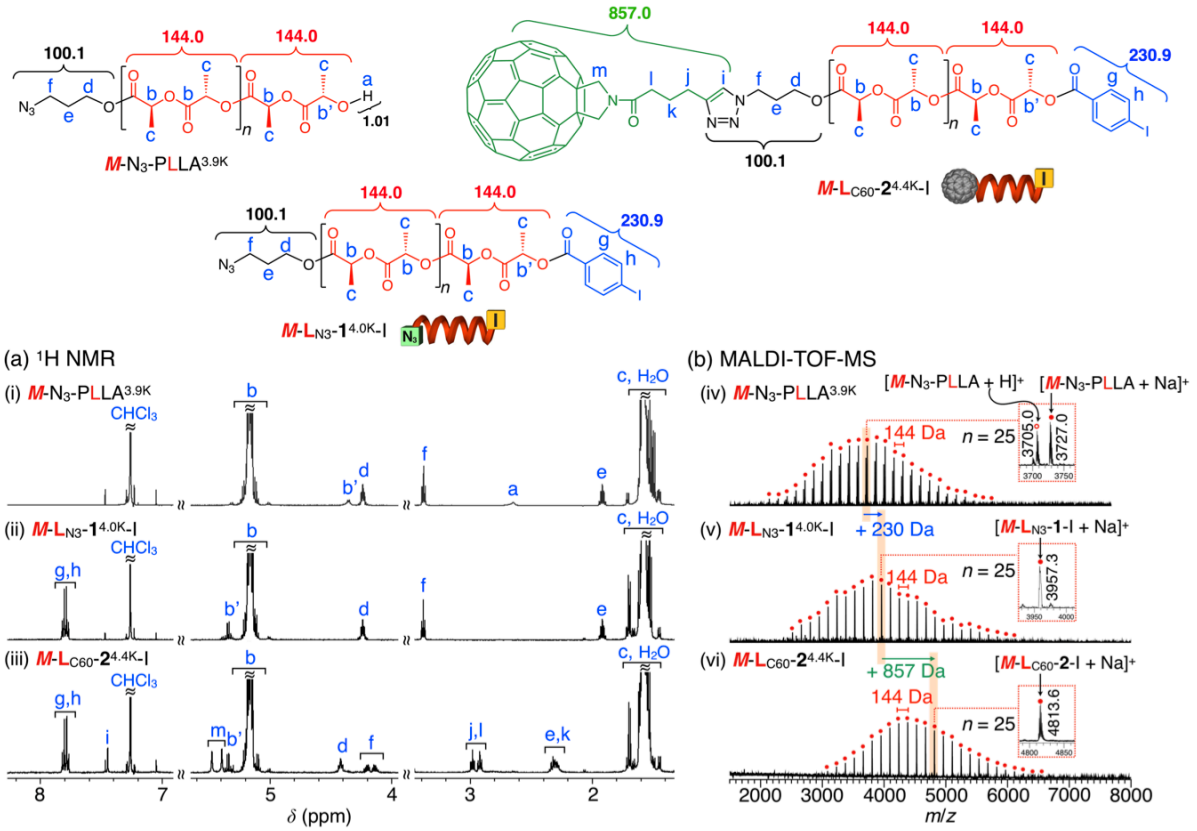

Figure 3-2. (a) ^{1}H NMR and (b) MALDI-TOF-MS spectra of ***M***-N_3–PLLA$^{3.9K}$, ***M***-**L**$_{N3}$-**1**$^{4.0K}$-I, and ***M***-**L**$_{C60}$-**2**$^{4.4K}$-I. The NMR spectra were measured in $CDCl_3$ at 25 °C and the MS measurements were performed using dithranol as a matrix and sodium iodide as a cationizing agent.

Table 3-1. Characteristics of PLA Prepolymers and C_{60}-Free and C_{60}-Bound *M*- and *P*-PLAs

entry	sample code	$M_{n,SEC}$ (10^3) [a]	M_w/M_n [a]	$M_{n,NMR}$ (10^3) [b]	$DP_{n,NMR}$ [c]	$f_{end\ group}$ (%) [d]	T_m (°C) [e]
1	***M*-N_3-PLLA$^{0.9K}$**	1.53	1.26	0.94	6.5	–	92
2	***M*-N_3-PLLA$^{2.1K}$**	3.55	1.11	2.08	14	–	130
3	***M*-N_3-PLLA$^{3.9K}$**	6.28	1.11	3.85	27	–	151
4	***M*-L_{N3}-1$^{1.0K}$-I**	1.61	1.19	0.95	6.6	>99	96
5	***M*-L_{N3}-1$^{2.3K}$-I**	4.14	1.11	2.30	16	>99	137
6	***M*-L_{N3}-1$^{4.0K}$-I**	6.53	1.12	4.01	28	>99	149
7	***M*-L_{C60}-2$^{1.0K}$-I**	1.82	1.24	0.99	6.9	>99	– [f]
8	***M*-L_{C60}-2$^{2.4K}$-I**	4.38	1.20	2.43	17	>99	141
9	***M*-L_{C60}-2$^{4.4K}$-I**	7.73	1.32	4.36	30	>99	146
10	***P*-N_3-PDLA$^{0.9K}$**	1.40	1.31	0.94	6.5	–	93
11	***P*-N_3-PDLA$^{2.3K}$**	3.82	1.12	2.28	16	–	136
12	***P*-N_3-PDLA$^{4.0K}$**	7.11	1.12	4.04	28	–	152
13	***P*-D_{N3}-1$^{1.0K}$-F**	1.62	1.23	0.98	6.8	>99	95
14	***P*-D_{N3}-1$^{2.4K}$-F**	4.15	1.11	2.41	17	>99	138
15	***P*-D_{N3}-1$^{4.1K}$-F**	7.38	1.12	4.11	29	>99	149
16	***P*-D_{C60}-2$^{1.0K}$-F**	1.63	1.41	1.00	6.9	>99	– [f]
17	***P*-D_{C60}-2$^{2.5K}$-F**	4.75	1.26	2.52	18	>99	141
18	***P*-D_{C60}-2$^{4.4K}$-F**	7.93	1.35	4.39	30	>99	146

[a] Estimated by SEC (polystyrene standards) with $CHCl_3$ as the eluent. [b] Determined by the ^{1}H NMR end-group analysis in $CDCl_3$. [c] Number-average degree of polymerization determined by $M_{n,NMR}$. [d] Functionality of the end-capped benzoate (entries 4–6 and 13–15) or C_{60} (entries 7–9 and 16–18) residue estimated by ^{1}H NMR in $CDCl_3$. [e] Melting point determined by DSC. [f] Not observed in the DSC thermogram.

Inclusion Complex Formation of C_{60}-Bound and C_{60}-Free PLAs with st-PMMA. As reported previously,[59] the st-PMMA/C_{60} complex gels in toluene were completely dissolved to form homogeneous solutions by heating above 90 °C, in which st-PMMA and C_{60} molecules are molecularly dispersed. On the basis of this observation, the encapsulation experiments of PLAs with st-PMMA were performed in toluene at 110 °C. As anticipated, the C_{60}-bound PLAs (***M*-L$_{C60}$-2**-I and ***P*-D$_{C60}$-2**-F) were efficiently encapsulated within the st-PMMA helical cavity during gelation of an optically inactive st-PMMA in toluene upon heating at 110 °C, followed by cooling to room temperature (Figure 3-3a),[59-62,75] which was almost independent of the $M_{n,NMR}$ of **2**. Typically, st-PMMA (10 mg) was dissolved in a toluene solution of ***M*-L$_{C60}$-2$^{4.4K}$**-I (3.0 mg/mL, 1.0 mL) at 110 ºC. After the solution was cooled to room temperature, the solution gelled within 10 min (Figure 3-3a, middle). The resulting soft gel was then centrifuged at 1700 *g* for 10 min (Figure 3-3a, right), and the supernatant containing the unencapsulated ***M*-L$_{C60}$-2$^{4.4K}$**-I was removed from the gel by decantation. The amount of the ***M*-L$_{C60}$-2$^{4.4K}$**-I encapsulated in the st-PMMA was estimated based on the differences in the absorption spectra between the feed ***M*-L$_{C60}$-2$^{4.4K}$**-I and the supernatant (Figure 3-S7) according to a previously reported method.[75] The inclusion complex formation results are summarized in Table 3-2. The encapsulated C_{60}-bound **2** content increased by using a higher concentrated C_{60}-bound **2** solution in toluene (>9.0 mg/mL) as the feed and reached an almost maximum value of ~24 wt% (run 5, Table 3-2).

The "helix-in-helix" superstructured inclusion complex formations were confirmed by differential scanning calorimetry (DSC) and X-ray diffraction (XRD) measurements of the st-PMMA complexed with C_{60}-bound **2** films containing about 15 wt% of C_{60}-bound **2** prepared from the gels, which revealed a crystalline structure of the st-PMMA/ C_{60}-bound **2** complexes (Figure 3-3c,d and Table 3-2) as supported by an apparent melting temperature (T_m) (ca. 180 °C) and a characteristic reflection at the *d*-spacing of ~1.8 nm due to the bundle structures of the helical st-PMMA chains, which are almost independent of the $M_{n,NMR}$ of **2**; the observed *d*-spacing is larger than that of the st-PMMA complexed with C_{60} (1.67 nm) but

smaller than that with larger fullerenes, such as C_{70} (1.92 nm) and C_{84} (2.04 nm),[59] and is almost identical to that with the C_{60}-bound *P*-L-peptide (Figure 3-1a) (1.80 nm).[75] The author also found that significant differences were not observed in the T_m and *d*-values when the encapsulated C_{60}-bound **2** content in the st-PMMA increased to 23.5 wt% (run 5, Table 3-2 and Figure 3-S8). Contrary to the expectation, the C_{60}-free PLA (***M***-$\mathbf{L}_{N3}$-$\mathbf{1}^{4.0K}$-I) was also found to form an inclusion complex with st-PMMA in toluene by heating followed by cooling to room temperature, resulting in gelation (Figure 3-3b). Compared with the previously reported C_{60}-free 10_3-helical peptides that could not form an inclusion complex with st-PMMA,[75] the PLA chains with the same helical geometry seem to more compatibly fit the helical cavities of the st-PMMA, leading to a larger enthalpy gain that mostly overcomes the entropic loss. The st-PMMA/C_{60}-free **1** inclusion complex film showed a slightly lower T_m value (174 °C) but a similar *d*-value (1.86 nm) as those of the st-PMMA/C_{60}-bound **2** complexes (Figure 3-3c–e, and Table 3-2). St-PMMA has been suggested to form a crystalline stereocomplex only with its complementary it-PMMA since its discovery in 1958.[92–94] Hence, the present finding will provide a rare opportunity for applications of the crystalline st-PMMA/PLA complexes as a practically useful hybrid plastic composed of biodegradable PLAs.

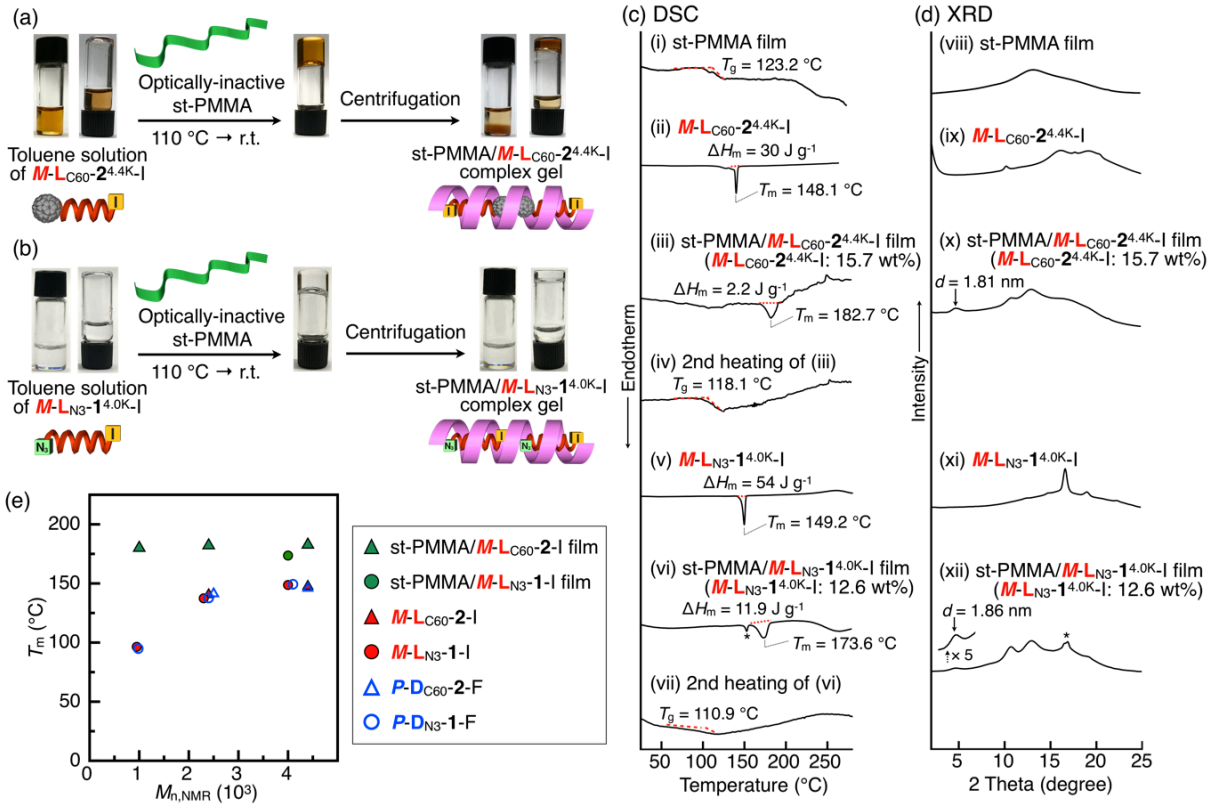

Figure 3-3. (a, b) Photographs of toluene solutions of ***M*-L$_{C60}$-2$^{4.4K}$-I** (a; 3.0 mg/mL, 1.0 mL; left) and ***M*-L$_{N3}$-1$^{4.0K}$-I** (b; 14.5 mg/mL, 0.80 mL; left), st-PMMA/***M*-L$_{C60}$-2$^{4.4K}$-I** (a) and st-PMMA/***M*-L$_{N3}$-1$^{4.0K}$-I** (b) gels after the addition of st-PMMA (10 mg (a) and 8 mg (b), respectively) with subsequent heating to 110 °C and then cooling to room temperature (middle), and the st-PMMA/***M*-L$_{C60}$-2$^{4.4K}$-I** (a) and st-PMMA/***M*-L$_{N3}$-1$^{4.0K}$-I** (b) complex gels after centrifugation at 1700 *g* for 10 min (right). (c) DSC thermograms of st-PMMA (i), ***M*-L$_{C60}$-2$^{4.4K}$-I** (ii), st-PMMA/***M*-L$_{C60}$-2$^{4.4K}$-I** complex film containing 15.7 wt% of ***M*-L$_{C60}$-2$^{4.4K}$-I** (iii), ***M*-L$_{N3}$-1$^{4.0K}$-I** (v), and st-PMMA/***M*-L$_{N3}$-1$^{4.0K}$-I** complex film containing 12.6 wt% of ***M*-L$_{N3}$-1$^{4.0K}$-I** (vi). These films were prepared by evaporating the solvents from the st-PMMA and st-PMMA/PLA complex gels in toluene. The DSC measurements were conducted after cooling the samples at –20 °C, followed by heating to 280 °C (10 °C/min) under nitrogen. The samples (iii) and (vi) were then cooled to –20 °C (40 °C/min), and then heated again ((iv) and (vii), respectively; 10 °C/min). The arrow to the left of the DSC data indicates the endothermic direction. Asterisk (*) in (vi) denotes the melting peak from the free ***M*-L$_{N3}$-1$^{4.0K}$-I**. (d) XRD profiles of st-PMMA (viii), ***M*-L$_{C60}$-2$^{4.4K}$-I** (ix),

st-PMMA/***M***-$\mathbf{L}_{C60}$-$\mathbf{2}^{4.4K}$-I complex film (15.7 wt%) (x), ***M***-$\mathbf{L}_{N3}$-$\mathbf{1}^{4.0K}$-I (xi), and st-PMMA/***M***-$\mathbf{L}_{N3}$-$\mathbf{1}^{4.0K}$-I complex film (12.6 wt%) (xii). Asterisk (*) in (xii) denotes the diffraction peak from the free ***M***-$\mathbf{L}_{N3}$-$\mathbf{1}^{4.0K}$-I. (e) Plots of melting temperature (T_m) of st-PMMA/PLAs complex films and PLAs versus the number-average molar mass of PLAs.

Table 3-2. Characteristics of Inclusion Complexes of C_{60}-Bound and C_{60}-Free *M*- and *P*-PLAs with st-PMMA [a]

run	PLA	st-PMMA/PLA inclusion complex		
		encapsulated PLA (wt%) [b]	*d* (nm) [c]	T_m (°C) [d]
1	***M***-$\mathbf{L}_{C60}$-$\mathbf{2}^{1.0K}$-I	15.2	1.77	180
2	***M***-$\mathbf{L}_{C60}$-$\mathbf{2}^{2.4K}$-I	15.3	1.82	181
3	***M***-$\mathbf{L}_{C60}$-$\mathbf{2}^{4.4K}$-I	15.7	1.81	183
4	***P***-$\mathbf{D}_{C60}$-$\mathbf{2}^{4.4K}$-F	16.8	–	–
5	***M***-$\mathbf{L}_{C60}$-$\mathbf{2}^{4.4K}$-I	23.5	1.86	181
6	***M***-$\mathbf{L}_{N3}$-$\mathbf{1}^{4.0K}$-I	12.6	1.86	174

[a] The st-PMMA/PLA complex gels were prepared by adding a toluene (runs 1–5) or toluene-d_8 (run 6) solution of PLA (3.0 mg/mL, 1.0 mL in runs 1–4, 9.0 mg/mL, 0.40 mL in run 5, and 14.5 mg/mL, 0.80 mL in run 6) to st-PMMA (10.0 mg in runs 1–4, 4.0 mg in run 5, and 8.0 mg in run 6) followed by heating to 110 °C and cooling to room temperature, and then centrifuged. [b] Determined by absorption (runs 1–5) and ^{1}H NMR (run 6) analyses. [c] Estimated by XRD of the st-PMMA/PLA complex films. [d] Melting point determined by DSC of the st-PMMA/PLA complex films.

Preferred-Handed Helix Formation in st-PMMA Induced by C_{60}-Bound and C_{60}-Free *M*- and *P*-PLAs. We anticipated that the one-handed helical C_{60}-bound and C_{60}-free *M*- and *P*-PLAs could induce one of the helices in st-PMMA once encapsulated in the st-PMMA helical cavity (Figure 3-1b), as observed for the inclusion complex formation with the C_{60}-bound *M*-D- and *P*-L-peptides.[75] In fact, the st-PMMA gels complexed with C_{60}-bound *M*- and *P*-C_{60}-**2** (15.6 – 18.5 wt%) showed mirror-image electric circular dichroism (ECD) and vibrational CD (VCD) spectra in the achiral fullerene chromophore and PMMA IR regions in toluene and toluene-d_8, respectively (Figures 3-4d,e and 3-S9f–i), while the C_{60}-bound PLAs (C_{60}-**2**) themselves exhibited negligibly weak ECD signals in the achiral fullerene chromophore regions in toluene-d_8 (Figures 3-4a and 3-S9b,c). The C_{60}-free *M*- and *P*-PLAs (N_3-**1**) also induced an excess of the one helical sense in st-PMMA, thus showing VCD signals in the PMMA IR regions (Figure 3-4f), which were different from those of the C_{60}-free *M*- and *P*-PLAs (N_3-**1**) (Figure 3-4c). The observed VCD spectral patterns of the st-PMMAs complexed with C_{60}-bound and C_{60}-free *M*- and *P*-PLAs agree well with those of the calculated *M*- and *P*-18_1-helical st-PMMAs, respectively (Figure 3-4g), thereby producing the helix-in-helix superstructures with the same-handedness to each other.[60,75] The inclusion complex structure of *M*-st-PMMA with C_{60}-bound and C_{60}-free *M*-PLA optimized by molecular mechanics calculations based on an 18_1-helical st-PMMA structure[66] support the helix-in-helix superstructure, in which the encapsulated C_{60}-bound and C_{60}-free *M*-PLA fill the st-PMMA helical nanotube while maintaining its 10_3-helical structures (Figure 3-S10).[78–80] The molecular arrangements of the C_{60}-bound and C_{60}-free *M*-PLAs within the st-PMMA helical cavity are not clear at present, but preferable stacking interactions between the C_{60} units of the C_{60}-bound-PLAs[59,75,94,95] may suggest a head-to-head packing array that may exist in part. The VCD intensities of the st-PMMAs induced by the C_{60}-bound and C_{60}-free *M*- and *P*-PLAs were relatively weaker than those induced by the (*R*)- and (*S*)-**3**[62] and C_{60}-bound *P*-L- and *M*-D-10_3-helical peptides.[75]

Interestingly, the encapsulated C_{60}-bound and C_{60}-free PLAs in the st-PMMA cavities could

be almost completely replaced by the achiral C_{60} as evidenced by the difference in the absorption or NMR spectra before and after the replacement (Figures 3-1b and 3-S12) due to a higher affinity of st-PMMA to C_{60} over the C_{60}-bound and C_{60}-free PLAs. More interestingly, the preferred-handed helical structures of the st-PMMAs induced by the C_{60}-bound and C_{60}-free *M*- and *P*-PLAs were retained after replacement by the achiral C_{60}, thus showing apparent ECDs in the C_{60} chromophore regions (Figure 3-5a), which were completely different from those of the st-PMMA complexed with *M*- and *P*-C_{60}-bound PLAs (Figure 3-4d), but were similar in their patterns to those of the st-PMMA/C_{60} complexes prepared from the isolated optically active *M*- and *P*-st-PMMAs complexed with C_{60},[59,62] indicating that the induced helical conformations of the st-PMMAs were memorized after the *M*- and *P*-C_{60}-bound and C_{60}-free PLAs were replaced by the achiral C_{60}.[59,60,62] The ECD intensities of the helicity-memorized *M*- and *P*-st-PMMA/C_{60} complexes were almost identical and independent of the terminal groups (C_{60} or azido group) of the PLA chains when the amounts of the encapsulated *M*- and *P*-PLA chains are the same (Figure 3-5b(ii–v)), indicating that the helical chirality of the *M*- and *P*-PLA chains play a dominant role to induce the preferred-handed helical conformation in st-PMMA. The ECD intensity of the helicity-memorized st-PMMA complexed with C_{60} tended to increase with an increase in the amount of the C_{60}-bound and C_{60}-free *M*- and *P*-PLAs encapsulated in the st-PMMA helical cavity during the helicity induction process (Figures 3-5b(i,ii) and 3-S13).

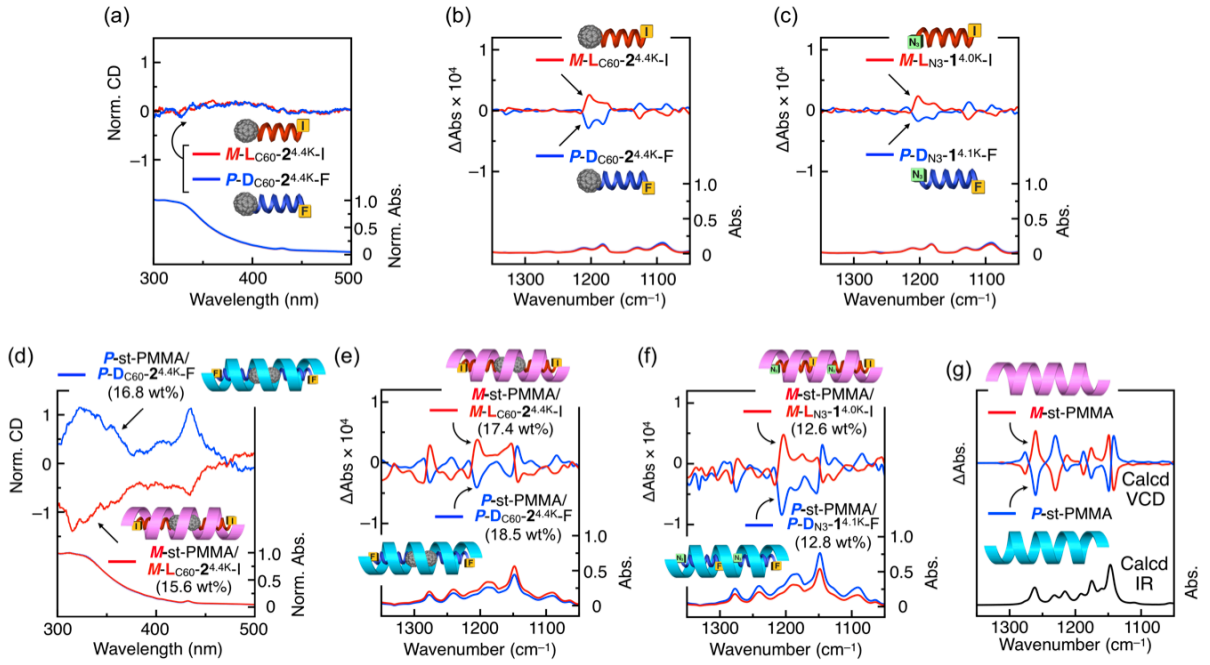

Figure 3-4. (a,d) ECD (top) and absorption (bottom) spectra of ***M*-L$_{C60}$-2$^{4.4K}$-I** (5.1×10^{-4} M) (red) and ***P*-D$_{C60}$-2$^{4.4K}$-F** (5.3×10^{-4} M) (blue) (a) in toluene-d_8 at 25 °C and those of st-PMMA/***M*-L$_{C60}$-2$^{4.4K}$-I** gel (15.6 wt%) (red) and st-PMMA/***P*-D$_{C60}$-2$^{4.4K}$-F** gel (16.8 wt%) (blue) (d) in toluene at 25 °C. The ECD and absorption spectra in (a,d) were normalized based on the corresponding absorption spectra at 25 °C. The contribution of the linear dichroism caused by the macroscopic anisotropy was negligible (d). The corresponding ECD and absorption spectra of st-PMMA/***M*-L$_{C60}$-2$^{4.4K}$-I** gel containing a higher content of ***M*-L$_{C60}$-2$^{4.4K}$-I** (25.5 wt%) are shown in Figure 3-S11. (b,e) VCD (top) and IR (bottom) spectra of ***M*-L$_{C60}$-2$^{4.4K}$-I** (5.1×10^{-4} M) (red) and ***P*-D$_{C60}$-2$^{4.4K}$-F** (5.3×10^{-4} M) (blue) (b) and those of st-PMMA/***M*-L$_{C60}$-2$^{4.4K}$-I** (17.4 wt%) (red) and st-PMMA/***P*-D$_{C60}$-2$^{4.4K}$-F** (18.5 wt%) (blue) complex gels (e) in toluene-d_8 at room temperature. (c,f) VCD (top) and IR (bottom) spectra of ***M*-L$_{N3}$-1$^{4.0K}$-I** (6.7×10^{-4} M) (red) and ***P*-D$_{N3}$-1$^{4.1K}$-F** (6.7×10^{-4} M) (blue) (c) and those of st-PMMA/***M*-L$_{N3}$-1$^{4.0K}$-I** (12.6 wt%) (red) and st-PMMA/***P*-D$_{N3}$-1$^{4.1K}$-F** (12.8 wt%) (blue) complex gels (f) in toluene-d_8 at room temperature. (g) Calculated VCD (top) and IR (bottom) spectra of *M*- (red line) and *P*- (blue line) helical st-PMMAs.[59]

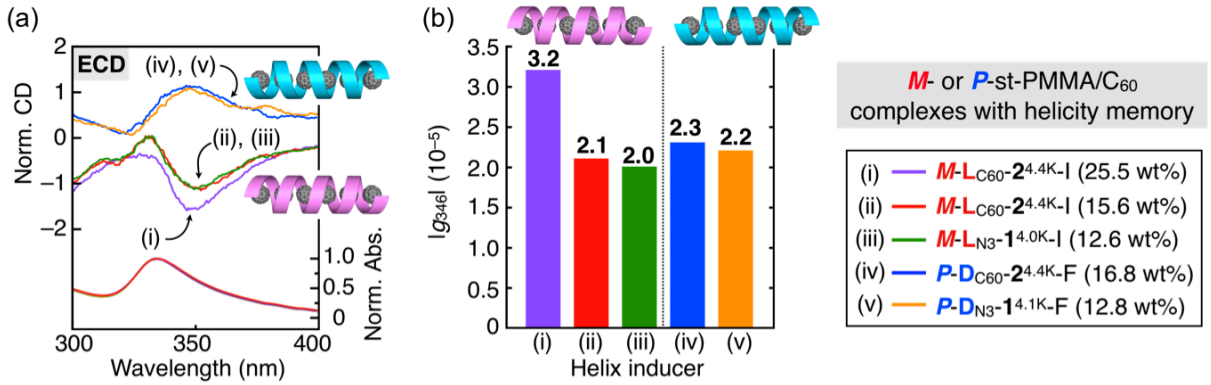

Figure 3-5. (a) ECD (top) and absorption (bottom) spectra of isolated st-PMMA/C_{60} complex gels in toluene prepared by complexation with ***M*-L**$_{C60}$-**2**$^{4.4K}$-I (i; 25.5 wt%, ii; 15.6 wt%), ***M*-L**$_{N3}$-**1**$^{4.0K}$-I (iii; 12.6 wt%), ***P*-D**$_{C60}$-**2**$^{4.4K}$-F (iv; 16.8 wt%), and ***P*-D**$_{N3}$-**1**$^{4.1K}$-F (v; 12.8 wt%) followed by replacement with the achiral C_{60}. Complete removal of the optically active PLAs was confirmed by ^{1}H NMR measurements of the isolated st-PMMA/C_{60} complexes (Figure 3-S12). The ECD and absorption spectra were normalized based on the corresponding absorption spectra at 25 °C. (b) Kuhn's dissymmetry factors at 346 nm ($|g_{346}|$) of the isolated st-PMMA/C_{60} complexes (i–v) in (a).

Helix-Sense-Selective Encapsulation of C_{60}-Bound and C_{60}-Free PLAs within the Helical Cavity of *M*- and *P*-st-PMMA with a Helicity Memory. Enantioselective extractions of the racemic C_{60}-bound (*rac*-C_{60}-**2**) and C_{60}-free (*rac*-N_3-**1**) *M*- and *P*-PLAs with a different $M_{n,NMR}$ and the end groups by the *M*- and *P*-st-PMMAs with a helicity memory were then performed (Figure 3-1c). The optically active *M*- and *P*-st-PMMAs with an excess single-handed helix were prepared according to a previously reported method using (*R*)- and (*S*)-**3** as the chiral solvent by heating at 110 °C, followed by cooling to room temperature, resulting in the gels composed of the *M*- and *P*-st-PMMAs, respectively, which were then repeatedly washed with toluene to completely remove (*R*)- and (*S*)-**3**, then isolated by centrifugation.[61,62]

Typically, the condensed *M*-st-PMMA gel (3.0 mg) prepared by (*R*)-**3** was suspended in a toluene solution of *rac*-C_{60}-$\mathbf{2}^{4K}$ composed of an equal mixture of ***M***-$\mathbf{L}_{C60}$-$\mathbf{2}^{4.4K}$-I and ***P***-$\mathbf{D}_{C60}$-$\mathbf{1}^{4.4K}$-F (1.8 mg/mL, 0.50 mL) with stirring at room temperature for 3 h to produce the *M*-st-PMMA/C_{60}-$\mathbf{2}^{4K}$ complex gel,[97] in which 0.47 mg of the nonracemic C_{60}-$\mathbf{2}^{4K}$ (52% yield) was encapsulated within the *M*-st-PMMA cavities as estimated by the ^{1}H NMR of the *M*-st-PMMA/C_{60}-$\mathbf{2}^{4K}$ complex dissolved in $CDCl_3$ (run 5 in Table 3-3). The yield of the encapsulated C_{60}-$\mathbf{2}^{4K}$ was almost consistent with that calculated from the difference in the absorption spectra of the racemic C_{60}-$\mathbf{2}^{4K}$ in toluene before and after the single extraction (Figure 3-S15a).[59,61,75] The ee value of the encapsulated C_{60}-$\mathbf{2}^{4K}$ was estimated to be 49% (***M***-$\mathbf{L}_{C60}$-$\mathbf{2}^{4.4K}$-I rich) by the ^{1}H NMR analysis (run 5 in Table 3-3 and Figure 3-6a(ii)). When the opposite (*S*)-**3** was used as the chiral solvent during the helix induction in st-PMMA, the resulting opposite *P*-st-PMMA with the helicity memory enantioselectively extracted the opposite enantiomer of C_{60}-$\mathbf{2}^{4K}$, giving 50% ee of C_{60}-$\mathbf{2}^{4K}$ (***P***-$\mathbf{D}_{C60}$-$\mathbf{2}^{4.4K}$-F rich) in 53% yield (run 6 in Table 3-3 and Figure 3-6a(iv) and 3-S14b). The author noted that the ee values of the unencapsulated C_{60}-$\mathbf{2}^{4K}$ remaining in the supernatants were also determined to be 53 (***P***-$\mathbf{D}_{C60}$-$\mathbf{2}^{4.4K}$-F rich) and 53% (***M***-$\mathbf{L}_{C60}$-$\mathbf{2}^{4.4K}$- rich) when the *M*- and *P*-st-PMMA gels were used, respectively (Figure 3-6a(iii,v)), which were in reasonably consistent agreement with

the calculated ee values based on the amounts and ee of the encapsulated C_{60}-**2**^{4K} (runs 5 and 6 in Table 3-3).

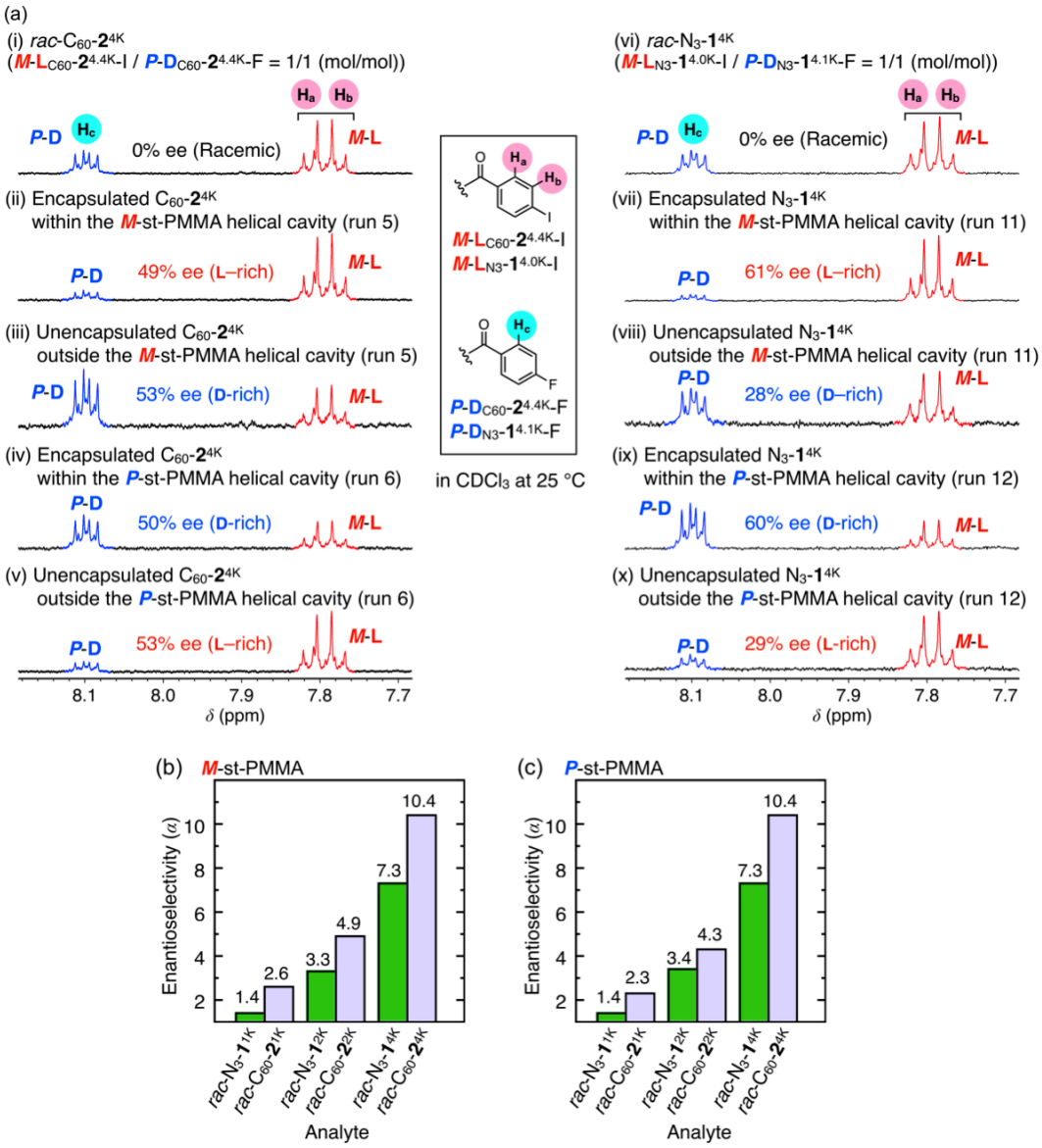

Figure 3-6. (a) ^{1}H NMR ($CDCl_3$, 25 °C) spectra of *rac*-C_{60}-**2**^{4K} (i) and helix-sense selectively encapsulated C_{60}-**2**^{4K} (L-rich (ii) or D-rich (iv)) and unencapsulated C_{60}-**2**^{4K} (D-rich (iii) or L-rich (v)) in the *M*- (ii and iii) (run 5, Table 3-3) and *P*- (iv and v) (run 6, Table 3-3) helical st-PMMA, respectively, and those of *rac*-N_3-**1**^{4K} (vi) and helix-sense selectively encapsulated N_3-**1**^{4K} (L-rich (vii) or D-rich (ix)) and unencapsulated N_3-**1**^{4K} (D-rich (viii) or L-rich (x)) in the *M*- (vii and viii) (run 11, Table 3-3) and *P*- (ix and x) (run 12, Table 3-3) helical st-PMMA, respectively. (b,c) Separation factors (enantioselectivity) (α) on *M*-st-PMMA (b) and *P*-st-PMMA (c) for *rac*-N_3-**1** (green bar) and *rac*-C_{60}-**2** (purple bar) with different molar masses.

The enantioselective extraction results of a series of *rac*-N_3-**1** and *rac*-C_{60}-**2** samples with a different $M_{n,NMR}$ and the end groups (azido or C_{60} group) are summarized in Table 3-3. The results revealed that the helical PLA segment of N_3-**1** and C_{60}-**2** that fit the helical cavities of the st-PMMAs with the same helical handedness as those of the PLAs are preferentially entrapped, which well agrees with the facts that the *M*-L-PLAs and *P*-D-PLAs induced the same *M*- and *P*-helical conformations in the st-PMMA backbone independent of the terminal residues (azido or C_{60} group), respectively, once encapsulated as previously described. The ee values of C_{60}-free **1** and C_{60}-bound **2** enantio- and helix-sense selectively entrapped in the optically active *M*- and *P*-st-PMMA are variable depending on the amounts (yields) of the encapsulated N_3-**1** and C_{60}-**2**, therefore, the author employed the separation factor (enantioselectivity) (α)[98–100] to evaluate the chiral recognition ability of the *M*- and *P*-st-PMMA toward the *rac*-N_3-**1** and *rac*-C_{60}-**2** (Table 3-3).

The C_{60}-bound PLAs (*rac*-C_{60}-**2**) were more efficiently and enantioselectively encapsulated in the helical cavity of the st-PMMA than the corresponding C_{60}-free *rac*-N_3-**1** under the similar experimental conditions using almost the identical $M_{n,NMR}$ of PLAs, probably because the terminal achiral C_{60} residues of the C_{60}-bound PLAs most likely contribute to enhancing the inclusion complexations with the st-PMMA, which could further enhance the hydrophobic interactions between the chiral PLA chains and the helical cavity of the st-PMMA, resulting in greater encapsulation yields and hence higher α values over the corresponding C_{60}-free PLAs. The enantioselectivity (α value) was highly dependent on the $M_{n,NMR}$ of the C_{60}-free and C_{60}-bound PLAs and showed a clear tendency that the α value significantly increased as the $M_{n,NMR}$ of the PLAs increased such that 1.4 < 3.3–3.4 < 7.3 and 2.3–2.6 < 4.3–4.9 < 10.4 for the C_{60}-free *rac*-N_3-**1** and C_{60}-bound *rac*-C_{60}-**2**, respectively (Figure 3-6b,c and Table 3-3). and eventually reached the excellent α value of ~10, thus giving approximately 50% ee for both the optically active ***M***- and ***P***-C_{60}-$\mathbf{2}^{4.4K}$ that could be isolated by a single extraction using *M*- and *P*-st-PMMA, when *rac*-C_{60}-**2** composed of an equal mixture of the highest molar mass PLAs, ***M***-$\mathbf{L}_{C60}$-$\mathbf{2}^{4.4K}$-I and ***P***-$\mathbf{D}_{C60}$-$\mathbf{2}^{4.4K}$-F, was used (runs 5 and 6 in Table 3-3). The observed

molar mass-dependent enhancement of the enantioselectivity is most likely due to the effective increases in the one-handed helical chain lengths of the *M*- and *P*-PLAs that allow further enhancement of the hydrophobic chiral interactions with the one-handed st-PMMA helical cavity. Furthermore, when the enantioselective extraction by *M*-st-PMMA with a helicity memory was further performed using nonracemic C_{60}-**2**^{4K} (53% ee (D-rich)) as an analyte that can be obtained by single extraction with *M*-st-PMMA (run 5 in Table 3-3), the ee value of the unencapsulated C_{60}-**2**^{4K} remaining in the supernatants increased to 87% ee (D-rich) (Figure 3-7 and run 13 in Table 3-3), thus providing a practically useful resolution method to obtain both helices of the PLAs with a high optical purity only by two extractions using *M*- or *P*-st-PMMA with a helicity memory.

Table 3-3. Helix-Sense-Selective Encapsulation of C_{60}-Bound Racemic and Nonracemic 2 and C_{60}-Free Racemic 1 by *M*- and *P*-Helical st-PMMA with Helicity Memory [a,b]

run	analyte	handedness of st-PMMA [c]	analyte/ st-PMMA in feed (w/w)	encapsulated analyte		ee (%) of free analyte [f]	separation factor (a) [g]
				yield (%) [d]	ee (%) [e]		
1	*rac*-C_{60}-$\mathbf{2}^{1K}$	*M*	0.40	46 (41)	26, *M*-L	19 (18), *P*-D	2.6 (2.4)
2	*rac*-C_{60}-$\mathbf{2}^{1K}$	*P*	0.40	47 (42)	22, *P*-D	20 (16), *M*-L	2.3 (2.2)
3	*rac*-C_{60}-$\mathbf{2}^{2K}$	*M*	0.37	50 (48)	38, *M*-L	33 (35), *P*-D	4.9 (4.7)
4	*rac*-C_{60}-$\mathbf{2}^{2K}$	*P*	0.37	50 (47)	34, *P*-D	34 (31), *M*-L	4.3 (3.8)
5	*rac*-C_{60}-$\mathbf{2}^{4K}$	*M*	0.30	52 (55)	49, *M*-L	53 (59), *P*-D	10.4 (11.5)
6	*rac*-C_{60}-$\mathbf{2}^{4K}$	*P*	0.30	53 (54)	50, *P*-D	53 (58), *M*-L	10.4 (11.0)
7	*rac*-N_3-$\mathbf{1}^{1K}$	*M*	0.23	12	13, *M*-L	2, *P*-D	1.4
8	*rac*-N_3-$\mathbf{1}^{1K}$	*P*	0.23	11	13, *P*-D	2, *M*-L	1.4
9	*rac*-N_3-$\mathbf{1}^{2K}$	*M*	0.25	23	43, *M*-L	10, *P*-D	3.3
10	*rac*-N_3-$\mathbf{1}^{2K}$	*P*	0.25	25	43, *P*-D	13, *M*-L	3.4
11	*rac*-N_3-$\mathbf{1}^{4K}$	*M*	0.22	32	61, *M*-L	28, *P*-D	7.3
12	*rac*-N_3-$\mathbf{1}^{4K}$	*P*	0.22	32	60, *P*-D	29, *M*-L	7.3
13[h]	53% ee of C_{60}-$\mathbf{2}^{4K}$ (D-rich)	*M*	0.030	53 (52)	22, *P*-D	87 (87), *P*-D	9.4 (9.2)

[a] Experimental conditions: st-PMMA, 3.0 mg (runs 1–12), 15.0 mg (run 13); (*R*)- or (*S*)-**3**, 75 μL (runs 1–12), (*R*)-**3**, 380 μL (run 13); *rac*-C_{60}-$\mathbf{2}^{1K}$ (***M***-$\mathbf{L}_{C60}$-$\mathbf{2}^{1.0K}$-I / ***P***-$\mathbf{D}_{C60}$-$\mathbf{2}^{1.0K}$-F = 50/50 (mol/mol)), 1.2 mg in 0.50 mL toluene (runs 1,2); *rac*-C_{60}-$\mathbf{2}^{2K}$ (***M***-$\mathbf{L}_{C60}$-$\mathbf{2}^{2.4K}$-I / ***P***-$\mathbf{D}_{C60}$-$\mathbf{2}^{2.5K}$-F = 50/50 (mol/mol)), 1.1 mg in 0.50 mL toluene (runs 3,4); *rac*-C_{60}-$\mathbf{2}^{4K}$ (***M***-$\mathbf{L}_{C60}$-$\mathbf{2}^{4.4K}$-I / ***P***-$\mathbf{D}_{C60}$-$\mathbf{2}^{4.4K}$-F = 50/50 (mol/mol)), 0.89 mg in 0.50 mL toluene (runs 5,6); *rac*-N_3-$\mathbf{1}^{1K}$ (***M***-$\mathbf{L}_{N3}$-$\mathbf{1}^{1.0K}$-I / ***P***-$\mathbf{D}_{N3}$-$\mathbf{1}^{1.0K}$-F = 50/50 (mol/mol)), 0.68 mg in 0.50 mL toluene (runs 7,8); *rac*-N_3-$\mathbf{1}^{2K}$ (***M***-$\mathbf{L}_{N3}$-$\mathbf{1}^{2.3K}$-I / ***P***-$\mathbf{D}_{N3}$-$\mathbf{1}^{2.4K}$-F = 50/50 (mol/mol)), 0.76 mg in 0.50 mL toluene (runs 9,10); *rac*-N_3-$\mathbf{1}^{4K}$ (***M***-$\mathbf{L}_{N3}$-$\mathbf{1}^{4.0K}$-I / ***P***-$\mathbf{D}_{N3}$-$\mathbf{1}^{4.1K}$-F = 50/50 (mol/mol)), 0.67 mg in 0.50 mL toluene (runs 11,12); 53% ee of C_{60}-$\mathbf{2}^{4K}$ (D-rich) (***M***-$\mathbf{L}_{C60}$-$\mathbf{2}^{4.4K}$-I / ***P***-$\mathbf{D}_{C60}$-$\mathbf{2}^{4.4K}$-F = 23/77 (mol/mol)), 0.44 mg in 2.5 mL toluene (run 13). [b] Average values of two runs. [c] *M* and *P* denote left- and right-handed helical senses, respectively. [d] Determined by ^{1}H NMR. In parentheses are shown the values estimated by absorption measurements (runs 1–6 and 13). [e] Determined by ^{1}H NMR. [f] Determined by ^{1}H NMR. In parentheses are shown the calculated ee values based on the yields determined by absorption measurements and the ee values of the encapsulated analytes (runs 1–6 and 13). [g] Calculated according to the equation $\alpha = (F_{major}\ (\%)/F_{minor}\ (\%))/(A_{major}\ (\%)/A_{minor}\ (\%))$, where

F_{major} and F_{minor} are the percentages of major and minor enantiomers of the free analyte in the supernatant solutions, respectively, and A_{major} and A_{minor} are those of major and minor enantiomers of the encapsulated analyte, respectively. F_{major}, F_{minor}, A_{major}, and A_{minor} are calculated from the yield and ee of the encapsulated analytes determined by ^{1}H NMR. In parentheses are shown the calculated ee values based on the yields determined by absorption measurements and the ee values of the encapsulated analytes (runs 1–6 and 13). [h] Values of a single experiment.

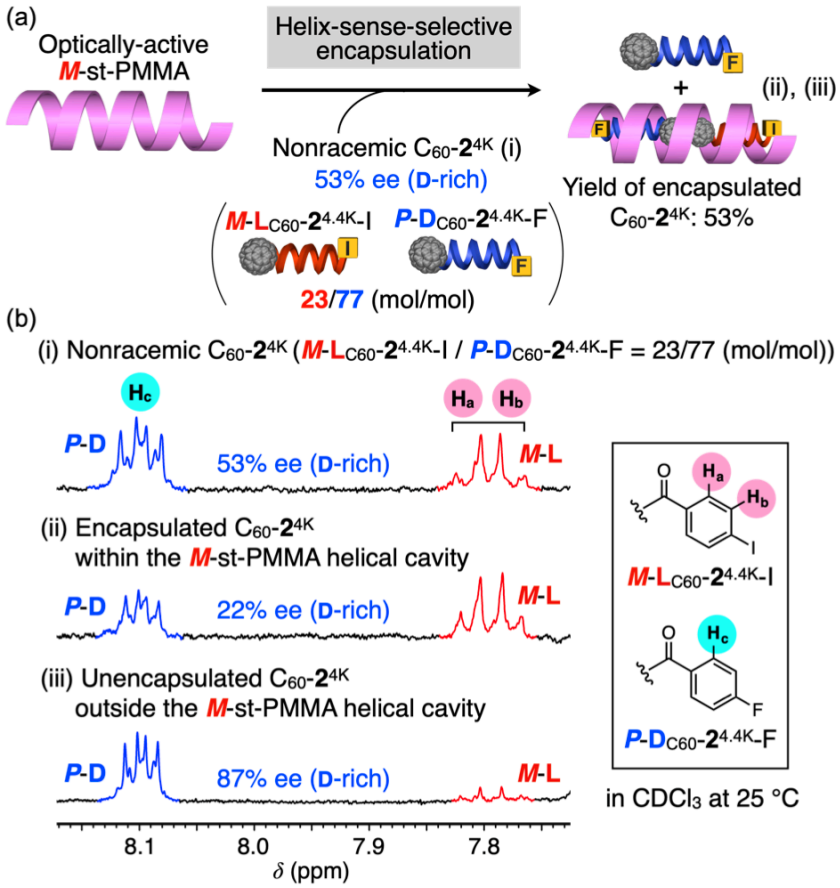

Figure 3-7. (a) Schematic illustration of the helix-sense-selective encapsulation of the C_{60}-bound nonracemic C_{60}-**2**^{4K} with *M*-st-PMMA with a helicity memory. (b) ^{1}H NMR ($CDCl_3$, 25 °C) spectra of 53% ee of C_{60}-**2**^{4K} (D-rich) (i) and helix-sense selectively encapsulated C_{60}-**2**^{4K} (D-rich; ii) and unencapsulated C_{60}-**2**^{4K} (D-rich; iii) in the *M*-st-PMMA (run 13, Table 3-3).

Conclusions

In summary, the author has found that the homochiral *M*-L- and *P*-D-PLAs are efficiently encapsulated in a highly helix-sense-selective manner within the helical cavity of an optically active st-PMMA with memory of the macromolecular helicity, which is readily prepared from inexpensive st-PMMA using chiral amines based on the "helicity induction and memory" strategy, thus producing unique crystalline "helix-in-helix" superstructured inclusion complexes with the same helical sense to each other. Contrary to the previously observed inclusion complex of st-PMMA with the C_{60}-bound *M*- and *P*-helical peptides,[75] the introduction of a C_{60} moiety at one end of the PLA chains is not necessarily required for the encapsulation in the st-PMMA hollow space, although the C_{60} unit as well as the longer helical chains of the *M*- and *P*-PLAs contributes to significant enhancement of the enantioselectivities during the "helix-in-helix" inclusion complex formations. The present results imply that other varieties of helical as well as nonhelical oligomers and polymers may form similar "helix-in-helix" superstructured inclusion complexes with a controlled handedness once encapsulated within the one-handed helical cavity of the st-PMMA. It should be emphasized that the observed α values of more than 2 (Table 3-3) are, in general, high enough for the complete baseline separation of enantiomers when used as a CSP for chiral HPLC,[99,100] indicating that the optically active st-PMMA with an excess one-handedness has the potential as a practically useful CSP for separating not only racemic PLAs, but also other racemic helical oligomers and polymers as well as chiral fullerenes[61] and aromatic compounds,[101] since st-PMMA has successfully been chemically bonded to silica particles by the surface-initiated living syndiotactic-specific anionic polymerization of MMA.[63] Such an immobilized st-PMMA-based CSP has a great advantage such that either an *M*- or *P*-helical st-PMMA can be induced using (*R*)- or (*S*)-**3** and subsequently memorized, thus providing a switchable CSP,[102,103] in which the elution order of chiral analytes can be switched in a reversible fashion.

Experimental Section

Instruments. The NMR spectra were measured using a Bruker Ascend 500 (Bruker Biospin, Billerica, MA) or a Varian 500AS (Agilent Technologies, Santa Clara, CA) spectrometer operating at 500 MHz for ^{1}H and 126 MHz for ^{13}C using tetramethylsilane (TMS) as the internal standard. The electron spray ionization mass spectra (ESI-MS) were recorded on a JEOL JMS-T100CS spectrometer (JEOL, Tokyo, Japan). The matrix-assisted laser desorption-ionization time-of-flight mass spectra (MALDI-TOF-MS) were measured using a Bruker autoflex maX (Bruker Scientific LLC, Billerica, MA) with a positive mode using 1,8,9-anthracenetriol (dithranol) as the matrix. The IR spectra were recorded on a JASCO FT/IR-680 spectrophotometer (JASCO, Tokyo, Japan). The optical rotations were taken using a JASCO P-1030 polarimeter in a 1.0-cm quartz cell equipped with a temperature controller. The absorption and electronic circular dichroism (ECD) spectra were obtained in 0.2-, 0.5-, and 1.0-mm quartz cells using a JASCO V750 spectrophotometer and a JASCO J-1500 spectropolarimeter, respectively. The concentrations of the polymers were calculated based on the monomer units. The temperature was controlled with a JASCO ETCS-900 apparatus. The vibrational circular dichroism (VCD) spectra were measured in a 0.15-mm BaF_2 cell with a JASCO FVS-6000 spectrometer. All spectra were collected for *ca*. 4–5 h at a resolution of 4 cm^{-1}. The temperature was controlled with a JASCO TCH-FVS apparatus. The differential scanning calorimetry (DSC) measurements were performed on a SEIKO EXSTAR6000 DSC 6200 under nitrogen (Hitachi High-Tech, Tokyo, Japan). The samples were sealed in aluminum pans. The melting temperature (T_m) and heat of melting (ΔH_m) were determined from the minimum of the endothermic peak and by the peak area, respectively. The X-ray diffraction (XRD) measurements were carried out using a Rigaku R-AXIS IV X-ray diffractometer with a rotating-anode generator with graphite monochromated Cu *K*α radiation (λ = 0.15418 nm) focused through a 0.3 mm pinhole collimator, which was supplied at 45 kV and 45 mA current, equipped with a flat imaging plate having a specimen-to-plate distance of 165 mm. The size exclusion chromatography (SEC) measurements were

performed with a JASCO PU-4580 liquid chromatograph equipped with a refractive index detector (JASCO RI-4030) and a column oven (JASCO CO-2060). The number-average molar mass (M_n) and its distribution (M_w/M_n) were determined at 40 ºC using a Tosoh TSKgel Multipore H_{XL}-M (30 cm) SEC column (Tosoh, Tokyo, Japan), and chloroform was used as the eluent at a flow rate of 0.5 mL/min. The molar mass calibration curve was obtained with polystyrene standards (Tosoh). The recycling preparative high-performance liquid chromatography (HPLC) was performed with an LC-918 liquid chromatography (JAI, Tokyo, Japan) equipped with a UV detector (JAI UV-310) at room temperature (eluent: chloroform; flow rate 3.5 mL/min). HPLC columns, JAIGEL-1H and JAIGEL-2H (60 cm × 2.0 cm (i.d.)), were connected in series, and chloroform was used as the eluent.

Materials. The st-PMMA was synthesized by the syndiotactic-specific polymerization of MMA in toluene at −95 ºC using a typical Ziegler-type catalyst derived from $Al(C_2H_5)_3$ and $TiCl_4$.[91] The M_n and M_w/M_n values and the tacticity (*mm*:*mr*:*rr*) were as follows: M_n = 616,000, M_w/M_n = 1.36, and *mm*:*mr*:*rr* = 0:4:96. The M_n and M_w/M_n values were measured by SEC in chloroform using PMMA standards (Shodex, Tokyo, Japan) for the calibration. The tacticity was determined from the ^{1}H NMR signals due to the α-methyl protons. D-Lactide was kindly supplied by Prof. Rong-Ming Ho (National Tsing Hua University, Taiwan) and purified by recrystallization from tetrahydrofuran (THF)/toluene (3/7, v/v) just before use. [60]Fullerene (C_{60}) (98%) was obtained from Frontier Carbon (Tokyo, Japan) and used as received. All starting materials and anhydrous solvents were purchased from Sigma-Aldrich (St. Louis, MO), Wako Pure Chemical Industries (Osaka, Japan), Kokusan Chemical Co. Ltd. (Tokyo, Japan), and Tokyo Kasei (Tokyo, Japan) unless otherwise noted. The C_{60}-free and C_{60}-bound *P*- and *M*-helical PLAs were prepared according to the reported procedures with modification.[83]

Synthetic Procedures

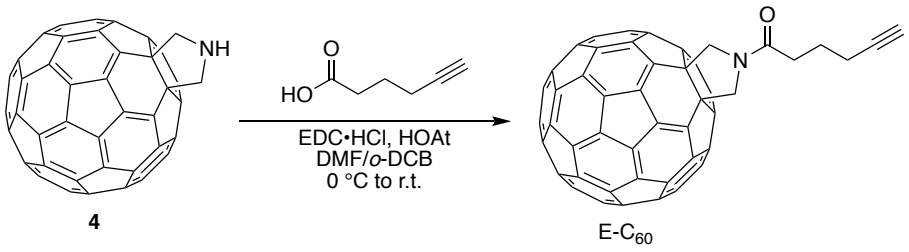

Scheme 3-S1. Synthesis of E-C_{60}.

Synthesis of E-C_{60}. To a mixture of 7-aza-1-hydroxy-1,2,3-benzotriazole (HOAt) (25 mg, 0.18 mmol) and 1-ethyl-3-(3-dimethylaminopropyl)-carbodiimide hydrochloride (EDC·HCl) (29 mg, 0.15 mmol) in anhydrous dichloromethane (1.3 mL) was added 5-hexynoic acid (17 mL, 0.15 mmol). The solution was degassed with three freeze-pump-thaw cycles and stirred at 0 ºC under nitrogen for 30 min. To this was then added a degassed solution of the fullerene derivative **4** (79 mg, 0.10 mmol) in *o*-dichlorobenzene (1.3 mL) at 0 ºC under nitrogen, and the reaction mixture was stirred at room temperature for 24 h. After removal of the solvents under reduced pressure, the residue was dissolved in chloroform, and the solution was washed with 1 N aqueous HCl, 5% aqueous $NaHCO_3$, and brine, and then dried over $MgSO_4$. Purification by column chromatography on silica gel using chloroform/EtOAc (9/1, v/v) as the eluent and further reprecipitation from chloroform to diethyl ether afforded E-C_{60} (36 mg, 42% yield) as a brown solid. HRMS (ESI+): *m*/*z* calcd for $C_{68}H_{11}NNaO$ ($M+Na^+$), 880.0733; found 880.0739. ^{1}H NMR (500 MHz, *o*-DCB-d_4, 25 ºC): δ 5.66 (s, 2H), 5.46 (s, 2H), 3.16 (t, J = 7.0 Hz, 2H), 2.72 (dt, J = 2.5, 7.0 Hz, 2H), 2.42 (quint, J = 7.0 Hz, 2H), 2.33 (dt, J = 0.5, 3.0 Hz, 1H). ^{13}C NMR (126 MHz, *o*-DCB-d_4, 25 ºC): δ 170.47, 153.84, 153.23, 147.38, 146.34, 146.12, 145.55, 145.51, 145.33, 144.46, 143.06, 142.66, 142.25, 142.09, 141.92, 140.23, 136.21, 135.73, 84.02, 71.26, 69.97, 69.71, 59.22, 57.58, 33.00, 24.34, 18.40. Mp: 135 ºC (dec.). IR (KBr, cm^{-1}): 1637 ($\nu_{C=O}$).

Synthesis of *M*-N_3–PLLA and *P*-N_3–PDLA. N_3-Polylactides (***M***-N_3–PLLA and ***P***-N_3–PDLA) were prepared by ring-opening polymerization of L- and D-lactides initiated with 3-azido-1-propanol in the presence of 1,8-diazabicyclo[5.4.0]-7-undecene (DBU) as a catalyst, respectively, in a similar way as previously reported.[90]

A typical procedure for the polymerization of D-lactide is described as follows. To a solution of D-lactide (0.30 g, 2.1 mmol) in anhydrous dichloromethane (2.1 mL) were added DBU (5.2 μL, 35 μmol) and 3-azido-1-propanol (28 μL, 0.30 mmol) at room temperature under nitrogen to initiate the polymerization. After 10 min, the polymerization was quenched by the addition of benzoic acid (30 mg, 0.25 mmol). The mixture was purified by reprecipitation from dichloromethane into cold methanol to give ***P***-N_3–$PDLA^{0.9K}$ (0.27 g, 91% yield) as a white solid. In the same way, ***P***-N_3–PDLA and ***M***-N_3–PLLA with different molar masses were prepared. The M_n and M_w/M_n values of the polymers were determined by SEC using polystyrene standards (Shodex, Tokyo, Japan) in chloroform. The M_n values were also estimated by ^{1}H NMR azido end-group analysis ($M_{n,NMR}$) in $CDCl_3$. The polymerization results are summarized in Table 3-S1.

Table 3-S1. Polymerization of L- and D-Lactides Initiated by 3-Azido-1-Propanol with DBU in CH_2Cl_2 at Room Temperature for 10 min [a]

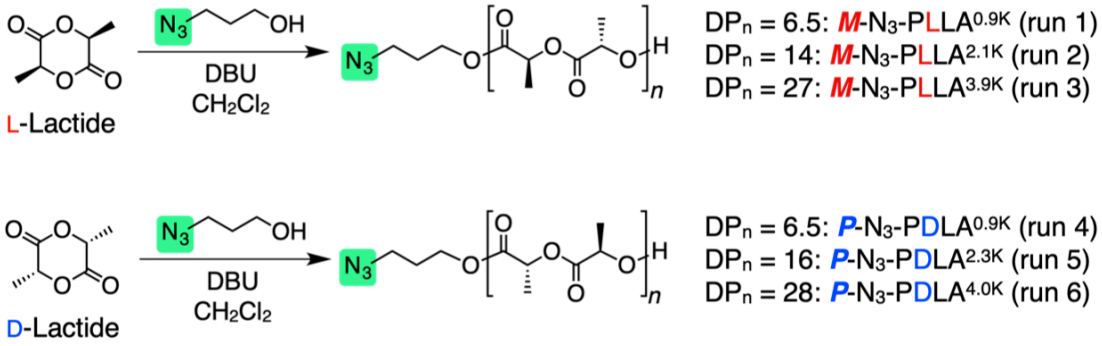

run	monomer	[monomer]/[initiator]	PLA prepolymer							
			sample code	yield (%)	$M_{n,SEC}$ (10^3) [b]	M_w/M_n [b]	$M_{n,NMR}$ (10^3) [c]	$DP_{n,NMR}$ [d]	$[\alpha]_D^{25}$ [e]	T_m (°C) [f]
1	L-lactide	7	***M***-N_3-PLLA$^{0.9K}$	87	1.53	1.26	0.94	6.5	–121.7	92
2	L-lactide	14	***M***-N_3-PLLA$^{2.1K}$	74	3.55	1.11	2.08	14	–132.0	130
3	L-lactide	26	***M***-N_3-PLLA$^{3.9K}$	87	6.28	1.11	3.85	27	–140.9	151
4	D-lactide	7	***P***-N_3-PDLA$^{0.9K}$	91	1.40	1.31	0.94	6.5	+124.9	93
5	D-lactide	15	***P***-N_3-PDLA$^{2.3K}$	90	3.82	1.12	2.28	16	+134.0	136
6	D-lactide	29	***P***-N_3-PDLA$^{4.0K}$	78	7.11	1.12	4.04	28	+139.1	152

[a] [Monomer] = 1.0 M, [DBU]/[monomer] = 0.01. The complete consumption of monomers was confirmed by ^{1}H NMR analysis in each run. [b] Estimated by SEC (polystyrene standards) with $CHCl_3$ as the eluent. [c] Determined by the ^{1}H NMR end-group analysis in $CDCl_3$. [d] Number-average degree of polymerization determined by $M_{n,NMR}$. [e] Measured in $CHCl_3$ at 25 °C. [f] Melting point determined by DSC.

Spectroscopic data of ***M***-N_3-PLLA$^{0.9K}$: IR (KBr, cm^{-1}): 2103 (N=N=N), 1759 (C=O), 1191 (C–O), 1094 (C–O). ^{1}H NMR (500 MHz, $CDCl_3$, 25 ºC): δ 5.24–5.10 (m, CH PLA backbone, 12H), 4.36 (q, J = 7.0 Hz, CH PLA backbone, 1H), 4.24 (dt, J = 6.2, 2.8 Hz, OCH_2, 2H), 3.39 (t, J = 6.7 Hz, N_3CH_2, 2H), 2.64 (br, OH, 1H), 1.94–1.89 (m, OCH_2CH_2, 2H), 1.61–1.49 (m, CH_3 PLA backbone, partially overlapping with H_2O signal) (for all the peak assignments including the end groups, see Figure 3-S2a(i)).

Spectroscopic data of ***M***-N_3-PLLA$^{2.1K}$: IR (KBr, cm^{-1}): 2103 (N=N=N), 1759 (C=O), 1185 (C–O), 1092 (C–O). ^{1}H NMR (500 MHz, $CDCl_3$, 25 ºC): δ 5.24–5.10 (m, CH PLA backbone,

28H), 4.35 (q, *J* = 7.0 Hz, CH PLA backbone, 1H), 4.24 (dt, *J* = 6.0, 3.0 Hz, OCH_2, 2H), 3.39 (t, *J* = 6.7 Hz, N_3CH_2, 2H), 2.65 (br, OH, 1H), 1.94–1.89 (m, OCH_2CH_2, 2H), 1.61–1.49 (m, CH_3 PLA backbone, partially overlapping with H_2O signal) (for all the peak assignments including the end groups, see Figure 3-S3a(i)).

Spectroscopic data of ***M***-N_3-PLLA$^{3.9K}$: IR (KBr, cm^{-1}): 2103 (N=N=N), 1759 (C=O), 1185 (C–O), 1092 (C–O). ^{1}H NMR (500 MHz, $CDCl_3$, 25 ºC): δ 5.24–5.10 (m, CH PLA backbone, 52H), 4.35 (q, *J* = 6.9 Hz, CH PLA backbone, 1H), 4.24 (dt, *J* = 6.0, 3.0 Hz, OCH_2, 2H), 3.38 (t, *J* = 6.7 Hz, N_3CH_2, 2H), 2.65 (br, OH, 1H), 1.94–1.89 (m, OCH_2CH_2, 2H), 1.61–1.49 (m, CH_3 PLA backbone, partially overlapping with H_2O signal) (for all the peak assignments including the end groups, see Figure 3-2a(i)).

Spectroscopic data of ***P***-N_3-PDLA$^{0.9K}$: IR (KBr, cm^{-1}): 2103 (N=N=N), 1760 (C=O), 1190 (C–O), 1094 (C–O). ^{1}H NMR (500 MHz, $CDCl_3$, 25 ºC): δ 5.24–5.10 (m, CH PLA backbone, 12H), 4.36 (q, *J* = 6.8 Hz, CH PLA backbone, 1H), 4.24 (dt, *J* = 6.3, 2.8 Hz, OCH_2, 2H), 3.38 (t, *J* = 6.7 Hz, N_3CH_2, 2H), 2.65 (d, *J* = 6.0 Hz, OH, 1H), 1.94–1.89 (m, OCH_2CH_2, 2H), 1.61–1.49 (m, CH_3 PLA backbone, partially overlapping with H_2O signal) (for all the peak assignments including the end groups, see Figure 3-S4a(i)).

Spectroscopic data of ***P***-N_3-PDLA$^{2.3K}$: IR (KBr, cm^{-1}): 2101 (N=N=N), 1759 (C=O), 1186 (C–O), 1093 (C–O). ^{1}H NMR (500 MHz, $CDCl_3$, 25 ºC): δ 5.24–5.10 (m, CH PLA backbone, 31H), 4.36 (q, *J* = 6.9 Hz, CH PLA backbone, 1H), 4.24 (dt, *J* = 6.0, 3.0 Hz, OCH_2, 2H), 3.39 (t, *J* = 6.7 Hz, N_3CH_2, 2H), 2.65 (br, OH, 1H), 1.94–1.89 (m, OCH_2CH_2, 2H), 1.61–1.49 (m, CH_3 PLA backbone, partially overlapping with H_2O signal) (for all the peak assignments including the end groups, see Figure 3-S5a(i)).

Spectroscopic data of ***P***-N_3-PDLA$^{4.0K}$: IR (KBr, cm^{-1}): 2103 (N=N=N), 1759 (C=O), 1185 (C–O), 1091 (C–O). ^{1}H NMR (500 MHz, $CDCl_3$, 25 ºC): δ 5.24–5.10 (m, CH PLA backbone, 55H), 4.36 (q, *J* = 7.0 Hz, CH PLA backbone, 1H), 4.24 (dt, *J* = 6.0, 3.0 Hz, OCH_2, 2H), 3.38 (t, *J* = 6.5 Hz, N_3CH_2, 2H), 2.65 (br, OH, 1H), 1.94–1.89 (m, OCH_2CH_2, 2H), 1.61–1.49 (m,

CH_3 PLA backbone, partially overlapping with H_2O signal) (for all the peak assignments including the end groups, see Figure 3-S6a(i)).

Synthesis of *M*-L$_{N3}$-1-I and *P*-D$_{N3}$-1-F. ***M*-L$_{N3}$-1**-I and ***P*-D$_{N3}$-1**-F were prepared by esterification of the terminal hydroxy groups of ***M*-N$_3$-PLLA** and ***P*-N$_3$-PDLA** with 4-iodo- and 4-fluoro-iodobenzoyl chlorides, respectively.

A typical procedure for the esterification of ***P*-N$_3$-PDLA$^{1.0K}$** is described as follows. To a solution of ***P*-N$_3$-PDLA$^{1.0K}$** (0.20 g, 0.19 mmol) in anhydrous dichloromethane/pyridine (3/1, v/v; 2.7 mL) was added 4-fluorobenzoyl chloride (0.67 mL, 5.6 mmol). After the reaction mixture was stirred at room temperature for 17 h under nitrogen, the solution was concentrated to ca. 0.5 mL. The residue was precipitated into methanol (2 mL), collected by centrifugation, and washed with methanol to afford ***P*-D$_{N3}$-1$^{1.0K}$**-F (0.17 g, 72% yield) as a white solid. In the same way, ***P*-D$_{N3}$-1**-F and ***M*-L$_{N3}$-1**-I and with different molar masses were prepared. The M_n and M_w/M_n values of the polymers were determined by SEC using polystyrene standards in chloroform. The M_n values were also estimated by ^{1}H NMR end-group analysis ($M_{n,NMR}$) in $CDCl_3$. The esterification results are summarized in Table 3-S2.

Table 3-S2. Esterification of *M*-N_3-PLLA and *P*-N_3-PDLA with 4-Iodo- and 4-Fluorobenzoyl Chloride, respectively, in CH_2Cl_2 at Room Temperature

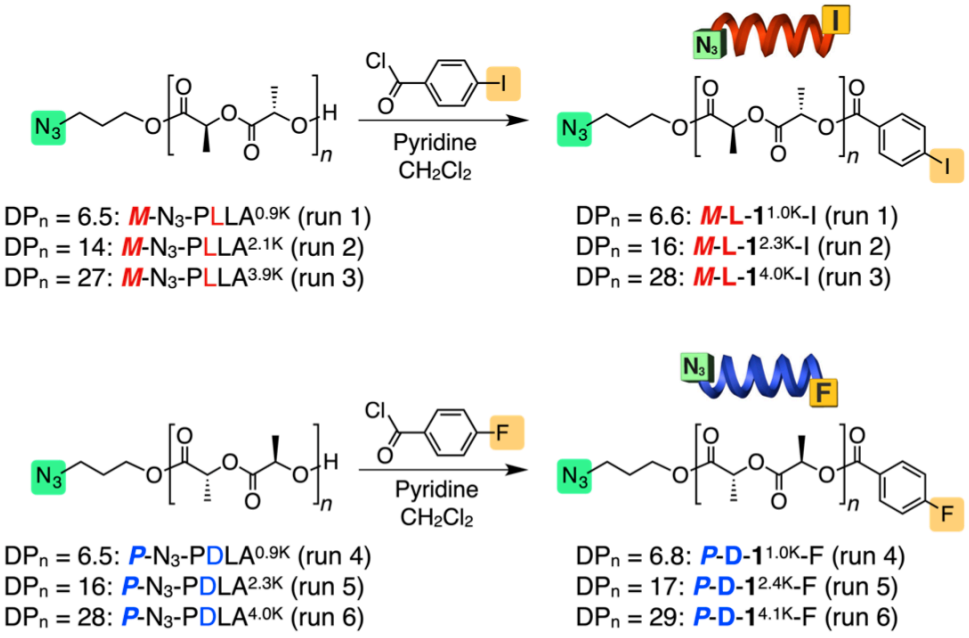

run	reactant	product	yield (%) [a]	$M_{n,SEC}$ (10^3) [b]	M_w/M_n [b]	$M_{n,NMR}$ (10^3) [c]	$DP_{n,NMR}$ [d]	$f_{benzoate}$ (%) [e]	T_m (°C) [f]
1	***M*-N_3-PLLA$^{0.9K}$**	***M*-L_{N3}-$1^{1.0K}$-I**	64	1.61	1.19	0.95	6.6	>99	96
2	***M*-N_3-PLLA$^{2.1K}$**	***M*-L_{N3}-$1^{2.3K}$-I**	69	4.14	1.11	2.30	16	>99	137
3	***M*-N_3-PLLA$^{3.9K}$**	***M*-L_{N3}-$1^{4.0K}$-I**	82	6.53	1.12	4.01	28	>99	149
4	***P*-N_3-PDLA$^{0.9K}$**	***P*-D_{N3}-$1^{1.0K}$-F**	72	1.62	1.23	0.98	6.8	>99	95
5	***P*-N_3-PDLA$^{2.3K}$**	***P*-D_{N3}-$1^{2.4K}$-F**	93	4.15	1.11	2.41	17	>99	138
6	***P*-N_3-PDLA$^{4.0K}$**	***P*-D_{N3}-$1^{4.1K}$-F**	98	7.38	1.12	4.11	29	>99	149

[a] Isolated yield after the purification by recycle SEC. [b] Estimated by SEC (polystyrene standards) with $CHCl_3$ as the eluent. [c] Determined by the ^{1}H NMR end-group analysis in $CDCl_3$. [d] Number-average degree of polymerization determined by $M_{n,NMR}$. [e] Functionality of the end-capped benzoate residue estimated by ^{1}H NMR in $CDCl_3$. [f] Melting point determined by DSC.

Spectroscopic data of ***M*-L_{N3}-$1^{1.0K}$-I**: IR (KBr, cm^{-1}): 2101 (N=N=N), 1759 (C=O), 1188 (C–O), 1094 (C–O). ^{1}H NMR (500 MHz, $CDCl_3$, 25 °C): δ 7.82–7.77 (m, Ar–H, 4H), 5.34 (q, J = 7.0 Hz, CH PLA backbone, 1H), 5.22–5.11 (m, CH PLA backbone, 12H), 4.24 (dt, J = 6.1, 2.5 Hz, OCH_2, 2H), 3.39 (t, J = 6.6 Hz, N_3CH_2, 2H), 1.94–1.89 (m, OCH_2CH_2, 2H),

1.70–1.51 (m, CH_3 PLA backbone, partially overlapping with H_2O signal) (for all the peak assignments including the end groups, see Figure 3-S2a(ii)).

Spectroscopic data of ***M*-$\mathbf{L}_{N3}$-$\mathbf{1}^{2.3K}$-I**: IR (KBr, cm^{-1}): 2103 (N=N=N), 1759 (C=O), 1185 (C–O), 1092 (C–O). ^{1}H NMR (500 MHz, $CDCl_3$, 25 ºC): δ 7.82–7.77 (m, Ar–H, 4H), 5.35 (q, J = 7.1 Hz, CH PLA backbone, 1H), 5.23–5.10 (m, CH PLA backbone, 31H), 4.24 (dt, J = 6.0, 2.5 Hz, OCH_2, 2H), 3.39 (t, J = 6.7 Hz, N_3CH_2, 2H), 1.94–1.89 (m, OCH_2CH_2, 2H), 1.72–1.44 (m, CH_3 PLA backbone, partially overlapping with H_2O signal) (for all the peak assignments including the end groups, see Figure 3-S3a(ii)).

Spectroscopic data of ***M*-$\mathbf{L}_{N3}$-$\mathbf{1}^{4.0K}$-I**: IR (KBr, cm^{-1}): 2103 (N=N=N), 1759 (C=O), 1184 (C–O), 1090 (C–O). ^{1}H NMR (500 MHz, $CDCl_3$, 25 ºC): δ 7.82–7.77 (m, Ar–H, 4H), 5.34 (q, J = 7.1 Hz, CH PLA backbone, 1H), 5.22–5.11 (m, CH PLA backbone, 55H), 4.24 (dt, J = 6.0, 2.5 Hz, OCH_2, 2H), 3.39 (t, J = 6.7 Hz, N_3CH_2, 2H), 1.94–1.89 (m, OCH_2CH_2, 2H), 1.72–1.52 (m, CH_3 PLA backbone, partially overlapping with H_2O signal) (for all the peak assignments including the end groups, see Figure 3-2a(ii)).

Spectroscopic data of ***P*-$\mathbf{D}_{N3}$-$\mathbf{1}^{1.0K}$-F**: IR (KBr, cm^{-1}): 2103 (N=N=N), 1759 (C=O), 1186 (C–O), 1092 (C–O). ^{1}H NMR (500 MHz, $CDCl_3$, 25 ºC): δ 8.11–8.08 (m, Ar–H, 2H), 7.13–7.10 (m, Ar–H, 2H), 5.35 (q, J = 7.1 Hz, CH PLA backbone, 1H), 5.24–5.10 (m, CH PLA backbone, 13H), 4.24 (dt, J = 6.0, 2.5 Hz, OCH_2, 2H), 3.38 (t, J = 6.7 Hz, N_3CH_2, 2H), 1.94–1.89 (m, OCH_2CH_2, 2H), 1.71–1.51 (m, CH_3 PLA backbone, partially overlapping with H_2O signal) (for all the peak assignments including the end groups, see Figure 3-S4a(ii)).

Spectroscopic data of ***P*-$\mathbf{D}_{N3}$-$\mathbf{1}^{2.4K}$-F**: IR (KBr, cm^{-1}): 2103 (N=N=N), 1759 (C=O), 1185 (C–O), 1092 (C–O). ^{1}H NMR (500 MHz, $CDCl_3$, 25 ºC): δ 8.11–8.08 (m, Ar–H, 2H), 7.13–7.10 (m, Ar–H, 2H), 5.35 (q, J = 7.1 Hz, CH PLA backbone, 1H), 5.24–5.10 (m, CH PLA backbone, 32H), 4.24 (dt, J = 6.0, 2.5 Hz, OCH_2, 2H), 3.38 (t, J = 6.7 Hz, N_3CH_2, 2H), 1.94–1.89 (m, OCH_2CH_2, 2H), 1.72–1.51 (m, CH_3 PLA backbone, partially overlapping with H_2O signal) (for all the peak assignments including the end groups, see Figure 3-S5a(ii)).

Spectroscopic data of ***P*-D$_{N3}$-1$^{4.1K}$-F**: IR (KBr, cm^{-1}): 2103 (N=N=N), 1759 (C=O), 1184 (C–O), 1090 (C–O). ^{1}H NMR (500 MHz, $CDCl_3$, 25 ºC): δ 8.11–8.08 (m, Ar–H, 2H), 7.14–7.10 (m, Ar–H, 2H), 5.35 (q, J = 7.1 Hz, CH PLA backbone, 1H), 5.22–5.11 (m, CH PLA backbone, 56H), 4.24 (dt, J = 6.0, 2.5 Hz, OCH_2, 2H), 3.39 (t, J = 6.7 Hz, N_3CH_2, 2H), 1.94–1.89 (m, OCH_2CH_2, 2H), 1.72–1.44 (m, CH_3 PLA backbone, partially overlapping with H_2O signal) (for all the peak assignments including the end groups, see Figure 3-S6a(ii)).

Synthesis of *M*-L$_{C60}$-2-I and *P*-D$_{C60}$-2-F. C_{60}-bound polylactides (***M*-L**$_{C60}$-**2**-I and ***P*-D**$_{C60}$-**2**-F) were prepared by the copper(I)-catalyzed click reaction of N_3-**1** PLAs with E-C_{60}.

A typical procedure for the copper(I)-catalyzed click reaction of ***P*-D**$_{N3}$-**1**$^{1.0K}$-F with E-C_{60} is described as follows. To a mixture of ***P*-D**$_{N3}$-**1**$^{1.0K}$-F (70 mg, 58 mmol) and E-C_{60} (59 mg, 69 mmol) in anhydrous dichloromethane/*o*-DCB (4 mL, 1/1, v/v) was added *N*,*N*,*N*′,*N*″,*N*″-pentamethyldiethylenetriamine (PMDETA) (15 mL, 72 mmol) under nitrogen, and the solution was degassed with three freeze-pump-thaw cycles. To this was added CuBr (12 mg, 84 mmol) under nitrogen and the reaction mixture was degassed again, and stirred at room temperature for 16 h. After removal of dichloromethane under reduced pressure, to this was added methanol (2 mL) to precipitate the desired product. The precipitate was collected by centrifugation and purified by SEC on Bio Beads S-X1 using dichloromethane as the eluent and preparative recycling SEC (JAIGEL-1H and -2H columns, chloroform) to give ***P*-D**$_{C60}$-**2**$^{1.0K}$-F (98 mg, 82% yield) as a brown solid. In the same way, ***P*-D**$_{C60}$-**2**-F and ***M*-L**$_{C60}$-**2**-I with different molar masses were prepared. The M_n and M_w/M_n of the polymers were determined by SEC using polystyrene standards in chloroform. The M_n values were also estimated by ^{1}H NMR end-group analysis ($M_{n,NMR}$) in $CDCl_3$. The copper(I)-catalyzed click reaction results are summarized in Table 3-S3.

Table 3-S3. Click Reaction of *M*-L_{N3}-1-I and *P*-D_{N3}-1-F with E-C_{60} in CH_2Cl_2/*o*-DCB (1/1, v/v) at Room Temperature

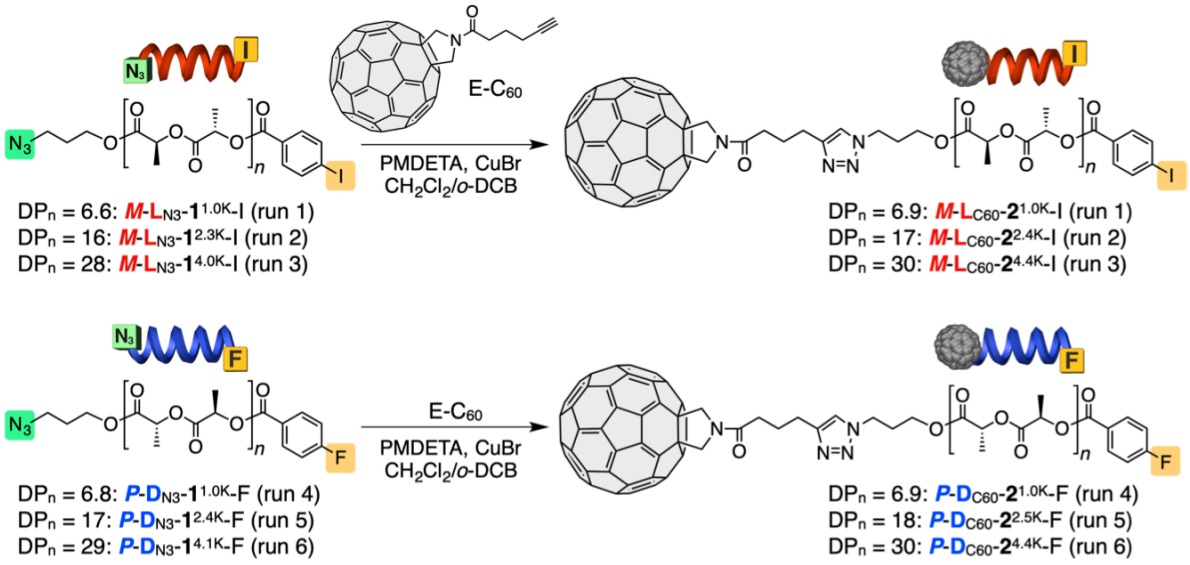

run	reactant	product	yield (%) [a]	$M_{n,SEC}$ (10^3) [b]	M_w/M_n [b]	$M_{n,NMR}$ (10^3) [c]	$DP_{n,NMR}$ [d]	f_{C60} (%) [e]	T_m (°C) [f]
1	***M*-L_{N3}-$1^{1.0K}$-I**	***M*-L_{C60}-$2^{1.0K}$-I**	88	1.82	1.24	0.99	6.9	>99	– [g]
2	***M*-L_{N3}-$1^{2.3K}$-I**	***M*-L_{C60}-$2^{2.4K}$-I**	79	4.38	1.20	2.43	17	>99	141
3	***M*-L_{N3}-$1^{4.0K}$-I**	***M*-L_{C60}-$2^{4.4K}$-I**	73	7.73	1.32	4.36	30	>99	146
4	***P*-D_{N3}-$1^{1.0K}$-F**	***P*-D_{C60}-$2^{1.0K}$-F**	82	1.63	1.41	1.00	6.9	>99	– [g]
5	***P*-D_{N3}-$1^{2.4K}$-F**	***P*-D_{C60}-$2^{2.5K}$-F**	94	4.75	1.26	2.52	18	>99	141
6	***P*-D_{N3}-$1^{4.1K}$-F**	***P*-D_{C60}-$2^{4.4K}$-F**	87	7.93	1.35	4.39	30	>99	146

[a] Isolated yield after the purification by recycle SEC. [b] Estimated by SEC (polystyrene standards) with $CHCl_3$ as the eluent. [c] Determined by the ^{1}H NMR end-group analysis in $CDCl_3$. [d] Number-average degree of polymerization determined by $M_{n,NMR}$. [e] Functionality of the end-capped C_{60} residue estimated by ^{1}H NMR in $CDCl_3$. [f] Melting point determined by DSC. [g] Not observed in the DSC thermogram.

Spectroscopic data of ***M*-L_{C60}-$2^{1.0K}$-I**: IR (KBr, cm^{-1}): 1759 (C=O), 1185 (C–O), 1092 (C–O). ^{1}H NMR (500 MHz, $CDCl_3$, 25 ºC): δ 7.82–7.77 (m, Ar–H,4H), 7.46 (s, C=CH, 1H), 5.48 (s, C_{60}–CH_2N, 2H), 5.40 (s, C_{60}–CH_2N, 2H), 5.35 (q, J = 7.1 Hz, CH PLA backbone, 1H), 5.23–5.08 (m, CH PLA backbone, 13H), 4.42 (dt, J = 6.7, 3.1 Hz, OCH_2, 2H), 4.23–4.11 (m,

NCH_2, 2H), 2.99 (t, J = 7.3 Hz, CH_2, 2H), 2.92 (t, J = 7.3 Hz, CH_2, 2H), 2.35–2.28 (m, OCH_2CH_2, 4H), 1.70–1.53 (m, CH_3 PLA backbone, partially overlapping with H_2O signal) (for all the peak assignments including the end groups, see Figure 3-S2a(iii)).

Spectroscopic data of ***M*-L$_{C60}$-2$^{2.4K}$**-I: IR (KBr, cm^{-1}): 1758 (C=O), 1184 (C–O), 1090 (C–O). ^1H NMR (500 MHz, $CDCl_3$, 25 ºC): δ 7.82–7.77 (m, Ar–H, 4H), 7.45 (s, C=CH, 1H), 5.48 (s, C_{60}–CH_2N, 2H), 5.40 (s, C_{60}–CH_2N, 2H), 5.34 (q, J = 7.1 Hz, CH PLA backbone, 1H), 5.23–5.08 (m, CH PLA backbone, 33H), 4.42 (dt, J = 6.7, 3.1 Hz, OCH_2, 2H), 4.24–4.11 (m, NCH_2, 2H), 2.98 (t, J = 7.3 Hz, CH_2, 2H), 2.92 (t, J = 7.4 Hz, CH_2, 2H), 2.35–2.28 (m, OCH_2CH_2, 4H), 1.72–1.53 (m, CH_3 PLA backbone, partially overlapping with H_2O signal) (for all the peak assignments including the end groups, see Figure 3-S3a(iii)).

Spectroscopic data of ***M*-L$_{C60}$-2$^{4.4K}$**-I: IR (KBr, cm^{-1}): 1758 (C=O), 1184 (C–O), 1090 (C–O). ^1H NMR (500 MHz, $CDCl_3$, 25 ºC): δ 7.82–7.77 (m, Ar–H, 4H), 7.45 (s, C=CH, 1H), 5.48 (s, C_{60}–CH_2N, 2H), 5.40 (s, C_{60}–CH_2N, 2H), 5.35 (q, J = 7.0 Hz, CH PLA backbone, 1H), 5.22–5.09 (m, CH PLA backbone, 59H), 4.42 (dt, J = 6.5, 3.0 Hz, OCH_2, 2H), 4.23–4.11 (m, NCH_2, 2H), 2.98 (t, J = 7.4 Hz, CH_2, 2H), 2.92 (t, J = 7.4 Hz, CH_2, 2H), 2.34-2.28 (m, OCH_2CH_2, 4H), 1.72–1.44 (m, CH_3 PLA backbone, partially overlapping with H_2O signal) (for all the peak assignments including the end groups, see Figure 3-2a(iii)).

Spectroscopic data of ***P*-D$_{C60}$-2$^{1.0K}$**-F: IR (KBr, cm^{-1}): 1758 (C=O), 1185 (C–O), 1091 (C–O). ^1H NMR (500 MHz, $CDCl_3$, 25 ºC): δ 8.12–8.08 (m, Ar–H, 2H), 7.45 (s, C=CH, 1H), 7.14–7.09 (m, Ar–H, 2H), 5.48 (s, C_{60}–CH_2N, 2H), 5.39 (s, C_{60}–CH_2N, 2H), 5.35 (q, J = 7.0 Hz, CH PLA backbone, 1H), 5.24–5.08 (m, CH PLA backbone, 13H), 4.42 (dt, J = 6.7, 3.1 Hz, OCH_2, 2H), 4.23–4.11 (m, NCH_2, 2H), 2.98 (t, J = 7.3 Hz, CH_2, 2H), 2.92 (t, J = 7.3 Hz, CH_2, 2H), 2.36 (m, OCH_2CH_2, 4H), 1.70–1.53 (m, CH_3 PLA backbone, partially overlapping

with H_2O signal) (for all the peak assignments including the end groups, see Figure 3-S4a(iii)).

Spectroscopic data of ***P*-D$_{C60}$-2$^{2.5K}$**-F: IR (KBr, cm^{-1}): 1759 (C=O), 1184 (C–O), 1091 (C–O). ^{1}H NMR (500 MHz, $CDCl_3$, 25 ºC): δ 8.12–8.08 (m, Ar–H, 2H), 7.45 (s, C=CH, 1H), 7.14–7.09 (m, Ar–H, 2H), 5.48 (s, C_{60}–CH_2N, 2H), 5.40 (s, C_{60}–CH_2N, 2H), 5.35 (q, J = 7.1 Hz, CH PLA backbone, 1H), 5.22–5.09 (m, CH PLA backbone, 34H), 4.42 (dt, J = 6.7, 3.1 Hz, OCH_2, 2H), 4.23–4.11 (m, NCH_2, 2H), 2.98 (t, J = 7.4 Hz, CH_2, 2H), 2.92 (t, J = 7.4 Hz, CH_2, 2H), 2.36–2.26 (m, OCH_2CH_2, 4H), 1.71–1.53 (m, CH_3 PLA backbone, partially overlapping with H_2O signal) (for all the peak assignments including the end groups, see Figure 3-S5a(iii)).

Spectroscopic data of ***P*-D$_{C60}$-2$^{4.4K}$**-F: IR (KBr, cm^{-1}): 1758 (C=O), 1184 (C–O), 1089 (C–O). ^{1}H NMR (500 MHz, $CDCl_3$, 25 ºC): δ 8.11–8.08 (m, Ar–H, 2H), 7.45 (s, C=CH, 1H), 7.14–7.09 (m, Ar–H, 2H), 5.48 (s, C_{60}–CH_2N, 2H), 5.40 (s, C_{60}–CH_2N, 2H), 5.35 (q, J = 7.1 Hz, CH PLA backbone, 1H), 5.22–5.08 (m, CH PLA backbone, 60H), 4.42 (dt, J = 6.7, 3.1 Hz, OCH_2, 2H), 4.23–4.11 (m, NCH_2, 2H), 2.98 (t, J = 7.4 Hz, CH_2, 2H), 2.92 (t, J = 7.4 Hz, CH_2, 2H), 2.35–2.28 (m, OCH_2CH_2, 4H), 1.72–1.54 (m, CH_3 PLA backbone, partially overlapping with H_2O signal) (for all the peak assignments including the end groups, see Figure 3-S6a(iii)).

Preparation of st-PMMA Films Complexed with the C_{60}-Free and C_{60}-Bound *M*- and *P*-PLAs. st-PMMA/PLA complex films for the DSC and XRD measurements were prepared according to the method reported previously for the preparation of st-PMMA/C_{60}-peptide complex films.[75] Typically, st-PMMA (10.0 mg) was dissolved in a toluene solution of ***M*-L**$_{C60}$-**2**$^{4.4K}$-I (3.0 mg/mL, 1.0 mL) at 110 ºC. After the solution was cooled to room temperature, the solution gelled within 10 min. The resulting soft gel was centrifuged at 1700 *g* for 10 min and the supernatant containing the unencapsulated ***M*-L**$_{C60}$-**2**$^{4.4K}$-I was removed from the gel by decantation. The condensed gel was washed with toluene and the solvent was removed by decantation after centrifugation. This procedure was repeated two times (0.5 mL × 2), affording the st-PMMA/***M*-L**$_{C60}$-**2**$^{4.4K}$-I complex gel (***M*-L**$_{C60}$-**2**$^{4.4K}$-I: 15.7 wt%) (run 3, Table 3-2). The encapsulated ***M*-L**$_{C60}$-**2**$^{4.4K}$-I content was estimated by absorption spectroscopy using the following equation: the encapsulated ***M*-L**$_{C60}$-**2**$^{4.4K}$-I content (mg) = ***M*-L**$_{C60}$-**2**$^{4.4K}$-I in feed (mg) × (Abs_0 – Abs)/Abs_0, where Abs_0 and Abs represent the absorbance at 313 nm of the feed ***M*-L**$_{C60}$-**2**$^{4.4K}$-I solution and that of the supernatant separated from the st-PMMA/***M*-L**$_{C60}$-**2**$^{4.4K}$-I gel after centrifugation, respectively (Figures 3a and S7). In the same way, st-PMMA gels complexed with ***M*-L**$_{C60}$-**2**$^{1.0K}$-I (15.2 wt%), ***M*-L**$_{C60}$-**2**$^{2.4K}$-I (15.3 wt%), and ***P*-D**$_{C60}$-**2**$^{4.4K}$-F (16.8 wt%) were prepared (runs 1, 2, and 4, Table 3-2). The st-PMMA/***M*-L**$_{C60}$-**2**$^{4.4K}$-I complex gel containing a higher content of ***M*-L**$_{C60}$-**2**$^{4.4K}$-I (23.5 wt%) was prepared by adding a toluene solution (0.4 mL) of ***M*-L**$_{C60}$-**2**$^{4.4K}$-I (9.0 mg/mL) to st-PMMA (4.0 mg) followed by heating to 110 °C and cooling to room temperature, and then centrifuged and washed with toluene (run 5, Table 3-2). The st-PMMA/***M*-L**$_{N3}$-**1**$^{4.0K}$-I complex gel (***M*-L**$_{N3}$-**1**$^{4.0K}$-I: 12.6 wt%) was also prepared by adding a toluene-d_8 solution (0.8 mL) of ***M*-L**$_{N3}$-**1**$^{4.0K}$-I (14.5 mg/mL) to st-PMMA (8.0 mg) followed by heating to 110 °C and cooling to room temperature, and then centrifuged and washed with toluene (run 6, Table 3-2). The encapsulated ***M*-L**$_{N3}$-**1**$^{4.0K}$-I content was estimated from the integral ratio of the methylene protons of the N_3-**1**$^{4.0K}$ end-group relative to the ^{13}C satellite peaks of the methoxy protons of st-PMMA due to ^{13}C–^{1}H coupling using ^{1}H NMR spectroscopy[104] instead of

absorption spectroscopy due to the lack of absorption in the region above 300 nm. The st-PMMA/PLA complex films were obtained by evaporating the solvents in the condensed gels under reduced pressure at room temperature for 12 h followed by drying under vacuum at 130 ºC for 50 h and then used for the DSC and XRD measurements (Figures 3-3c,d and 3-S8).

Molecular Modeling of the st-PMMA/*M*-L$_{C60}$-2$^{4.4K}$-I and *M*-L$_{N3}$-1$^{4.0K}$-I Complexes. The molecular modeling was performed on a Windows 10 PC with the Materials Studio package (Version 8.0; Dassault Systèmes BIOVIA, San Diego, CA, USA). The initial structures of ***M*-L$_{C60}$-2$^{4.4K}$-I**, ***M*-L$_{N3}$-1$^{4.0K}$-I**, and st-PMMA/***M*-L$_{C60}$-2$^{4.4K}$-I** and st-PMMA/***M*-L$_{N3}$-1$^{4.0K}$-I** inclusion complexes were constructed according to the following procedures: first, the PLA segments of ***M*-L$_{C60}$-2$^{4.4K}$-I** and ***M*-L$_{N3}$-1$^{4.0K}$-I** were constructed based on the Cartesian coordinates of the atoms of the lactide residue and the bond lengths, bond angles, and internal rotation angles reported for the α-form poly(L-lactic acid) (PLLA) crystal.[105,106] The end groups of ***M*-L$_{C60}$-2$^{4.4K}$-I** and ***M*-L$_{N3}$-1$^{4.0K}$-I** were then added to the PLA chains and selectively optimized by the molecular mechanics (MM) calculations (Compass II force field[107] as implemented in the Materials Studio package). An initial left-handed 18_1 ***M*-st-PMMA** (576mer) helical model (18 monomer units/turn) was built according to the reported method.[66] The geometry-optimized ***M*-L$_{C60}$-2$^{4.4K}$-I** and ***M*-L$_{N3}$-1$^{4.0K}$-I** were then manually inserted into the helical cavity of the ***M*-st-PMMA** helical model to generate initial ***M*-st-PMMA/*M*-L$_{C60}$-2$^{4.4K}$-I** and ***M*-st-PMMA/*M*-L$_{N3}$-1$^{4.0K}$-I** inclusion complexes. The relative positions of the ***M*-st-PMMA** and ***M*-L$_{C60}$-2$^{4.4K}$-I** or ***M*-L$_{N3}$-1$^{4.0K}$-I** helices were determined in order to avoid any unfavorable van der Waals contacts. The ***M*-L$_{C60}$-2$^{4.4K}$-I** and ***M*-L$_{N3}$-1$^{4.0K}$-I** chains included in the ***M*-st-PMMA** helix except for the PLA backbones were then selectively geometry-optimized by the MM calculations (Compass II force field) (Figure 3-S10).

General Procedures for VCD Measurements of st-PMMA Gels Complexed with the C_{60}-Free and C_{60}-Bound *M*- and *P*-PLAs. A typical experimental procedure is described below. st-PMMA (8.0 mg) was dissolved in a toluene-d_8 solution of ***M*-L**$_{C60}$-**2**$^{4.4K}$-I (3.0 mg/mL, 2.0 mL) at 110 °C. After the solution was cooled to room temperature, the solution gelled within 10 min. The resulting soft gel was centrifuged at 1700 *g* for 10 min and the supernatant containing the unencapsulated ***M*-L**$_{C60}$-**2**$^{4.4K}$-I was removed from the gel by decantation. The condensed gel was then washed with toluene-d_8 and the solvent was removed by decantation after centrifugation. This procedure was repeated two times (0.2 mL × 2). The obtained st-PMMA/***M*-L**$_{C60}$-**2**$^{4.4K}$-I gel was suspended in a small amount of toluene-d_8, and then subjected to the IR and VCD measurements. In the same way, st-PMMA/***P*-D**$_{C60}$-**2**$^{4.4K}$-F and st-PMMA/*rac*-C_{60}-**2**^{4K} (*rac*-C_{60}-**2**$^{4.4K}$ = a 1:1 mixture of ***M*-L**$_{C60}$-**2**$^{4.4K}$-I and ***P*-D**$_{C60}$-**2**$^{4.4K}$-F) complex gels were prepared and their IR and VCD spectra were measured. The VCD spectrum of the st-PMMA/*rac*-C_{60}-**2**^{4K} complex gel was subtracted from the VCD spectra of the st-PMMA/***M*-L**$_{C60}$-**2**$^{4.4K}$-I and st-PMMA/***P*-D**$_{C60}$-**2**$^{4.4K}$-F complex gels in toluene-d_8 after appropriate base-line corrections (Figure 3-4e). In the same way, st-PMMA gels complexed with ***M*-L**$_{C60}$-**2**$^{1.0K}$-I, ***P*-D**$_{C60}$-**2**$^{1.0K}$-F, ***M*-L**$_{C60}$-**2**$^{2.4K}$-I, ***P*-D**$_{C60}$-**2**$^{2.5K}$-F, ***M*-L**$_{N3}$-**1**$^{4.0K}$-I, and ***P*-D**$_{N3}$-**1**$^{4.1K}$-F were prepared in toluene-d_8, which were used for the IR and VCD measurements (Figures 3-4f and 3-S9h,i).

Preparation of st-PMMA/*M*- and *P*-PLA Complex Gels in Toluene and Replacement with C_{60}. A typical experimental procedure is described below. st-PMMA (8.0 mg) was dissolved in a toluene solution of ***M*-L**$_{C60}$-**2**$^{4.4K}$-I (3.0 mg/mL, 2.0 mL) at 110 °C. After the solution was cooled to room temperature, the solution gelled within 10 min. The obtained soft gel was collected by centrifugation at 1700 *g* for 10 min and the supernatant was removed from the gel by decantation. The condensed gel was then washed with toluene to remove the unencapsulated ***M*-L**$_{C60}$-**2**$^{4.4K}$-I by centrifugation followed by decantation. This procedure was repeated 2 times (0.2 mL × 2). The obtained st-PMMA/***M*-L**$_{C60}$-**2**$^{4.4K}$-I gel (***M*-L**$_{C60}$-**2**$^{4.4K}$-I:

15.6 wt%) was suspended in a small amount of toluene, and then subjected to the absorption and ECD measurements.

To replace the encapsulated ***M*-L$_{C60}$-2$^{4.4K}$-I** (15.6 wt%) with the achiral C_{60}, the st-PMMA/***M*-L$_{C60}$-2$^{4.4K}$-I** complex gel was suspended in a toluene solution of C_{60} (1.7 mg/mL, 1.0 mL). The mixture was vigorously stirred at room temperature by a magnetic stirrer. After 30 min, the obtained gel particles were recovered by centrifugation at 1700 *g* for 10 min and the supernatant containing the ***M*-L$_{C60}$-2$^{4.4K}$-I** released from the st-PMMA and unencapsulated C_{60} was removed by decantation. This procedure was repeated 10 times (1.0 mL × 10). The condensed gel was then washed with toluene and the solvent was removed by decantation after centrifugation. This procedure was repeated 2 times (0.5 mL × 2). Removal of ***M*-L$_{C60}$-2$^{4.4K}$-I** was confirmed by the ^{1}H NMR spectrum of the isolated st-PMMA/C_{60} complex (Figure 3-S12). The obtained gel was suspended in a small amount of toluene, and then subjected to the absorption and ECD measurements.

Helix-Sense-Selective Encapsulation of the Racemic *M*- and *P*-PLAs with *M*- and *P*-st-PMMA with a Helicity Memory. An optically-active *M*- or *P*-st-PMMA gel was prepared according to a previously reported method.[61,62] A typical experimental procedure is described below. st-PMMA (3.0 mg) was dissolved in (*R*)-1-phenylethylamine ((*R*)-**3**) (75 mL) at 110 ºC. After the solution was cooled to 3 °C, the solution gelled within 3 h. The obtained gel was washed with toluene to remove (*R*)-**3** completely by centrifugation followed by decantation. This procedure was repeated five times (0.15 mL × 7), affording an optically-active *M*-st-PMMA with helicity memory. The gel was then suspended in a toluene solution of an equimolar mixture of ***M*-L$_{C60}$-2$^{4.4K}$-I** and ***P*-D$_{C60}$-2$^{4.4K}$-F** (1.8 mg/mL, 0.50 mL). The mixture was vigorously stirred at room temperature for 3 h by a magnetic stirrer, thus producing soft gel particles. The obtained *M*-st-PMMA/nonracemic C$_{60}$-**2**$^{4.4K}$ complex gel was collected by centrifugation at 1700 *g* for 10 min and the supernatant containing the

unencapsulated C_{60}-**2**$^{4.4K}$ was recovered by decantation. The encapsulated C_{60}-**2**$^{4.4K}$ content was estimated from the integral ratio of the methoxy and methine protons of the *M*-st-PMMA and C_{60}-**2**$^{4.4K}$ in the ^{1}H NMR spectrum, respectively, and also determined from absorption spectroscopy. After evaporation of the solvents in the *M*-st-PMMA/C_{60}-**2**$^{4.4K}$ complex gel and of its supernatant, the residues were dissolved in $CDCl_3$, and the ee values of the encapsulated and unencapsulated C_{60}-**2**$^{4.4K}$ were determined by ^{1}H NMR (Figure 3-6a(ii,iii)). In the same way, the helix-sense-selective encapsulations of other C_{60}-bound *rac*-**2** and C_{60}-free *rac*-**1** with different molar masses were conducted using the *M*- and *P*-helical st-PMMA gels with helicity memory prepared by (*R*)- and (*S*)-**3**, respectively, and the results are summarized in Table 3-3.

PLA Chain Exchange Reactions Between the C_{60}-Bound Helical *M*- or *P*-PLAs Encapsulated in the *M*-st-PMMA Helical Cavity and Free C_{60}-Bound Helical *M*- or *P*-PLAs. An optically-active *M*-st-PMMA gel with helicity memory was prepared in (*R*)-**3**. The gel consisting of *M*-st-PMMA (6.0 mg) was then suspended in a toluene solution of ***M***-$\mathbf{L}_{C60}$-**2**$^{4.4K}$-I (1.8 mg/mL, 0.50 mL). The mixture was vigorously stirred at room temperature for 3 h by a magnetic stirrer, thus producing soft gel particles. The obtained *M*-st-PMMA/***M***-$\mathbf{L}_{C60}$-**2**$^{4.4K}$-I complex gel was collected by centrifugation at 1700 *g* for 10 min and the supernatant containing the unencapsulated ***M***-$\mathbf{L}_{C60}$-**2**$^{4.4K}$-I was recovered by decantation. The encapsulated ***M***-$\mathbf{L}_{C60}$-**2**$^{4.4K}$-I content was determined from absorption spectroscopy. The supernatant solution and the *M*-st-PMMA/***M***-$\mathbf{L}_{C60}$-**2**$^{4.4K}$-I complex gel were then mixed again, followed by adding a toluene solution of ***P***-$\mathbf{D}_{C60}$-**2**$^{4.4K}$-F (1.8 mg/mL, 0.50 mL). The mixture was vigorously stirred at room temperature for 3 h by a magnetic stirrer. The obtained *M*-st-PMMA/nonracemic C_{60}-**2**$^{4.4K}$ complex gel was collected by centrifugation at 1700 *g* for 10 min and the supernatant containing the unencapsulated C_{60}-**2**$^{4.4K}$ was recovered by decantation. The encapsulated C_{60}-**2**$^{4.4K}$ content was estimated by ^{1}H NMR

spectroscopy After evaporation of the solvents in the *M*-st-PMMA/C_{60}-**2**$^{4.4K}$ complex gel and of its supernatant, the residues were dissolved in $CDCl_3$, and the ee values of the encapsulated and unencapsulated C_{60}-**2**$^{4.4K}$ were determined by ^{1}H NMR. In the same way, the PLA chain exchange reaction between ***P***-**D**$_{C60}$-**2**$^{4.4K}$-F encapsulated in the ***M***-st-PMMA helical cavity and free ***M***-**L**$_{C60}$-**2**$^{4.4K}$-I were conducted, and the results are summarized in Figure 3-S14a,b.

Helix-Sense-Selective Encapsulation of the Nonracemic C_{60}-Bound PLA with *M*- and *P*-st-PMMA with a Helicity Memory. An optically-active *M*-st-PMMA gel with helicity memory was prepared in (*R*)-**3**. The gel consisting of *M*-st-PMMA (15.0 mg) was then suspended in a toluene solution of 53% ee of C_{60}-**2**$^{4.4K}$ (***P***-**D**$_{C60}$-**2**$^{4.4K}$-F rich) (0.18 mg/mL, 2.5 mL). The mixture was vigorously stirred at room temperature for 3 h by a magnetic stirrer, thus producing soft gel particles. The obtained *M*-st-PMMA/nonracemic C_{60}-**2**$^{4.4K}$ complex gel was collected by centrifugation at 1700 *g* for 10 min and the supernatant containing the unencapsulated C_{60}-**2**$^{4.4K}$ was recovered by decantation. The encapsulated C_{60}-**2**$^{4.4K}$ content was estimated by ^{1}H NMR and absorption spectroscopies. After evaporation of the solvents in the *M*-st-PMMA/C_{60}-**2**$^{4.4K}$ complex gel and of its supernatant, the residues were dissolved in $CDCl_3$, and the ee values of the encapsulated and unencapsulated C_{60}-**2**$^{4.4K}$ were determined by ^{1}H NMR (Figure 3-7b(ii,iii)).

References

(1) Bishop, R.; Dance, I. G. *Top. Curr. Chem.* **1988**, *149*, 137–188.

(2) Star, A.; Steuerman, D. W.; Heath, J. R.; Stoddart, J. F. *Angew. Chem., Int. Ed.* **2002**, *41*, 2508–2512.

(3) Kim, O.-K.; Je, J.; Baldwin, J. W.; Kooi, S.; Pehrsson, P. E.; Buckley, L. J. *J. Am. Chem. Soc.* **2003**, *125*, 4426–4427.

(4) Li, C.; Numata, M.; Bae, A.-H.; Sakurai, K.; Shinkai, S. *J. Am. Chem. Soc.* **2005**, *127*, 4548–4549.

(5) Sanji, T.; Kato, N.; Kato, M.; Tanaka, M. *Angew. Chem., Int. Ed.* **2005**, *44*, 7301–7304.

(6) Ikeda, M.; Furusho, Y.; Okoshi, K.; Tanahara, S.; Maeda, K.; Nishino, S.; Mori, T.; Yashima, E. *Angew. Chem., Int. Ed.* **2006**, *45*, 6491–6495.

(7) Sanji, T.; Kato, N.; Tanaka, M. *Org. Lett.* **2006**, *8*, 235–238.

(8) Frampton, M. J.; Claridge, T. D. W.; Latini, G.; Brovelli, S.; Cacialli, F.; Anderson, H. L. *Chem. Commun.* **2008**, 2797–2799.

(9) Numata, M.; Shinkai, S. *Chem. Commun.* **2011**, *47*, 1961–1975.

(10) Kumar, K.; Woortman, A. J. J.; Loos, K. *Biomacromolecules* **2013**, *14*, 1955–1960.

(11) Klug, A. *Angew. Chem., Int. Ed. Engl.* **1983**, *22*, 565–582.

(12) Egan, P.; Sinko, R.; LeDuc, P. R.; Keten, S. *Nat. Commun.* **2015**, *6*, 7418.

(13) Luo, Q.; Hou, C.; Bai, Y.; Wang, R.; Liu, J. *Chem. Rev.* **2016**, *116*, 13571–13632.

(14) Pieters, B. J. G. E.; van Eldijk, M. B.; Nolte, R. J. M.; Mecinović, J. *Chem. Soc. Rev.* **2016**, *45*, 24–39.

(15) Wilson, C. J.; Bommarius, A. S.; Champion, J. A.; Chernoff, Y. O.; Lynn, D. G.; Paravastu, A. K.; Liang, C.; Hsieh, M.-C.; Heemstra, J. M. *Chem. Rev.* **2018**, *118*, 11519–11574.

(16) Yuan, C.; Ji, W.; Xing, R.; Li, J.; Gazit, E.; Yan, X. *Nat. Rev. Chem.* **2019**, *3*, 567–588.

(17) Tomasik, P.; Schilling, C. H. *Adv. Carbohydr. Chem. Biochem.* **1998**, *53*, 345–426.

(18) Frampton, M. J.; Anderson, H. L. *Angew. Chem., Int. Ed.* **2007**, *46*, 1028–1064.

(19) Putseys, J. A.; Lamberts, L.; Delcour, J. A. *J. Cereal Sci.* **2010**, *51*, 238–247.

(20) Alberts, B.; Johnson, A.; Lewis, J.; Morgan, D.; Raff, M.; Roberts, K.; Walter, P.*; Molecular biology of the cell, 6th ed., Garland Science*: New York, 2015.

(21) Kadokawa, J. *Synlett* **2020**, *31*, 648–656.

(22) Barrow, S. J.; Kasera, S.; Rowland, M. J.; del Barrio, J.; Scherman, O. A. *Chem. Rev.* **2015**, *115*, 12320–12406.

(23) Li, J.; Yim, D.; Jang, W.-D.; Yoon, J. *Chem. Soc. Rev.* **2017**, *46*, 2437–2458.

(24) Liu, Z.; Nalluri, S. K. M.; Stoddart, J. F. *Chem. Soc. Rev.* **2017**, *46*, 2459–2478.

(25) Murray, J.; Kim, K.; Ogoshi, T.; Yao, W.; Gibb, B. C. *Chem. Soc. Rev.* **2017**, *46*, 2479–2496.

(26) Prochowicz, D.; Kornowicz, A.; Lewiński, J. *Chem. Rev.* **2017**, *117*, 13461–13501.

(27) Kumar, R.; Sharma, A.; Singh, H.; Suating, P.; Kim, H. S.; Sunwoo, K.; Shim, I.; Gibb, B. C.; Kim, J. S. *Chem. Rev.* **2019**, *119*, 9657–9721.

(28) Ogoshi, T.; Kakuta, T.; Yamagishi, T. *Angew. Chem., Int. Ed.* **2019**, *58*, 2197–2206.

(29) Blanco-Gómez, A.; Cortón, P.; Barravecchia, L.; Neira, I.; Pazos, E.; Peinador, C.; García, M. D. *Chem. Soc. Rev.* **2020**, *49*, 3834–3862.

(30) Xia, D.; Wang, P.; Ji, X.; Khashab, N. M.; Sessler, J. L.; Huang, F. *Chem. Rev.* **2020**, *120*, 6070–6123.

(31) Biros, S. M.; Rebek, J. J. *Chem. Soc. Rev.* **2007**, *36*, 93–104.

(32) Saalfrank, R. W.; Maid, H.; Scheurer, A. *Angew. Chem., Int. Ed.* **2008**, *47*, 8794–8824.

(33) Yoshizawa, M.; Klosterman, J. K.; Fujita, M. *Angew. Chem., Int. Ed.* **2009**, *48*, 3418–3438.

(34) Brown, C. J.; Toste, F. D.; Bergman, R. G.; Raymond, K. N. *Chem. Rev.* **2015**, *115*, 3012–3035.

(35) Rizzuto, F. J.; von Krbek, L. K. S.; Nitschke, J. R. *Nat. Rev. Chem.* **2019**, *3*, 204–222.

(36) Yoshizawa, M.; Catti, L. *Acc. Chem. Res.* **2019**, *52*, 2392–2404.

(37) Pilgrim, B. S.; Champness, N. R. *ChemPlusChem* **2020**, *85*, 1842–1856.

(38) Sun, Y.; Chen, C.; Liu, J.; Stang, P. J. *Chem. Soc. Rev.* **2020**, *49*, 3889–3919.

(39) Hill, D. J.; Mio, M. J.; Prince, R. B.; Hughes, T. S.; Moore, J. S. *Chem. Rev.* **2001**, *101*, 3893–4011.

(40) Ho, R.-M.; Chiang, Y.-W.; Lin, S.-C.; Chen, C.-K. *Prog. Polym. Sci.* **2011**, *36*, 376–453.

(41) Pfukwa, R.; Kouwer, P. H. J.; Rowan, A. E.; Klumperman, B. *Angew. Chem., Int. Ed.* **2013**, *52*, 11040–11044.

(42) Yashima, E.; Ousaka, N.; Taura, D.; Shimomura, K.; Ikai, T.; Maeda, K. *Chem. Rev.* **2016**, *116*, 13752–13990.

(43) Ferrand, Y.; Huc, I. *Acc. Chem. Res.* **2018**, *51*, 970–977.

(44) John, E. A.; Massena, C. J.; Berryman, O. B. *Chem. Rev.* **2020**, *120*, 2759–2782.

(45) Legrand, B.; Aguesseau-Kondrotas, J.; Simon, M.; Maillard, L. *Catalysts* **2020**, *10*.

(46) Rinaldi, S. *Molecules* **2020**, *25*.

(47) Tamura, K.; Sam, N. S. M.; Ikai, T.; Okamoto, Y.; Yashima, E. *Bull. Chem. Soc. Jpn.* **2011**, *84*, 741–747.

(48) Zheng, M.; Jagota, A.; Semke, E. D.; Diner, B. A.; McLean, R. S.; Lustig, S. R.; Richardson, R. E.; Tassi, N. G. *Nat. Mater.* **2003**, *2*, 338–342.

(49) Sakurai, K.; Uezu, K.; Numata, M.; Hasegawa, T.; Li, C.; Kaneko, K.; Shinkai, S. *Chem. Commun.* **2005**, 4383–4398.

(50) Nishino, S.; Mori, T.; Tanahara, S.; Maeda, K.; Ikeda, M.; Furusho, Y.; Yashima, E. *Mol. Cryst. Liq. Cryst.* **2007**, *471*, 29–38.

(51) Akazaki, K.; Toshimitsu, F.; Ozawa, H.; Fujigaya, T.; Nakashima, N. *J. Am. Chem. Soc.* **2012**, *134*, 12700–12007.

(52) Chung, W.; Nobusawa, K.; Kamikubo, H.; Kataoka, M.; Fujiki, M.; Naito, M. *J. Am. Chem. Soc.* **2013**, *135*, 2374–2383.

(53) Deria, P.; Von Bargen, C. D.; Olivier, J.-H.; Kumbhar, A. S.; Saven, J. G.; Therien, M. J. *J. Am. Chem. Soc.* **2013**, *135*, 16220–16234.

(54) Sun, J. Z.; Qin, A.; Tang, B. Z. *Polym. Chem.* **2013**, *4*, 211–223.

(55) Schroeder, V.; Savagatrup, S.; He, M.; Lin, S.; Swager, T. M. *Chem. Rev.* **2019**, *119*, 599–663.

(56) Haraguchi, S.; Numata, M.; Li, C.; Nakano, Y.; Fujiki, M.; Shinkai, S. *Chem. Lett.* **2009**, *38*, 254–255.

(57) Shiraki, T.; Tsuchiya, Y.; Noguchi, T.; Tamaru, S.; Suzuki, N.; Taguchi, M.; Fujiki, M.; Shinkai, S. *Chem. - Asian J.* **2014**, *9*, 218–222.

(58) Peters, K. *Smart Mater. Struct.* **2011**, *20*, 013002.

(59) Kawauchi, T.; Kumaki, J.; Kitaura, A.; Okoshi, K.; Kusanagi, H.; Kobayashi, K.; Sugai, T.; Shinohara, H.; Yashima, E. *Angew. Chem., Int. Ed.* **2008**, *47*, 515–519.

(60) Kawauchi, T.; Kitaura, A.; Kumaki, J.; Kusanagi, H.; Yashima, E. *J. Am. Chem. Soc.* **2008**, *130*, 11889–11891.

(61) Kawauchi, T.; Kitaura, A.; Kawauchi, M.; Takeichi, T.; Kumaki, J.; Iida, H.; Yashima, E. *J. Am. Chem. Soc.* **2010**, *132*, 12191–12193.

(62) Kitaura, A.; Iida, H.; Kawauchi, T.; Yashima, E. *Chem. Lett.* **2011**, *40*, 28–30.

(63) Sato, M.; Kato, T.; Ohishi, T.; Ishige, R.; Ohta, N.; White, K. L.; Hirai, T.; Takahara, A. *Macromolecules* **2016**, *49*, 2071–2076.

(64) Vidal, F.; Falivene, L.; Caporaso, L.; Cavallo, L.; Chen, E. Y. X. *J. Am. Chem. Soc.* **2016**, *138*, 9533–9547.

(65) Sato, M.; Kato, T.; Shimamoto, H.; Kamitani, K.; Ohta, N.; Hirai, T.; Takahara, A. *ACS Macro Lett.* **2018**, *7*, 148–152.

(66) Kumaki, J.; Kawauchi, T.; Okoshi, K.; Kusanagi, H.; Yashima, E. *Angew. Chem., Int. Ed.* **2007**, *46*, 5348–5351.

(67) Stereocomplex formation has been applied to construct supramolecular nanostructures, see refs. 68–74.

(68) Kawauchi, T.; Kumaki, J.; Yashima, E. *J. Am. Chem. Soc.* **2006**, *128*, 10560–10567.

(69) Goh, T. K.; Tan, J. F.; Guntari, S. N.; Satoh, K.; Blencowe, A.; Kamigaito, M.; Qiao, G. G. *Angew. Chem., Int. Ed.* **2009**, *48*, 8707–8711.

(70) Ren, J. M.; Ishitake, K.; Satoh, K.; Blencowe, A.; Fu, Q.; Wong, E. H. H.; Kamigaito, M.; Qiao, G. G. *Macromolecules* **2016**, *49*, 788–795.

(71) Ren, J. M.; Lawrence, J.; Knight, A. S.; Abdilla, A.; Zerdan, R. B.; Levi, A. E.; Oschmann, B.; Gutekunst, W. R.; Lee, S.-H.; Li, Y.; McGrath, A. J.; Bates, C. M.; Qiao, G. G.; Hawker, C. J. *J. Am. Chem. Soc.* **2018**, *140*, 1945–1951.

(72) Ren, J. M.; Knight, A. S.; van Ravensteijn, B. G. P.; Kohl, P.; Bou Zerdan, R.; Li, Y.; Lunn, D. J.; Abdilla, A.; Qiao, G. G.; Hawker, C. J. *J. Am. Chem. Soc.* **2019**, *141*, 2630–2635.

(73) Vidal, F.; Watson, E. M.; Chen, E. Y. X. *Macromolecules* **2019**, *52*, 7313–7323.

(74) Abdilla, A.; Dolinski, N. D.; de Roos, P.; Ren, J. M.; van der Woude, E.; Seo, S. E.; Zayas, M. S.; Lawrence, J.; Read de Alaniz, J.; Hawker, C. J. *J. Am. Chem. Soc.* **2020**, *142*, 1667–1672.

(75) Ousaka, N.; Mamiya, F.; Iwata, Y.; Nishimura, K.; Yashima, E. *Angew. Chem., Int. Ed.* **2017**, *56*, 791–795.

(76) Kawauchi, T.; Ohnishi, K.; Kajihara, K.; Kawauchi, M.; Takeichi, T. *Macromolecules* **2019**, *52*, 5067–5073.

(77) *Poly(Lactic Acid): Synthesis, Structures, Properties, Processing, and Applications*; Auras, R., Lim, L. T., Selke, S. E. M., Tsuji, H., Eds.; John Wiley & Sons. Inc.: NJ, 2010.

(78) De Santis, P.; Kovacs, A. J. **1968**, *6*, 299–306.

(79) Sasaki, S.; Asakura, T. *Macromolecules* **2003**, *36*, 8385–8390.

(80) Wasanasuk, K.; Tashiro, K.; Hanesaka, M.; Ohhara, T.; Kurihara, K.; Kuroki, R.; Tamada, T.; Ozeki, T.; Kanamoto, T. *Macromolecules* **2011**, *44*, 6441–6452.

(81) Tonelli, A. E. *Macromolecules* **1992**, *25*, 3581–3584.

(82) Topol, I. A.; Burt, S. K.; Deretey, E.; Tang, T.-H.; Perczel, A.; Rashin, A.; Csizmadia, I. G. *J. Am. Chem. Soc.* **2001**, *123*, 6054–6060.

(83) Mamiya, F. Studies on Synthesis of Chiral Cyclic Supramolecules and Supramolecular Helical Complex Formation of Syndiotactic Poly(methyl methacrylate) with Chiral Fullerene Derivatives. Ph.D. Thesis, Nagoya University, Japan, **2019**. http://hdl.handle.net/2237/00029969.

(84) Nolte, R. J. M.; Van Beijnen, A. J. M.; Drenth, W. *J. Am. Chem. Soc.* **1974**, *96*, 5932–5933.

(85) Okamoto, Y.; Mohri, H.; Nakano, T.; Hatada, K. *J. Am. Chem. Soc.* **1989**, *111*, 5952–5954.

(86) Miyabe, T.; Iida, H.; Banno, M.; Yamaguchi, T.; Yashima, E. *Macromolecules* **2011**, *44*, 8687–8692.

(87) Ohya, Y.; Takamido, S.; Nagahama, K.; Ouchi, T.; Ooya, T.; Katoono, R.; Yui, N. *Macromolecules* **2007**, *40*, 6441–6444.

(88) Kaneko, Y.; Ueno, K.; Yui, T.; Nakahara, K.; Kadokawa, J.-i. *Macromol. Biosci.* **2011**, *11*, 1407–1415.

(89) Tanaka, T.; Sasayama, S.; Yamamoto, K.; Kimura, Y.; Kadokawa, J.-i. *Macromol. Chem. Phys.* **2015**, *216*, 794–800.

(90) Isono, T.; Kondo, Y.; Otsuka, I.; Nishiyama, Y.; Borsali, R.; Kakuchi, T.; Satoh, T. *Macromolecules* **2013**, *46*, 8509–8518.

(91) Abe, H.; Imai, K.; Matsumoto, M. *J. Polym. Sci., Part C* **1968**, *23*, 469–485.

(92) Fox, T. G.; Garrett, B. S.; Goode, W. E.; Gratch, S.; Kincaid, J. F.; Spell, A.; Stroupe, J. D. *J. Am. Chem. Soc.* **1958**, *80*, 1768–1769.

(93) Liquori, A. M.; Anzuino, G.; Coiro, V. M.; D'Alagni, M.; De Santis, P.; Savino, M. *Nature* **1965**, *206*, 358–362.

(94) Worch, J. C.; Prydderch, H.; Jimaja, S.; Bexis, P.; Becker, M. L.; Dove, A. P. *Nat. Rev. Chem.* **2019**, *3*, 514–535.

(95) Effing, J.; Jonas, U.; Jullien, L.; Plesnivy, T.; Ringsdorf, H.; Diederich, F.; Thilgen, C.; Weinstein, D. *Angew. Chem., Int. Ed. Engl.* **1992**, *31*, 1599–1602.

(96) Pantoş, G. D.; Wietor, J.-L.; Sanders, J. K. M. *Angew. Chem., Int. Ed.* **2007**, *46*, 2238–2240.

(97) The PLA chain exchange reactions between the C_{60}-bound helical ***M***- or ***P***-PLAs encapsulated in the *M*-st-PMMA helical cavity and free C_{60}-bound helical ***M***- or ***P***-PLAs proceeded to reach an equilibrium within 3 h at room temperature (see Figure 3-S14 and Experimental Section).

(98) The α value is a useful measure in chiral chromatography to evaluate the chiral resolving abilities of CSPs toward racemic analytes, see refs. 99 and 100.

(99) Okamoto, Y.; Yashima, E. *Angew. Chem., Int. Ed.* **1998**, *37*, 1020–1043.

(100) Shen, J.; Okamoto, Y. *Chem. Rev.* **2016**, *116*, 1094–1138.

(101) Kawauchi, T.; Kawauchi, M.; Kodama, Y.; Takeichi, T. *Macromolecules* **2011**, *44*, 3452–3457.

(102) Shimomura, K.; Ikai, T.; Kanoh, S.; Yashima, E.; Maeda, K. *Nat. Chem.* **2014**, *6*, 429–434.

(103) Ishidate, R.; Sato, T.; Ikai, T.; Kanoh, S.; Yashima, E.; Maeda, K. *Polym. Chem.* **2019**, *10*, 6260–6268.

(104) Harrell, M. L.; Bergbreiter, D. E. *J. Chem. Educ.* **2017**, *94*, 1668–1673.

(105) Hoogsteen, W.; Postema, A. R.; Pennings, A. J.; ten Brinke, G.; Zugenmaier, P. *Macromolecules* **1990**, *23*, 634–642.

(106) Alemán, C.; Lotz, B.; Puiggali, J. *Macromolecules* **2001**, *34*, 4795–4801.

(107) Sun, H.; Jin, Z.; Yang, C.; Akkermans, R. L. C.; Robertson, S. H.; Spenley, N. A.; Miller, S.; Todd, S. M. *J. Mol. Model.* **2016**, *22*, 47.

Supporting Data

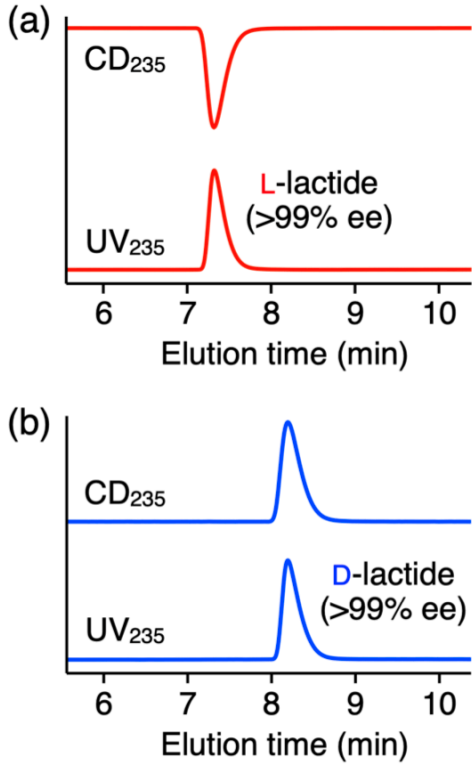

Figure 3-S1. Verification of high optical purities (>99% ee) of L-lactide (a) and D-lactide (b) by chiral HPLC on a CHIRALPAK IA-3 column (15 cm × 0.46 cm (i.d.)). Chromatograms show UV (bottom) and CD (top) traces recorded at 235 nm. Eluent, hexane/2-propanol (90/10, v/v); flow rate, 1.0 mL/min; temperature, ca. 20 °C.

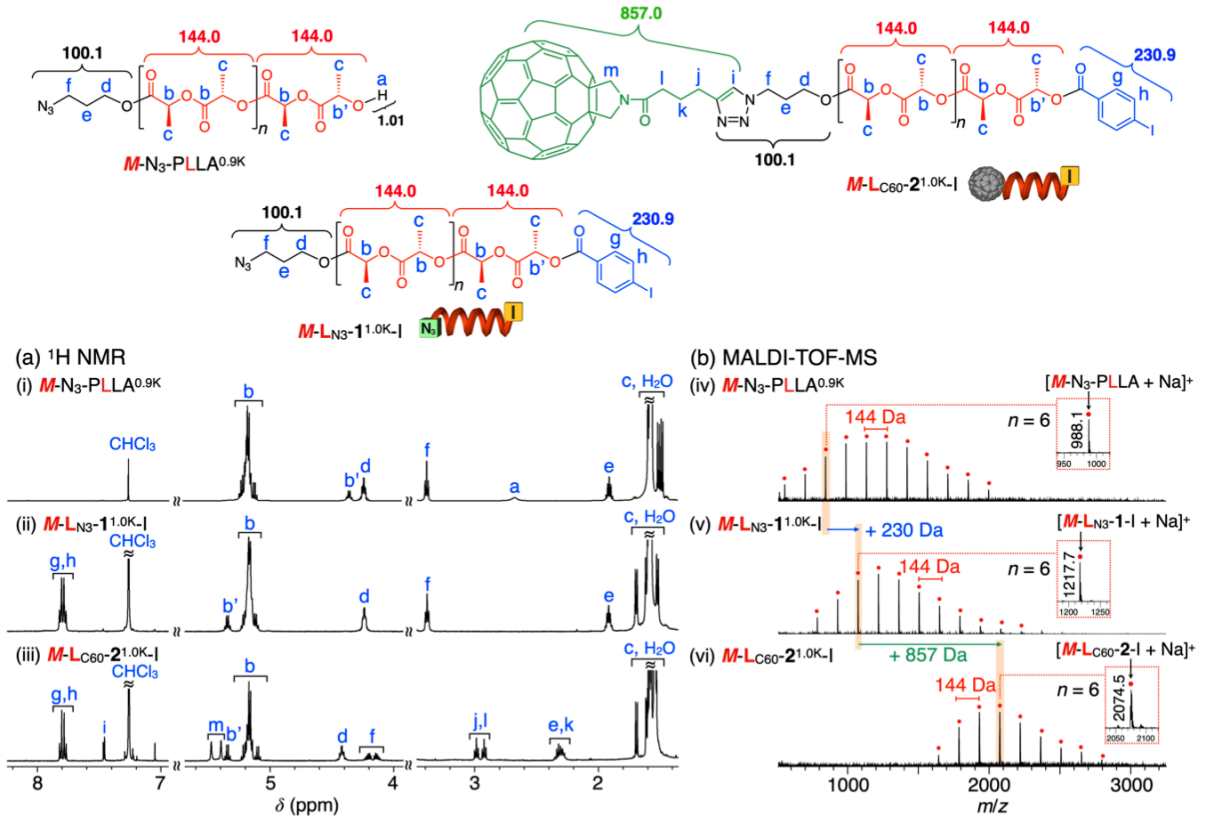

Figure 3-S2. (a) ^{1}H NMR and (b) MALDI-TOF-MS spectra of ***M***-N$_3$-PLLA$^{0.9K}$, ***M***-**L**$_{N3}$-**1**$^{1.0K}$-I, and ***M***-**L**$_{C60}$-**2**$^{1.0K}$-I. The NMR spectra were measured in $CDCl_3$ at 25 °C and the MS measurements were performed using dithranol as a matrix and sodium iodide as a cationizing agent.

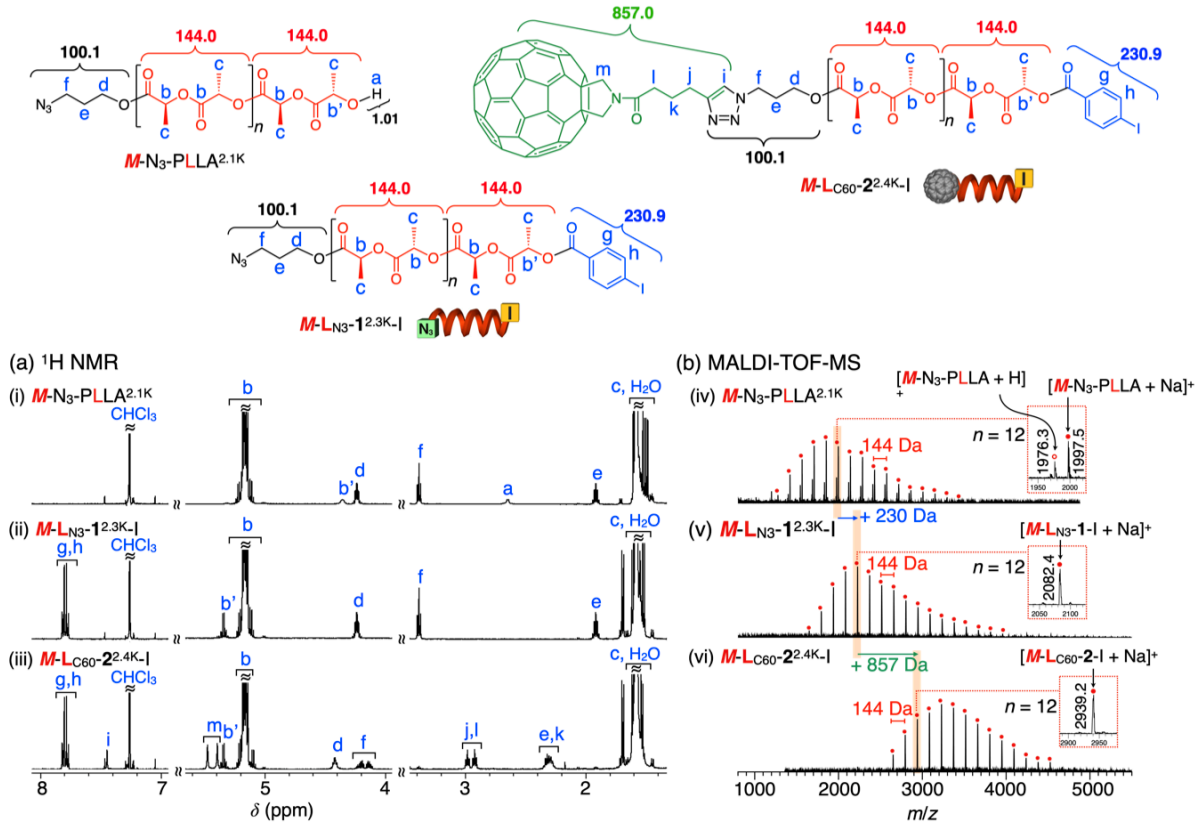

Figure 3-S3. (a) ^{1}H NMR and (b) MALDI-TOF-MS spectra of ***M***-N_3-PLLA$^{2.1K}$, ***M***-L_{N3}-**1**$^{2.3K}$-I, and ***M***-L_{C60}-**2**$^{2.4K}$-I. The NMR spectra were measured in $CDCl_3$ at 25 °C and the MS measurements were performed using dithranol as a matrix and sodium iodide as a cationizing agent.

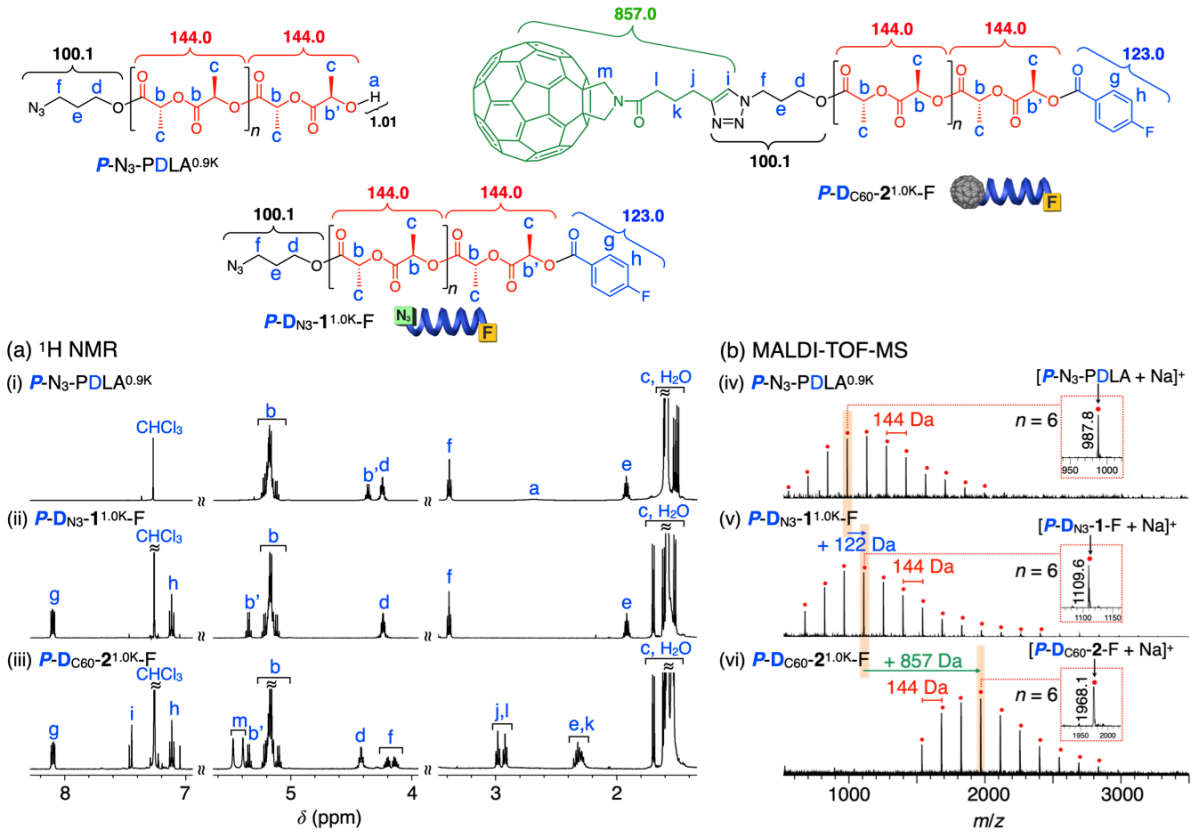

Figure 3-S4. (a) ^{1}H NMR and (b) MALDI-TOF-MS spectra of ***P***-N_3-PDLA$^{0.9K}$, ***P***-**D**$_{N3}$-**1**$^{1.0K}$-F, and ***P***-**D**$_{C60}$-**2**$^{1.0K}$-F. The NMR spectra were measured in $CDCl_3$ at 25 °C and the MS measurements were performed using dithranol as a matrix and sodium iodide as a cationizing agent.

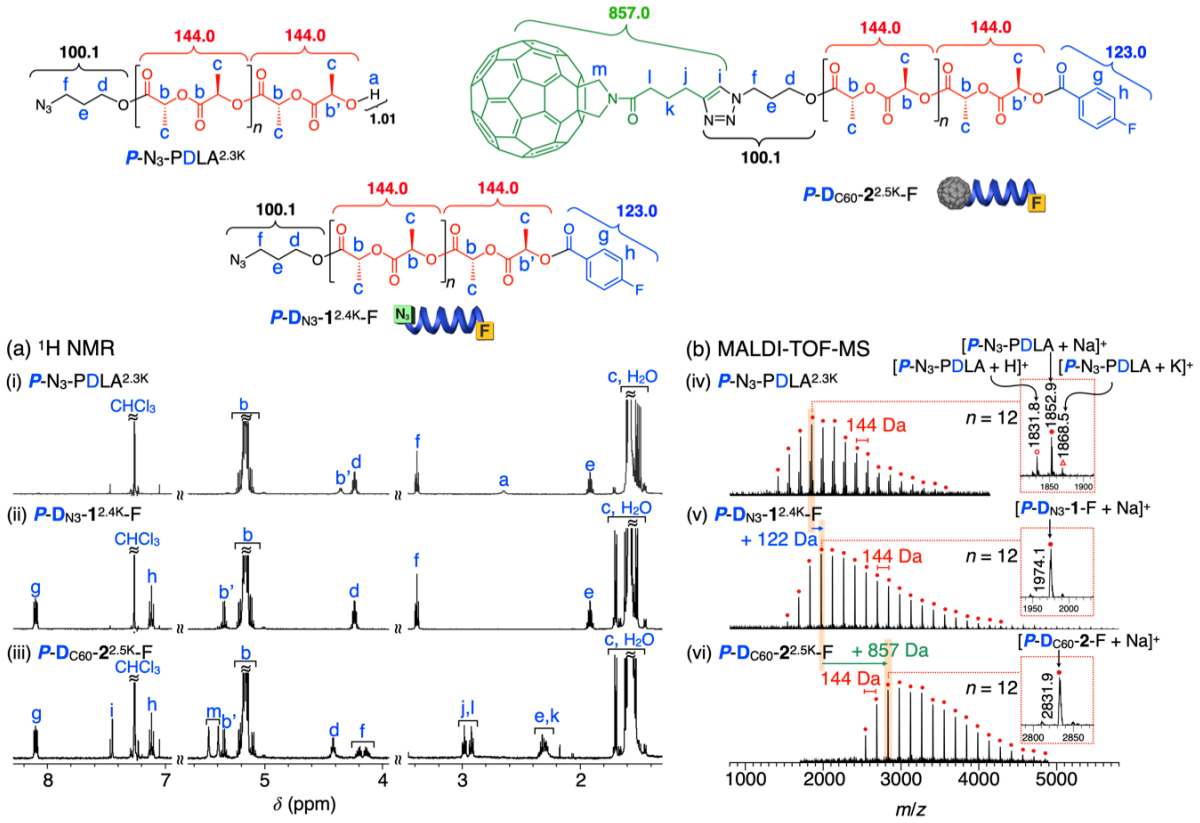

Figure 3-S5. (a) ^{1}H NMR and (b) MALDI-TOF-MS spectra of ***P***-N_3-PDLA$^{2.3K}$, ***P***-$\mathbf{D}_{N3}$-$\mathbf{1}^{2.4K}$-F, and ***P***-$\mathbf{D}_{C60}$-$\mathbf{2}^{2.5K}$-F. The NMR spectra were measured in $CDCl_3$ at 25 °C and the MS measurements were performed using dithranol as a matrix and sodium iodide as a cationizing agent.

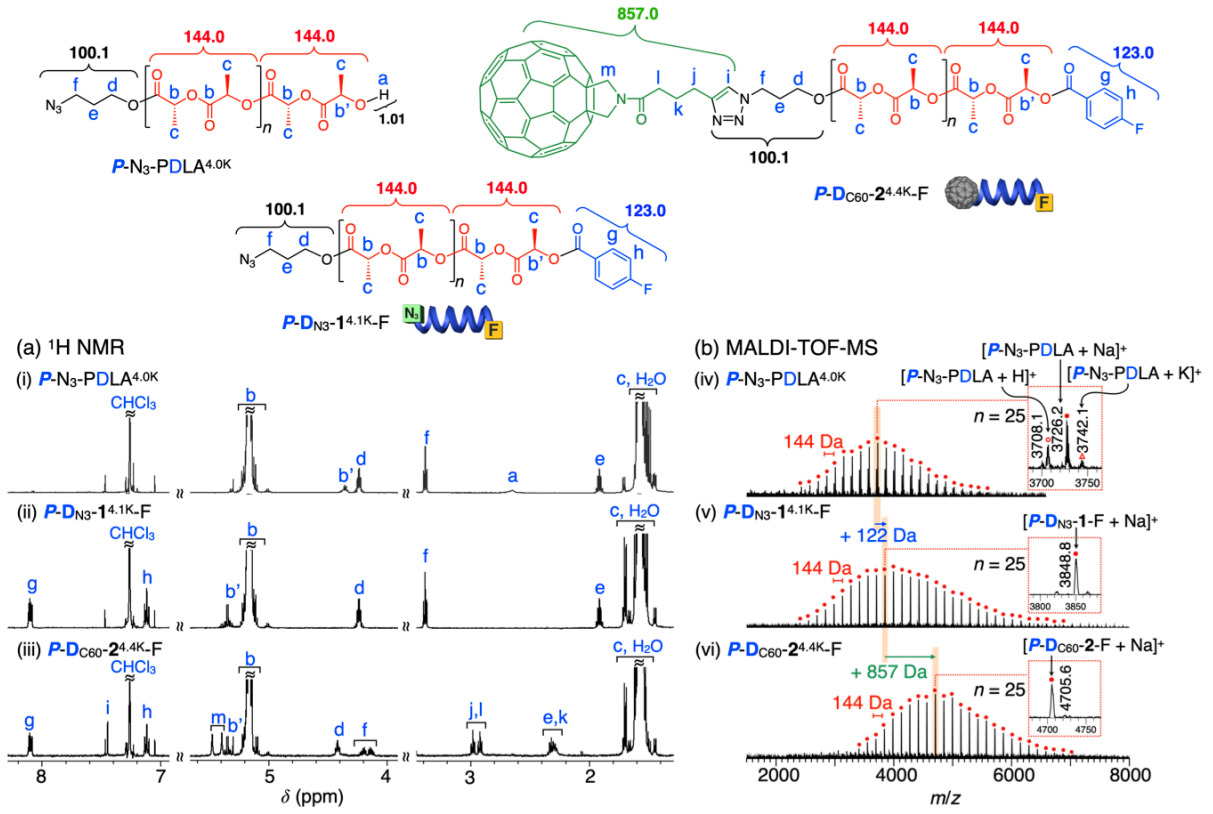

Figure 3-S6. (a) ^{1}H NMR and (b) MALDI-TOF-MS spectra of ***P***-N_3-PDLA$^{4.0K}$, ***P***-**D**$_{N3}$-**1**$^{4.1K}$-F, and ***P***-**D**$_{C60}$-**2**$^{4.4K}$-F. The NMR spectra were measured in $CDCl_3$ at 25 °C and the MS measurements were performed using dithranol as a matrix and sodium iodide as a cationizing agent.

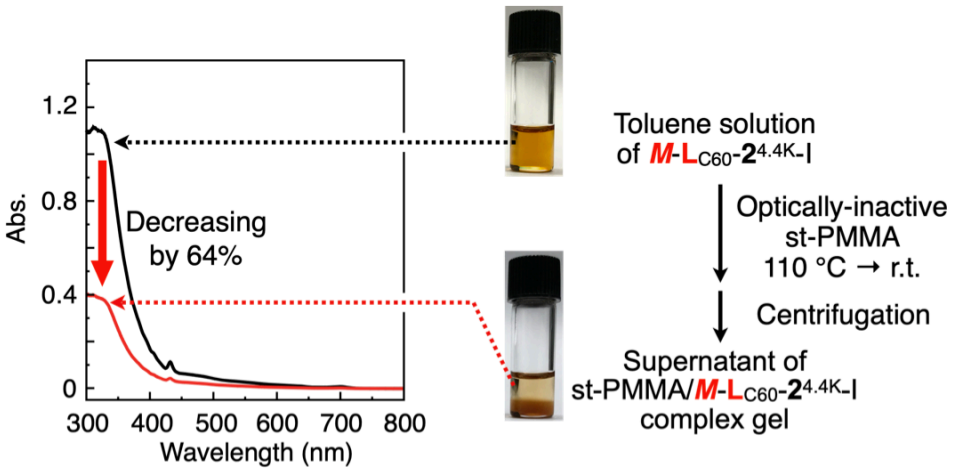

Figure 3-S7. Absorption spectra of the toluene solution of the feed ***M*-L$_{C60}$-2$^{4.4K}$-I** (3.0 mg/mL, 1.0 mL) and the supernatant isolated from the st-PMMA/***M*-L$_{C60}$-2$^{4.4K}$-I** complex gel after the addition of **s**t-PMMA (10 mg) with subsequent heating at 110 °C followed by cooling to r.t. and then centrifuged at 1700 *g* for 10 min.

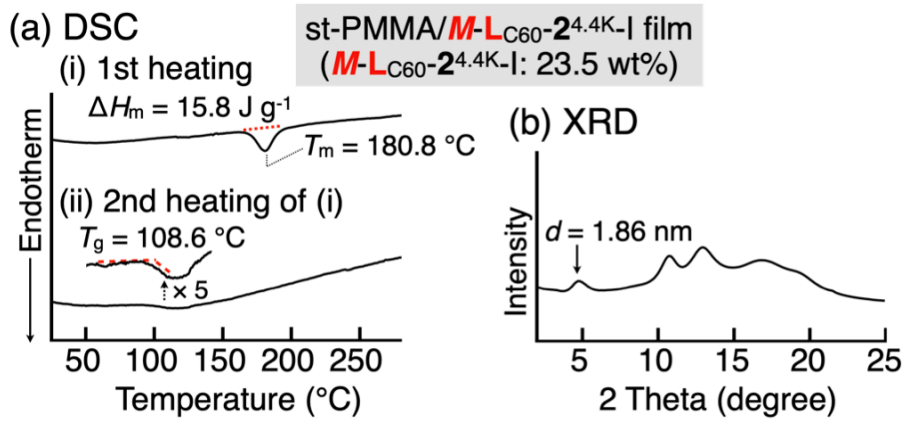

Figure 3-S8. (a) DSC thermograms of st-PMMA/***M*-L$_{C60}$-2$^{4.4K}$-I** complex film containing 23.5 wt% of ***M*-L$_{C60}$-2$^{4.4K}$-I** (i). The film was prepared by evaporating the solvent from the st-PMMA/***M*-L$_{C60}$-2$^{4.4K}$-I** complex gel in toluene. The DSC measurement was conducted after cooling the sample at –20 °C, followed by heating to 280 °C (10 °C/min) under nitrogen. The sample (i) was then cooled to –20 °C (40 °C/min), and then heated again ((ii); 10 °C/min). The arrow to the left of the DSC data indicates the endothermic direction. (b) XRD profile of st-PMMA/***M*-L$_{C60}$-2$^{4.4K}$-I** complex film (23.5 wt%).

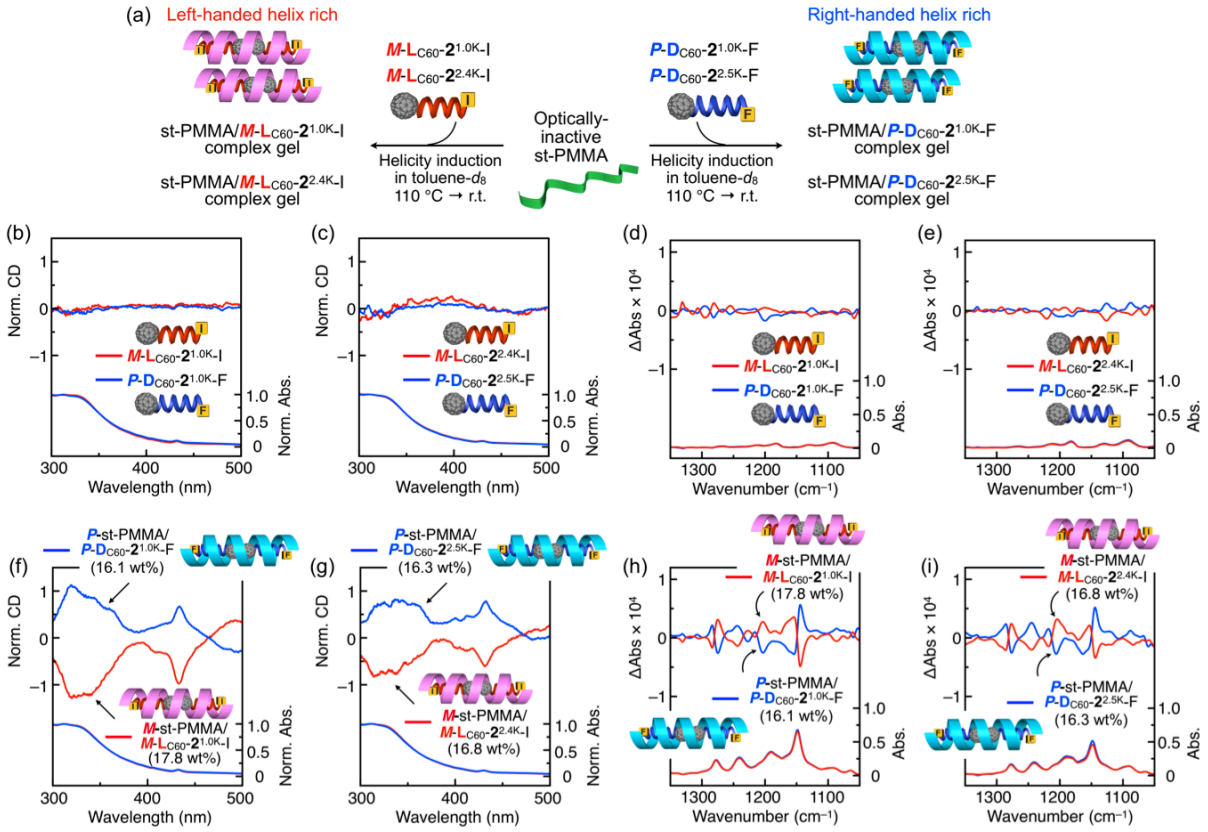

Figure 3-S9. (a) Schematic illustration of *M*- (left) and *P*- (right) helicity induction in st-PMMA upon encapsulation of ***M*-L**$_{C60}$**-2**-I and ***P*-D**$_{C60}$**-2**-F, respectively. (b,f) ECD (top) and absorption (bottom) spectra of ***M*-L**$_{C60}$**-2**$^{1.0K}$-I (1.3×10^{-3} M) (red) and ***P*-D**$_{C60}$**-2**$^{1.0K}$-F (1.4×10^{-3} M) (blue) (b) and those of st-PMMA/***M*-L**$_{C60}$**-2**$^{1.0K}$-I gel (17.8 wt%) (red) and st-PMMA/***P*-D**$_{C60}$**-2**$^{1.0K}$-F gel (16.1 wt%) (blue) (f) in toluene-d_8 at 25 °C. (c,g) ECD (top) and absorption (bottom) spectra of ***M*-L**$_{C60}$**-2**$^{2.4K}$-I (8.3×10^{-4} M) (red) and ***P*-D**$_{C60}$**-2**$^{2.5K}$-F (7.8×10^{-4} M) (blue) (c) and those of st-PMMA/***M*-L**$_{C60}$**-2**$^{2.4K}$-I gel (16.8 wt%) (red) and st-PMMA/***P*-D**$_{C60}$**-2**$^{2.5K}$-F gel (16.3 wt%) (blue) (g) in toluene-d_8 at 25 °C. The ECD and absorption spectra in (b,c,f,g) were normalized based on the corresponding absorption spectra at 25 °C. The contribution of the linear dichroism caused by the macroscopic anisotropy was negligible. (d,h) VCD (top) and IR (bottom) spectra of ***M*-L**$_{C60}$**-2**$^{1.0K}$-I (1.3×10^{-3} M) (red) and ***P*-D**$_{C60}$**-2**$^{1.0K}$-F (1.4×10^{-3} M) (blue) (d) and those of st-PMMA/***M*-L**$_{C60}$**-2**$^{1.0K}$-I gel (17.8 wt%) (red) and st-PMMA/***P*-D**$_{C60}$**-2**$^{1.0K}$-F gel (16.1 wt%) (blue) complex gels (h) in toluene-d_8 at room temperature. (e,i) VCD (top) and IR (bottom) spectra of ***M*-L**$_{C60}$**-2**$^{2.4K}$-I (8.3×10^{-4} M)

(red) and ***P***-$\mathbf{D}_{C60}$-$\mathbf{2}^{2.5K}$-F (7.8×10^{-4} M) (blue) (e) and those of st-PMMA/***M***-$\mathbf{L}_{C60}$-$\mathbf{2}^{2.4K}$-I gel (16.8 wt%) (red) and st-PMMA/***P***-$\mathbf{D}_{C60}$-$\mathbf{2}^{2.5K}$-F gel (16.3 wt%) (blue) complex gels (i) in toluene-d_8 at room temperature.

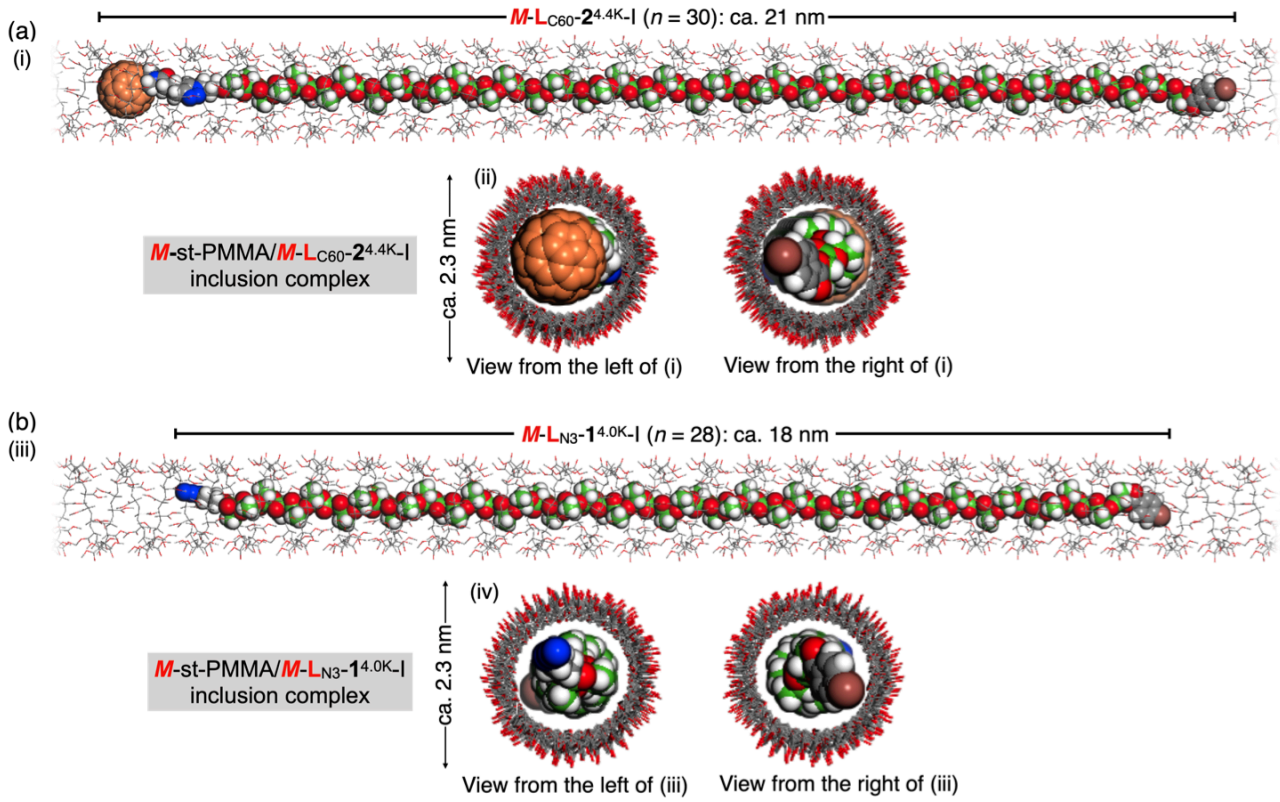

Figure 3-S10. Side (i and iii) and top (ii and iv) views of the geometry-optimized structures of the inclusion complexes between the left-handed 18_1 helical ***M***-st-PMMA and the left-handed 10_3 helical ***M***-$\mathbf{L}_{C60}$-$\mathbf{2}^{4.4K}$-I (a) and the left-handed 10_3 helical ***M***-$\mathbf{L}_{N3}$-$\mathbf{1}^{4.0K}$-I (b) obtained by the molecular mechanics (MM) calculations (Compass II force field). Hydrogen atoms of st-PMMA are omitted for clarity. The carbon atoms of the polylactide and C_{60} moieties are highlighted in green and orange, respectively.

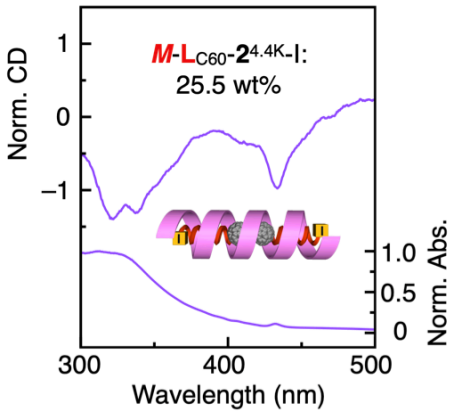

Figure 3-S11. ECD (top) and absorption (bottom) spectra of st-PMMA/***M***-$\mathbf{L}_{C60}$-$\mathbf{2}^{4.4K}$-I gel (25.5 wt%) in toluene at 25 °C. The contribution of the linear dichroism caused by the macroscopic anisotropy was negligible.

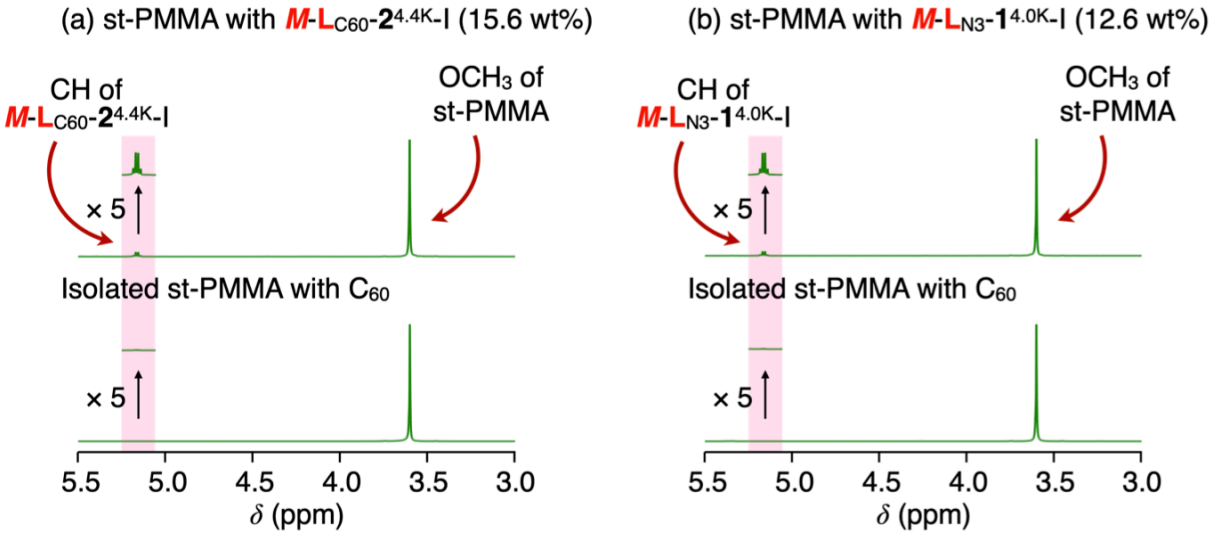

Figure 3-S12. ^{1}H NMR spectra of st-PMMA in the presence of ***M***-$\mathbf{L}_{C60}$-$\mathbf{2}^{4.4K}$-I (15.6 wt%) (a) and ***M***-$\mathbf{L}_{N3}$-$\mathbf{1}^{4.0K}$-I (12.6 wt%) (b) (top) and those of the isolated helicity-memorized st-PMMA with C_{60} (bottom) in $CDCl_3$ at 25 °C.

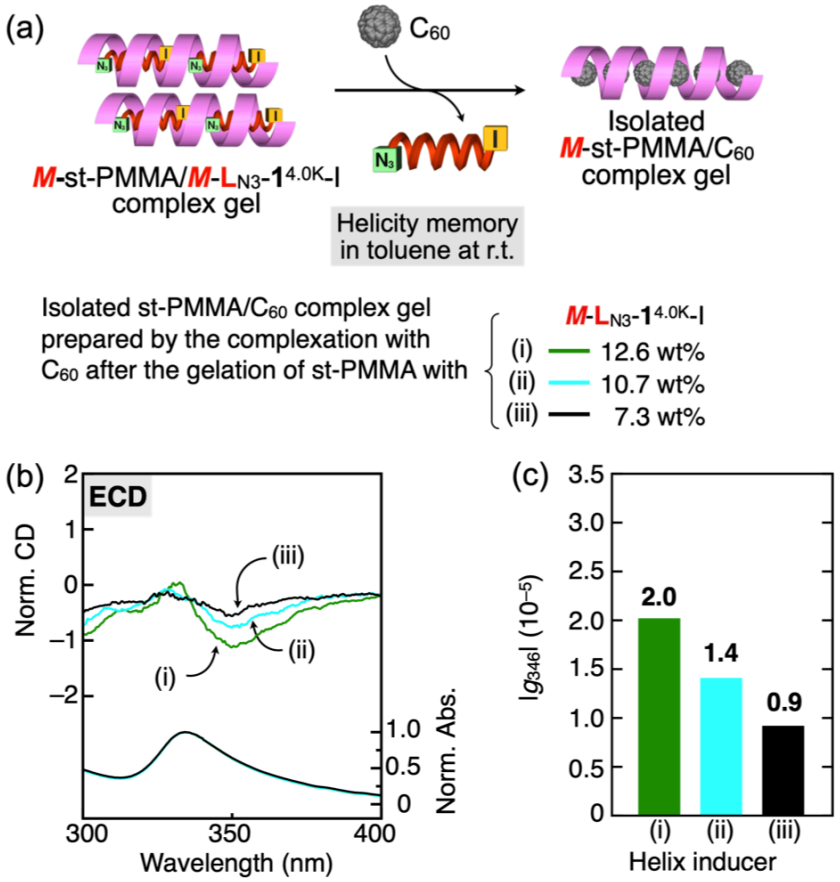

Figure 3-S13. (a) Schematic illustration of memory of the macromolecular helicity in st-PMMA induced by inclusion complexation with ***M***-**L**$_{N3}$-**1**$^{4.0K}$-I followed by replacement with the achiral C_{60}. (b) ECD (top) and absorption (bottom) spectra of isolated st-PMMA/C_{60} complex gels in toluene prepared by complexation with ***M***-**L**$_{N3}$-**1**$^{4.0K}$-I (i; 12.6 wt%, ii; 10.7 wt%, iii; 7.3 wt%) followed by replacement with the achiral C_{60}. Complete removal of ***M***-**L**$_{N3}$-**1**$^{4.0K}$-I was confirmed by ^{1}H NMR measurements of the isolated st-PMMA/C_{60} complexes. The ECD and absorption spectra were normalized based on the corresponding absorption spectra at 25 °C. (c) Kuhn's dissymmetry factors at 346 nm ($|g_{346}|$) of the isolated st-PMMA/C_{60} complexes (i–iii) in (b).

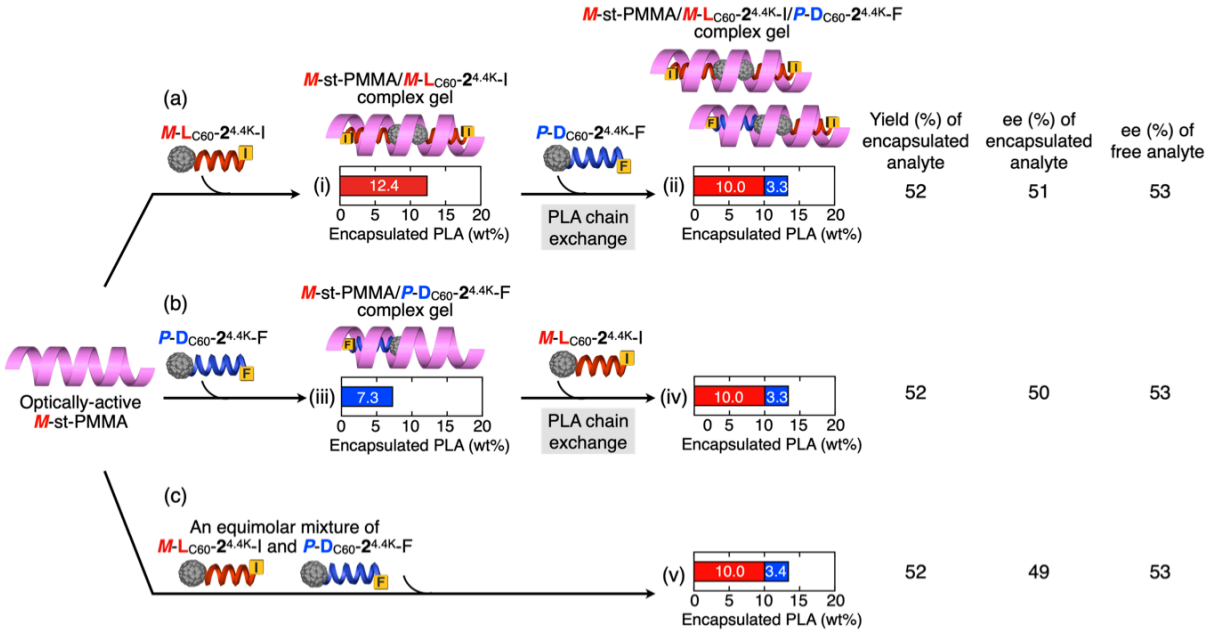

Figure 3-S14. Schematic illustrations of the PLA chain exchange reactions between the encapsulated PLAs and free PLAs. (a) Changes in the encapsulated ***M*-L**$_{C60}$-**2**$^{4.4K}$-I in the helical cavity of *M*-st-PMMA before (left, i) and after adding an equimolar amount of ***P*-D**$_{C60}$-**2**$^{4.4K}$-F with stirring at room temperature for 3 h (right, ii). (b) Changes in the encapsulated ***P*-D**$_{C60}$-**2**$^{4.4K}$-F in the helical cavity of *M*-st-PMMA before (left, iii) and after adding an equimolar amount of ***M*-L**$_{C60}$-**2**$^{4.4K}$-I with stirring at room temperature for 3 h (right, iv). (c) Encapsulation of an equal amount of ***M*-L**-$_{C60}$-**2**$^{4.4K}$-I and ***P*-D**$_{C60}$-**2**$^{4.4K}$-F (*rac*-C_{60}-**2**^{4K}) in the helical cavity of *M*-st-PMMA (v) (run 5 in Table 3-3). The amounts of the encapsulated PLAs in *M*-st-PMMA were estimated by absorption (i, iii) and ^{1}H NMR (ii, iv, v) analyses. The molar ratios of the encapsulated nonracemic PLAs in *M*-st-PMMA (ii, iv, v) were estimated by ^{1}H NMR analyses.

The results clearly indicated that the PLA chain exchange reactions proceeded to reach an equilibrium within 3 h at room temperature.

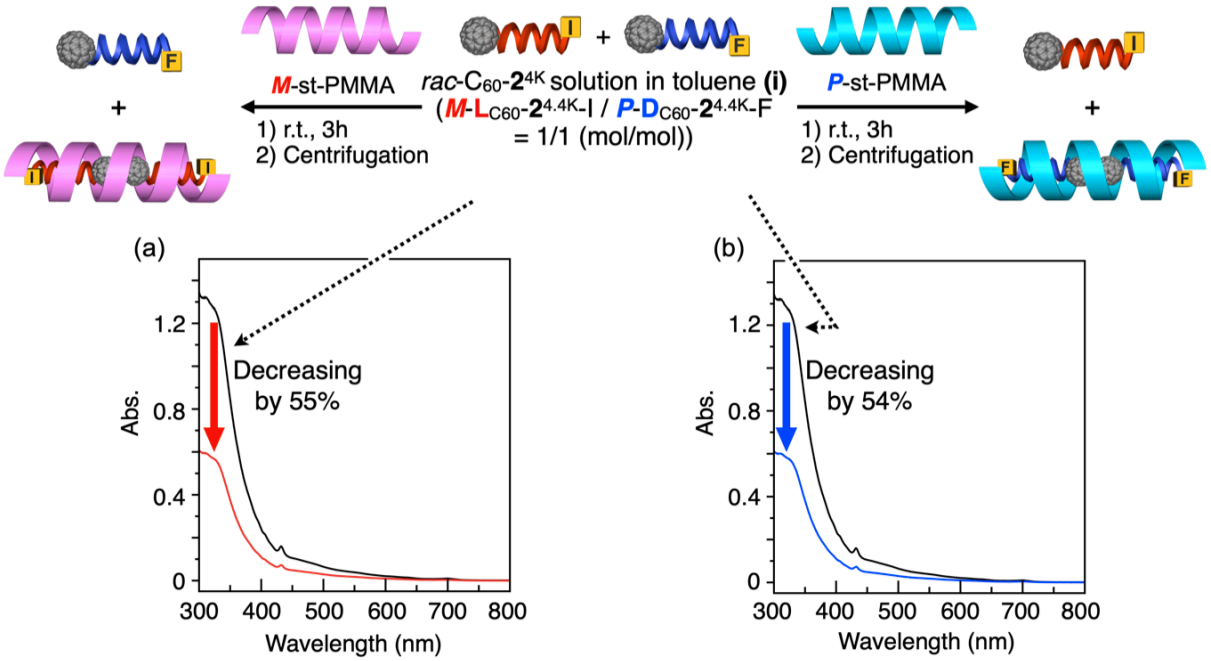

Figure 3-S15. (a, b) Absorption spectra of toluene solutions of the feed *rac*-C_{60}-**2**^{4K} (an equimolar mixture of ***M***-$\mathbf{L}_{C60}$-**2**$^{4.4K}$-I and ***P***-$\mathbf{D}_{C60}$-**2**$^{4.4K}$-F; 1.8 mg/mL, 0.50 mL) and the supernatant isolated from the st-PMMA/nonracemic C_{60}-**2**^{4K} complex gels after the addition of ***M***-st-PMMA (a) and ***P***-st-PMMA (b) (3.0 mg) with subsequent stirring at r.t. for 3 h and then centrifuged at 1700 *g* for 10 min.

List of Publications

Papers

1. "Allosteric Regulation of Metal-Binding Sites Inside an Optically-Active Helical Foldamer and Its Tubular Assemblies"
   Satoshi Kawabata, Naoki Ousaka, and Eiji Yashima
   Chem. Commun. **2018**, *54*, 2417–2420.

2. "Chiral Amplification of Supramolecular Coassemblies of Chiral and Achiral Acylhydrazine-Functionalized Biphenyls and Their Copolymers"
   Tomoyuki Ikai, Satoshi Kawabata, Shogo Okuda, Naoki Ousaka, and Eiji Yashima
   Polym. J. **2021**, in press (DOI: 10.1038/s41428-021-00550-7).

3. "Helix-Sense-Selective Encapsulation of Helical Poly(lactic acid)s within a Helical Cavity of Syndiotactic Poly(methyl methacrylate) with Helicity Memory"
   Tomoyuki Ikai, Satoshi Kawabata, Fumihiko Mamiya, Daisuke Taura, Naoki Ousaka, and Eiji Yashima
   J. Am. Chem. Soc. **2020**, *142*, 21913–21925.

Acknowledgment

The present study was carried out at the Department of Molecular and Macromolecular Chemistry, Graduate School of Engineering, Nagoya University, during 2016–2021.

The author wishes to express his grateful acknowledgment to Professor Eiji Yashima whose encouragement and helpful suggestions have been indispensable to the completion of the present thesis. He would also like to acknowledge Drs. Tomoyuki Ikai, Naoki Ousaka, Daisuke Taura, and Nozomu Suzuki for their constant guidance, encouragement, pertinent and tolerant advice, and helpful discussion. The author thanks Prof. Rong-Ming Ho (National Tsing Hua University, Taiwan) for his kind supply of D-lactide.

It is pleasure to express his appreciation to the colleagues of Professor Yashima Laboratory for their encouragement and friendship, especially to Drs. Kouhei Shimomura, Junki Tanabe, Shinya Yamamoto, Ryoma Ishidate, Fumihiko Mamiya, Akio Urushima, Raj Kumar Roy, Xiang Wang, and Wei Zheng and Messrs. Yoshimasa Suzuki, Takahide Tsuda, Kenta Katsura, Kouhei Watanabe, Takuya Iwata, Masayuki Ueda, Naomichi Horimoto, Chiaki Yokota, Noriyuki Hayashi, Masaki Ito, Tomoyuki Kurake, and Shogo Okuda.

He is very grateful to the Fellowship of the Program for Leading Graduate Schools "Integrative Graduate Education and Research in Green Natural Sciences" during 2016–2021, and the Research Fellowship of the Japan Society for the Promotion of Science for Young Scientists during 2019–2021.

He also gratefully appreciates his family members, Rina, Tomoshi, and Chisaki for their supports and understandings.

Finally, he would like to give his special thanks to Professors Masami Kamigaito and Kentaro Tanaka for serving on his dissertation committee.

August, 2021

Satoshi KAWABATA